Experimental study and modeling of methane hydrates cristallization under flow from emulsions with variable fraction of water and anti-agglomerant

Aline Mendes Melchuna

NNT : *2016 EMSE 0811*

THÈSE

présentée par

Aline MENDES MELCHUNA

pour obtenir le grade de
Docteur de l'École Nationale Supérieure des Mines de Saint-Étienne

Spécialité : Génie des Procédés

ÉTUDE EXPERIMENTALE ET MODELISATION DE LA CRISTALLISATION D'HYDRATES DE METHANE EN ECOULEMENT A PARTIR D'UNE EMULSION A POURCENTAGES VARIABLES D'EAU ET D'ANTI-AGGLOMERANT

soutenue à Saint-Etienne, le 04 janvier 2016

Membres du jury

Président :		
Rapporteurs :	Rigoberto MORALES	Professeur, Universidade Tecnológica Federal do Paraná, Curitiba, Brésil
	Amadeu SUM	Maître-Assitant, Colorado School of Mines, Golden, USA
Examinateur(s) :	Ana CAMEIRAO	Maître-Assistante, ENS des Mines de Saint-Etienne, Saint-Etienne, France
	Fabienne ESPITALIER	Professeur, ENS des Mines d'Albi-Carmaux, Albi, France
	Philippe GLENAT	Ingénieur Recherche, TOTAL-CSTJF, Pau, France
Directeur(s) de thèse :	Jean-Michel HERRI	Professeur, ENS des Mines de Saint-Etienne, Saint-Etienne, France

Spécialités doctorales	Responsables :	Spécialités doctorales	Responsables
SCIENCES ET GENIE DES MATERIAUX	K. Wolski Directeur de recherche	MATHEMATIQUES APPLIQUEES	O. Roustant, Maître-assistant
MECANIQUE ET INGENIERIE	S. Drapier, professeur	INFORMATIQUE	O. Boissier, Professeur
GENIE DES PROCEDES	F. Gruy, Maître de recherche	IMAGE, VISION, SIGNAL	JC. Pinoli, Professeur
SCIENCES DE LA TERRE	B. Guy, Directeur de recherche	GENIE INDUSTRIEL	A. Dolgui, Professeur
SCIENCES ET GENIE DE L'ENVIRONNEMENT	D. Graillot, Directeur de recherche	MICROELECTRONIQUE	S. Dauzere Peres, Professeur

EMSE : Enseignants-chercheurs et chercheurs autorisés à diriger des thèses de doctorat (titulaires d'un doctorat d'État ou d'une HDR)

ABSI	Nabil	CR	Génie industriel	CMP
AVRIL	Stéphane	PR2	Mécanique et ingénierie	CIS
BALBO	Flavien	PR2	Informatique	FAYOL
BASSEREAU	Jean-François	PR	Sciences et génie des matériaux	SMS
BATTAIA-GUSCHINSKAYA	Olga	CR	Génie industriel	FAYOL
BATTON-HUBERT	Mireille	PR2	Sciences et génie de l'environnement	FAYOL
BERGER DOUCE	Sandrine	PR2	Sciences de gestion	FAYOL
BIGOT	Jean Pierre	MR(DR2)	Génie des Procédés	SPIN
BILAL	Essaid	DR	Sciences de la Terre	SPIN
BLAYAC	Sylvain	MA(MDC)	Microélectronique	CMP
BOISSIER	Olivier	PR1	Informatique	FAYOL
BONNEFOY	Olivier	MA(MDC)	Génie des Procédés	SPIN
BORBELY	Andras	MR(DR2)	Sciences et génie des matériaux	SMS
BOUCHER	Xavier	PR2	Génie Industriel	FAYOL
BRODHAG	Christian	DR	Sciences et génie de l'environnement	FAYOL
BRUCHON	Julien	MA(MDC)	Mécanique et ingénierie	SMS
BURLAT	Patrick	PR1	Génie Industriel	FAYOL
COURNIL	Michel	PR0	Génie des Procédés	DIR
DAUZERE-PERES	Stéphane	PR1	Génie Industriel	CMP
DEBAYLE	Johan	CR	Image Vision Signal	CIS
DELAFOSSE	David	PR0	Sciences et génie des matériaux	SMS
DELORME	Xavier	MA(MDC)	Génie industriel	FAYOL
DESRAYAUD	Christophe	PR1	Mécanique et ingénierie	SMS
DOLGUI	Alexandre	PR0	Génie Industriel	FAYOL
DRAPIER	Sylvain	PR1	Mécanique et ingénierie	SMS
FAVERGEON	Loïc	CR	Génie des Procédés	SPIN
FEILLET	Dominique	PR1	Génie Industriel	CMP
FRACZKIEWICZ	Anna	DR	Sciences et génie des matériaux	SMS
GARCIA	Daniel	MR(DR2)	Génie des Procédés	SPIN
GAVET	Yann	MA(MDC)	Image Vision Signal	CIS
GERINGER	Jean	MA(MDC)	Sciences et génie des matériaux	CIS
GOEURIOT	Dominique	DR	Sciences et génie des matériaux	SMS
GONDRAN	Natacha	MA(MDC)	Sciences et génie de l'environnement	FAYOL
GRAILLOT	Didier	DR	Sciences et génie de l'environnement	SPIN
GROSSEAU	Philippe	DR	Génie des Procédés	SPIN
GRUY	Frédéric	PR1	Génie des Procédés	SPIN
GUY	Bernard	DR	Sciences de la Terre	SPIN
HAN	Woo-Suck	MR	Mécanique et ingénierie	SMS
HERRI	Jean Michel	PR1	Génie des Procédés	SPIN
KERMOUCHE	Guillaume	PR2	Mécanique et Ingénierie	SMS
KLOCKER	Helmut	DR	Sciences et génie des matériaux	SMS
LAFOREST	Valérie	MR(DR2)	Sciences et génie de l'environnement	FAYOL
LERICHE	Rodolphe	CR	Mécanique et ingénierie	FAYOL
LI	Jean-Michel		Microélectronique	CMP
MALLIARAS	Georges	PR1	Microélectronique	CMP
MAURINE	Philippe	Ingénieur de recherche	Microélectronique	CMP
MOLIMARD	Jérôme	PR2	Mécanique et ingénierie	CIS
MONTHEILLET	Frank	DR	Sciences et génie des matériaux	SMS
MOUTTE	Jacques	CR	Génie des Procédés	SPIN
NEUBERT	Gilles	PR	Génie industriel	FAYOL
NIKOLOVSKI	Jean-Pierre	Ingénieur de recherche		CMP
NORTIER	Patrice	PR1		SPIN
OWENS	Rosin	MA(MDC)	Microélectronique	CMP
PICARD	Gauthier	MA(MDC)	Informatique	FAYOL
PIJOLAT	Christophe	PR0	Génie des Procédés	SPIN
PIJOLAT	Michèle	PR1	Génie des Procédés	SPIN
PINOLI	Jean Charles	PR0	Image Vision Signal	CIS
POURCHEZ	Jérémy	MR	Génie des Procédés	CIS
ROBISSON	Bruno	Ingénieur de recherche	Microélectronique	CMP
ROUSSY	Agnès	MA(MDC)	Génie industriel	CMP
ROUSTANT	Olivier	MA(MDC)	Mathématiques appliquées	FAYOL
ROUX	Christian	PR	Image Vision Signal	CIS
STOLARZ	Jacques	CR	Sciences et génie des matériaux	SMS
TRIA	Assia	Ingénieur de recherche	Microélectronique	CMP
VALDIVIESO	François	PR2	Sciences et génie des matériaux	SMS
VIRICELLE	Jean Paul	DR	Génie des Procédés	SPIN
WOLSKI	Krzystof	DR	Sciences et génie des matériaux	SMS
XIE	Xiaolan	PR1	Génie industriel	CIS
YUGMA	Gallian	CR	Génie industriel	CMP

M

ise à

jour :

29/06/

2015

ENISE : Enseignants-chercheurs et chercheurs autorisés à diriger des thèses de doctorat (titulaires d'un doctorat d'État ou d'une HDR)

BERGHEAU	Jean-Michel	PU	Mécanique et Ingénierie	ENISE
BERTRAND	Philippe	MCF	Génie des procédés	ENISE
DUBUJET	Philippe	PU	Mécanique et Ingénierie	ENISE
FEULVARCH	Eric	MCF	Mécanique et Ingénierie	ENISE
FORTUNIER	Roland	PR	Sciences et Génie des matériaux	ENISE
GUSSAROV	Andrey	Enseignant contractuel	Génie des procédés	ENISE
HAMDI	Hédi	MCF	Mécanique et Ingénierie	ENISE
LYONNET	Patrick	PU	Mécanique et Ingénierie	ENISE
RECH	Joël	PU	Mécanique et Ingénierie	ENISE
SMUROV	Igor	PU	Mécanique et Ingénierie	ENISE
TOSCANO	Rosario	PU	Mécanique et Ingénierie	ENISE
ZAHOUANI	Hassan	PU	Mécanique et Ingénierie	ENISE

To my parents who were there all along the way.

“You have to be brave to be afraid.” (Unknown Author)

Acknowledgement

The road until the end of a thesis has some difficult obstacles, still, at the same time, it has a wonderful view. This view is possible, partially, due to the magic of science and, partially, due to the people that are with you throughout this journey.

Foremost, I would like to express my sincere gratitude to my supervisors M. Jean-Michel HERRI and Ms. Ana CAMEIRAO for the continuous support during the development of my research. Their knowledge, motivation and guidance were decisive factors and helped me to overcome every obstacle of this road. I could not have imagined having better mentors.

In time, I would like to thank the collaboration of M. Philippe GLENAT, in name of TOTAL S.A., always giving a new perspective about the obtained results, which allowed the research to achieve the required industrial level.

Besides, I would like to thank the other members of my thesis committee: M. Rigoberto MORALES, M. Amadeu SUM and, particularly, Ms. Fabienne ESPITALIER, who introduced me to this PhD opportunity.

The greatness of a PhD research requires a great team of technicians; I would like to take this opportunity to thank every technician of EMSE that helped me in this journey, including the ones which the help was a word of motivation. In particular, I would like to thank M. Fabien CHAUVY, Ms. Yamina OUABBAS, M. Alain LALLEMAND, Jean-Pierre POYET, M. Marc ROUVIERE and Richard DROGO.

A large fraction of these three years of thesis was passed in the bureau; I take this moment to thank everyone that divided this place with me (for longer or shorter period), specially: Jêrome, Aurélie, Wuchang and Rafael. They were of special importance either by the company either by the help to solve quotidian problems.

I also would like to express my gratitude to all my PhDs and non-PhDs colleagues, it would be impossible to name each one of them that represent a huge importance during these years. Although, I need to highlight some names: Orianne, for the support in every dimension since the beginning of these three years; Aurélie, for being my guide when I needed the most; and Kien, for being the one who will continue this project that means so much to me.

Last, but not least, I need to thank everyone that supported me in long distance from Brazil. To all my friends, there are no words to express the gratitude; you were, constantly, my fun even miles away. To my family, particularly, my parents, my sisters, my aunts and my grandmother, simply, I would not be here without you. To my best friend, my fiancé, every single time you were the light that pointed out the way.

Summary

Nomenclature

Latin Letters

Symbol	Description	Unity
A_{GL}	surface of the gas-liquid interface	m^2
C^*	interfacial concentration	$mol.L^{-1}$
C_b	concentration in the liquid bulk	$mol.L^{-1}$
C_{ext}	interfacial concentration at the gas-liquid equilibrium	$mol.L^{-1}$
C_i	molar concentration of the solute i	$mol.L^{-1}$
C_i^{eq}	molar concentration of the solute i in equilibrium	$mol.L^{-1}$
C_j^i	Langmuir constant of the component j in the cavity i	-----
C_w^0	initial concentration of gas in water	$mol.L^{-1}$
D_f	fractal diameter	-----
F_c	capillary forces	N
F_d	dispersion force	N
H_L	head loss	m
K^*	constant of hydrate growth	
K_g	global growth rate constant	$m^2.s^{-1}$
M_w	water molar mass	$g.mol^{-1}$
N_0	numerical concentration of water droplets	-----
N_1	numerical concentration of primary particles	-----
N_h	quantity of gas consumed to form the hydrate	mol
N_c	quantity of formed crystal c	mol
N_{cf}	quantity of gas solubilized into the emulsion	mol
N_{ct}	quantity of gas solubilized into the emulsion with time	$mol.s^{-1}$
$N_{i,j}$,	numerical concentration of initial agglomerates	-----
P_c	critical pressure	Pa
P_{eq}	pressure at equilibrium	Pa or MPa
R'	agglomerate radius	m
T_R	reduced temperature	-----
T_c	critical temperature	K
V_{Hyd}	hydrate volume	m^3
V_{cells}	cell volume	m^3
V_{total}	total volume	m^3
a_i	activity of the solute i	-----
a_i^{eq}	activity of the solute i in equilibrium	-----
a_w^L	water activity in the liquid phase	-----
f_{eq}	equilibrium fugacity	MPa
f_{gi}	fugacity od the specie i in the gas phase	MPa
k_L	mass transfer constant at the gas-liquid interface	$m.s^{-1}$
k_{agg}	agglomeration kernel	$m^3.s^{-1}$
k_d	constant of transfer	$m.s^{-1}$
k_g	constant rate of crystallization	$m^3.s^{-1}$
k_i	constant of integration rate	$m^2.s^{-1}$
k_{i+1}^F	breakage kernel	$m^3.s^{-1}$

k_n	constant of nucleation	-----
m_w	water mass	g
n_{CH_4}	quantity of methane consumed	mol
n_{cells}	quantity of hydrate cells	-----
n_{crw}	quantity of crystallized water	mol, molecules
n_i	quantity of gas i in a unit cell of hydrate	mol
n_{iwater}	Initial quantity of water	mol
n_w	quantity of water in a unit cell of hydrate	mol
r'	primary particle radius	m
r_c	critical cluster radius	m
$\bar{v}$	molar volume	$L.mol^{-1}$
v_h	volume of a hydrate cell	L
v_H	molar volume of hydrates particles	$L.mol^{-1}$
v_i	quantity of cavities type i	-----
v_w	volume of water molecule in a solution	L
x_b	gas molar fraction in the liquid bulk in equilibrium with the hydrate phase	-----
x_{int}	gas molar fraction in the liquid in equilibrium with the gas at the interface	-----
x_j	molar fraction of the molecule j	
$y_{a,i}$	the activity coefficient of the solute i	-----
$y_{a,i}^{eq}$	the activity coefficient of the solute i in equilibrium	-----
ΔG_{cr}	critical Gibbs' free energy	$J.mol^{-1}$
ΔG_s	surface excess Gibbs' free energy	$J.mol^{-1}$
ΔG_v	volume excess Gibbs' free energy	$J.mol^{-1}$
h	distance, enthalpy	m, $J.mol^{-1}$
A	Hamaker constant, crystal surface area	J, m^2
B	nucleation rate	$nuclei.m^{-3}.s^{-1}$
C	bulk concentration	$mol.L^{-1}$
D	diffusion coefficient, diameter	$m^2.s^{-1}$, m
F	force	N
L	length	m
P	pressure	Pa or MPa
Q	flow rate	$m^3.h^{-1}$
R	ideal gas constant	$J.K^{-1}.mol^{-1}$
Re	Reynolds' Number	-----
S	supersaturation, structure factor	-----
T	temperature	K
Y	solute fraction in the gas phase	-----
Z	compressibility factor	-----
f	fugacity	MPa
f	Fugacity, Fanning friction factor	MPa, -----
g	gravity	$m.s^{-2}$
k	Boltzmann constant	$J.K^{-1}$
k	Boltzmann constant	$J.K^{-1}$
r, a	radius	m
s	surface	m^2

t	time	s
u	velocity	m.s^{-1}
v	mean velocity, molar volume	m.s^{-1}, L.mol^{-1}
y	height	m

Greek Letters

Symbol	Description	Unity
Φ_2	second moment of the particle size distribution	-----
$\dot{\gamma}$	shear rate	s^{-1}
θ_j^i	occupancy factor of cavities type i per gas molecule j	-----
θ_p	contact angle	-----
μ_0	continuous phase dynamic viscosity	Pa.s
μ_s	suspension dynamic viscosity	Pa.s
$\xi_i^{L,eq}$	chemical potential of the specie i in the saturated solution	J.mol^{-1}
ξ_i^L	chemical potential of the specie i in the solution	J.mol^{-1}
τ_0	critical shear stress	Pa
φ^*	volume fraction of the dispersed phase from which the relative viscosity becomes 100	-----
φ_{eff}	effective volume fraction of the dispersed phase	-----
φ_{max}	dispersed phase maximum compact fraction	-----
φ_{water}	Water volume fraction	-----
Δ	difference operator	-----
Φ	particle size distribution	-----
δ	boundary layer thickness	m
μ	dynamic viscosity	Pa.s
ξ	chemical potential	J.mol^{-1}
ρ	density	Kg.m^{-3}
σ	surface tension	N.m^{-1}
τ	shear stress	Pa
φ	dispersed phase volume fraction	-----
ω	acentric factor	-----
η	conversion rate	-----

Figures Summary

Tables Summary

Introduction

Gas clathrates, also called gas hydrates, are ice-like structures formed by crystallization process. In this structure, hydrogen bonded water molecules cage a *guest* molecule, small enough to fit in different types of cavities and typically belonging to the lightest hydrocarbon group: usually methane, ethane, propane, butane and carbon dioxides.

Gas hydrates can form during the extraction of petroleum, commonly in subsea pipelines, when the required low temperature and high pressure conditions of formation are found. After massive hydrate formation and agglomeration, a large pressure drop increase is observed and, in some cases, the formation of an impermeable plug can occur (Hill *et al.*, 2010). This represents a real concern for the petroleum industry. In addition to the environmental risk; the hydrate plug occurrence can interrupt the process of petroleum extraction that results in financial costs.

During the process of petroleum extraction, a mixture of water and oil (with or without free gas phase) is transported in the flow lines. The mixture of water and oil is commonly named emulsion, since it is formed by two immiscible liquids, where one liquid is dispersed into another which is called continuous phase. Water and oil form an unstable mixture, which morphology depends on the water cut (*i.e.*, water volume fraction), the flow regime, the chemistry of the oil and the additives. The water cut varies during hydrate formation, as water is consumed to form the hydrates. This modifies the water-oil mixture morphology. Inversely, the properties of the water-oil mixture modify the crystallization process and deeply affect the agglomeration.

As the petroleum field matures, the water fraction usually increases. Therefore, industry is facing a system where the continuous phase of the liquid-liquid mixture is unknown, oil or water (Joshi *et al.*, 2013). Since the last decade, this kind of system became the focus of researches and there is a clear interest in studying this issue to provide better management of the hydrate formation during petroleum extraction.

The methods to manage hydrate formation and/or agglomeration are numerous, such as: maintaining the pipeline in a secure temperature zone by insulating the pipe, removing water from the system (dehydration), using additives as thermodynamic hydrate inhibitors (THIs), or most recently, using low dosage hydrate inhibitors (LDHIs), including kinetic hydrate inhibitors (KHIs) and anti-agglomerants (AAs).

In this work, the process of hydrate formation in flow lines was investigated by evaluating the influence of different water cuts varying the flow rate. Sets of experiments were done without and with the presence of a commercial anti-agglomerant additive (AA-LDHI). The main goal of this work is to enhance the understanding of the hydrate formation and agglomeration from different kinds of emulsions and also comprehend the mechanism by which a dispersant additive avoids the agglomeration and the pipeline plugging.

The experiments were performed in the *Archimède* flow loop installed at the *Ecole des Mines de Saint-Etienne (EMSE)*. The experimental dispositive works in similar conditions than the ones found in deep-sea pipelines, it simulates a flow of water and oil mixture at controlled pressure (until 100 bar), temperature (0°C to 14°C) and flow rate (0.3 $m.s^{-1}$ to 1.8 $m.s^{-1}$). The flow loop is equipped with probes measuring the pressure drop, the flow rate, the relative pressure, the temperature, the density and the particles (droplets and hydrates) size. The probes used to follow the particles properties are: a Focused Beam Reflectance Measurements probe (FBRM) and a Particle Video Microscope probe (PVM) to observe the shape of particles and agglomerates.

This thesis manuscript is composed of four chapters. The first one gives a bibliographic revue divided in three parts: (1) notions of emulsions and suspension, (2) notions of gas hydrates and (3) flow lines with hydrates, which gives a brief introduction about flow lines, an overview about the hydrate formation in this kind of facility and, finally, how it can be avoided. The second chapter describes the experimental device, the probes and the experimental protocol. Lastly, the third and the fourth chapters are devoted to the experimental results obtained from the experimental study. The third chapter presents experimental results of shear stabilized emulsion and hydrate formation experiments at the *Archimède* flow loop. In the fourth chapter the discussion is deepened, presenting a topological model for the process of hydrate formation without and with anti-agglomerant, suggesting a mechanism to explain how the additive avoid the hydrate agglomeration.

Introduction

Les clathrates (ou hydrates de gaz) sont des structures similaires à la glace qui sont formées par un processus de cristallisation. Dans ces structures, les molécules d'eau liées par des ponts d'hydrogène forment un réseau cristallin qui piège une molécule « invitée ». En règle générale celle-ci est assez petite pour s'ajuster à différents types de cavités et appartient au groupe des hydrocarbures les plus léger : habituellement le méthane, l'éthane, le propane, le butane et les dioxydes de carbone.

Les hydrates de gaz peuvent se former pendant l'extraction du pétrole, généralement dans des conduites sous-marines, où se trouvent les conditions requises pour sa formation : basse température et haute pression. Une importante formation et agglomération d'hydrates est suivi par une forte augmentation de la perte de charge. Dans certains cas, la formation d'un bouchon imperméable d'hydrates peut se produire (Hill *et al.*, 2010). Cela représente une réelle préoccupation pour l'industrie pétrolière. Au-delà du risque environnemental, l'occurrence d'un bouchon d'hydrates peut interrompre le processus d'extraction de pétrole qui entraîne des coûts financiers importants.

Au cours du processus d'extraction de pétrole, un mélange d'eau et d'huile (avec ou sans phase gazeuse libre) est transporté dans les conduites d'écoulement. Le mélange d'eau et d'huile est communément appelé émulsion, formé par deux liquides non miscibles, où un liquide est dispersé dans un autre, appelé phase continue. L'eau et l'huile forment un mélange instable, dont la morphologie dépend de la fraction d'eau (généralement mesurée en volume), le régime d'écoulement, la composition chimique de l'huile et des additifs. La fraction d'eau du système varie pendant la formation d'hydrates au fur et à mesure que l'eau est consommée pour former des hydrates, en modifiant aussi la morphologie du mélange d'eau et d'huile. A l'inverse, les propriétés du mélange d'eau et d'huile influent sur le processus de cristallisation et affectent profondément l'agglomération.

Le vieillissement des champs de pétrole correspond souvent à une augmentation de la fraction d'eau extraite avec le pétrole. Par conséquent, l'industrie fait face à un système dans lequel la phase continue du mélange liquide-liquide est inconnue, soit l'huile ou l'eau à l'inverse de ce qui est habituellement admis en cas de faible fraction d'eau où la phase continue est l'huile (Joshi *et al.*, 2013). Les études réalisés les derniers dix ans se sont concentrés sur ces systèmes de façon à fournir

une meilleure gestion de la formation d'hydrates lors de l'extraction de pétrole à haute fraction d'eau

Les techniques de management de la formation d'hydrates et / ou l'agglomération sont nombreuses, tels que : la conservation de la température du pipeline dans une zone en dehors de la zone de formation d'hydrates par isolation de la conduite ; l'élimination de l'eau du système par un processus de déshydratation ; l'utilisation d'additifs tels que les inhibiteurs thermodynamiques (THI), ou les inhibiteur d'hydrates à faible dosage (LDHI) qui comprennent les inhibiteurs cinétiques (KHI) et anti-agglomérants (AA).

Dans ce travail, le processus de formation d'hydrates en écoulement a été étudié par évaluation de l'influence de différentes fractions d'eau et débits de circulation, ainsi que avec et sans la présence d'un additif commercial anti-agglomérant (AA-LDHI). L'objectif principal de ce travail est d'améliorer la compréhension de la formation et de l'agglomération d'hydrates à partir de différents types d'émulsions et de comprendre également le mécanisme par lequel l'additif anti-agglomérant évite l'agglomération et le bouchage des pipelines.

Les expériences ont été effectuées dans la boucle d'écoulement *Archimède* installée à *l'Ecole des Mines de Saint-Etienne (EMSE)*. Le dispositif expérimental reproduit les conditions trouvées dans les pipelines en mer profonde. Il simule l'écoulement d'un mélange d'eau et d'huile à pression (jusqu'à 100 bar), température (0°C à 14°C) et débit (0,3 $m.s^{-1}$ à 1,8 $m.s^{-1}$) contrôlés. La boucle d'écoulement est équipée avec des sondes qui mesurent la perte de charge, le débit, la pression relative, la température, la masse volumique et la taille des gouttelettes et hydrates (par une sonde granulométrique *in situ* (FBRM). La forme et structure des gouttelettes et agglomérats sont observés par une sonde microscopique *in situ* (PVM).

Ce manuscrit est composé de quatre chapitres. Le premier chapitre présente une étude bibliographique divisée en trois parties: (1) notions d'émulsion et de suspension, (2) notions d'hydrates de gaz et (3) lignes d'écoulement avec hydrates, qui donne une brève introduction sur les lignes d'écoulement, un aperçu de la formation d'hydrates dans ce type d'installation et, enfin, comment la formation d'hydrates peut être gérée. Le deuxième chapitre décrit le dispositif expérimental, les sondes et le protocole expérimental. Finalement, les troisième et quatrième chapitres sont consacrés aux résultats expérimentaux obtenus à partir de l'étude expérimentale. Le troisième chapitre présente les résultats expérimentaux de l'étude de formation de l'émulsion

stabilisée par cisaillement et des hydrates dans la boucle d'écoulement *Archimède*. La discussion est approfondie dans le quatrième chapitre, qui présente un modèle topologique du processus de formation d'hydrates avec et sans anti-agglomérant, en proposant un mécanisme pour expliquer comment l'additif évite l'agglomération d'hydrates.

Chapter I – Bibliographic Review

"Somewhere, something incredible is waiting to be known" (Carl Sagan)

The understanding of a research lies on the knowledge of specifics scientific concepts from the studied area. Chapter I will be an overview about the required knowledge to understand the process of hydrate formation in a petroleum flow line.

Firstly, it will be introduced a discussion about dispersions (emulsions and suspensions) (§ I.1), from the basic concepts until its rheology. Finally, the petroleum dispersion, which is of interest in this research, will be presented. In section (§ I.2), notions about hydrates will be presented. It will be discussed their structure and properties, every step of their formation process, thermodynamics and the methane hydrate, the one studied in this research. Finally, in section § I.3, the main scope of the actual research will be introduced: the hydrate formation in flow lines and the means to deal with this event.

I.1 Notions of Emulsions and Suspensions

I.1.1 Basic Concepts on Emulsions

An emulsion is a mixture (dispersion) of immiscible liquids, formed by droplets (dispersed phase, also known as internal phase) dispersed in a continuous phase (also known as external phase). The emulsions are formed by an aqueous phase (called water) and a hydrocarbon phase (called oil). When water is the continuous phase, the mixture is named oil-in-water emulsion (O/W), also known as direct emulsion. On the contrary, if oil is the continuous phase, the mixture is named water-in-oil emulsion (W/O), also known as inverse emulsion. It is also possible to find emulsions with more complexity, for example, oil-in-water-in-oil emulsions (O/w/O) or water-in-oil-in-water (W/o/W), called multiple emulsions (or double emulsions).

Emulsion properties (such as size distribution, viscosity and stability) can vary with the properties of the chemical substances used and the method applied to form it. The emulsions are divided in three groups following the droplets size (Sjoblom, 2006):

(1) Nano-emulsions: presenting droplets with diameter inferior to 0.1 μm;
(2) Mini-emulsions: presenting droplets with diameter between 0.2 μm and 1 μm;
(3) Emulsions: presenting droplets with diameter superior to 1 μm.

The process of emulsion formation is called emulsification and its objective is to obtain the maximum interface between the dispersed and the continuous phases. This is normally obtained by applying high shear rates, however, others methods of emulsion formation are possible (Sjoblom, 2006). Generally, in the process of emulsification, an emulsifying agent (or stabilizer) is used in order to facilitate the droplets dispersion in the continuous phase and, also, to increase the stability of the formed emulsion (Brochette, 2013).

The stability of an emulsion is evaluated from the behavior of the droplets, which should keep a uniform distribution in the continuous phase. Nevertheless, there is no natural tendency to keep this stability, in the opposite the system tends to form larger droplets and to separate the two liquid phases, reducing the interfacial area, thus, reducing the free energy (thermodynamically unstable). An emulsion can only be stable from a kinetic point of view, *i.e.*, the emulsion keeps the droplets dispersed in the liquid phase during a period of time (Sjoblom, 2006).

There are several processes which could work to destabilize the emulsion. They are represented in Figure I.1 and briefly discussed in sequence:

- Flocculation (aggregation): It is a reversible process which consists on the formation of droplets clusters, which can favor others mechanisms as creaming and sedimentation. The origin of this effect is the movement of the droplets. If they collide while moving and the attractive forces between them are enough, they will keep together, without losing their original identities (Brochette, 2013).
- Sedimentation and creaming: They are reversible processes which consist on the formation of droplets clusters. The clusters are displaced to the bottom, for the sedimentation, and to the top, for the creaming. This process has the same mechanical origin as the flocculation and the displacement of the cluster will depend on the properties of continuous and dispersed phases (Brochette, 2013).
- Ostwald Ripening: It is an irreversible process which consists on the migration of molecules forming smaller droplets to form larger ones. The mechanism occurs due to the difference in the chemical potential between droplets. This arose from the difference in droplets' radius curvature (Taylor, 1998). The evolution of the Ostwald Ripening mechanism will end with the separation of the two phases.
- Coalescence: It is an irreversible process which consists on the fusion of two droplets in order to form a larger one. It is the phenomenon opposite to the droplets breakup during the

emulsion formation. In general the process is divided in three parts: (1) the droplets approach each other due to their own movement (likewise the process of flocculation, sedimentation and creaming) and a film is formed between the droplets interface, (2) which gets thinner over time; and, finally, (3) disrupts and forms a larger droplet (Brochette, 2013). Evolution of the coalescence mechanism will end with the separation of the two phases.

- Phase inversion: It is an irreversible process where the continuous phase becomes the dispersed one (and vice versa). It is known by some researchers as a catastrophic event, once it happens suddenly due to a gradual change in the system conditions (Preziosi *et al.*, 2013).

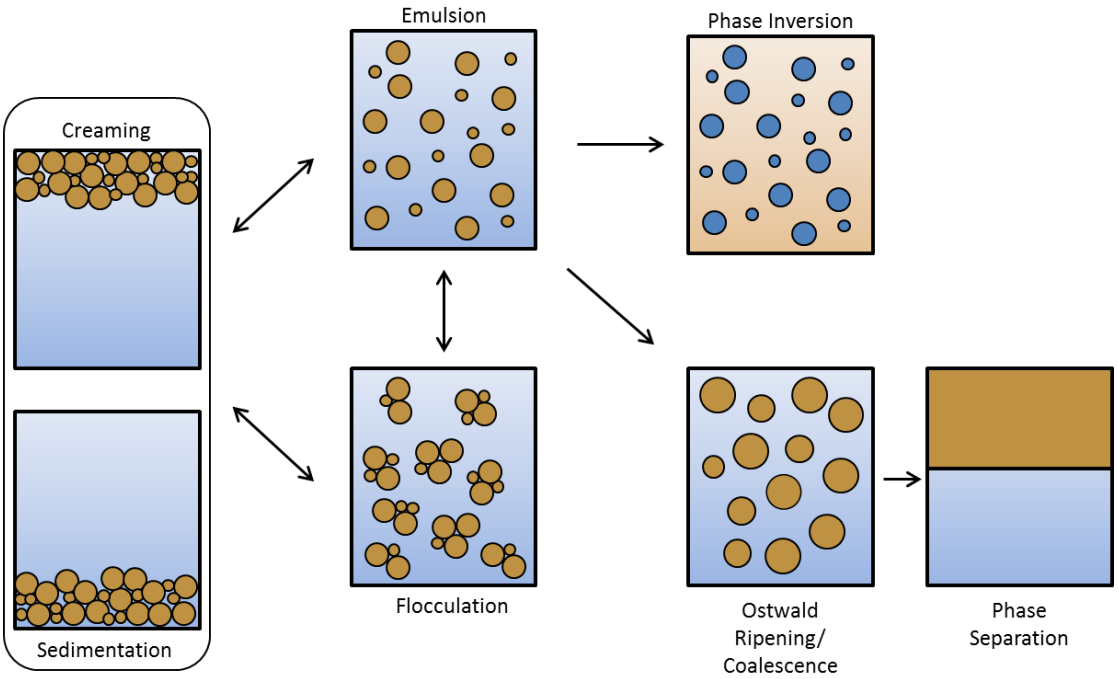

Figure I.1 – Schematic representation of the emulsion destabilization mechanisms (modified from Taylor, 1998).

I.1.2 Basic Concepts on Suspensions

Suspension is a mixture (dispersion) of solid and liquid phases, where the solid phase is insoluble in the liquid one. Usually, the suspension is formed by the dispersion of the solid (dispersed/internal phase) into the liquid (continuous/external phase) by a mechanical agitation procedure. In practice, the particles in suspension usually have diameter larger than 0.2µm with upper limit ranging between 50 µm and 100 µm (Schramm, 2005).

As emulsions, suspensions can only be stable kinetically and for a certain period of time. Thus, mechanisms of emulsion destabilization (as flocculation/aggregation, creaming, sedimentation and coalescence, here mostly named agglomeration) are still valid for suspensions.

I.1.3 Dispersions Rheology

The rheology science studies equations of motion (force balance) and rheological properties of materials (independent of the system). This science allows linking experimental results of macroscopically observable forces and displacements (Midoux, 1993) with the rheological state of the fluid. In other words, the rheology is the study of system's deformation and flow under influence of an applied force.

The rheology is responsible for evaluating the flow of different sorts of materials, ranging from liquids to solids. In all cases, independently of the elapsed time to start the flow, the laws characterizing the observed behavior are the same. The rheological classification of materials is made from their behavior under simple shear. The shear can be studied by considering two plane parallel surfaces (P and P', see Figure I.2Figure I.2) with a distance dy between them. The fluid moves between the surfaces with a velocity $u + du$, generating a tangential friction force τ and an angle of rotation γ.

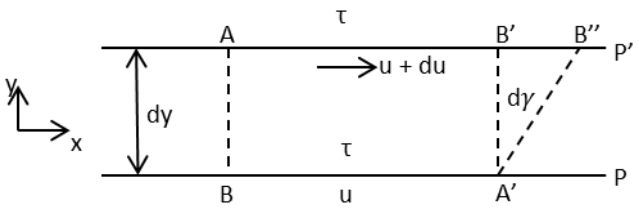

Figure I.2 – Shear study between two parallel surfaces (Midoux, 1993).

The shear stress (τ) is calculated by equation I.1 from the applied force (F), having a constant value at any point of the surface (s):

$$\tau = \frac{dF}{ds} \tag{I.1}$$

The shear rate or velocity gradient ($\dot{\gamma}$) depends on the shear stress and the type of fluid, it refers to the velocity variation (du) between two adjacent fluid layers (dy), represented mathematically by,

$$\dot{\gamma} = \frac{du}{dy} \tag{I.2}$$

The relation between the shear stress (τ) and the shear rate ($\dot{\gamma}$) is expressed by the viscosity (μ), which is dependent on the temperature and the fluid properties, and indicates the internal resistance of the fluid to flow. The viscosity for a laminar regime (Figure I.3) is represented by,

$$\tau = \mu\dot{\gamma} \tag{I.3}$$

If the flow regime is turbulent (Figure I.3), the moving layers are mixed. The distinction between laminar and turbulent flow is indicated by the Reynolds' Number (Re):

$$Re = \frac{\rho v L}{\mu} \tag{I.4}$$

where ρ is the fluid density, v is the mean velocity and L is the characteristic length (depending on the geometry of the flow, usually, the diameter of the pipe). In pipelines, the flow generally is laminar for Re < 2000 and turbulent for Re > 4000 (Livelli, 2010). A transitional regime can happen between laminar and turbulent flow (Figure I.3). The values of the flow regime transitions can change for other configurations and different fluids (Schramm, 2005). In general, lower Reynolds represents a laminar flow and higher Reynolds a turbulent flow.

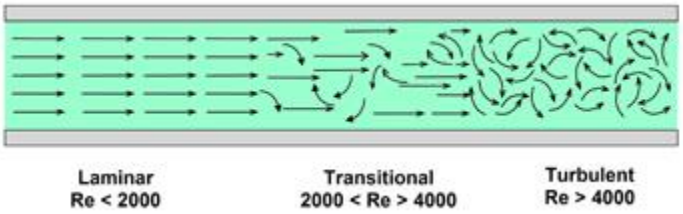

Figure I.3 – Fluid regimes in a pipe (Livelli, 2010).

The behavior of simplest fluids (Newtonian fluids), as oil and water, is expressed by the equation I.3. However, there are several equations to calculate the viscosity for different systems (for which, the reader is referred to Midoux, 1993). The rheological classification is performed by evaluating values of shear stress (τ), shear rate ($\dot{\gamma}$) and viscosity (μ). A simple analysis can be done from a rheogram (Figure I.4), a graph of shear stress (τ) versus shear rate ($\dot{\gamma}$), where the slope gives the viscosity (μ).

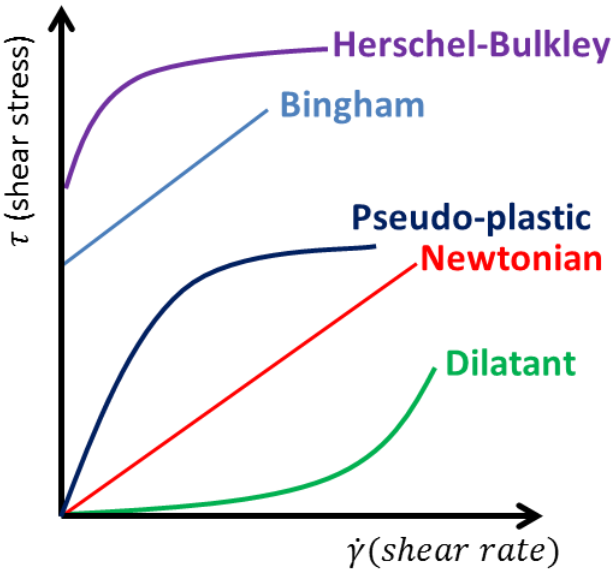

Figure I.4 – Types of fluids behavior (Modified from Midoux, 1993).

From the presented classification (Figure I.4), the fluid can be:

(1) Shear thinning or pseudo-plastic fluids are characterized by the decrease in viscosity with shear rate.

(2) Newtonian fluids have constant viscosity, independent of the shear rate.

(3) Shear thickening or dilatant fluids are characterized by the viscosity increase with the shear rate.

(4) Bingham plastic fluids are characterized by perfect solid behavior for low shear stress and viscous fluids for larger shear stress.

(5) Plastic Fluid fluids of the type Herschel-Bulkley are characterized by a complex nonlinear relationship between fluid deformation and applied shear stress.

The prediction of a dispersion (*e.g.*, emulsions and suspensions) viscosity is preferably performed in terms of continuous phase viscosity (μ_0) and amount of dispersed phase (in volume fraction, φ). The majority of equations developed until now are extensions of the Einstein's equation (1906) for a dilute suspension of non-interacting spheres (Schramm, 2005):

$$\mu = \mu_0(1 + 2.5\varphi) \tag{I.5}$$

The volume fraction of dispersed phase (φ) must be less than 0.02 to the best application of Einstein's equation. Beyond this value, the equation works as good approximation to values between

0.05 and 0.1. Above 0.1 the dispersion viscosity increases and can become non-Newtonian. The maximum volume fraction of the dispersed phase is 0.74, considering a dispersed phase formed by uniform and incompressible spheres. Higher values can be observed in emulsions due to droplet distortion (Schramm, 2005). The increase in the volume fraction of the dispersed phase (concentrated dispersions) increases the difficulty on predicting the viscosity behavior.

The first author who developed a model for high volume fraction ($\varphi \leq 0,62$) was Thomas (1965). In his equation, the collision phenomena and the particles rearrangement are considered. Several researchers have identified models to calculate the viscosity after him (Darbouret, 2005). Until today, the most important and most used model is the Mills model (1985):

$$\mu = \mu_0 \left[\frac{1-\varphi}{\left(1-\frac{\varphi}{\varphi_{max}}\right)^2} \right] \tag{I.6}$$

where φ_{max} is the maximum compact fraction. This value represents the volume fraction in which all particles are in contact and the dispersion tends to behave like a solid.

There are some rheological studies developed to predict the emulsion viscosity. One that is worthwhile to mention is the model developed by Pal & Rhodes (1989) due to its applicability in the petroleum field. This model is useful for Newtonian and non-Newtonian emulsions. The viscosity equation is given by:

$$\mu = \mu_0 \left[1 + \frac{\left(\varphi/\varphi^*\right)}{\left(1.187-\left(\varphi/\varphi^*\right)\right)} \right]^{2.49} \tag{I.7}$$

where φ^* is the dispersed phase volume fraction from which the relative viscosity (μ/μ_0) becomes 100.

The viscosity of emulsions will be dependent on the droplet size and properties. For example, the emulsion viscosity will be higher when droplets sizes are relatively homogeneous. The emulsion viscosity will also increase with increasing the dispersed phase volume due to droplet “crowding” or structural viscosity. As consequence, the fluid can become non-Newtonian (Schramm, 2005).

I.1.2 Petroleum Dispersions

Petroleum is important for our society. It provides secondary products for energy and other industries, for heating and transportation (Speight, 2014). Chemically, petroleum is formed by a

complex mixture of hydrocarbons (the percentage of hydrocarbon molecules considering the different sizes will determine the state – liquid or gaseous – of the mixture; smaller molecules form gaseous mixture and larger ones form liquid mixtures). The petroleum mixture usually contains small amounts of other chemical compounds: oxygen, nitrogen, sulfur and some traces of metals.

Petroleum is extracted from the reservoir rock through flow lines. The reservoir rocks contain natural water inside it, as well as, additional water that is injected in the system to enhance the extraction. Consequently, the product obtained at the end of this process is a mixture of water and petroleum, which forms an emulsion during its transport from the reservoir until the surface. Some types of petroleum have natural constituents (*e.g.*, asphaltenes, high weight molecules that can work as emulsifying agent), which increase the stability of formed emulsions (Speight, 2014). The higher stability of the formed emulsion can represent a problem in some processing steps.

The presence of water during petroleum extraction can induce another problem. Once the petroleum extracted from a reservoir can be a mixture of liquid and gaseous phases, which can form solid compounds called hydrates in the right conditions of temperature and pressure. Hydrates can circulate suspended in the petroleum/water mixture. However, its formation (in some levels) harms, or even interrupts, the petroleum production. Hydrates are the major subject of this research, being deeply discussed in section §I.2. Later in section §I.3, some notions of flow lines with hydrates will be introduced.

I.2 Notions of Hydrates

Hydrates are crystalline compounds (ice-like structures) formed by one or more *guest* molecules (gas or liquid) trapped inside a *host* molecule network, generally comprising hydrogen bonded water molecules. The *guest* molecule stabilizes the formed structure by weak van der Waals forces. Hydrates can only be formed in suitable conditions of pressure, temperature and concentration of its components. Scientifically, hydrates are recognized as clathrates from the Latin *clatratus*, *i.e.*, *enclosed or protected by cross bars of a grating* (Nolas, 2014).

The first valid documentation mentioning hydrates in the science history was written by Sir Humphrey David (1811), who was able to form hydrates from oxymuriatic (chlorine) gas (Sloan & Koh, 2007). From this period until the mid-1930s, hydrates were only seen as a curiosity in science. However, in 1934, Hammerschmidt published an article showing that natural gas (methane, ethane, propane and isobutene) hydrates were being the responsible of causing blockage in gas transmission lines (Hammerschmidt, 1934). From then on, gas hydrates awaken the interest of industry and scientific research, showing importance for several researches branches: flow assurance in gas and oil flow lines, gas transport and storage, climate change, refrigeration, water desalination, among others (Eslamimanesh *et al.*, 2012). From now on, the focus of this review will be the gas hydrates.

I.2.1 Gas Hydrates Structure and Properties

The hydrates structure was not known for a long time. Only in 1949, von Stackelberg used the X-ray diffraction to identify them, starting the study on this topic (von Stackelberg, 1949). Later, new characterization techniques began to be used, as NMR (Nuclear Magnetic Resonance) and vibrational spectroscopy, which improved the knowledge on this field (Ripmeester, 2000).

The hydrates crystalline structure is generally sustained by hydrogen bonded water molecules (*host* molecule), while the *guest* molecules stabilize the structure by weak van der Waals forces between them and the water molecules. The hydrogen bonded water form polyhedral cages, with oxygen atoms occupying the vertices, while hydrogen bonds are represented by the edges. Six different kinds of polyhedrons were identified (Figure I.5).

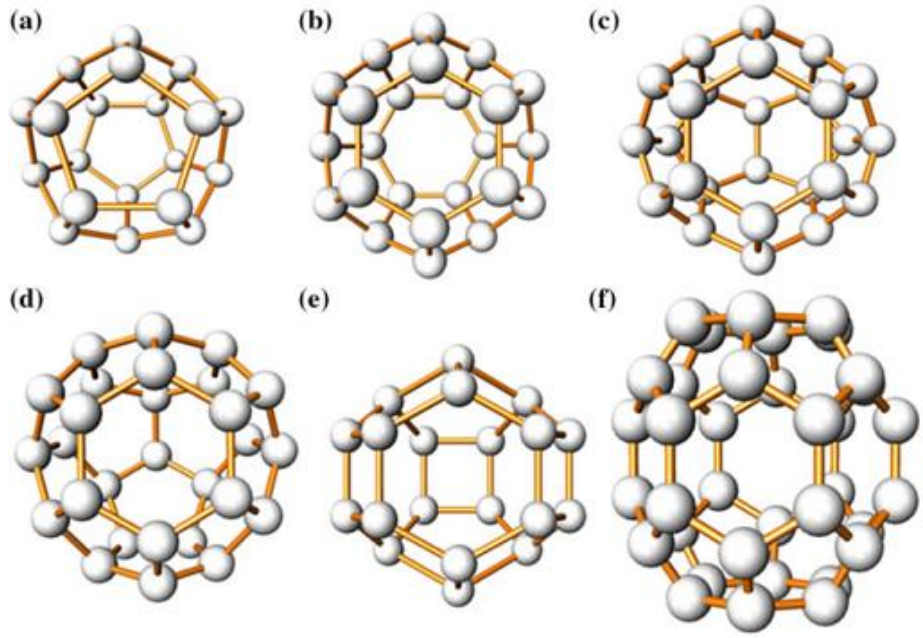

Figure I.5 – Differents polyhedrons forming clathrate-types structures (a) the pentagonal dodecahedron, 5^{12}, (b) the tetrakaidecahedron, $5^{12}6^2$, (c) the pentakaidecahedron, $5^{12}6^3$ (d) the hexakaidecahedron, $5^{12}6^4$, (e) the 12-faced $4^3 5^6 6^3$ polyhedron and (f) the 20-faced $5^{12}6^8$ polyhedron (Nolas, 2014).

In order to facilitate the understanding of the different kinds of polyhedrons, Jeffrey (1984) suggested the $n_i^{m_i}$ nomenclature; where n_i represents the number of edges of a polyhedron i and m_i is the number of times that the geometrical faces appear in this polyhedron i. Different types of polyhedrons can be combined in different ways to form a hydrate structure, the three main hydrates structures (sI, sII and sH - the ones that form the majority of known hydrates) and its properties are presented in Table I.1.

Firstly, between 1959 and 1967, two main structures were identified: cubic structure (sI) and cubic structure (sII). Another five (III - VII) structures were proposed by Jeffrey (1984), which are less representative in nature. More recently, in 1987, with the advent of new techniques, a new structure was discovered: the hexagonal structure (sH), very rare in nature.

Generally, cubic structures (sI and sII) form hydrates with single guest molecules. However, the hexagonal structure (sH) requires two types of guest molecules to achieve stabilization: smaller molecules (e.g., methane) will occupy small and medium cages, while larger molecules (e.g., 2,2-dimethylbutane) will occupy large cages (Sloan & Koh, 2007).

Table I.1 – Characteristics of the different hydrates structures (Sloan & Koh, 2007).

Hydrates Structure	S_I		S_{II}		S_H		
System	Cubic		Face-Centered Cubic		Hexagonal		
	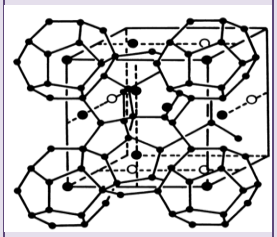		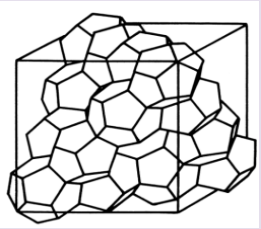		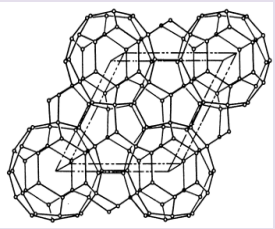		
Cage	Small	Large	Small	Large	Small	Medium	Large
Type of Cages	5^{12}	$5^{12}6^2$	5^{12}	$5^{12}6^4$	5^{12}	$4^35^66^3$	$5^{12}6^8$
Number of Cages	2	6	16	8	3	2	1
Average Cage Rayon (Å)	3.95	4.33	3.91	4.73	3.91[c]	4.06[c]	5.71[c]
Variation in Radius[a], %	3.4	14.4	5.5	1.73	Not Available		
Coordination Number[b]	20	24	20	28	20	20	36
Water Molecules /Unity	46		136		34		
Gas Examples	Methane, Ethane, CO_2		Propane, Butane, O_2		CH_4 + 2,2-dimethylbutane, Xe + Cycloheptene		

(a) Variation in distance of oxygen atoms from the cage center.
(b) Number of oxygens at the periphery of each cage.
(c) Estimates of structure H cages by geometrical model.

Hydrates can be represented by a stoichiometric equation (I.8):

$$m + nH_2O \leftrightarrow m.nH_2O \tag{I.8}$$

where m represents the *guest* molecule and n represents the hydration number.

Nevertheless, experimental studies (*e.g.*, Huo *et al.*, 2002; Ripmeester & Davidson, 1981) and the statistical thermodynamic developed by van der Waals and Platteeuw (1959) have shown that the cages present in hydrates structures are not really fully occupied by *guest* molecules. For this matter, hydrates are classified as non-stoichiometric species.

The ideal hydration number is obtained considering that all cages of the hydrate structure are filled. In general, each cage contains one guest molecule. At very high pressures, some molecules (*e.g.*, methane) can occupy together large cages (Sloan & Koh, 2007). Considering, that both cages of sI and sII structures are filled with a single molecule, the ideal hydration number is 5.75 and 5.67, respectively. For sH structure, the simplest case is to consider that one specie X occupies the two smallest cages and another specie Y occupies the largest cage, giving a hydration number of $5X.1Y.34H_2O$ (Sloan and Koh, 2007).

As previously stated, the hydrate cages are not fully occupied; consequently, real hydrates will always have more water molecules than an ideal structure (which has 85 % mol. of water). Due to high amount of water in the hydrate structure, some of the mechanic, thermodynamic and thermal properties observed in frozen water (ice) are also observed in hydrates. More deeply, even some structural characteristics of ice (hexagonal structure) and hydrates are very close (Sloan and Koh, 2007).

The characteristics of the *guest* molecule are very important in the goal of understanding the hydrates. Such that the hydrates can be classified considering: (1) the chemical nature and (2) the shape and size (influenced by the hydration number and, generally, its non-stoichiometric behavior) of the *guest* molecule (Sloan & Koh, 2007).

The chemical nature of the *guest* molecule was studied, firstly, by von Stackelberg (1956), who related it with the molecule size. Later, Jeffrey and McMullan (1967) classified the *guest* molecule, in four groups (hydrophobic compounds, water-soluble acid gases, water-soluble polar compounds, water-soluble ternary or quaternary alkylammonium salts) according to different characteristics. Finally, Jeffrey (1984) summarized the study of the *guest* molecule chemical nature by stating that the *guest* molecule should not have any strong hydrogen-bonding, once it can destabilize the hydrogen-bonding of the crystalline structure, destabilizing the hydrate.

Shape and size (geometry) of *guest* molecules were studied by many scientists. Knowledge about *guest* molecule geometry can be used to determine the filling ability of the hydrate cage, which depends on the temperature, pressure and *guest* composition (Sloan & Koh, 2007). In order to determine the possibility of a *guest* molecule to occupy certain hydrate cages, Davidson (1971) proposed to calculate the ratio between the guest diameter and the cage diameter (obtained by subtracting the van der Waals radius of the water molecule to the average cage radius). The ratio obtained by this method should have a value between 0.76 and 1.0 in order to stabilize the hydrate. Ratios under 0.76 mean that the molecular attractive forces contribution for the cage stability is not enough. Ratios above 1.0 mean that the guest molecule does not fit the cage. The relation of the cage size and hydrate structure with the appropriate guest molecule is given in Figure I.6. The same figure shows the relation between the hydration number and the guest molecule size.

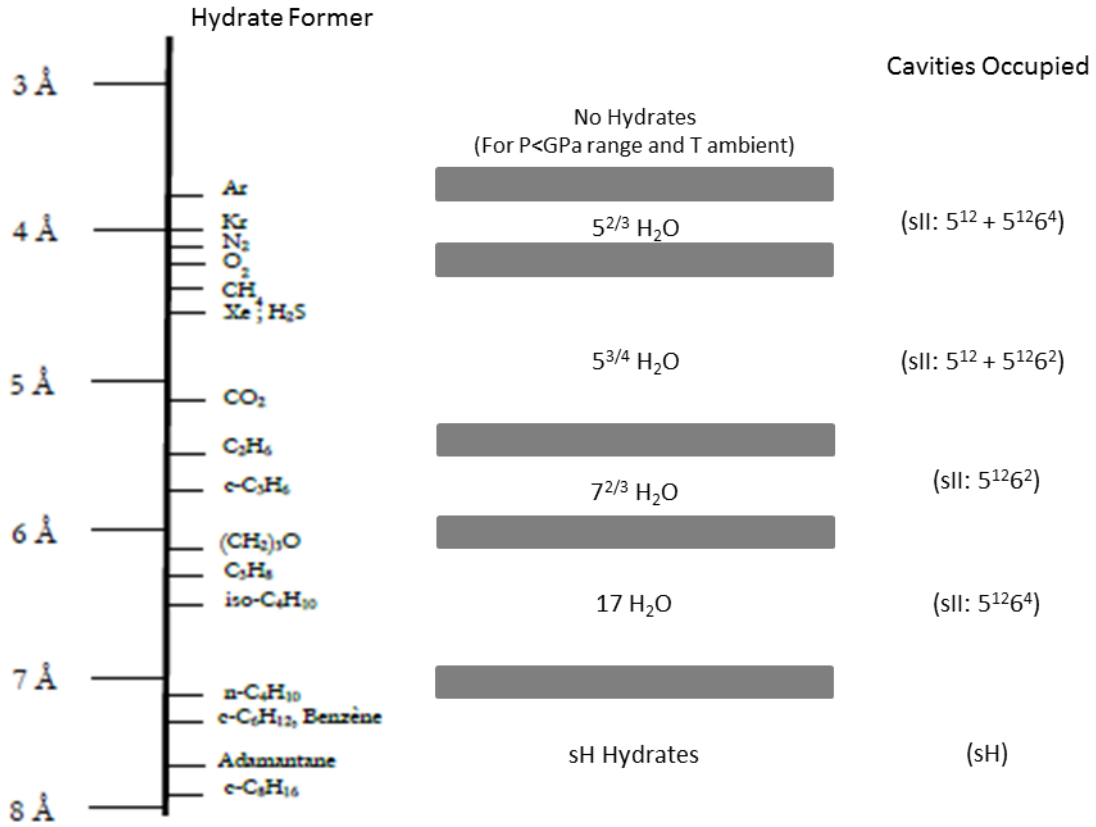

Figure I.6 – Relation of guest molecule sizes with the cavities occupied in different hydrates structure (diagram of von Stackelberg (1949) modified for Sloan & Koh (2007)).

I.2.2 Gas Hydrate Formation - Crystallization

Gas hydrates are formed by a process of crystallization. In the crystallization process, thermodynamic conditions are created to allow the molecules to approach and to regroup in highly organized structures (crystals). The crystallization process, such as the hydrate formation process, is divided in: (1) nucleation, (2) growth, (3) aggregation (agglomeration) and (4) dissociation. These four steps are time-dependent, increasing the difficulty of the phenomenon comprehension.

The driving force of crystallization is called supersaturation. In order to understand the supersaturation, it is necessary to previously understand the saturation process.

A solution is considered as saturated when the maximum amount of solute is solubilized into the solvent volume. If the solution is saturated, it means that the equilibrium was reached; in other words, the difference between the chemical potentials (equation I.9) of the specie *i* in each phase (solution and saturated solution) must be zero. For a supersaturated solution (non-equilibrium state),

this difference presents a value larger than zero; this means that the solution has more solute dissolved than it can normally contain. For this matter, the supersaturated solution *looks forward* to return to the equilibrium state by crystallizing the solute. Consequently, the supersaturation and the number of crystals formed during the crystallization are directly dependent. The supersaturated mixture is in a very unstable state; allowing the nucleation to start which determines the number of crystals initially created. Furthermore, the supersaturation also influences the crystal growth and its evolution, as well as, its properties, such as the size.

$$\Delta\xi_i = \xi_i^L - \xi_i^{L,eq} \tag{I.9}$$

The equation I.9 can be represented in terms of activity (a), in terms of molar concentration (C) or in terms of supersaturation (S),

$$\Delta\xi_i = RTln\left(\frac{a_i}{a_i^{eq}}\right) = RTln\left(\frac{y_{a,i}C_i}{y_{a,i}^{eq}C_i^{eq}}\right) = RTlnS \tag{I.10}$$

where a_i is the solute i activity, a_i^{eq} is the solute i activity in equilibrium, $y_{a,i}$ is the activity coefficient of the solute i, $y_{a,i}^{eq}$ is the activity coefficient of the solute i in equilibrium, C_i is the molar concentration of the solute i, C_i^{eq} is the molar concentration of the solute i in equilibrium.

Supersaturated solutions are metastable states, which can be achieved in the gas hydrate formation systems by decreasing the temperature (supercooling) or by increasing the pressure which increases the gas (solute) concentration. Conventionally, the supersaturation for hydrate formation is defined as the difference between the chemical potentials of the water in the liquid phase (ξ_{old_phase}) and in the hydrate phase (ξ_{new_phase}), as shown in equation I.11. Actually, the most general equation (I.11) to describe the supersaturation in hydrate systems was developed by Kashchiev and Firoozabadi (2002a) and Anklam and Firoozabadi (2004), assuming a fixed composition of the hydrate.

$$\Delta\xi = \xi_{old\_phase} - \xi_{new\_phase} = \sum_i n_i(T,P_e,Y)kTln\left[\frac{f_{gi}(T,P,Y)}{f_{gi}(T,P_e,Y)}\right] + n_w v_w(P-P_{eq}) - v_h(P-P_{eq}) = RTlnS \tag{I.11}$$

where n_i is the number of gas molecule i in the unit cell of hydrate, n_w is the number of water molecules in the unit cell of hydrate, T is the temperature, P is the pressure, P_{eq} is the pressure at equilibrium, Y is the solute fraction in the gas phase, k is the Boltzmann constant, f_{gi} is the fugacity

of the specie i in the gas phase, v_w is the volume of water molecule in the solution and v_h is the volume of hydrate cell.

I.2.2.1 Nucleation

The nucleation is a transition stage between two states of a species, aiming to create a solid dispersed phase in a liquid volume or on an inert surface (Myerson, 2002). During nucleation, small entities (crystal nuclei) are formed, which often have unclear structure. In industrial crystallization, different types of nucleation (as it can be seen in Myerson, 2002) have been verified, the most relevant for this study are the following:

1. Homogeneous nucleation (spontaneous, formation in the solution body – primary nucleation).
2. Heterogeneous nucleation (formation induced by inert particles – primary nucleation).
3. Contact or Secondary nucleation (formation induced by crystals).

The nucleation nomenclature does not have a general agreement until now (Mullin, 2001). It was chosen here to consider the primary nucleation (homogenous and heterogeneous) occurring in systems without any crystal formed from the solute. The homogeneous nucleation takes place in an environment containing only the mother phase - liquid supersaturated phase without any heterogeneity, impurities or interfaces. In reality, it is almost impossible to find this type of nucleation due to the presence of the equipment walls, dust, bubbles, etc. which could act as support to form the first crystal nuclei, this consists of heterogeneous nucleation. Otherwise, the solid surface of the formed crystals itself could be the crystallization agent, generating small fragments that can be transformed into new nuclei, the so-called secondary nucleation.

The majority of the studies aiming to understand the nucleation process are related to primary homogeneous nucleation, which is not clearly understood. From the classical nucleation theory, the primary homogeneous nucleation phenomenon can be briefly described as follows (Kashchiev and Firoozabadi, 2002b):

- In the supersaturated solution, a set of continuous reactions between ions or molecules acts forming clusters (embryos).
- The clusters stability are influenced by aggregation forces, related to the total volume, and by the disaggregation forces, related to the surface of the aggregate formed.

- The clusters will combine themselves until the formation of a critical size cluster (thermodynamically stable nuclei – see Figure I.7).

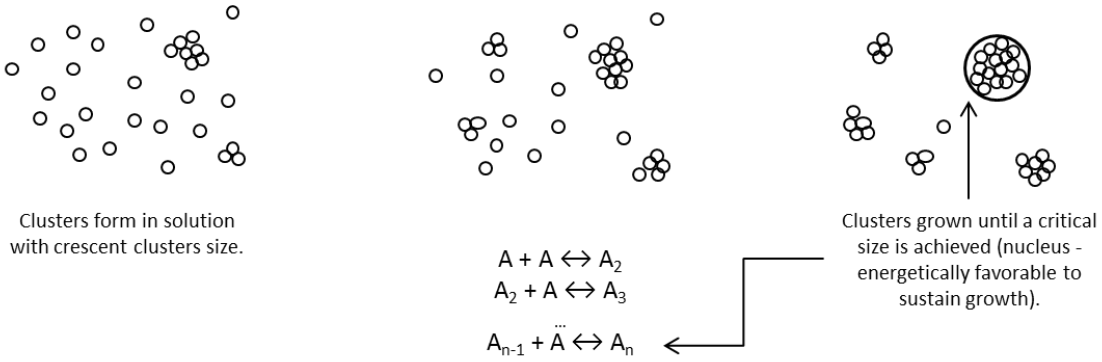

Figure I.7 – Clusters formation by the Classical Nucleation theory (Sloan & Koh, 2007, from T. Sobrel, Personal Communication, October 24, 2006).

The study of nucleation kinetics is also mainly related to primary nucleation, as the secondary nucleation is a complex phenomenon and not clearly understood (Myerson, 2002). The usual equation of the rate (B) for primary homogeneous nucleation is given by:

$$B = k_n \exp\left(-\frac{(16\pi/3)\sigma\bar{v}^2}{T^3 ln^2 S}\right) \quad \text{(I.12)}$$

where k_n is the constant of nucleation, the ratio $16\pi/3$ comes from the geometric factor, σ refers to the surface tension and $\bar{v}$ is the molar volume.

Clearly, the nucleation rate increases with temperature and supersaturation, and decreases with the surface tension. Primary homogeneous nucleation rate is developed from the value of the free energy when clusters achieve the critical size (ΔG_{cr}). A relation between free energy and cluster size was firstly proposed by Mullin, in 1972, like shown in Figure I.8.

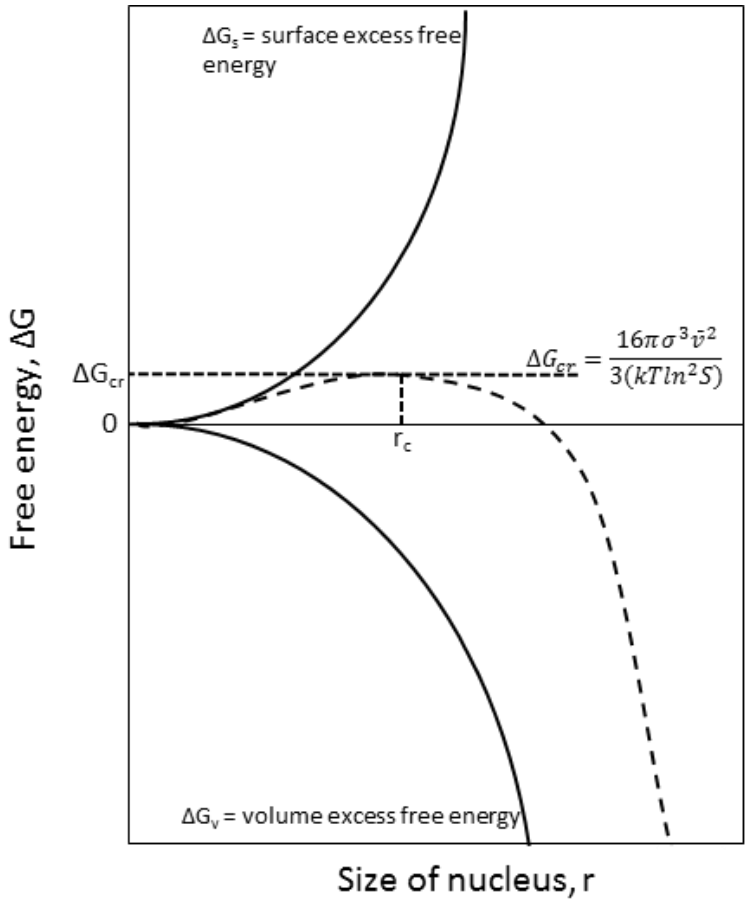

Figure I.8 – Free energy as a function of cluster size (adapted from Mullin, 2001)

The interval from the moment the solution achieves its supersaturation until the moment of the first cluster formation is known as induction or lag time. The induction time until the nucleation beginning can vary even when the same conditions are applied. This means that the nucleation is a stochastic (unpredictable) event.

The observation by naked eye of the gas hydrate nucleation is not possible. In order to understand this process, it is necessary to develop models involving the vapor/liquid interface (where gas hydrate nucleation generally begins) and the phenomena (*e.g.*, supersaturation and subcooling) related to the driving forces of gas hydrate nucleation.

The first model developed to explain the hydrate nucleation was proposed by Sloan (1990). It is called "Labile (unstable) Cluster". According to this model, the nucleation occurs by agglomeration of labile clusters in the liquid or in the vapor side of the interface until the nucleus reaches a critical size. A change in this model was proposed by Long (1994) and Kvamme (1996), based on adsorption and

aggregation only in the vapor side of the interface. Finally, the most recent mechanism refuses the "Labile Cluster" theory, Radhakrishnan and Trout (2002) found out by molecular simulations that the labile clusters were more likely to disaggregate than to aggregate. So, they proposed a model based on the local clustering hypothesis. The model supposed that the *guest* molecules arrange themselves in similar configuration to the one they present in the hydrate phase until this arrangement exceed the one present in a critical nucleus, then forming the first crystal nucleus. The most realistic model is to consider that all these mechanisms may be combined to form the first nucleus.

An interesting effect observed by some researchers is related to the *historic* of the water that hydrates are formed from, the so-called "memory effect". It was observed that hydrates form more rapidly (induction time lesser than expected) from solutions where hydrates have been formed before. Two opposing hypotheses were presented by Sloan & Koh (2007) to explain this behavior: (1) the hydrate structure (not visible by naked-eye) remains in solution or (2) the dissolved gas remain in solution. Although, others researchers have presented evidences from experiments that this effect does not exist, this phenomena remains without consensus in the hydrate literature.

I.2.2.2 Growth

After clusters reach a critical size (nucleation), forming the crystal nucleus, the growth process begins. The crystals start to grow by the addition of solute molecules from the supersaturated solution (Myerson, 2002). The agitation or circulation rate, the degree of supersaturation, the temperature, etc. are parameters which act in the growth rate and the final product characteristics (alongside with nucleation).

There are several theories trying to explain the crystal growth, while scientists focus mainly in crystal growth by equilibrium or thermodynamic view, the industrial crystallization is more interested in kinetic view (growth rate). In general, the crystal growth process is assumed to present a layer-by-layer mechanism, by this way molecules from the solute will bond in a place at the forming crystal surface with the maximum of neighborhood surface, representing the most energetically favorable site (Myerson, 2002).

The Diffusion Layer Model is one of the simplest models explaining crystal growth and it can be used to explain hydrate growth. It is based on the concept of a concentration gradient around the growing crystal due to the transfer of solute from solution to crystal. Once solute concentration

decreases around the growing crystal, the solute that is far from the crystal surface will diffuse towards it. A conceptual representation of the model is proposed in Figure I.9.

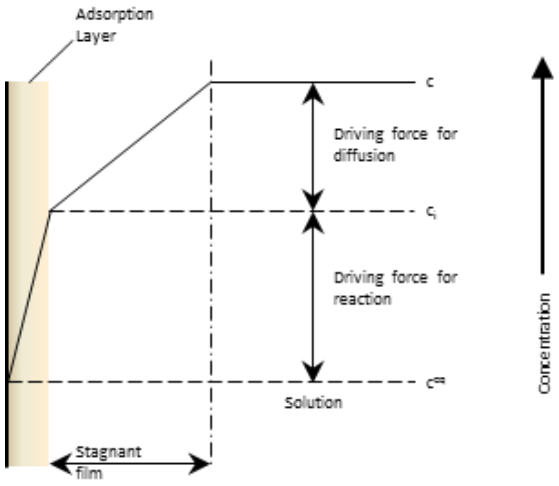

Figure I.9 – Conceptual picture of the Diffusion Layer Model (Sloan and Koh, 2007)

The representation proposed in Figure I.9 considers a single unidimensional case. In this matter, the mass increase rate of the crystal can be calculated by the equation (I.13) and the rate of solution integration to crystal surface by the equation (I.14) from Myerson (2002):

$$\frac{dN_c}{dt} = k_d A\,(C - C_i) \tag{I.13}$$

$$\frac{dN_c}{dt} = k_i A\,(C_i - C)^i \tag{I.14}$$

where $\frac{dN_c}{dt}$ is the number of moles of crystal c formed with time (t), k_d is the constant of transfer given by $\left({}^{D}/_{\delta}\right)$, D is the diffusion coefficient, δ is the boundary layer thickness, k_i is the integration rate constant, A is the crystal surface area, C and C_i are the bulk and interfacial concentrations, respectively. In equation (I.14), i has a value between 1 and 2; for $i = 1$, the equations (I.13) and (I.14) can be combined, eliminating the interfacial concentration that is difficult to obtain, and giving an equation associated to the global growth rate constant of transfer (K_g).

$$\frac{dN_c}{dt} = K_G A \Delta C \tag{I.15}$$

with,

$$\frac{1}{K_G} = \frac{1}{k_d} + \frac{1}{k_i} \tag{I.16}$$

This equation can work as an indicative of what process controls the crystal growth rate,

- If $k_d \ll k_i \rightarrow K_G = k_d$, the process is controlled by the diffusion.
- If $k_i \ll k_d \rightarrow K_G = k_i$, the process is controlled by the solute incorporation to the crystal.

Several researchers worked to develop models to exclusively explain the hydrate growth process; even so, the amount of data on hydrate growth is much limited. In general, researchers consider the supersaturation as the driving force of growth, but in cases of hydrates at this step the heat and mass transfer are more important regarding the process of crystals formation (Sloan & Koh, 2007).

In general, growth models for hydrates were developed in high-pressure reactors, so their accuracy is related to this condition, limiting the models validation for more complex systems (*e.g.*, flowlines). Until now, it is considered that hydrates may grow as: a single crystal, a film (shell) in the hydrocarbon-water interface (typical method) or multiple crystals in a stirred system (Sloan & Koh, 2007). The most important models describing the hydrate growth process will be discussed in later section (§I.1.2.2.1), in general, they focus on: (1) the kinetic of growth, (2) the mass transfer and (3) the heat transfer.

I.2.2.2.1 Hydrate Growth Models

Hydrates literature's is filled with several models trying to explain the hydrate growth process. In the following section, some models will be described, for more information the reader is refereed to Ribeiro & Lage (2008).

The Model of Englezos-Bishnoi

Englezos *et al.* (1987) performed kinetic experiments in a high pressure stirred reactor for a maximum experiment time of 200 min., later developing a model for hydrate growth in these conditions. The authors used as *guest* molecules: methane, ethane and their mixtures. They proposed that the hydrate growth is divided in three steps:

1. Gas diffusion from the gas-liquid interface until the liquid bulk;
2. Gas diffusion from the liquid bulk until the hydrate-liquid interface;

3. Adsorption “reaction”: the gas is incorporated to the water structure at the hydrate crystal interface.

The model was developed from the basis of the crystallization theory (without considering agglomeration) and the diffusion layer model for growth, assuming a spherical particle with outside surface equal to the inside one. The model considers as driving force for hydrate formation the difference between the fugacity of the dissolved gas in the liquid ($f(P,T)$) and at the equilibrium ($f_{eq}(P,T)$). So, the growth rate per particle is given by:

$$\left(\frac{dN_h}{dt}\right)_p = K^* A\left(f - f_{eq}\right) \tag{I.17}$$

where $\left(\frac{dN_h}{dt}\right)_p$ is the number of moles of gas consumed by unit of time during the hydrate formation, A is the particle surface and K^* is the constant of hydrate growth – similar to K_G (global growth rate constant of transfer) in the diffusion layer model – which takes into account the resistance (in series) of steps 2 (gas diffusion from the bulk liquid to the hydrate-liquid interface) and 3 (adsorption of the gas to the hydrate structure) of the proposed mechanism of hydrate formation.

The overall reaction rate is obtained by integrating the equation (I.17) over the whole particle population (size distribution) and considering homogeneously distributed spherical particles. Step 1 (diffusion from the gas-liquid interface until the bulk liquid) of the mechanism is taken into account by applying the two-film theory (mass transfer) in the upper part of the reactor, allowing to calculate the fugacity profile at the film interface.

The model of Englezos-Bishnoi remained for a long time as the most complete model for the hydrate growth, although its restrictions, such as (Sloan & Koh, 2007, and Ribeiro & Lage, 2008):

- The model was developed for simple hydrate formers (methane, ethane, carbon dioxide) which give rise to sI structures in the same experimental device, with total gas consumption smaller than 0.1 mole and under identical hydrodynamic conditions. This imposes some caution for using the model with sII and sH structure or even in different conditions than those it was developed from.
- Skovborg & Rasmussen (1994) remarked that an increase of gas consumption is predicted for a longer operating time than the one observed experimentally.

- The model is very sensitive to the moles of gas consumed at the place where hydrates are first seen, which is very hard to detect.
- The model considers that the hydrate surface pressure is equal to the equilibrium pressure at operating temperature to calculate the critical radius. If this happened, a pressure gradient should be seen in the reactor, followed by a force imbalance.
- The model considers rather the kinetics from the hydrate growth process than the mass and heat transfer roles, which seems to be more important in some kinds of systems (*e.g.*, turbulent pipeline flow).

The Model of Skovborg-Ramussen

After analyzing the model proposed by Englezos *et al.* (1987), Skovborg & Rasmussen (1994) proposed to simplify it by removing the population balance, by considering that all the particles have the same size and grow at the same rate. They have also assumed that the hydrate formation is only limited by the mass transfer during the diffusion of the dissolved gas from the gas-liquid interface into the liquid bulk. After their simplifications, the following equation was proposed:

$$\frac{dN_h}{dt} = k_L A_{GL} C_w^0 (x_{int} - x_b) \tag{I.18}$$

where k_L the mass transfer coefficient at the gas-liquid interface, A_{GL} the surface of gas-liquid interface, C_w^0 is the initial concentration of gas in water, x_{int} is the gas mole fraction in the liquid in equilibrium with the gas at the interface and x_b is the gas mole fraction in the liquid bulk in equilibrium with the hydrate phase.

The model proposed by Skovborg & Rasmussen (1994) represented a great advance, showing a good mathematical agreement to the growth process, which is controlled by mass transfer. However, it was verified that the model is very sensitive to errors in the driving force calculations. Moreover, the model reliability probably is related to the use of the same kind of apparatus.

The Model of Herri-Pic-Gruy-Cournil

Despite the advance observed with the model proposed by Skovborg & Rasmussen (1994), their model just presents some modifications from the one proposed by Englezos *et al.* (1987). It was with the model proposed by Herri *et al.* (1999a) that real progress was reached, presenting a model

including nucleation, growth and agglomeration steps. The developed model was able to reproduce experimental trends. However, numerical comparisons with the experimental data were not shown.

The model of Herri *et al.* (1999a) considers the importance of the gas-liquid interface for the diffusion of the dissolved gas (as well as Skovborg & Rasmussen (1994)). However, Herri *et al.* (1999 stated that the model should be based on the theory of crystallization, including the population balance which, at this time, could be evaluated with the arising of new techniques of crystal size measurement for hydrates.

The experimental study developed by Herri *et al.* (1999a) was done in a stirred reactor at constant pressure and temperature, while measuring throughout the experiment: (1) the consumption of methane during hydrate formation and (2) the particle size distribution of methane hydrates during formation by a turbidimetric sensor.

The performed experiments at different stirring rates showed that this parameter affected the mean diameter, the total number of particles and the absorption of methane. In order to understand this behavior, Herri *et al.* (1999a) proposed a new kinetic model, divided in two parts:

(1) Mass and Population balances, distinguishing two zones of behavior in the stirred reactor:
   (a) the interfacial zone, with small thickness (where the concentration of dissolved methane is constant). In this zone, only primary nucleation is prone to occur due to the high supersaturation at the interface;
   (b) the bulk zone, with uniform methane concentration. In this zone, it is possible to find all the classic crystallization steps: primary nucleation, growth, agglomeration and secondary nucleation
(2) Modelling of the stirring rate effect on the particle size distribution.

The first part of the model can be described by the two following differential equations. The mass balance for the gas in the bulk zone (1),

$$\frac{dC_b}{dt} = k_L A(C_{ext} - C_b) - \frac{4\pi K_g \Phi_2}{v_H} \tag{I.19}$$

where C_{ext} is the methane interfacial concentration imposed by gas-liquid equilibrium, C_b is the methane concentration in the liquid bulk, Φ_2 is the second moment of particle size distribution and v_H is the molar volume of hydrates particle. The first term of this equation is related to the gas

absorption at gas-liquid interface and the second term is related to gas consumption due to the hydrate formation.

And the population balance equation for hydrates crystals (2),

$$\frac{\partial \Phi}{\partial t} + K_g \frac{\partial \Phi}{\partial r} = B'(r) - D'(r) \quad \text{(I.20)}$$

where r is the particle radius, $\Phi(r,t)$ is the particle size distribution function, $B'(R)$ is the birth term related to the contributions of primary and secondary nucleation, growth and agglomeration, and $D'(r)$ is the death term essentially due to agglomeration.

In order to model the stirring rate effect on the particle size distribution (second part of the model), Herri *et al.* (1999b) tested four different additional models: (1) secondary nucleation in the liquid layer around the crystal, (2) breakage by attrition leading to new nuclei, (3) binary breakage into two equal particles and (4) ternary breakage. From them, only breakage by attrition was able to explain the experimental trends.

Recent Models for Hydrate Growth in Presence of an Oil Phase

Talatori *et al.* (2008) developed a kinetic model from experiments of hydrate formation in presence of an oil phase in pressurized cells for different stirring rates. The model was based on the KJMA (Kolmogorov – Jonhson – Mehl – Avrami) theory of crystallization in case of polynuclear mechanism, from what is possible to determine two mechanisms: (1) instantaneous nucleation (IN) and (2) progressive nucleation (PN).

Data obtained by the experiments of Talatori *et al.* (2008) fit well with the model. Later Talatori & Barth (2012) presented a deeper discussion on the model, where they observed different growth rate behaviors varying the quantity of water (water cut) in the system: the higher was the water cut; the lower was the growth rate.

In 2009, Turner *et al.* performed several experiments of hydrate formation in presence of an oil phase in autoclave cell, varying the shear rate and the pressure. From the experiments, they developed an inward growing shell model (the hydrates are formed in the water droplets interface and grow into the droplet center). They considered the gas diffusion through the gas-oil interface, the bulk liquid and the formed hydrate phase, which could cause some limitations in the growth rate.

The model of Turner *et al.* (2009) fit well with the experimental data. However, it under-estimated the initial gas consumption, while over-estimated the long-term consumption. The authors explained this behavior by two assumptions of the model: (1) constant droplet size and (2) considering zero thickness at the beginning of hydrate shell growth, whereas, in reality, the shell has some finite thickness. The overcome of the model is showing that the hydrate shell growth could provoke a higher hydrate particles fraction, even with low conversion, due to the water encapsulation inside the hydrate shell.

One of the most recent models for the hydrate growth process in presence of oil phase was proposed by Shi *et al.* (2011). The authors presented an advance by developing an inward/outward hydrate shell growth model (the hydrates are formed in the water droplets interface and grow into the droplet center and also into the exterior of the droplet) from experiments performed in a flow loop at low water cut (*i.e.*, high quantity of oil). The model considers kinetics, mass and heat transfer limitations.

Experimental and simulated data obtained by Shi *et al.* (2011) presented a good agreement one another. They found out that hydrate formation rate was related with water cut, quantity of gas dissolved in the system and ratio surface/volume of the particles, which depends on the fluid properties and the flow conditions.

I.2.2.3 Agglomeration

Agglomeration is the process describing the combination (aggregation) of several dispersed particles which consolidate to form an agglomerate. The aggregation is an intermediate step of the agglomeration: if the particles remain together the agglomerate is formed, if not the aggregate is disrupted in the original particles.

The aggregation is the result of collisions between particles in a suspension, leading sometimes to agglomeration. The collisions can be classified in two different types (Jones, 2002):

(1) Perikinetic due to Brownian motion (small particles, less than 1µm);
(2) Ortokinetic due to larger particles (more than 1µm) entrained in fluid velocity gradients;

both mechanisms are represented in Figure I.10.

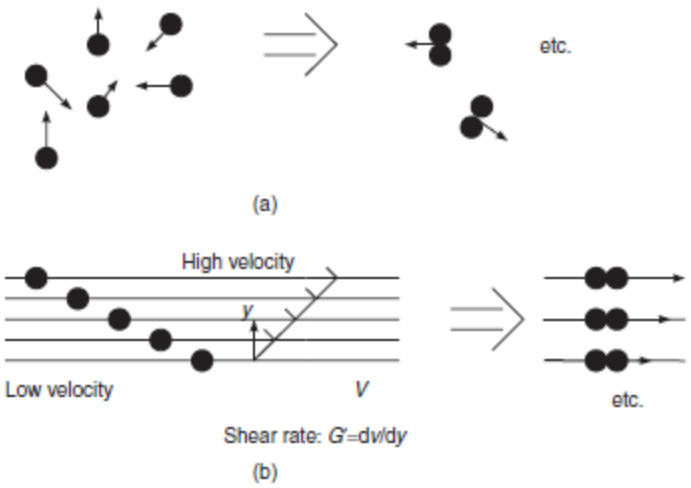

Figure I.10 – (a) Periknetic aggregation; (b) Ortokinetic aggregation (Jones, 2002).

In general, there are three main types of forces between particles: (1) Van der Walls attraction, (2) electrostatic forces and (3) steric forces. These interactions depend on shape and size of the particle, surface charge, solution composition (pH, ionic strength, etc.), temperature and distance between the particles.

Concerning the mechanisms of hydrate agglomeration, the forces acting in this process are mainly (Anklan *et al.*, 2008):

(1) Dispersion forces (F_d): these forces are London—Van der Walls type, characterized by weak attraction between particles. The dispersion forces between two spherical particles can be calculated by equation (I.21), from which is possible to see that a great distance between particles (h) corresponds to a weak dispersion force:

$$F_d = \frac{aA}{12h^2} \tag{I.21}$$

where a is the particle radius and A is the Hamaker constant.

(2) Capillary forces (F_c): hydrates have hydrophilic characteristics, thus, liquid water would be able to form a bridge between hydrate particles, holding them together. The capillary forces between the particles depend on surface tension (σ) and contact angle (θ_p) between water and hydrate particle (see Figure I.11). The equation (I.22) describing the capillary force is given below, from which is possible to see that a low surface tension corresponds to a weak capillary force, decreasing the possibility of agglomeration:

$$\frac{F_c}{a} = 2\pi\sigma cos\theta_p \quad \text{(I.22)}$$

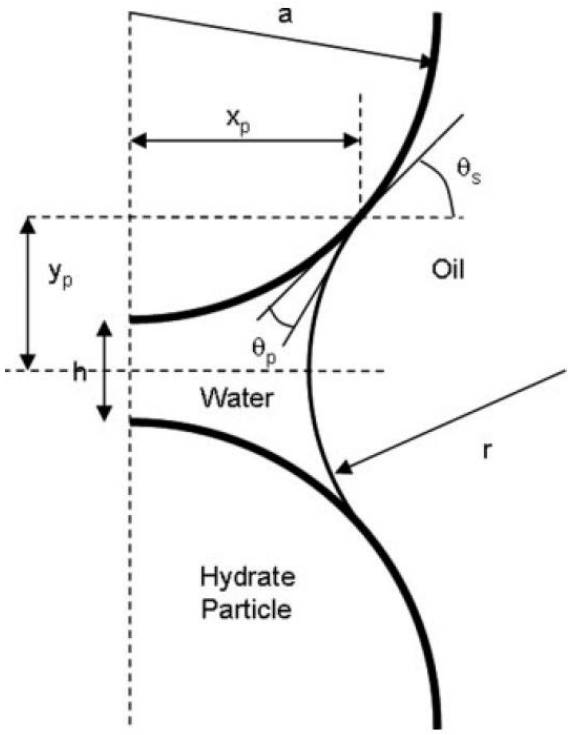

Figure I.11 – Liquid water bridge connecting two spherical hydrate particles dispersed in oil (From Anklan *et al.*, 2008).

I.2.2.3.1 Hydrate Agglomeration Models

The hydrate agglomeration represents a great risk in the oil & gas industry, for example, the evolution of the hydrate agglomeration in a petroleum flow line can lead to flow line plug, damaging the pipe and interrupting the production. Several models intending to describe the mechanism of hydrate agglomeration were proposed in literature. Some of these models will be shown in the following sections.

Contact Induced Agglomeration Model

After performing experiments in a flow-loop for hydrate formation at low water cut under the influence of additive, Fidel-Dufour *et al.* (2005) proposed a mechanism of agglomeration by contact. They have observed an increase in the viscosity, explained by the formation of hydrates agglomerates. Assuming that agglomerates are porous, their formation occupies a larger volume than the dispersed particles, consequently, increasing the viscosity.

The agglomeration model (Fidel-Dufour *et al.*, 2005) considers that agglomerates formed by a quantity i or j of primary particles (droplets completely converted in hydrates, 1) will agglomerate by intermediate of a water droplet, which forms a bridge (by capillary forces) between both particles. This process can be represented by the quasi-chemical reaction (considering a favorable ternary collision) forming an agglomerate of $(i+j+1)$ crystallized particles:

$$(i)+(0)+(j)\rightarrow(i+j+1) \tag{I.23}$$

In the system, there are three different populations, with the numerical concentrations: N_0, N_1 and $N_{i,j}$, corresponding to water droplets, primary particles and initial agglomerates, respectively. The primary particles formation rate ($\frac{dN_1}{dt}$) is proportional to the numerical concentration of water droplets:

$$\frac{dN_1}{dt}=k_gN_0 \tag{I.24}$$

where k_g is the constant rate of crystallization, which is a fitting parameter.

The formed agglomerates will always contain an odd number of primary particles (*i.e.*, $i=2k-1, k\geq 2$). Evolution of the numerical concentration of agglomerates is performed by two distinct equations:

(1) $k=1$, formation of an agglomerate from the primary particles:

$$\frac{dN_1}{dt}=k_gN_0-k_{agg}N_0N_1\sum_{h=1}^{\infty}N_h \tag{I.25}$$

(2) $k\geq 2$, formation of agglomerates from others agglomerates already formed:

$$\frac{dN_k}{dt}=\frac{1}{2}k_{agg}N_0\sum_{i=1,i+h=k}^{k-1}N_iN_h-k_{agg}N_0N_k\sum_{h=1}^{\infty}N_h \tag{I.26}$$

where k_{agg} is the agglomeration kernel, which is a fitting parameter. The presented equations were made dimensionless and solved by classical ordinary differential equations solver.

The dynamic viscosity of the suspension (μ_s) was based on the equation of Mills (1985):

$$\frac{\mu_s}{\mu_0} = \frac{1-\varphi_{eff}}{\left(1-\frac{\varphi_{eff}}{\varphi_{max}}\right)^2} \quad \text{(I.27)}$$

where μ_0 is the dynamic viscosity of the continuous phase, φ_{eff} is the effective volume fraction of the dispersed phase and $\varphi_{max} = 4/7$ is the volume fraction corresponding to a close packing. From Mills (1985), the effective volume fraction should be influenced by all agglomerates, considered as fractal morphologies, which are calculated by,

$$\frac{R'}{r'} = \left(\frac{i}{S}\right)^{1/D_f} \quad \text{(I.28)}$$

where R' is the agglomerate radius, r' is the primary particle radius, S is the structure factor and D_f the fractal diameter. Then, φ_{eff} is determined (I.29) in function of the water volume fraction, the different populations numerical concentrations and the fractal diameter (the relation between the radius is cubed to take into account the volume).

$$\varphi_{eff} = \varphi_{water}\left(N_0 + N_1 + \sum_{k=2}^{\infty}\left(\frac{2k-1}{S}\right)^{3/D_f} N_k\right) \quad \text{(I.29)}$$

The developed model is limited to low water cut systems. Nevertheless, it was able to describe the evolution of the viscosity during hydrate formation, with good agreement between model and experimental data. The model also justifies the viscosity increase with increase of the quantity of water present in the system (but still at low water cut), due to formation of agglomerates with larger porosity.

Palermo *et al.* (2005) developed a similar model to the precedent one (agglomeration by contact), but more simplified. Based on experiments in a high pressure cell at low water cut, they propose that agglomeration will occur by simple contact of water droplet and hydrate particle, following the pseudo-chemical reaction below,

$$(i) + (0) \rightarrow (i+1) \quad \text{(I.30)}$$

where an agglomerate formed by i primary particles under contact with a water droplet (not-converted, 0) will form a agglomerate $(i+1)$.

After this simplification, the authors modified the model proposed by Fidel-Dufour *et al.* (2005), including the influence of the gas solubilization on the system. The data obtained from the model showed good agreement with experimental results, but is still only valid for low water cut systems.

Shear-Limited Agglomeration Model

The contact induced agglomeration model achieved to demonstrate the viscosity evolution during hydrate formation for low water cut systems, where all water droplets were converted into hydrates, without considering any breakage during the process. However, when it comes to systems outside these conditions, the model fails in predicting the final viscosity. Pauchard *et al.* (2007) accomplish to predict this value by using a shear-limited agglomeration model.

Pauchard *et al.* (2007) performed experiments of hydrate formation in presence of a black crude oil (low water cut) using a multiphase flow loop. The viscosity found for the experiments was then compared to the shear-limited agglomeration model. The model also uses the Mills (1985) equation (I.27) to predict the dynamic viscosity of the suspension. Though, they consider that hydrate particles final size is dependent (I.31) on the shear stress (τ). The effective volume fraction (φ_{eff}) is therefore calculated (I.32) from the hydrates final size:

$$\frac{R'}{r'} = \left(\frac{\tau_0}{\tau}\right)^m \tag{I.31}$$

$$\varphi_{eff} = \varphi_{water}\left(\frac{\tau_0}{\tau}\right)^{(3-D_f)m} \tag{I.32}$$

where m depends upon the breakage mechanism (between 0.3 and 0.5, (Potanin, 1991)) and τ_0 is the critical shear stress.

Combined Agglomeration Model

Considering the two models described above, Colombel *et al.* (2009) developed a model in order to demonstrate that the two types of agglomeration model could fit together, giving a more accurate model to understand the process of hydrate agglomeration. In one hand, the contact induced agglomeration model can well-describe the viscosity evolution during the hydrate formation. On the other hand, the shear-limited agglomeration model can predict correctly the final viscosity of the

hydrate slurry. Thus, the two models can be unified in a more precise one. The model proposed by Colombel *et al.* (2009) is described by the following pseudo-chemical reactions:

$$(0) \xrightarrow{k_g} (1) \tag{I.33}$$

$$(i) + (0) \xrightarrow{k_{agg}} (i+1) \tag{I.34}$$

$$(i+1) \xrightarrow{k_{i+1}^F} (i) + (1) \tag{I.35}$$

where k_g is the constant rate of crystallization, k_{agg} is the agglomeration kernel (constant value and non-dependent of the agglomerates size) and k_{i+1}^F is the breakage kernel (related to the shear stress and the fractal diameter). These values are calculated accordingly to the system. The first two parameters are related to the contact induced model and the last one to the shear-limited model. The evolution of the formed agglomerates can be calculated by,

$$\frac{dN_1}{dt} = k_g N_0 - k_{1,agg} N_0 N_1 + 2k_2^F N_2 + \sum_{i>2}^{\infty} k_i^F N_i \tag{I.36}$$

$$\frac{dN_i}{dt} = k_{i-1,agg} N_0 N_{i-1} - k_{i,agg} N_0 N_i + k_{i+1}^F N_{i+1} - k_i^F N_i \tag{I.37}$$

$$N_0 = 1 - \sum_{i\geq 1}^{\infty} i N_i \tag{I.38}$$

The combined agglomeration model also uses the Mills (1985) equation (I.27) to calculate the suspension dynamic viscosity. The effective volume fraction (φ_{eff}) is now given as,

$$\varphi_{eff} = \varphi_{water} \left(N_0 + \sum_{i\geq 1}^{\infty} i^{3/D_f} N_i \right) \tag{I.39}$$

Data obtained from the model was compared with results of viscosity measured (by a rheometer) during triclorofluromethene hydrate formation (in low water cut). Results obtained by Colombel *et al.* (2009) were well described by the model. Nevertheless, authors recognize that some improvement must be made to better describe the breakage kernel.

I.2.2.4 Dissociation

The process of hydrate disruption is called dissociation. It is an endothermic process, characterized by hydrogen bonds breakage of water molecules (*host* molecule). Dissociation is also characterized by vanishing of the weak van der Waals attraction forces between water and *guest*

molecule, leading to hydrates structure disruption. The methods used to produce dissociation are: depressurization, thermal stimulation, thermodynamic inhibitor injection or a combination of all methods (Sloan & Koh, 2007).

The majority of hydrates dissociation models are based on the dissociation limited by heat transfer, that is normally used to provoke hydrate dissociation, but there are also models involving mass transfer and kinetics. Furthermore, the use of molecular dynamic simulations is commonly applied to understand the process of hydrate dissociation.

The actual research in hydrate dissociation considers two main types of models to describe the process (Liu & Gamwo, 2012): equilibrium and kinetic models. Liu & Gamwo (2012) made a comparison between equilibrium and kinetic models of hydrate dissociation, performing a parametric study with the constants of each model. They found that the equilibrium model can be considered a limiting case of the kinetic model.

I.2.3 Gas Hydrate Phase Equilibria - Thermodynamics

The concept of phase equilibria is related to simultaneous existence of different phases from the same molecular structure in the same system, without any external intervention. The gas hydrate phase equilibria properties can be defined and easily evaluated by phase diagrams (Pressure vs. Temperature – fixed composition) and approximate methods. An example of an approximate method is the gas gravity method, where the gas gravity is calculated for one specified temperature, then the pressure of hydrate formation is defined, or vice versa.

Another method to evaluate the gas hydrate phase equilibria is the development of phase equilibria calculations, which are better accurate and comprehensive than the other ones. The first model to make this calculation was proposed by Van der Waals & Platteeuw (1959), which developed a statistical theory to model the hydrates thermodynamic properties. The model assumptions are:

(1) Spectrum of the *host* lattice is not affected by the presence of solute molecules;
(2) G*uest* molecules in the cages are located in spherical cavities containing only one *guest* molecule;
(3) Mutual interaction of the *guest* molecule is neglected;
(4) Classical statistics are valid;
(5) G*uest* molecule can freely rotate inside the cavity;

(6) G*uest* molecule potential energy can be calculated from the spherically symmetrical potential for a limited distance of the cage center.

Hydrates in thermodynamic equilibrium present the same values for the difference between the chemical potential ($\Delta\xi$) of water in hydrate phase (H) and a hypothetical reference phase (β) and the difference between the chemical potential ($\Delta\xi$) of the liquid water (L) and a hypothetical reference phase (β), represented by:

$$\Delta\xi_w^{H-\beta} = \Delta\xi_w^{L-\beta} \tag{I.40}$$

where $\Delta\xi_w^{H-\beta}$ is determined by statistical thermodynamics (I.41), while $\Delta\xi_w^{L-\beta}$ is determined from the classical thermodynamics (I.45).

$$\Delta\xi_w^{H-\beta} = RT\sum_i v_i ln\left(1-\sum_j \theta_j^i\right) \tag{I.41}$$

where R is the universal gas constant, T is the temperature, v_i is the number of cavities type i per water molecule and θ_j^i is the occupancy factor of cavities type i per gas molecule j, which varies between 0 and 1.

The occupancy factor is very important to define the thermodynamic equilibrium and determine the hydrates properties. Its value is described by a model based on the analogy with the Langmuir adsorption (Sloan, 1998). From several assumptions, the value of the occupancy factor is given by I.42. Then, I.41 is rewritten in I.43.

$$\theta_j^i = \frac{C_j^i f_j(T,P,x_j)}{1+\sum_j C_j^i f_j(T,P,x_j)} \tag{I.42}$$

$$\Delta\xi_w^{H-\beta} = RT\sum_i v_i ln\left(1-\sum_j C_j^i f_j(T,P,x_j)\right) \tag{I.43}$$

In equations I.42 and I.43, $f_j(T,P,x_j)$ is the fugacity of the *guest* molecule j with molar fraction, x_j, at thermodynamic equilibrium. The occupancy factor is directly proportional to the fugacity (in any phase). Thus, an increase in the fugacity (so, an increase in the pressure) will increase the occupancy factor. C_j^i is the Langmuir constant of the component j in the cavity i, describing the interaction between the *guest* molecule in the symmetrically spherical cage and the water molecules forming it.

$$C_j^i = \frac{4\pi}{kT}\int_0^\infty \exp\left(-\frac{w(r)}{kT}\right) r^2 dr \quad \text{(I.44)}$$

where k is the Boltzmann constant, w is the interaction potential between the *guest* molecule and the water molecules (*host*) relative to the distance r separating them.

The difference between the chemical potential of the liquid water and a hypothetical reference phase ($\Delta\xi_w^{L-\beta}$) is calculated by the classical thermodynamics equation of Gibbs-Duhem, related to the variation of the free enthalpy with the temperature (T) and the pressure (P). This relation is written by,

$$\Delta\xi_w^{L-\beta} = T\frac{\Delta\xi_w^{L-\beta}\big|_{T^0,P^0}}{T^0} - T\int_{T^0}^{T}\frac{\Delta h_w^{L-\beta}\big|_{P^0}}{T}dT + \int_{P^0}^{P}\Delta\bar{v}_W^{L-\beta}\Big|_T dT - RTln\, a_w^L|_{T,P} \quad \text{(I.45)}$$

where a_w^L is the water activity in the liquid phase (a second order parameter), $\Delta h_w^{L-\beta}$ and $\Delta\bar{v}_W^{L-\beta}$ are, respectively, the partial molar enthalpy and the partial molar volume for the *guest* molecule. These parameters are of first order, both found in the literature. For example, the model developed by Van der Waals and Platteeuw (1959) was studied by Herri *et al.* (2010), who estimated some of these model parameters.

I.2.4 Hydrates Wettability

Discussing hydrates wettability is of interest because hydrate formation can occur from water/oil emulsion structure. The wettability phenomena can be related to the phase inversion of an emulsion/suspension and to hydrates agglomeration (Fotland & Askvik, 2008). It measures the tendency of one fluid to spread in a solid phase (in presence of another immiscible phase), in other words, it measures the solid *preference* of being in contact with a certain liquid (Abdallah *et al.*, 2007). Analyzing Figure I.12, there is a droplet of liquid B on a solid surface with contact angle (θ) near zero in the extreme left. The solid surface is surrounded by liquid A, *i.e.,* it *prefers* to be wetted by liquid A. Opposite behavior is observed in the extreme right, where it can be seen that liquid B completely wets the solid surface. In this case, the solid surface *prefers* to be wetted by the liquid B (contact angle, θ, near 180°). Between these two cases, there is an intermediate case where the solid surface is wetted by liquid A and B, and the surface and interfacial forces which determine the contact angle (θ) are balanced.

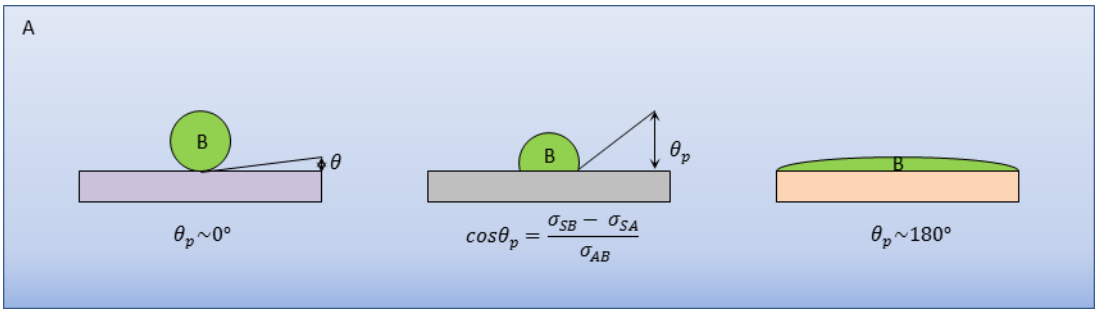

Figure I.12 – Contact angle (θ_p) in wettability: liquid A (blue), liquid B (green), solid surface (rectangular form), σ_{SA} (interfacial tension between the solid surface and the liquid A), σ_{SB} the (interfacial tension between the solid surface and the liquid B) and σ_{BA} (interfacial tension between the liquid A and the liquid B) (modified from Abdallah *et al.*, 2007).

There are several methods to measure the wettability. In the case of hydrates, where the surface energy (interfacial tension) has an important role, measurement of contact angles (from Young's equation) is the more suitable to be used in laboratory scale. It uses the relationship between interfacial tension and contact angle given by the Young's equation:

$$cos\theta_p = \frac{\sigma_{SB} - \sigma_{SA}}{\sigma_{AB}} \quad \text{(I.46)}$$

If the contact angle is lower than 90°, the surface is wetted by the liquid A. In contrast, if the contact angle is higher than 120°, the surface is wetted by the liquid B. For intermediate angles, the surface has no *preference* for any of the liquid phases (see Figure I.12).

The type of wettability (oil-wet particles or water-wet particles) will be important regarding suspension stability and, consequently, phase inversion. In resume, oil-wet particles tend to stabilize water-in-oil suspensions, while water-wet particles tend to stabilize oil-in-water suspensions (Hoiland *et al.*, 2005b). The wettability can also be associated to the flow line plug tendency. Studies from Hoiland *et al.* (2005a) showed that crude oil systems generating oil-wet hydrates form dispersions, while crude oil systems generating water-wet or intermediate wet hydrates form plugs. In resume, the kind of crude oil system forming hydrates influences the hydrate wettability and the hydrate wettability influences the tendency of forming plugs.

Hoiland *et al.* (2005a, b) formed *in situ* Freon hydrates from different water in crude oil emulsions at low water cut (but with enough water to consume all Freon during hydrate formation). They have also considered the interaction between hydrates and liquid phase at high water cuts, aiming to explore how the hydrate presence can promote or delay the inversion of water-crude oil

suspensions. This event was associated with the wetting parameters of the system. They have concluded that hydrates wettability is governed by the type and stability of suspensions, where it is possible to correlate the phase inversion with the particles wettability.

In this matter, Fotland & Askvik (2008) related the type of emulsion before hydrate formation with the hydrates wettability. The possible relations between these characteristics will have different effects on hydrate formation (Table I.2). After analyzing the system characteristics, it could be possible to determine when phase inversion or agglomeration (aggregation) is prone to occur, showing a link between agglomeration and wettability.

Table I.2 – Characteristics relating the kind of emulsion, the hydrate wettability and the effects on hydrate formation (Fotland & Askvik ,2008).

	Water Wetted	**Oil Wetted**
Water-in-oil	Destabilization, separation, phase inversion. Growth inhibition of hydrate before inversion. Aggregate formation is likely.	Stabilization, rupture of droplets, more interface is generated. Hydrate growth promoted instantly. The dispersion is likely.
Oil-in-water	Stabilization and possible rupture of droplets. New interface formed in water and the hydrate growth will probably accelerate. Possible aggregation is likely.	Destabilization, droplets growth and the oil separates from the water. Eventual inversion may occur. Initially hydrate growth is inhibited due to the decrease of the interfacial surface.
Separated/Stratified	Oil in water emulsion can be formed. The interfacial area increases, and the hydrate growth is favored. Aggregation is likely.	Water in oil emulsion can be formed. Increasing the interfacial area promotes growth of hydrates. Dispersions due to wetting by oil are likely.

I.2.5 Methane Hydrates

Methane hydrate is commonly known by its famous picture as “burning ice” (Figure I.13). It is formed by methane gas molecules (CH_4) trapped by water molecules, normally forming a hydrate with sI structure (see characteristics in Table I.1). Methane hydrate can be found in sediments, which could be a great energy source in the future. Concerning the flow assurance in Oil & Gas industry, methane hydrates are responsible for damaging the production by forming large agglomerates or plugs, alongside with other natural gases.

Figure I.13 – Methane hydrate: "burning ice" (Alexiades, 2009).

From thermodynamic point of view, methane hydrates evaluation can be simply made by analyzing a phase diagram according to the temperature and pressure for fixed gas composition, as in Figure I.14. In this diagram, methane hydrate formation is associated to ocean depth. The diagram shows four zones of stability separated by dashed lines; each area is associated with a different condition (pressure and temperature). The intersection point between the dashed lines represents equilibrium conditions where the four phases coexist.

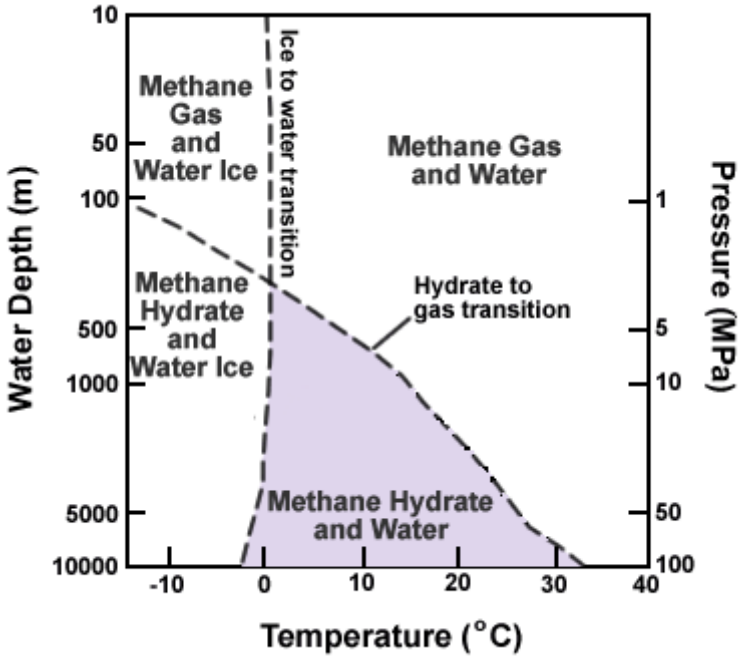

Figure I.14 – Methane Hydrate Phase Diagram (Ruppel *et al,* 2012).

The hydrate density can be calculated based on the crystal unit, Sloan & Koh (2007) performed this calculation for methane hydrate and obtained a value of $0.91\ g.cm^{-3}$.

I.2.5.1 Methane Solubilization

Gas hydrate formation from water or emulsion is influenced by gas solubilization in the system. Gas phase solubilizes into the liquid phase until it achieves its saturation, then hydrate formation starts, if the system is under right conditions of pressure and temperature. After supersaturation, as gas consumption is re-started, it is possible to assume that hydrates are under crystallization.

From literature (Clever, 1987), methane solubility is known to be higher in alkane liquids (oil fluids) than in water. Experimentally, the equation of state can be used to calculate the compressibility factor (Z) which allows obtaining the quantity of gas consumed by the liquid phase.

The Peng-Robinson equation of state is commonly used in hydrate studies, it is given by:

$$P = \frac{RT}{v-b} - \frac{a}{v(v+b)+b(v-b)} \tag{I.47}$$

where P is the pressure, R is the universal gas constant, T the temperature, v is the molar volume,

$$a = a(T_c)\alpha(T_R, \omega) \tag{I.48}$$

$$b = 0.07780\frac{RT_c}{P_c} \tag{I.49}$$

$$a(T_c) = 0.45724\frac{R^2{T_c}^2}{P_c} \tag{I.50}$$

$$\alpha(T_R, \omega) = \left(1 + K\sqrt{1 - T_R}\right)^2 \tag{I.51}$$

$$K = 0.37464 + 1.54226\omega - 0.26992\omega^2 \tag{I.52}$$

$$T_R = \frac{T}{T_c} \tag{I.53}$$

ω is the acentric coefficient, T_c is the critical temperature and P_c is the critical pressure (for the methane these values are 0.008, $160.60\ K$, and $45.4\ Pa$, respectively).

The equation of state (I.47) can be written in the cubic form by,

$$Z^3 - (1 - B)Z^2 + (A - 3B^2 - 2B)Z - (AB - B^2 - B^3) = 0 \tag{I.54}$$

where,

$$A = \frac{aP}{R^2T^2} \quad \text{(I.55)}$$

$$B = \frac{bP}{RT} \quad \text{(I.56)}$$

For pressures ranging between 1 to 10 MPa and temperatures ranging between 0 and 10 Celsius degrees, the compressibility factor (Z) can be simplified, as shown by Fidel-Dufour (2004):

$$Z = -0.0196P(MPa) + 0.994 \quad \text{(I.57)}$$

This simplification can be used in the ideal gas equation (I.58), allowing to calculate the gas consumption (number of moles or molar concentration) with the pressure variation.

$$PV = nZRT \quad \text{(I.58)}$$

where V the volume occupied by the gas.

I.3 Flow lines and Hydrates

A flow line is used during the petroleum extraction to transport the petroleum dispersion from the wellhead to the process unit.

I.3.1 Pressure Drop in Flow Lines

An important characteristic when designing flow lines is the knowledge on the pressure drop that the system is exposed to. By applying some concepts of fluid mechanics, the pressure drop in pipeline can be evaluated.

In spite of its limitations for steady, incompressible, non-viscous, isothermal flow; the energy conservation equation for steady-state fluid flow can be applied to represent the pressure drop in pipeline systems. This equation is developed from the assumption that all mechanical energy of the system is conserved between two points (1 and 2). For real systems, terms referring to gains and losses of energy can be included in the Bernoulli equation to improve the representation. For the target system here, the best representation of the Bernoulli equation is given by:

$$h_1 + \frac{P_1}{\rho_1 g} + \frac{v_1^2}{2g} = h_2 + \frac{P_2}{\rho_2 g} + \frac{v_2^2}{2g} + H_L \quad \text{(I.59)}$$

The equation can be simplified to (the density, ρ, is maintained constant between the two points and g is the gravity):

$$(P_2 - P_1) = \rho g(h_1 - h_2) + \rho \frac{v_1^2 - v_2^2}{2} - \rho g H_L \quad \text{(I.60)}$$

From the above equation the difference of pressure between two points $(P_2 - P_1)$ can be calculated from three different contributions:

(1) The contribution of static pressure difference (ΔP_{st}) due to the difference of height between two points $(h_1 - h_2)$:

$$\Delta P_{st} = \rho g(h_1 - h_2) \quad \text{(I.61)}$$

(2) The contribution of dynamic pressure difference (ΔP_{dyn}) due to the difference of velocity between two points ($v_1^2 - v_2^2$). This contribution is influenced by the system geometry.

$$\Delta P_{st} = \rho \frac{v_1^2 - v_2^2}{2} \quad \text{(I.62)}$$

(3) The contribution of pressure drop due to friction (ΔP_f), which can be related to the head loss (H_L). The friction force is opposite to the flow movement. As consequence, there is some energy lost into the pipe wall. This contribution can be calculated from the Fanning friction factor (f, mostly used in chemical engineering) and the flow velocity (v):

$$H_L = 2\frac{f v^2 L}{gD} \quad \text{(I.63)}$$

$$\Delta P_f = \rho g H_L = 2\frac{f \rho v^2 L}{D} \quad \text{(I.64)}$$

The pressure drop due to the friction (ΔP_f) can also be calculated from the Hagen-Poiseuille equation:

$$\Delta P_f = 128\frac{\mu L Q}{\pi D^4} \quad \text{(I.65)}$$

where L the pipeline length, D the internal diameter of the pipe and Q the flow rate.

From equations I.64 and I.65, it is possible to calculate the friction factor for laminar flows (once the Hagen-Poiseuille equation is only valid in this condition). Matching these equations, the friction factor for laminar flow is obtained as,

$$f = \frac{16}{Re} \quad \text{(I.66)}$$

The friction factor calculation for transition flow is impossible due to the inconsistency of the flow pattern. For turbulent flow, the friction factor will be dependent on the Reynolds' number and the pipe roughness. For this study, the pipe is considered smooth. In this condition, the friction factor is calculated from the Blasius equation:

$$f = 0.079 Re^{-0.25} \quad \text{(I.67)}$$

As it can be seen, the study of the flow regime in pipelines is performed in terms of friction factor, Reynolds number and pipe roughness. This kind of analysis can be summarized by the Moody Diagram, as represented in Figure I.15.

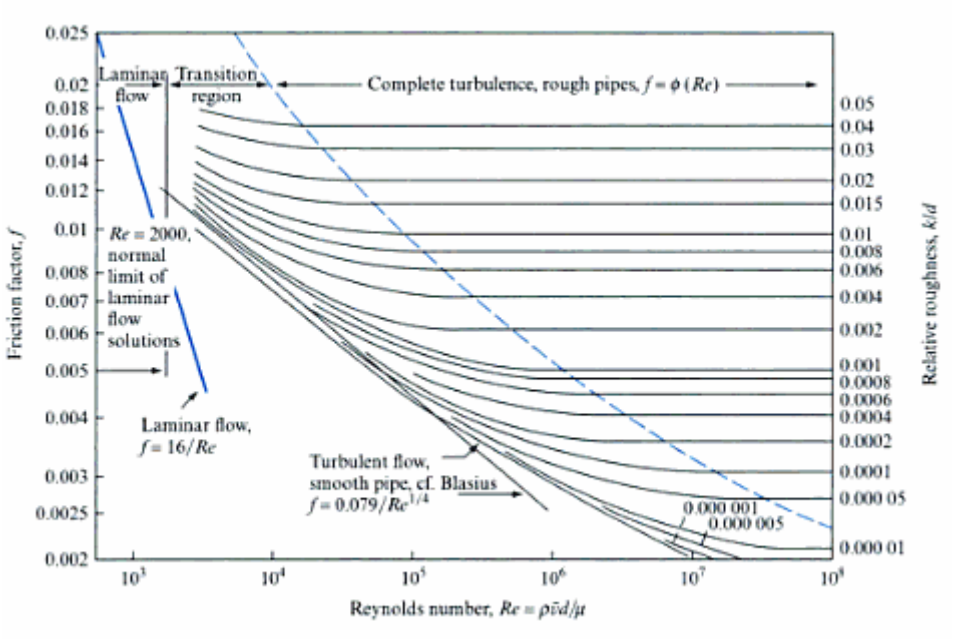

Figure I.15 – Moody Diagram considering the Fanning friction factor variation with Reynolds number and the pipe wall roughness for ducts of circular cross section (Douglas, 2005).

I.3.3 Hydrates Formation and Plugging in Flow Lines

As introduced in § I.1.2, hydrates can be formed from oil and water dispersions during the petroleum extraction process. The hydrate formation process in flow lines was first identified by Hammerschimidt (1934), in extreme cases, it can lead to flow line plug, generating interruption of petroleum extraction, leading to financial losses.

Hydrates can be formed from dispersions of water with oil and/or gas. Whatever the gas, hydrate formation process is not entirely known and very sensitive to system conditions (*e.g.*, water cut: amount of water). Topological models trying to explain this process have been described in literature (Sloan *et al.*, 2011). In general, topological models of hydrate formation from oil, water and gas mixtures can be separated in three distinct conditions: (1) oil is the predominant external phase, (2) water is the predominant external phase and (3) gas is the most important phase. For the first two conditions, an important factor influencing the hydrate formation process is the presence of free gas phase, which works increasing the surface of contact between gas and liquid phases, what can facilitate the hydrate formation.

In literature, topological models were proposed by Sloan *et al.* (2011). The focus of the present work is the hydrate formation from water and oil emulsions. For this matter, topological models of hydrate formation concerning these systems will be followed discussed.

Oil as predominant phase

Figure I.17 presents a conceptual model developed by Sloan et al. (2011). The model is valid for systems with oil (in brown), gas (in green) and water (in blue), with water cut equal or inferior to 50%. The model is divided in four steps:

(1) Water-in-oil emulsion formation occurs due to shear (flow) and oil chemical properties (some water can remain in the system as free water phase depending on these conditions). The water will disperse in the oil phase forming droplets with size inferior to 50μm.

(2) Once the system enters in the gas hydrate zone (*i.e.*, low temperature, high pressure and gas supersaturation), hydrates are formed in the droplet interface, giving rise to the appearance of a shell around it (Figure I.16).

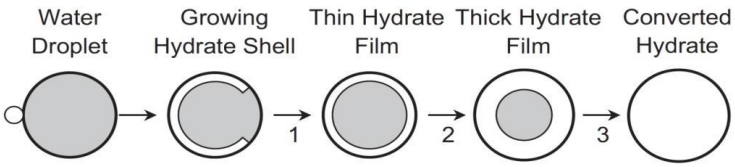

Figure I.16 – Hydrate formation on an emulsified water droplet (Sloan *et al.*, 2011).

(3) The formed hydrates shell continues to grow (into the droplets interior - see Figure I.16) due to mass and heat transfer. Alongside, agglomeration begins through the presence of free water or water inside the droplet shells, increasing the capillary forces between the hydrate droplets.

(4) As agglomeration continues, the hydrates can plug the pipeline. These agglomerates are firstly composed by entrapped water and can block the liquid flow.

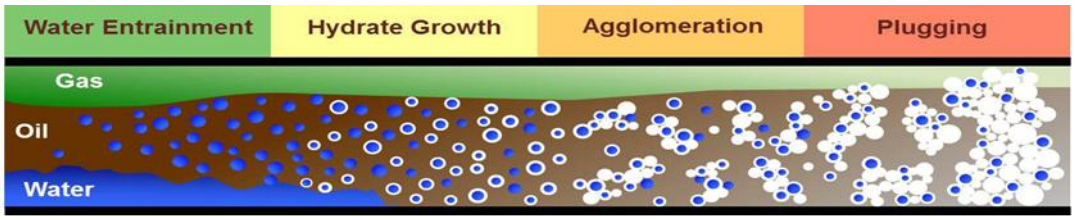

Figure I.17 - Conceptual model for hydrate formation in oil-dominated multiphase flow systems consisting of gas, oil, and water (Sloan *et al.*, 2011).

This behavior model represents great advance in understanding hydrate formation in flow lines, when oil is the predominant phase. However, it is necessary to highlight some of its limitations:

- Despite the consideration of free gas and water phases, the model does not take into account hydrate formation at these interfaces;
- The model supposes that oil will be the external phase only for water cut lower than 50%. In practice, it is known that oil can be the external phase even at higher water cut, depending on chemical properties of the oil;
- The model considers the formation of simple water-in-oil emulsions, disregarding the possibility of more complex emulsion formation (*e.g.*, oil-in-water-in oil).

Water as predominant external phase

The majority of the researches which investigate hydrate formation in flow lines are focused in oil dominant systems. For this reason, systems containing high amount of water are less understood than systems containing high amount of oil. In petroleum reservoirs, the quantity of water increases as the field matures.

Sloan *et al.* (2011) proposed a model for systems with water as predominant phase. The model is presented in Figure I.18 and it is valid for systems containing oil (gray), gas (light gray) and water (black), with water cut equal or superior to 50%. It can be divided in four steps:

(1) The model considers that the quantity of water is high, making the dispersion of this phase into the oil phase impracticable. Consequently, it is observed the water phase with some entrained oil (bottom) and the oil phase with some entrained water (top).
(2) Hydrates start to form at all possible interfaces, having gas and water available.
(3) Hydrates start to agglomerate in the respective phases due to capillary forces.

(4) Hydrates continue to form, as well as, agglomerate, increasing the system viscosity.

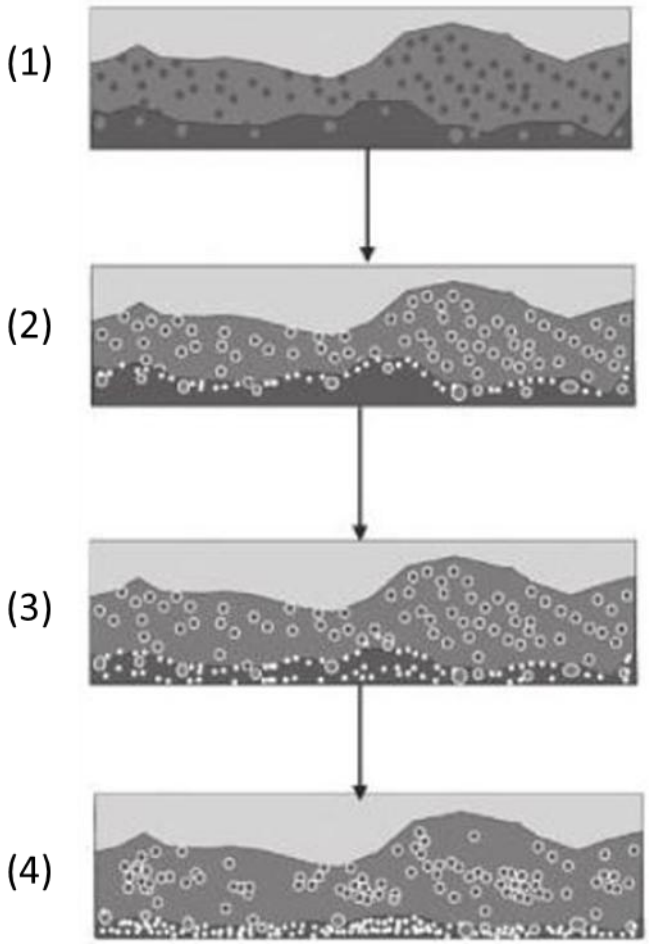

Figure I.18 – Hypothesis of hydrate formation in water dominated systems (Joshi, 2008).

As the authors of the model recognize, this is only a first effort to represent the hydrate formation for water dominant systems. The model neglects some important stages of the process:

- The growth process in the liquid droplets;
- The formation of more complex emulsions instead of two continuous phase;
- The model does not consider the possibility of having single oil continuous phase for systems with high amount of water.
- The agglomeration process is not well-developed, pipeline plug is not proposed.

In conclusion, it is observed that deeper studies of hydrate formation process in flow lines need to be performed to increment the knowledge of this process in systems with water or oil as

predominant phase. This knowledge will be able to support the development of techniques to avoid flow lines plugging.

Actually, there are several ways to avoid flow lines plugging:

(1) Dehydration: water removal;
(2) Thermal insulation, heating: maintain the temperature outside hydrate zone;
(3) Addition of inhibitors:
    a. Thermodynamic Hydrate Inhibitors (THIs);
    b. Low Dosage Hydrate Inhibitors (LDHIs):
        i. Kinetic Hydrate Inhibitors (KHIs);
        ii. Anti-agglomerants (AAs).

Different methods can be combined; but actually, the most common approach to deal with the hydrate formation is the chemical inhibition. The first type of additive to be studied/developed were the thermodynamic hydrate inhibitors (THIs), which act at the hydrate equilibrium conditions, changing it to higher pressures and lower temperatures. The high amount of THIs needed (high cost) to prevent the hydrate formation pushed the researchers to find other ways to handle the problem.

Most recently, in order to decrease the high cost on applying THIs, the researchers focus changed from preventing the hydrate formation to avoiding the pipeline blockage by the use of low dosage hydrate inhibitors (LDHIs) including kinetic hydrate inhibitors (KHIs) and anti-agglomerants (AAs). The first acts by delaying the first steps of the hydrate formation process (nucleation and growth) and the second works by preventing agglomeration.

A deeper discussion on the mechanisms used to deal with the hydrate formation will be presented in sequence.

I.3.3.1 Thermodynamic Hydrate Inhibition

Thermodynamic hydrate inhibition is achieved by injecting inorganic salts (*e.g.*, NaCl, NaOH, $CaCl_2$) or alcohols/glycols (*e.g.*, methanol, monoethylene glycol – mostly used in Oil & Gas industry) during petroleum extraction (Sum *et al.*, 2009). The goal on using a THI is maintaining the system outside the zone of hydrate formation (Figure I.19).

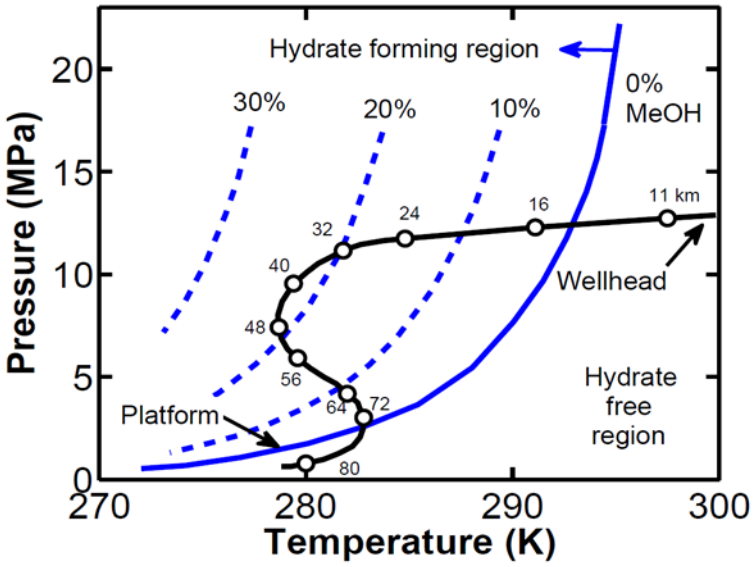

Figure I.19 – Pressure vs. Temperature in a typical subsea flow line in function of the methanol concentration (MeOH) in free water for a given gas mixture. Adapted from Sloan *et al.*, 2011.

The mechanism of inhibition (of glycols/alcohols) arises from the inhibitors chemical structure. For example, in alcohols/glycols, the oxygen atoms naturally attract the neighboring water molecules through hydrogen bond (Sloan *et al.* 2011). The same mechanism of hydrogen bond is required to form hydrates cage (attraction between the water molecules). The competition for hydrogen bond, between the water itself and the water and the inhibitor, prevents the formation of cages by eliminating the participation of water molecules in the hydrate structure, preventing hydrate formation. This is a time independent mechanism.

As consequence of the aforementioned mechanism, the hydrate equilibrium temperature is decreased and the hydrate equilibrium pressure is increased, shifting the hydrate equilibrium curve (Figure I.19). The quantity of THI used is calculated from the quantity of water in the reservoir (in wt. %). From Figure I.19, the amount of methanol (MeOH) needed to avoid hydrate formation increases by following the operatory conditions way (black line in Figure I.19). In some flow lines (Sloan et al., 2011), with higher water fraction, the required quantity of THI achieves values as high as 60 wt. %. This large amount represents high operational cost, one of the motivations to develop new kinds of additive.

The mechanism of inorganic salts inhibition is not exactly the same one observed with the use of alcohols/glycols. The inorganic salt ionizes the solution, interacting with the dipoles of water

molecules, in much stronger way that water molecules interact between themselves. Thus, similarly with what happens in the hydrate inhibition mechanism using alcohols and glycols, the hydrates cage will be prevented of forming, preventing the hydrate formation. A secondary effect observed with the use of inorganic salts for hydrate inhibition is the decrease of the solubilization of the potential *guest* molecule in the water phase (Sloan & Koh, 2007).

I.3.3.2 Kinetic Hydrate Inhibition

Poly(vinyl pirrolidone) (PVP) and poly(vinyl caprolactam) (PVCap) are examples of successful kinetic hydrate inhibitors (KHIs). In general, KHIs are low-molecular-weight polymers or co-polymers dissolved in a carrier solvent. KHIs are used in low dosage (calculated from the water fraction) and injected in the water phase. The use of KHIs has the advantages of not disturbing the dispersion flow and not requiring a recovery system (necessary with THIs). The goal on using KHIs is to delay nucleation and growth steps, avoiding blockage (Sloan *et al.*, 2011).

The principle of polymers and co-polymers kinetic inhibition also arises from its chemical structure. The KHIs adsorb on the hydrate surface: polymers and co-polymers have a pendant group that will work as a “pseudo-guest” into a hydrate cage (Sloan *et al.*, 2011). By this way, the polymers will be anchored in the hydrates surface, making a barrier for hydrate growth and nucleation. This is a time dependent process, because the additive needs to be effective during fluids transport in the flow line. The process effectiveness also depends on the degree of subcooling provided to the system.

In fact, KHIs molecular mechanism is not entirely understood, limiting its effective application in every kind of system (Sun *et al.*, 2009). There are several issues related to the appliance of KHIs: operational cost, environmental impact, performance in limit conditions, among others (Kelland, 2000). However, they represent a great advance when comparing to THIs, once they are used as successful hydrate inhibitors in some fields (with concentration as low as 1 wt. %).

I.3.2.3 Anti-Agglomeration

Anti-agglomerants (AAs, or dispersant additives) are long molecules (surfactants) characterized by their double chemical affinity for polar (hydrophilic group: water-soluble) and non-polar (lipophilic group: oil-soluble) substances (Figure I.20). The longer is each group chain, the higher is the surfactant tendency to solubilize in the respective phase (oil or water).

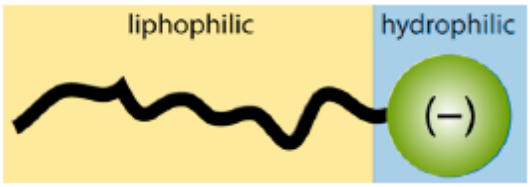

Figure I.20 – Scheme of a surfactant molecule. From Zerpa, 2013.

The characteristics of a system can be changed due to the use of surfactants, which have properties able to decrease the surface/interfacial tension, modify the contact angle between oil and water phases, modify the solid surface wettability, among other influences (Shah, 1977). Concerning hydrate formation, surfactants can promote it by increasing the gas solubility in the water phase and increasing the interfacial area for hydrate formation. They can also avoid hydrate agglomeration by keeping the formed hydrates dispersed in the oil phase. Dispersed hydrates can flow in a pipeline without blocking it until a liquid loading (percentage of hydrate volume regarding the total volume) of 50% (Sloan *et al.*, 2011).

In order to understand the anti-agglomeration mechanism, it is necessary to understand the agglomeration process. Actually, there are two mechanisms that can explain why anti-agglomerants avoid hydrates to stick together:

(1) The surfactant forms a special kind of emulsion with small droplets of water dispersed in the oil phase. These droplets will fully convert into small hydrates, which will circulate, as dry particles, dispersed in the oil phase without aggregation due to the anti-agglomerant (Kelland, 2014).

(2) The surfactant will attach to the hydrate surface from a “hydrate-philic” head group; the other group of the surfactant is lipophilic. If surfactant continues to attach to the hydrate surface, the hydrate crystal will become hydrophobic (or oil-wet), and then kept dispersed in the liquid hydrocarbon phase. From this method, there is no need on forming a well dispersed water-in-oil emulsion (Kelland, 2014).

It is important to mention that some crude oils naturally have chemical substances acting like artificial anti-agglomerants, thus, avoiding flow line plugging (Sloan *et al.*, 2011).

As for the others inhibitors, anti-agglomerant dosage is based on the water amount in the reservoir. Successful application of anti-agglomerant in dosage until 1 wt. % has been registered in

literature. The use of AAs in offshore fields is becoming more common nowadays. Before, they have been successfully used in start-up wells (Kelland, 2014).

The anti-agglomerant study, as the kinetic hydrate inhibitor study, is very recent and not completely understood. There is a lack of information in literature about the anti-agglomerant mechanism in systems with high amount of water, providing a new scope for futures researches.

The goal of using additives in petroleum flow lines can be resumed by Figure I.21. In systems where no inhibitors are used, hydrates will likely form and plug is highly possible (1). If thermodynamic inhibitors are added in the system, hydrate formation will be avoided (2), but sometimes this represents high costs regarding the entire process. If kinetic inhibitors are used, no hydrate formation is guaranteed for a short time (3), but for longer time hydrates can form and plug the flow line (3). The limited time of the kinetic inhibitor effectiveness represent an operational risk, beyond other limitations that the use of KHIs imposes (*e.g.*, subcooling). If anti-agglomerants are used, hydrates are supposed to keep dispersed in the liquid phase (4) without plug, still, this effect is not guaranteed for systems with large water amount.

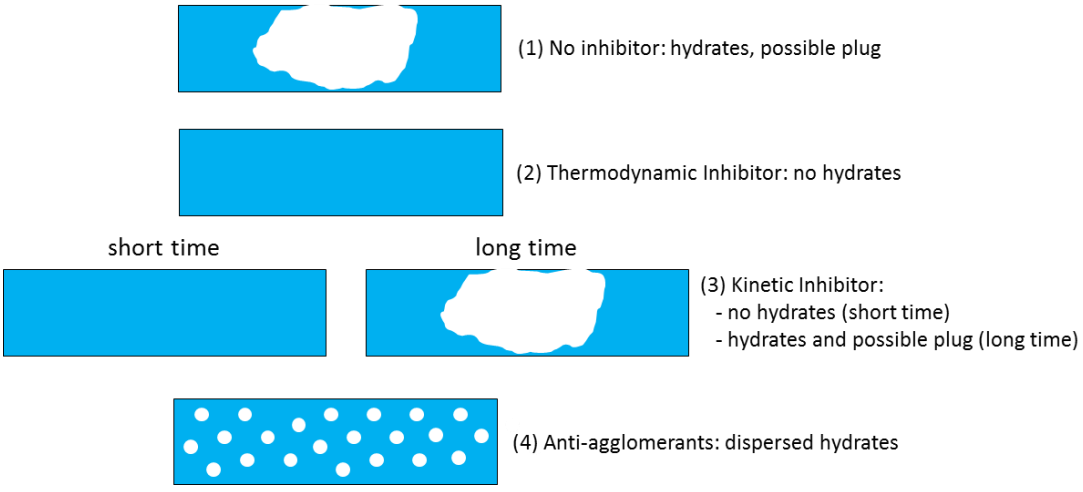

Figure I.21 – Scheme summarizing the effect of the different inhibitors. Modified from Frostman, 2000.

I.4 Chapter Highlights in French – Aperçu du Chapitre I

La recherche dans un domaine précis passe tout d'abord par l'étude des concepts scientifiques spécifiques du domaine étudié. Le premier chapitre était un aperçu sur les connaissances nécessaires pour la compréhension du processus de formation d'hydrates dans une conduite pétrolière.

Tout d'abord (§I.1), il a été introduite une discussion à propos des dispersions en allant des concepts de base jusqu'à la rhéologie (l'étude de la déformation et l'écoulement du système sous l'influence d'une force appliquée). Les dispersions étudiées sont :

1. Emulsions : mélange de liquides non miscibles (une phase aqueuse et une phase hydrocarbure), formée par gouttelettes (phase dispersée / interne) dispersées dans une phase continue / externe. Lorsque la phase aqueuse est la phase continue, le mélange est appelé huile-dans-eau (H / E), également connue comme émulsion directe. Au contraire, si l'huile est la phase continue, le mélange est appelé émulsion eau-dans-huile (E / H) ou émulsion inverse.
2. Suspensions : mélange d'une phase solide dans une phase liquide, dans laquelle la phase solide est insoluble dans le liquide. Habituellement, la suspension est formée par la dispersion du solide (phase dispersée / interne) dans le liquide (phase continue / externe) par un processus d'agitation mécanique. Les particules en suspension ont généralement un diamètre supérieur à 0,2 µm avec une limite supérieure comprise entre 50 µm et 100 µm.

Postérieurement, dans la section § I.2, des notions sur les hydrates ont été présentées. Cette section a comporté une révision bibliographique sur la structure et les propriétés des hydrates, chaque étape de leur processus de formation, leur thermodynamique surtout celle de l'hydrate de méthane, lequel sera étudié pendant ce travail de recherche.

Les hydrates sont des composés cristallins (avec une structure similaire à la glace) formés par une ou plusieurs molécules « invitées » (liquide ou gaz) piégées à l'intérieur du réseau cristallin formé par les molécules « hôte ». Les molécules hôte sont les molécules d'eau liées par des ponts d'hydrogène. La molécule « invitée » stabilise la structure en se liant aux molécules d'eau à travers des forces de van der Waals.

Les hydrates peuvent être formés seulement dans des conditions appropriées de pression, température et concentration de ses composants.

Les hydrates de gaz éveillent l'intérêt de l'industrie et de la recherche scientifique, notamment dans ce qui concerne le maintiens de l'écoulement en lignes de transport de gaz et d'huile, pour le transport et le stockage de gaz, les hydrates sédimentaires, la réfrigération, le dessalement et la purification de l'eau, parmi d'autres (Eslamimanesh *et al.*, 2012).

Les hydrates de gaz sont formés par un processus de cristallisation. Dans la cristallisation, des conditions thermodynamiques sont créés pour permettre aux molécules de s'approcher et de se regrouper dans des structures hautement organisées (cristaux). Le processus de cristallisation, dont le processus de formation des hydrates, est divisé en : (1) nucléation, (2) croissance, (3) agrégation (agglomération) et (4) dissociation. Ces quatre étapes sont dépendantes du temps, ce qui augmente la difficulté de la compréhension de ces phénomènes. La force motrice de la cristallisation est appelée sursaturation.

Les propriétés d'équilibre de phases concernant les hydrates de gaz peuvent être définies et facilement évaluées par diagrammes de phases (pression en fonction de la température à composition fixe), par méthodes approximatives (corrélations) ou de façon plus complexe par le développement de modèles d'équilibre de phases. Le concept d'équilibre de phases est lié à l'existence simultanée de différentes phases de la même structure moléculaire dans le même système, sans aucune intervention externe.

L'hydrate de méthane est communément connu par sa célèbre image de la « glace qui brûle ». Il est formé par molécules de gaz méthane (CH_4) piégées par les molécules d'eau. L'hydrate de méthane peut être trouvé dans la nature dans les sédiments, ce qui pourrait être une future source d'énergie. En ce qui concerne l'assurance des lignes d'écoulement dans l'industrie, les hydrates de méthane sont responsables d'endommagement des lignes de production pétrolière par la formation de gros agglomérats ou de bouchons.

Enfin, dans la section § I.3, le champ principal de cette recherche a été introduit : la formation d'hydrates dans les conduites d'écoulement et les moyens pour faire face à cet événement. La ligne d'écoulement est utilisée lors de l'extraction de pétrole pour le transport de la dispersion de pétrole à partir de la tête de puits jusqu'à l'unité de traitement. La formation d'hydrates dans les conduites d'écoulement a été identifiée d'abord par Hammerschmidt (1934), et dans les cas extrêmes, elle peut

conduire au bouchage des lignes et, par conséquence, à l'interruption de l'extraction du pétrole, en conduisant à d'importantes pertes financières.

Le processus de formation d'hydrates de gaz n'est pas entièrement maitrisé et est très sensible aux conditions du système (par exemple, fraction d'eau). Quelques modèles topologiques essaient d'expliquer ce processus (Sloan *et al.*, 2011). En général, les modèles topologiques de formation d'hydrates à partir de mélanges de pétrole, d'eau et de gaz peuvent être séparées en trois conditions distinctes : (1) l'huile est la phase externe prédominante, (2) l'eau est la phase externe prédominante et (3) le gaz est la phase prédominante. Pour les deux premières conditions, un facteur important pour le processus est la présence de la phase gazeuse libre, qui augmente la surface de contact entre les phases gazeuse et liquide, qui peut faciliter la formation d'hydrates.

En fait, il y a plusieurs façons d'éviter le bouchage des lignes d'écoulement :

(1) La déshydratation : élimination de l'eau ;
(2) L'isolation thermique, chauffage : maintiens de la température en dehors de la zone de formation d'hydrate ;
(3) L'addition d'inhibiteurs :
    a. Inhibiteur thermodynamique d'hydrates (THI) ;
    b. Inhibiteur d'hydrates à faible dosage (LDHI) :
        i. Inhibiteur cinétique d'hydrates (KHIs) ;
        ii. Anti-agglomérants (AAs).

Différentes méthodes peuvent être combinées pour manager la formation d'hydrates, mais l'approche la plus commune pour faire face à la formation d'hydrates est l'addition d'inhibiteurs. Quand les inhibiteurs ne sont pas utilisés, les hydrates vont se former et très probablement agglomérer pour finir par boucher le système. L'utilisation d'inhibiteurs thermodynamiques représente des coûts trop élevés car leur proportion dans le volume total peut aller de 30 % à 60%. Les inhibiteurs cinétiques qui bloquent les vitesses de formation pendant une courte période, peuvent se montrer inefficaces pour de longues périodes non maitrisées (arrêt de production par exemple), pendant lesquelles les hydrates peuvent se former et boucher la conduite. L'efficacité limitée par le temps de l'inhibiteur cinétique représente un risque opérationnel, au-delà d'autres limitations que l'utilisation de ce type d'additif impose (par exemple, le sous-refroidissement). Par contre si des anti-agglomérants sont utilisés, les hydrates sont censés rester dispersées dans la phase

liquide sans bouchage. Cependant cet effet n'est pas garanti pour les systèmes avec une quantité d'eau importante.

Chapter II – Materials and Methods

"If you don't know, the thing to do is not to get scared, but to learn." (Ayn Rand)

Studies of hydrate formation in flow lines from oil emulsion structures require more complex systems than the ones investigated in reactors or pressurized cells. The use of an experimental pilot plant (flow loop) is a major asset to reproduce the conditions found in flow lines during petroleum extraction.

The study of methane hydrate formation developed in this thesis was performed in a flow loop (presented in § II.1) from shear stabilized emulsions formed by water and Kerdane® (C11 – C14), without and with anti-agglomerant. The materials used in the experiments are presented in § II.2 and the experimental protocol is presented in § II.3.

II.1 Experimental Apparatus

The so-called *Archimède* flow loop was the experimental apparatus (Figure II.1) used in this work. It was constructed during the PhD thesis of Fidel-Dufour (2004) to study transport and aggregation of methane hydrates. The apparatus is able to work in similar conditions to the ones found during the flow of deep-sea petroleum extraction (*i.e.*, high pressure and low temperature) which are the thermodynamic conditions for hydrates formation.

The flow loop consists in a horizontal section downsloping (Figure II.2) of 36.12 m with 1.02 cm of internal diameter, a riser pipe of 10 m directed towards the gas separator and a descending pipe of 10 m directed to the horizontal section. The vertical section (Figure II.2) has an internal diameter of 1.73 cm. The horizontal section coils around itself in three different levels, with 6 m length, 3 m width and 2 m height. The flow loop liquid volume capacity is 11.5L; the total volume is 15L when accounting the gas separator. The curves connecting the pipes were designed in order to not disturb the flow, for example with large diameter curvature elbows.

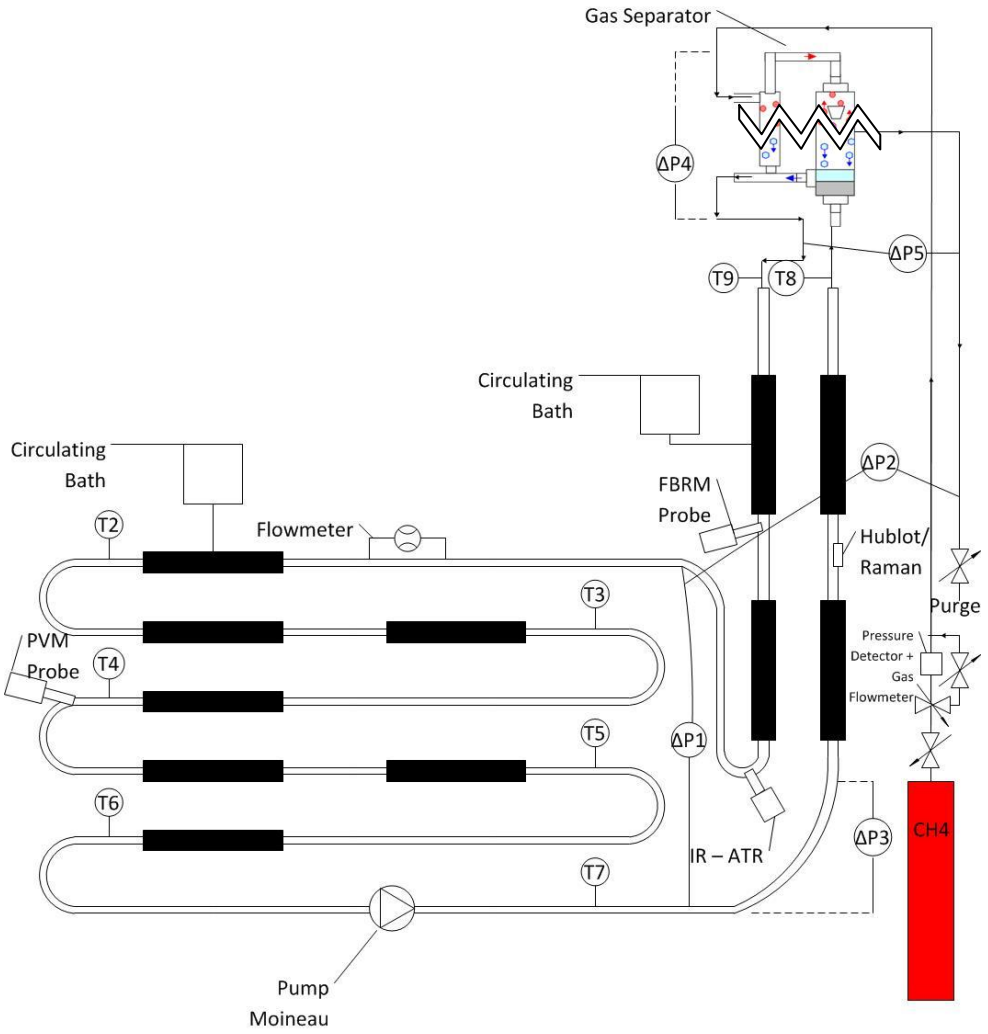

Figure II.1 – Flow loop scheme.

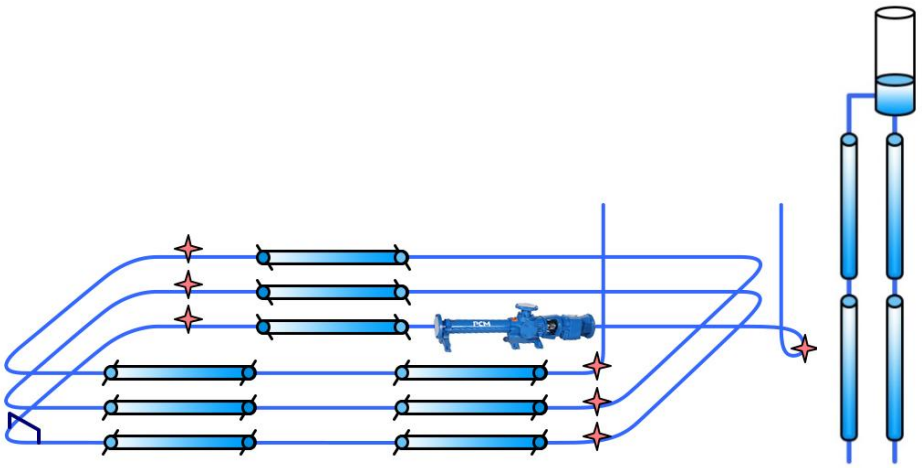

Figure II.2 – Horizontal and vertical sections.

Since 2004, some devices were added in order to improve the accuracy of the hydrate formation study performed with the flow loop. The actual flow loop set up is equipped with several instruments working to keep constant flow rate (100 to 500 $L.h^{-1}$, operational velocity: 0 to 1.7 $m.s^{-1}$), pressure (0 to 100 bar) and temperature (0 to 10°C). In addition, improvements on the monitoring system were also implemented. They work to follow the temperature, the pressure drop, the density (and flow rate), the shape and size of the droplets and hydrates and the gas consumption. These instruments will be presented in the next section (§ II.1.1).

II.1.1 Instruments

II.1.1.1 Moineau® Pump – Progressive Cavity Pump

The *Archimède* flow loop is equipped with a Moineau® pump type MR 6I20 S (Figure II.3) provided by *PCM pompes*. The Moineau® pump is a sort of progressive cavity pump, consisted of a helical rotor turning inside a helical stator (PCM Instruction Manual). The rotational movement generates an axial displacement of the closed cells, transferring the product from the intake to the discharge without smashing the crystal (PCM® Instruction Manual). This is a very important factor considering the actual interest on evaluating the hydrate formation, once the particles, aggregates and agglomerates of hydrates are not destroyed by the pump.

The Moineau® pump (Figure II.3) feeds the flow loop with the prepared liquid mixture and allows keeping constant flow rate throughout the experiment. The pump installed in the flow loop allows flow rate up to $500L.h^{-1}$, working temperature until 20°C and pressure until 105 bar, with a maximum pressure drop of 10 bar.

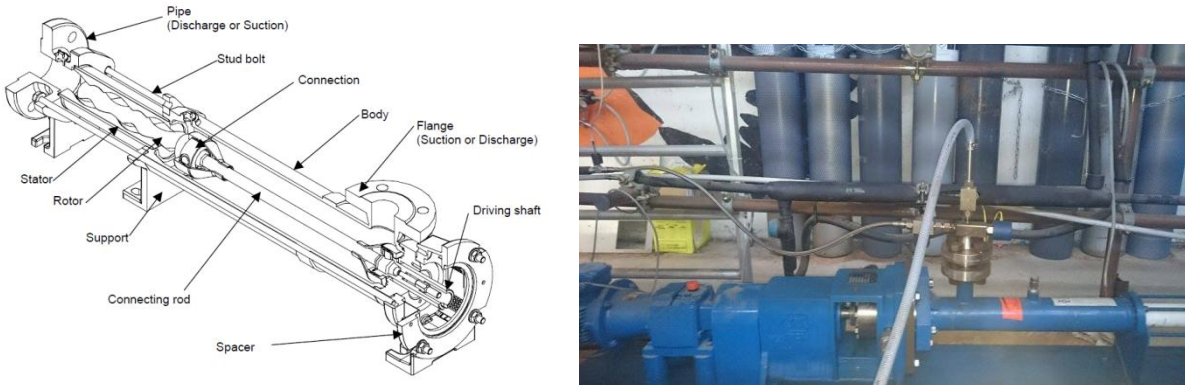

Figure II.3 – Moineau® pump (PCM Instruction Manual).

II.1.1.2 System of Pressure Injection and Control

The methane gas is injected in the flow loop at the top of the riser section, into the gas separator (see Figure II.1 and Figure II.2). Gas is solubilized into the mixture in the separator, where the mixture arriving from the riser under a geyser shape rains down in the pipe parallel to the riser. Through the bottom section of the separator the liquid phase with or without solid goes into the flow loop without gas phase, by gravity effect. In the top of the separator, there is a pressure sensor (provided by KELLER®) measuring the relative pressure inside the flow loop system.

The gas separator (Figure II.4) has 5.1 cm of external diameter and 2.2 m of height, it receives the mixture from the flow loop directly from the riser, placed inside the separator until a height of 1.5 m. When the mixture arrives to the separator as a geyser shape, it collides with a Teflon piece (Figure II.4 (a)) that breaks the liquid jet, increasing the contact surface between liquid and gas phases. The gas separator is connected to a second separator (Figure II.4 (a)) with smaller external diameter (0.6 cm) aiming to recuperate any residual droplet of liquid or gas. Both separators are connected with the descending pipe that sends the liquid, charged with gas, back to the flow loop.

(a) (b)

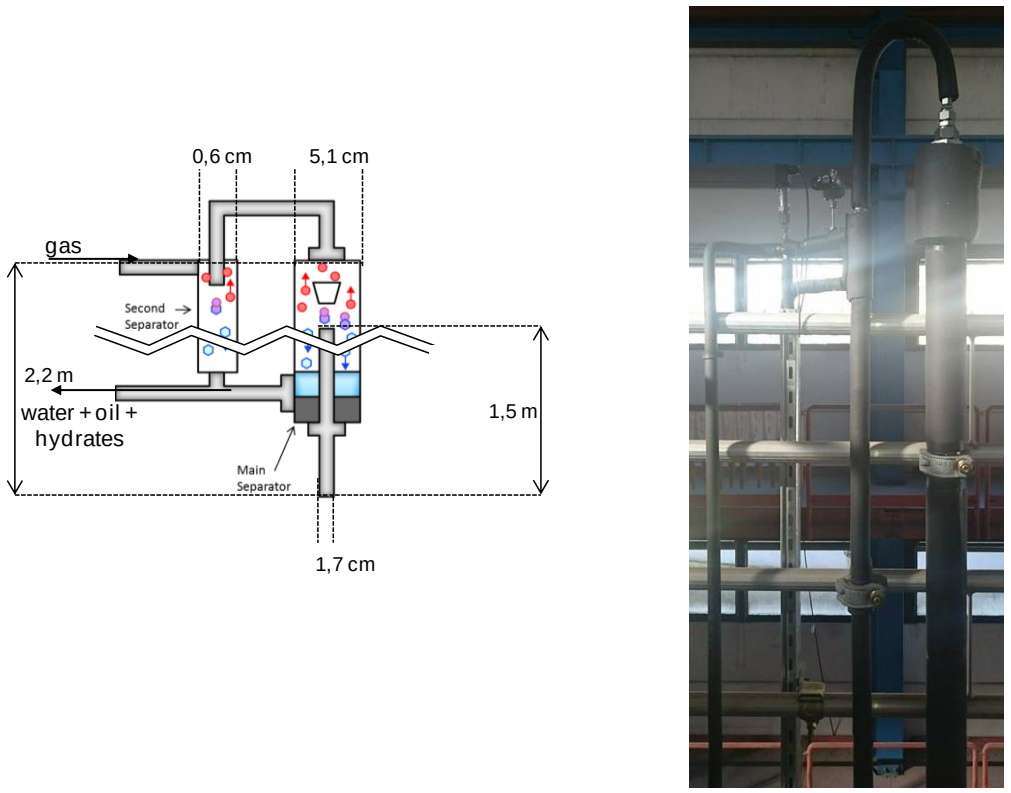

Figure II.4 – Gas separator (a) scheme (red circle: gas; blue hexagon: water) and (b) installed at the flow loop.

The relative pressure is maintained constant by the pressure controller (Figure II.5), provided by Brooks®, that compensates the pressure decrease by injecting gas at the top of the separator. Pressure controller comprises a valve that opens/closes automatically when a difference between measured pressure and set point (80 bar) is detected. The valve is designed to support the maximum pressure of 100 bar. The injected gas flow rate is recorded what makes possible solving the mass balance in order to calculate the conversion of water into hydrates. Gas flow rate is recorded in normal liter per minute ($ln.min^{-1}$), meaning that the measurement is given for normal conditions (0°C and 1.013 bar).

The pressure controller set-up (Figure II.5) is bypassed to allow gas injection by another valve without automatic control. When the pressure controller system is used; this valve shall remain closed during the operation; if not, the valve keeps opened and injection is manually controlled.

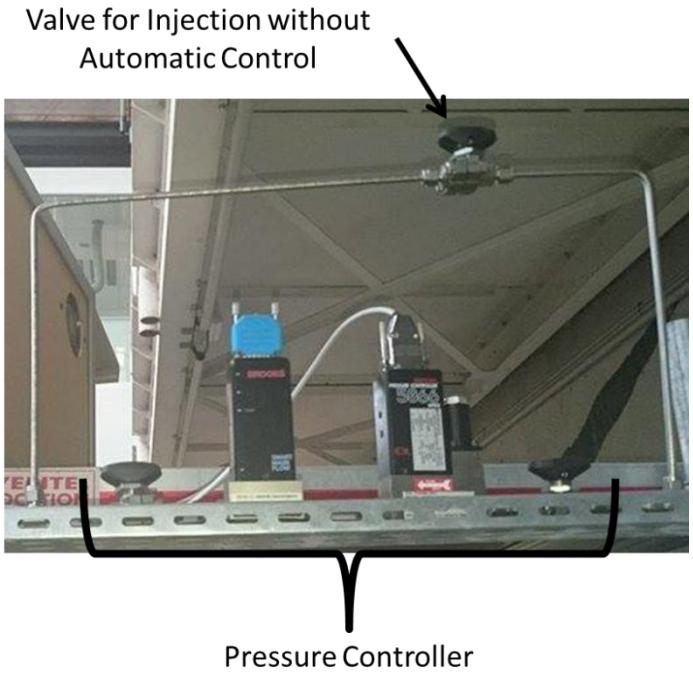

Figure II.5 – Pressure Controller System.

II.1.1.3 System of Temperature Control

Temperature is controlled by a cooling system composed by two circulating baths (one for the horizontal section and other for the vertical section), provided by Huber® (Model CC 250, polystat CC 1), which send a refrigerated fluid (mixture of water and ethanol) to the heat exchanger pipe. This pipe is concentric with different sections of the flow loop pipelines (in black in Figure II.1 and detailed

in Figure II.6). In order to prevent heat losses, the entire flow loop, including the heat exchangers, is jacketed with an insulating material.

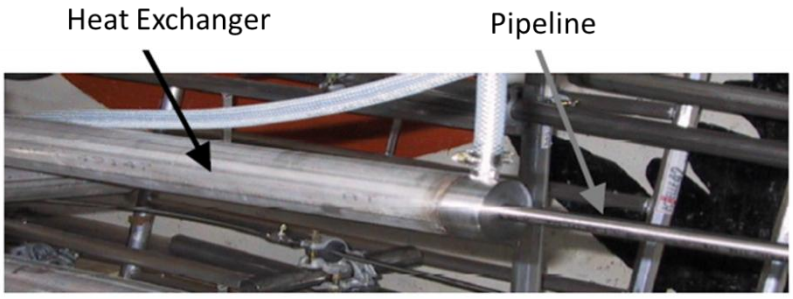

Figure II.6 – Heat exchanger.

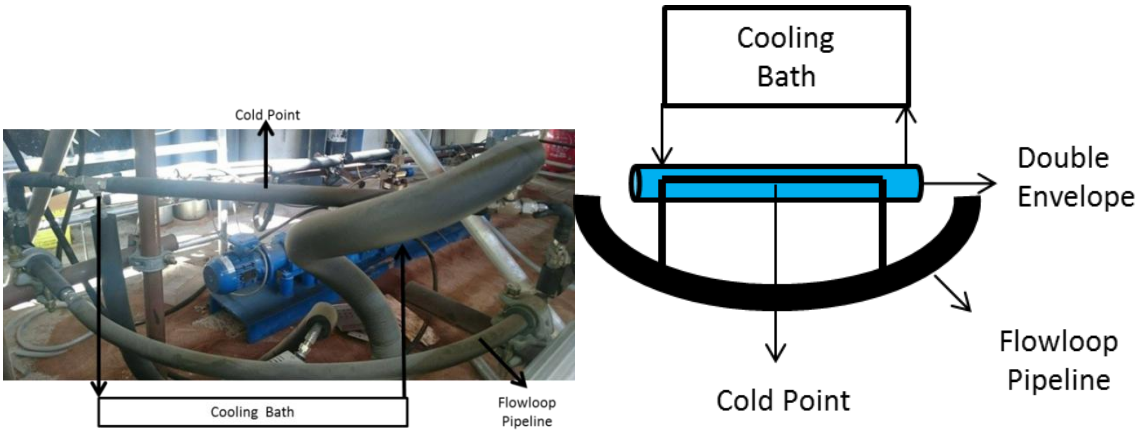

Figure II.7 – *Cold point* device.

A third and smaller cooling bath, also provided by Huber® (Model ministat) is used to refrigerate the *cold point* (Figure II.7). Ethanol is used as refrigerated fluid in this bath. The *cold point* (or crystallizer) is a section consisting of a small heat exchanger around a pipe (1.10 m long with 0.635 cm of external diameter). This pipe bypasses the second floor of the horizontal section. The goal on using the *cold point* is to accelerate the crystallization beginning by forming ice and adding it to the flow loop mixture. Thus, the third circulating bath is set in lower temperature (until -25°C) than the one set for the two others circulating baths. The flow rate in this spot is negligible to produce temperature decrease in the entire flow loop. There is the possibility of blocking the *cold point* due to the lower temperature applied. However, this does not represent risk, once this line is blocked, the mixture can normally circulate in the principal flow loop line.

II.1.1.4 Temperature Probes

Throughout the experiments, temperature of the mixture is monitored by a set of temperature probes (type PT100) distributed over the entire length of the flow loop (see Figure II.1). The room temperature is also recorded by a temperature probe installed outside the system.

II.1.1.5 Pressure Drop Probes

The flow loop is equipped with five differential pressure sensors (sensor-transmitter piezoresistive type, provided by KELLER®). The sensors can measure from 0 to 10 bar with a minimum span of 0.10 bar. Figure II.8 shows the location of each sensor relating it to the distance (h) which each differential pressure measurement is performed. Knowledge about this distance allows establishment of the pressure balance, as shown by Fidel-Dufour (2004).

Each pressure drop present in Figure II.8 is explained as follows: pressure drop by flow in the entire horizontal section is given by ΔP_1, pressure drop between the descending pipe and the gas phase (in the separator) is given by ΔP_2, pressure drop between the beginning and the end of one loop of the horizontal section is given by ΔP_3, pressure drop at the separator is given by ΔP_4 and pressure drop between the riser and the gas phase (in the separator) is given by ΔP_5.

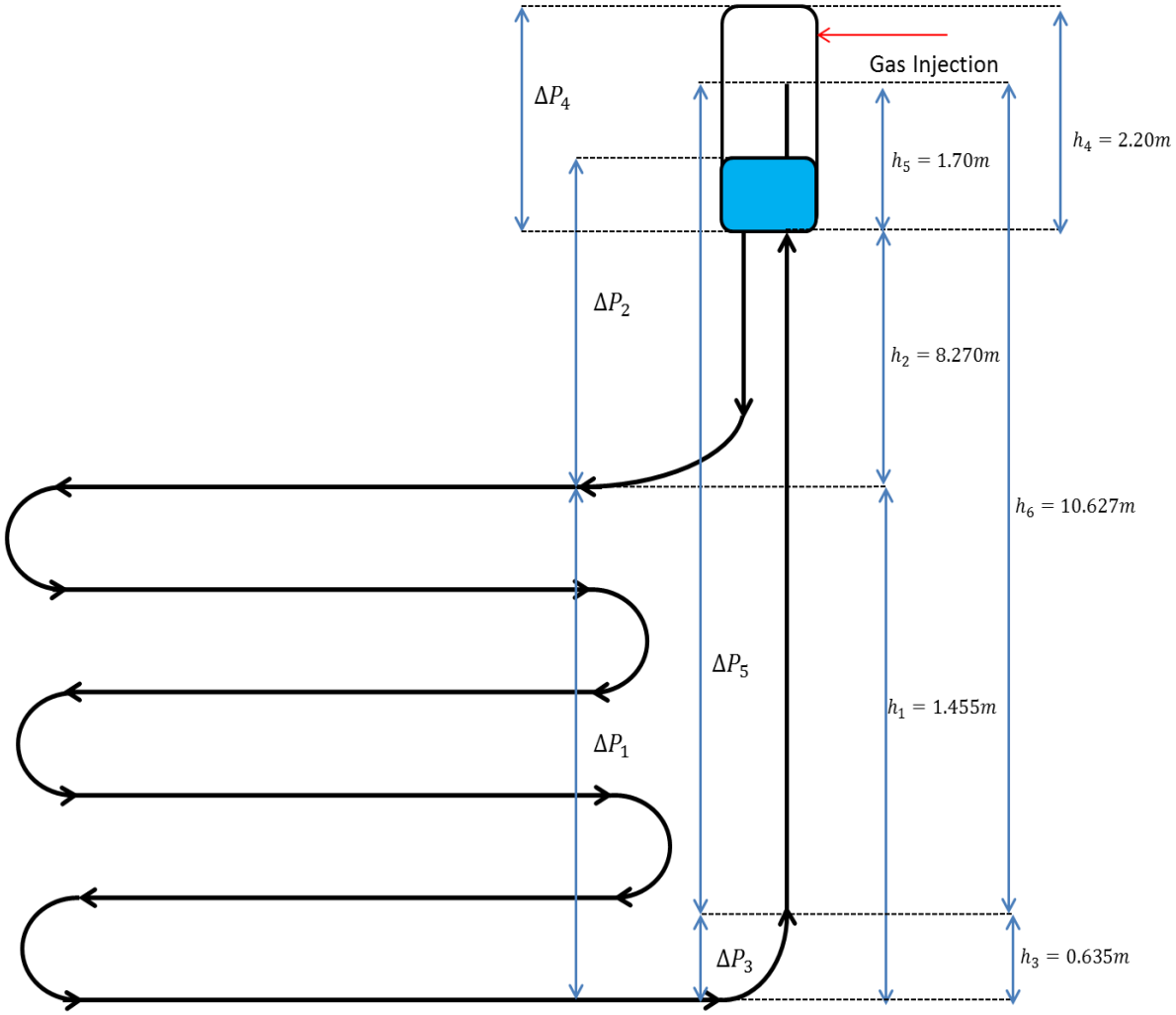

Figure II.8 – Differential pressure sensors disposition at the flow loop.

II.1.1.6 Flowmeter and Densimeter

A mass flowmeter with densimeter (provided by MICRO MOTION®) is installed in the descending pipe, before the connection with the horizontal section. It measures the flow rate and the density of the mixture and operates until 100 bar. The accuracy and repeatability of the measurements on liquids and slurries is provided in Table II.1 (Micromotion® Instruction Catalogue) for a test with water at 20 to 25°C and 1 to 2 bar.

Table II.1 - Accuracy and repeatability of the measurements on liquids and slurries (Micromotion® Instruction Catalogue).

Performance Specification	Calibration code Y	Calibration code A
Mass Flow Accuracy[(1)]	$\pm$ 0.5% of rate	$\pm$ 0.4% of rate
Volume Flow Accuracy[(1)]	$\pm$ 0.5% of rate[(2)]	
Mass Flow Repeatability	$\pm$ 0.25% of rate	$\pm$ 0.2% of rate
Volume Flow Repeatability	$\pm$ 0.25% of rate	
Density Accuracy	$\pm$ 0.01 g. cm^{-3} ($\pm$10.0 kg. m^{-3})	$\pm$ 0.003 g. cm^{-3} ($\pm$3.0 kg. m^{-3})
Density Repeatability	$\pm$ 0.005 g. cm^{-3} ($\pm$5.0 kg. m^{-3})	$\pm$ 0.0015 g. cm^{-3} ($\pm$1.5 kg. m^{-3})

[(1)]Stated flow accuracy includes the combined effects of repeatability, linearity, and hysteresis.
[(2)]Valid at calibration conditions.

The flow rate is measured by *Coriolis Effect*. Tubes measuring the flow rate (which the fluid passes through) are forced to oscillate what produces a sine wave (Figure II.9). Without flow the waves are in phase, with flow the phases shift as the tubes twist due to Coriolis forces. Time difference between the waves is measured and it is proportional to the flow rate (Micromotion® Instruction Catalogue).

The density measurement is consequence of change in the natural frequency of the measuring tubes; as the mass of fluid passing inside the tubes changes, a corresponding change is observed in the frequency, which can be used to calculate the density.

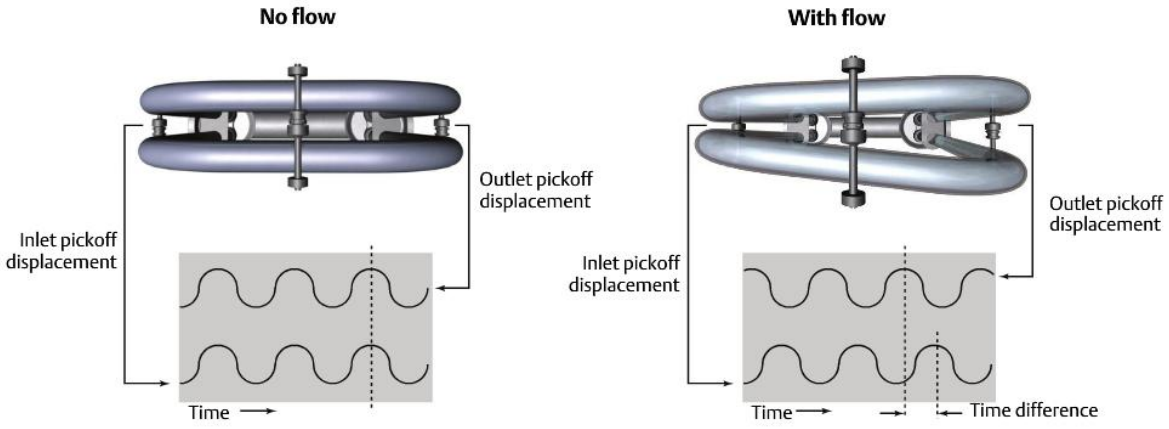

Figure II.9 – Flowmeter measuring tubes (Micromotion® Instruction Catalogue).

II.1.1.7 Focus Beam Reflectance Measurement – FBRM

Focused Beam Reflectance Measurements (FBRM) is an in-situ particle analyzer provided by Mettler-Toledo Lasentec®. It consists of infrared laser with wavelength of 785 nm which can switch its scan speed from 2 to 8 $m.s^{-1}$ (here 2 $m.s^{-1}$). The FBRM probe (D600 type L) is installed at the descending pipe of the flow loop (forming an angle of 45° with it - Figure II.1). The interval between each chord length distribution measurement can be set manually (here 5 seconds). The laser is transmitted through optical fiber to the probe. Rotating optical lens emit the laser at the probe tip (Figure II.10 (a)). Facing an emulsion or a suspension, the emitted laser scans across the particle system in a circular path (with 2 cm of diameter and focal point at 2 mm). When laser encounters the surface of a particle/droplet (the particles linear speed is inferior to the laser speed), it is reflected and detected by the probe as a pulse, measured from an edge of the particle until the opposite one (Figure II.10 (b)). Determination of the chord length is obtained by the product of each pulse duration (measured by the probe) and laser scan speed. Thousands of chords are detected at each measurement and grouped in a chord length distribution for each corresponding time.

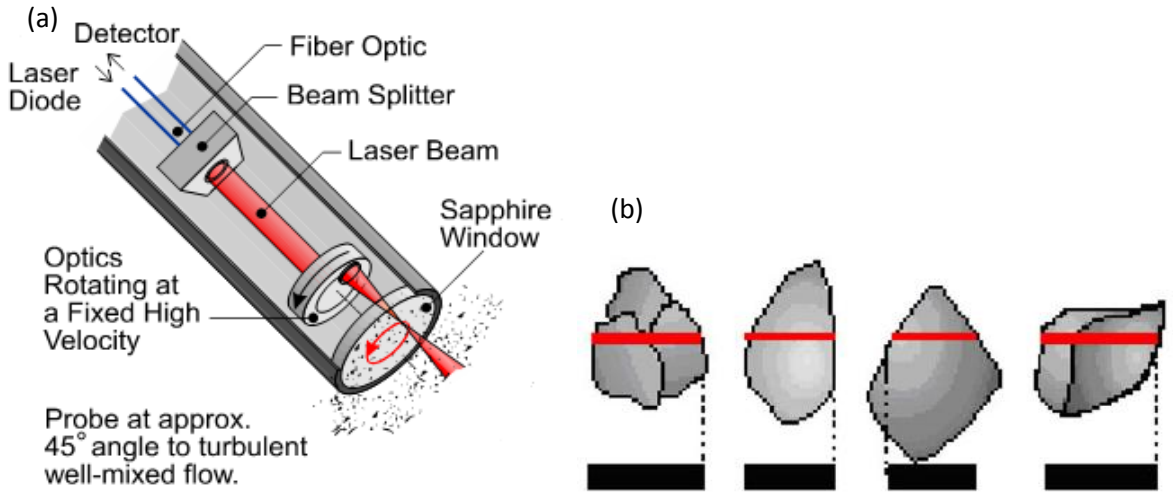

Figure II.10 – (a) FBRM probe description and (b) examples of chords detection (from FBRM Lasentec® Manual).

Figure II.11 shows examples of chord length distribution signal (the detected chord length is in log scale) during three steps of hydrate crystallization experiment: (1) emulsion - before hydrate formation, (2) suspension – beginning of the hydrate formation and (3) suspension - at the end of the experiment, before dissociation. The FBRM probe detection range varies between 0.5 µm and 3000 µm. In fact, it is important to notice that the FBRM measures chord lengths instead of single

diameters. For example, a population of monodisperse and spherical particles of diameter D will give a distribution of chord length between 0 and D.

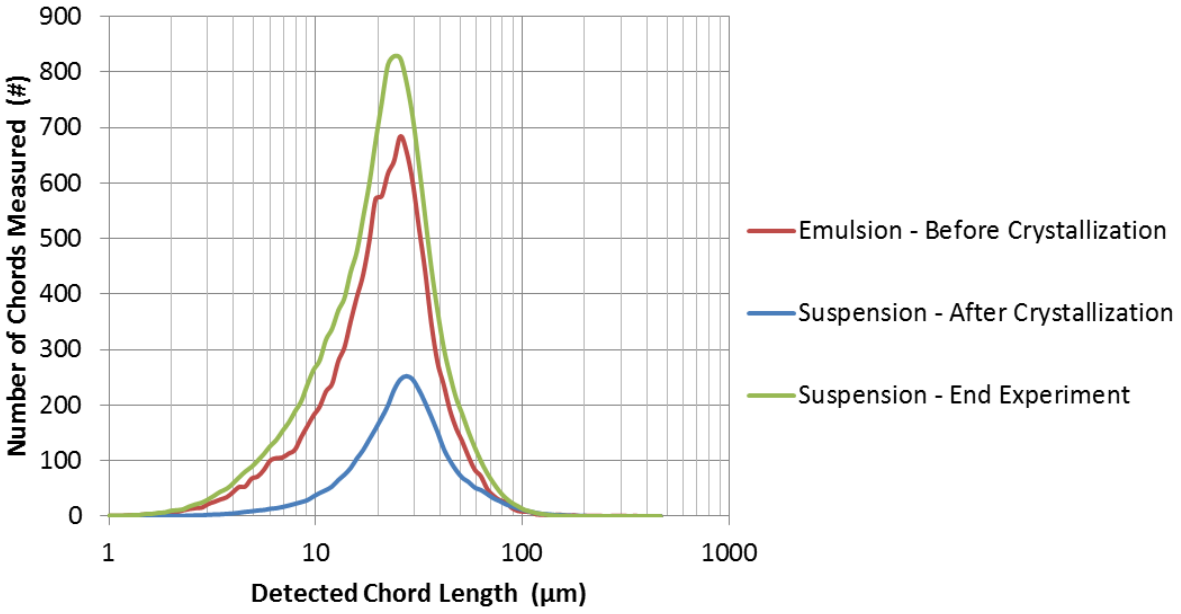

Figure II.11 – Example of Chord Length Distribution (70% water cut, 400L.h^{-1}, without additive)

Another important remark, as proposed by Le Ba (2009), is that the measured chord lengths are inferior to the real chord length probably due to: (1) particles transparency, (2) little optical contrast between the solution and the particles and (3) irregular particle geometry. Relating to the particles characteristics, Turner *et al.* (2005) performed hydrate formation experiments from water-in-oil emulsion and showed that the number of particles detected by the FBRM depends on the particles reflection: the more reflective is the particle, the more particles will be detected.

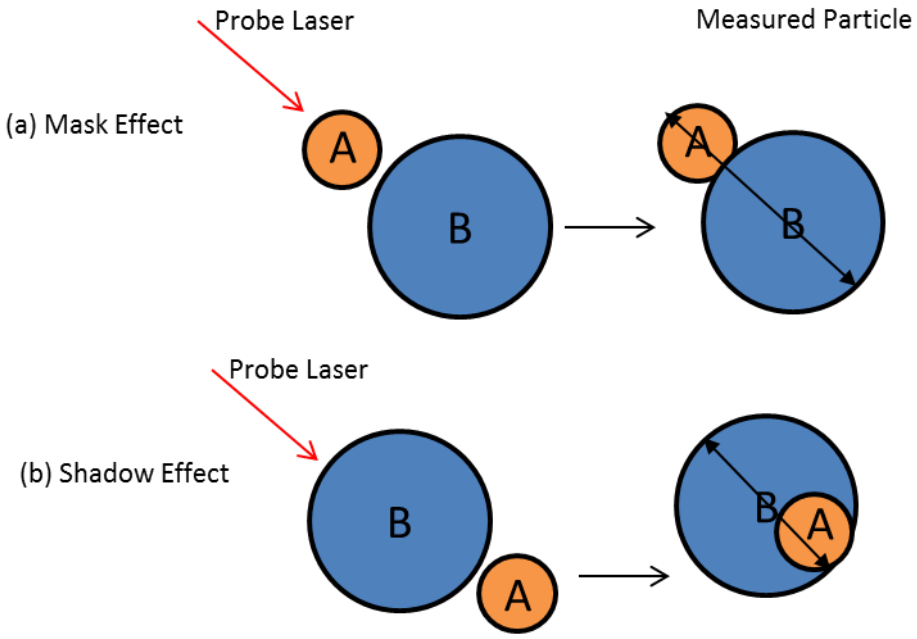

Figure II.12 – Mask and Shadow effect.

Another effect observed throughout measurements using FBRM probe (mainly in concentrated solutions) is the mask and the shadow effect (Le Ba, 2009). The mask effect (Figure II.12 (a)) is related to the particles superposition, when a smaller particle (A) is placed in front of and very close to another larger particle (B). As consequence, the probe will measure a single particle. The shadow effect (Figure II.12 (b)) happens when a larger particle (B) overshadow a smaller particle (A). As consequence, the probe measure only the size related to the larger particle.

II.1.1.8 Particle Video Measurement – PVM

Particle Video Microscope (PVM) is an in-situ particle analyzer also provided by Mettler-Toledo Lasentec®. It (Figure II.13) consists of six independent lasers illuminating a fixed area in front of the probe face, a camera that records the digital images passing in front of the probe face and objective lens allowing adjusting the image focus.

The PVM probe is installed at the second loop of the horizontal section (forming an angle of 45° with it). In all cases, the instrument was set to save one image each 40 seconds (+/- 15), giving images of 1050 x 800 µm (Figure II.14).

Figure II.14 shows images from a hydrate crystallization experiment, the recorded images show the shape and the size of droplets and hydrate particles. Oil or water droplets present well-rounded

shape with clear surface on which is possible to see six laser reflections (Figure II.14 (a)). During hydrate formation, texture of the droplet surface changes and shape becomes irregular. At hydrate formation beginning, reflection of six laser beams is still observed (partially converted droplets), but becomes null after deep conversion (Figure II.14 (b)). The color of hydrates is whiter than the liquid.

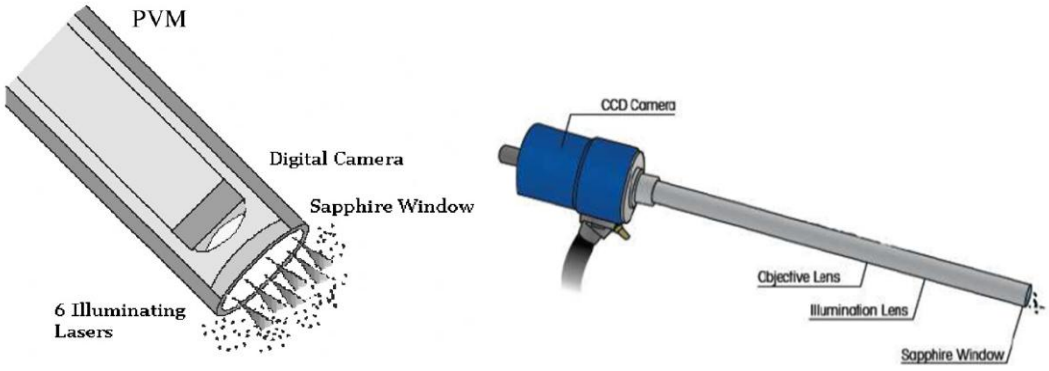

Figure II.13 – PVM probe description (from PVM Lasentec® Manual).

(a) (b)

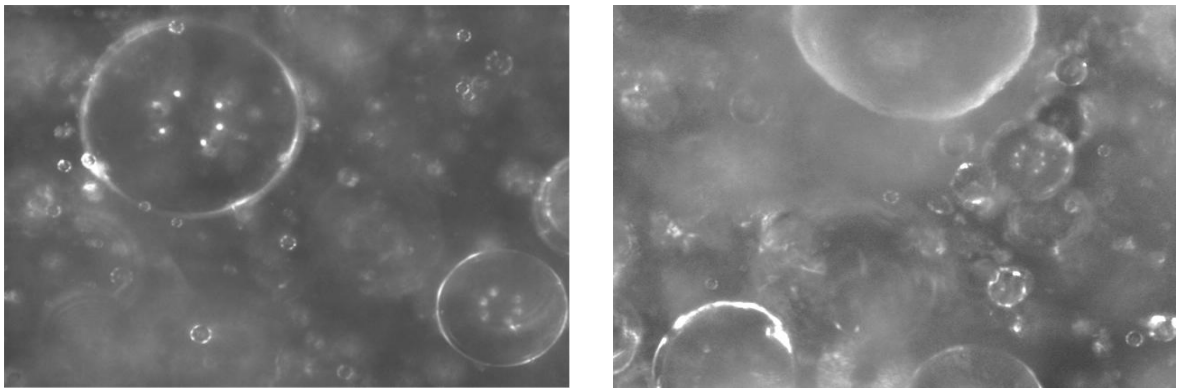

Figure II.14 – PVM image from (a) the emulsion at 80% water cut and 400L/h without AA-LDHI and (b) hydrates particles during the experiment at 80% water cut and 400L/h without AA-LDHI.

Unfortunately, experiments performed with anti-agglomerant additive did not provide good images for analysis. In general, images obtained in this group of experiments were totally white due to the light diffusion in the small droplet.

II.2 Materials

II.2.1 Kerdane®

The experiments are performed with Kerdane® oil. Kerdane® is the commercial denomination of an organic liquid supplied by TOTAL *Fluides*. It is composed by a variable and complex mixture of paraffinic and cyclic hydrocarbons (C11 – C14).

The Kerdane® has well-known properties (as density, viscosity) and it is a low volatile liquid, reducing the risk of losing mass. Both factors facilitate the experimental analysis, supporting the choice of Kerdane® as the oil phase in the studied systems. Moreover, the oil is transparent, which allows better study of the particle sizes and shapes once the FBRM accuracy depends on the laser diffusion in the continuous phase and the quality of the PVM image depends on the contrast between dispersed and continuous phase.

The Kerdane® viscosity in function of the temperature was calculated by Le Ba (2009) from experiments performed at the *Archimède* flow loop (atmospheric pressure). The experimental viscosity (Figure II.15) is calculated from the pressure drop, using the Hagen-Poiseuille equation in laminar regime. The obtained values are shown in Figure II.15. At 20°C, the viscosity provided by Total *Fluides* is approximately 1.68 mPa.s. For the same conditions, the value experimentally obtained is 1.93 mPa.s, this represents an error of 14.5% which is acceptable for the developed study. The flow is in laminar regime, as required by the equation used to calculate the viscosity.

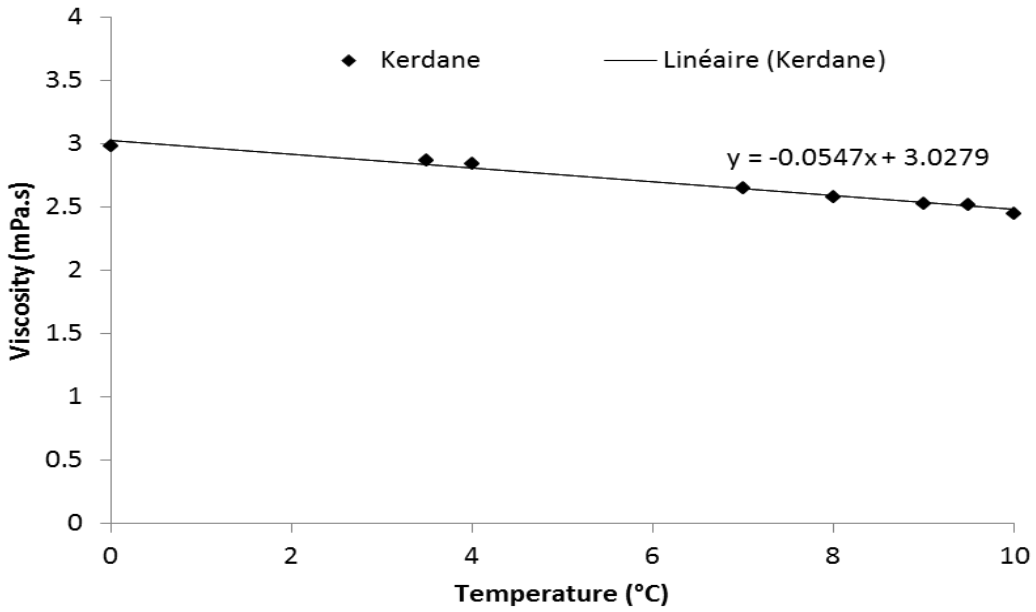

Figure II.15 – Kerdane® experimental viscosity in function of the temperature and in atmospheric pressure (Le Ba, 2009).

II.2.2 Water

Experiments were performed with ultrapure water (type I). The ultrapure water is obtained by a purification system (Milli-Q® Advantage A10) provided by Merck KGaG. The system eliminates any ionic or organic contaminants, reducing the water conductivity and the total amount of organic carbon (less than 5 ppb).

The water viscosity (Figure II.16) in function of the temperature was determined from experiments performed at the *Archimède* flow loop (atmospheric pressure), following the same procedure used to calculate the Kerdane® viscosity. It is interesting to notice that the water viscosity decreases abruptly between 4 and 5°C, probably due to the anomalous behavior of water around these temperatures. For this reason it is not possible to define a linear tendency to describe the experimental points. At 5°C, the dynamic viscosity of water is approximately 1.52 mPa.s (Engineering ToolBox). For the same conditions, the value experimentally obtained is 3.06 mPa.s. This represents an experimental error of 50%. The high error is explained because the laminar regime was not achieved, even with the flow loop working in the lowest flow rate possible so the applied method to measure the viscosity was not adapted to the provided conditions and affected the accuracy of the experimental measurement of water viscosity. Also, data from literature were obtained for pure water, whereas the flow loop can contain traces of mixtures used in precedent experiments, then the water purity cannot be guaranteed.

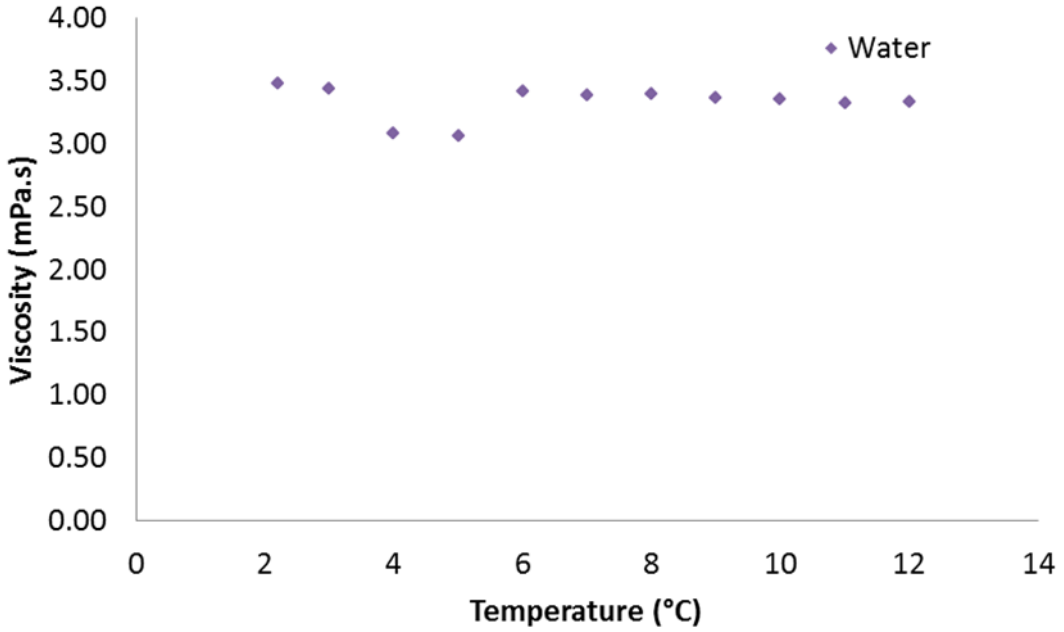

Figure II.16 – Water experimental viscosity while varying the temperature (in atmospheric pressure).

II.2.3 Methane

Methane (CH_4) is used in the experiments to form hydrates. Pure methane (99.99%) is supplied by AIR LIQUIDE.

Methane solubility in water is given in Table II.2 (Duan *et al.*, 1992). Methane solubility in Kerdane® was calculated from experiments at the *Archimède* flow loop (at 80 bar, approximately). The results are given in **Erreur ! Source du renvoi introuvable.**. Performing a linear interpolation with the solubility values for temperatures of 0°C and 30°C (Table II.2) it was obtained the solubility values at 4°C and pressures of 50 bar and 100 bar. In sequence, another linear interpolation was performed with values of pressure of 50 bar and 100 bar aiming to obtain the methane solubility in water at 80 bar and 4°C. Finally, the solubility at 80 bar and 4°C was obtained as being approximately 0.13 mol of CH_4 per Kg of water is obtained for methane solubilization in water. These conditions concern to the hydrate formation experiments performed for the study developed during this thesis. For similar experimental conditions (**Erreur ! Source du renvoi introuvable.**), methane solubilization in Kerdane® was approximately 2.27 mol of CH_4 per Kg of Kerdane®. This proves the higher solubility of methane in oil than in water.

Table II.2 – Methane solubility in water (mol /kg water) (Duan *et al.*, 1992)

	T (°C)		
P (bar)	0	30	60
1	0.0023	0.0012	0.0008
50	0.0974	0.0547	0.0412
100	0.1623	0.0949	0.0736

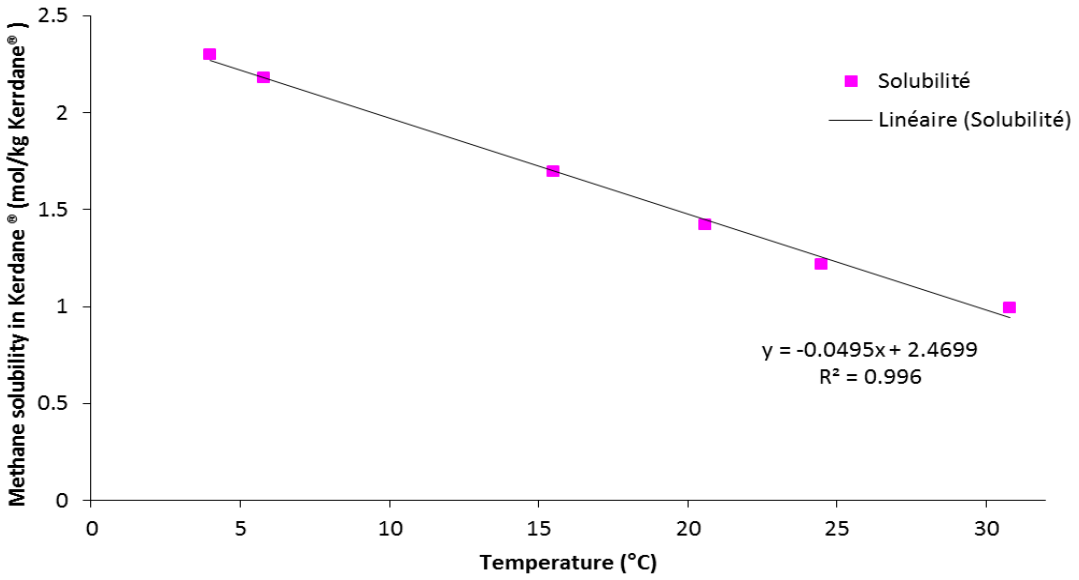

Figure II.17- Methane solubility in Kerdane® (at 80 bar).

II.2.4 Anti-Agglomerant Additive - Dispersant

The dispersant additive used in this study is a commercial anti-agglomerant provided by TOTAL. The additive is a water soluble mixture, mostly composed by a natural oil-based surfactant (30% to 60%, proprietary formula) and methanol (40% to 50%). The density of the mixture is 0.8637 $g.mL^{-1}$.

II.3 Experimental Protocol

A total of 110 experiments were performed using the *Archimède* flow loop installed at the *Ecole Nationale Supérieure des Mines de Saint-Etienne.* The aim of the study was to understand the hydrate formation from shear stabilized emulsions composed of water and oil (Kerdane®). Parametric modifications of the variables were used to access the hydrate formation properties. The systematically varied parameters were the water cut and the flow rate, while the additive dosage was varied accordingly to experimental observations (explained in Chapter III).

For this purpose, a set of experiments (Table II.3) without anti-agglomerant additive (AA-LDHI) was firstly performed and analyzed, aiming to better understand the process of hydrate formation. These experiments are the blanks. Later, a set of experiments (Table II.4) with AA-LDHI was performed, analyzed and compared to the blanks, aiming to understand the additive effect on the system. All experiments were analyzed in terms of pressure drop, gas consumption, density, chord length distribution and particles shape. Some experiments were repeated in order to confirm the obtained results namely when hydrate formation was very slow.

Table II.3– Set of Experiments without Additive AA-LDHI.

Water Cut (vol. % at room temperature)	Flow Rate (L/h)	Liquid Loading (%)
100	200 (2) 400 (1)	100 100
90	200 (1) 400 (1)	100 100
80	200 (7) 400 (5)	100 100
70	200 (6) 400 (3)	100 100
60	200 (4) 400 (3)	100 100
50	200 (1) 400 (1)	100 100
40	200 (2) 400 (2)	100 100
30	200 (1) 400 (1)	100 100

Table II.4 – Set of Experiments with Additive AA-LDHI.

Water Cut (vol. % at room temperature)	Flow Rate (L/h)	Additive AA-LDHI (% vs. w)	Liquid Loading (%)
90	200 (2) 400 (4)	0.005 0.005	100 100
80	200 (2) 400 (1)	0.005 0.005	100 100
80	200 (1) 400 (1)	0.01 0.01	100 100
70	200 (1) 400 (1)	0,01 0.01	100 100
60	200 (1) 400 (1)	0.01 0.01	100 100
50	200 (3) 400 (4)	0.01 0.01	100 100
50	200 (2)	0.1	100
40	200 (1) 400 (1)	0.01 0.01	100 100
40	200 (3) 400 (1)	0.05 0.05	100 100
30	200 (1) 400 (1)	0.01 0.01	100 100
30	200 (3) 400 (1)	0.05 0.05	100 100

(*)The value in parenthesis represents the number of experiments done in the same conditions.

II.3.1 Emulsification

The protocol of shear stabilized emulsion formation (emulsification) was performed before every experiment in the flow loop. The purpose was to form homogeneous and stable emulsions under flow, understanding their formation. The emulsification needs to be performed before every experiment; because once the shear stabilized emulsion rests quiescent overnight in the flow loop, it separates in the two original phases.

The characteristics of the formed shear stabilized emulsions will have an influence on the hydrate formation process, the reason why it is of major importance to have homogeneous and stable emulsions under flow. The mixture is homogeneous and shear stabilized under flow and during time when chord length distribution (and average chord length) and pressure drop are stable for long period (more than 10 minutes) when compared to the beginning of the process.

For each couple of experimental conditions (water cut and additive percentage), in the first day of experiment 11.5 L of shear stabilized emulsion was prepared in the flow loop and studied by the rheological study. In the following day, using the same mixture, the hydrates crystallization was studied at 200 $L.h^{-1}$ and, in the third day, the hydrates crystallization from the shear stabilized emulsion was studied at the other flow rate (400 $L.h^{-1}$), still with the same emulsion.

The protocol started by feeding the flow loop with the desired mixture of water and Kerdane® (and additive when necessary) at room temperature. The water cut is determined in terms of volume (the total volume of the flow loop is 11.5 L) at room temperature. Thus, water cut of 30% (volume) means that the quantity of water and Kerdane® in the mixture should be 3.45 L and 8.05 L, respectively. The calculated volume of water and Kerdane® is multiplied by its respective density (1000 $Kg.m^{-3}$ for the water and 800 $Kg.m^{-3}$ for the Kerdane®) to determine the weighed mass of each liquid. The quantity of additive is determined from the mass of water used in the experiment. So, if the water cut was 30%, the mass of water used was 3450 g, consequently, an additive dosage of 0.05% (mass) means that 1.725 g of AA-LDHI should be added into the mixture. All components were put together in the feeding vessel (Figure II.18) connected to the flow loop through the Moineau® pump, which feeds the flow loop with the liquid in the vessel.

The shear stabilized emulsion forms through shear of the mixture with the pipe wall, by circulating the mixture in the flow loop until homogeneity and stability criteria are achieved (always at atmospheric pressure). Flow rate and temperature of the emulsification process change accordingly to the experiment which is going to be performed next, being:

- 100 $L.h^{-1}$ (0.4 $m.s^{-1}$) before the rheological study (room temperature);
- the same flow rate of the hydrate formation (200 $L.h^{-1}$ (0.7 $m.s^{-1}$) or 400 $L.h^{-1}$ (1.4 $m.s^{-1}$)) in the crystallization experiments (≈4°C).

Figure II.18 – Feeding vessel.

Figure II.19 shows an example of the pressure drop evolution with time for three emulsifications with water cut of 80% and for three different constant flow rates (before rheological study and before hydrate formation). It is observed that the pressure drop is constant or approximately constant at end of the emulsification, what confirms that the criterion of homogeneity and stability concerning the pressure drop was achieved.

Homogeneity and stability criterion concerning the chord length distributions states that they must keep the same shape during time. An example is given in Figure II.20 for experiment with water cut of 40%; where the expected behavior can be observed (the color map at the right is related to the number of chords detected in the system).

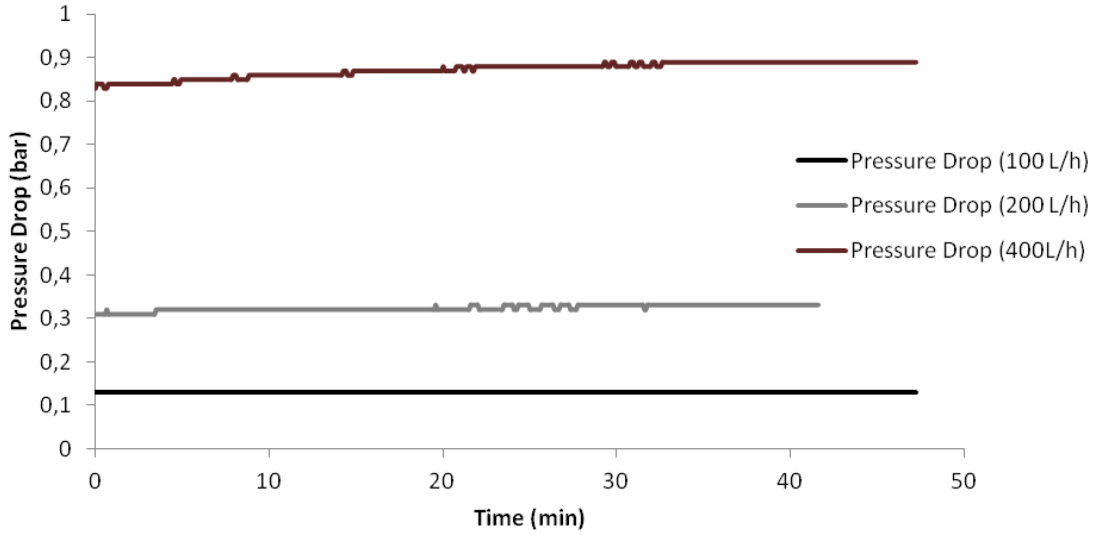

Figure II.19 – Pressure drop evolution with time during emulsification for the experiment with 80% water cut.

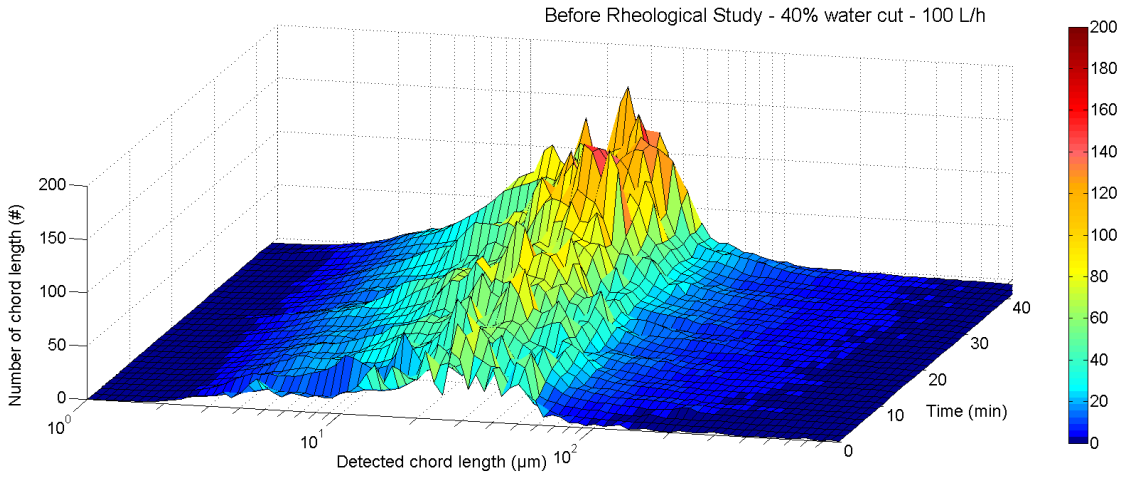

Figure II.20 – Chord Length Distribution during emulsification for the experiment with 40% water cut.

II.3.2 Rheological Study

The shear stabilized emulsion rheological behavior is also important to the understanding of hydrate formation process. The rheology of a system is usually studied in terms of fluids viscosity. Throughout the rheological study, firstly, the emulsion homogeneity and stability under flow is confirmed by varying the flow rate, step by step, verifying if the pressure drop is the same for the same flow rate. Secondly, the flow regime (laminar, transition or turbulent) correspondent to each flow rate is determined by the friction factor in function of the Reynolds' number. Finally, the shear

stabilized emulsion viscosity is calculated (Hagen-Poiseuille equation – I.65) from pressure drop measurements in the laminar regime.

The rheological study (at atmospheric pressure) starts after emulsification at 100 $L.h^{-1}$ and is performed by varying the flow rate (100 $L.h^{-1}$, 200 $L.h^{-1}$, 300 $L.h^{-1}$ and 400 $L.h^{-1}$) and measuring the pressure drop (ΔP, bar). The flow rate is changed once the pressure drop measurement is constant or approximately constant over time. An example is given in Figure II.21; it can be observed that the pressure drop measurements are close for different steps of the same flow rate. This can be used as parameter to indicate that the emulsion is homogeneous and stable under flow, even if real stability is not possible once the Kerdane® does not present any emulsifying property. Consequently, when the flow is stopped, the two phases separate. The shear stabilized emulsion with additive presented higher stability due to the fact that the surfactant prevents destabilization.

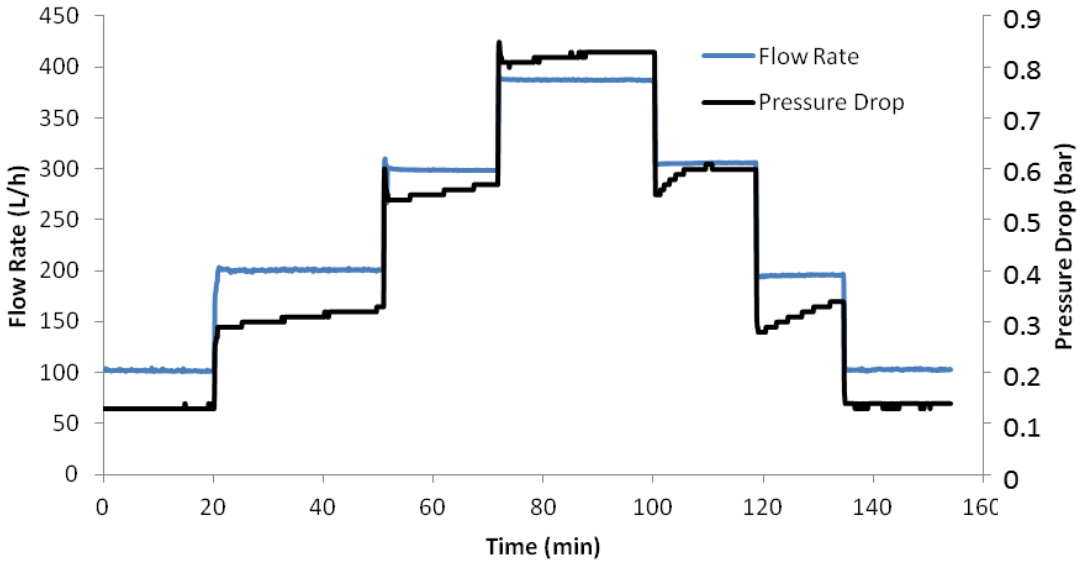

Figure II.21 – Rheological study for the experiment at 80% water cut.

With data obtained during the rheological study, it is possible to calculate the experimental Fanning friction factor (f, equation I.63) and the Reynolds' Number (Re, equation I.4). After it, the regime (laminar, transition or turbulent) for each flow rate is determined based on the Moody Scheme (Figure I.15), as shown by Figure II.22 (80% water cut). In this case, the lowest flow rate 100 $L.h^{-1}$ is in laminar regime (black line), while the flux of 200 $L.h^{-1}$ is in transition zone and the two highest flow rates, 300 $L.h^{-1}$ and 400 $L.h^{-1}$, in turbulent regime (dashed line). Finally, the viscosity for

laminar flow is determined by Hagen-Poiseuille equation (I.65). For the referred experiment at 80% water cut, the viscosity is approximately 5.13 mPa.s.

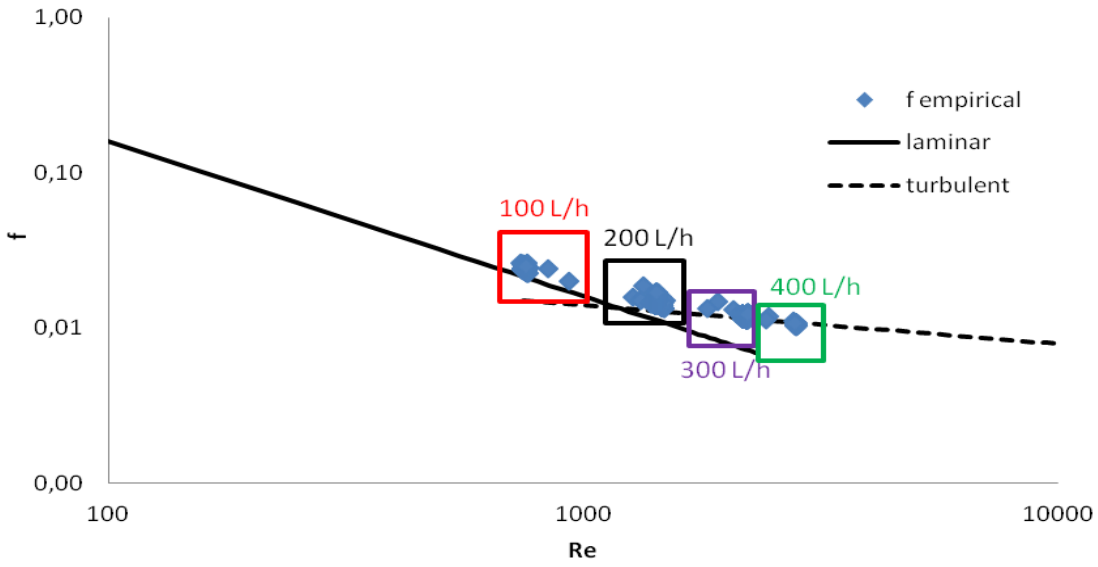

Figure II.22 – Fanning friction factor vs. Reynolds' Number (experiment at 80% water cut).

II.3.3 Gas transfer to the shear stabilized emulsion

At the beginning of hydrates crystallization experiments, before hydrate formation, the gas transfer to the shear stabilized emulsion is studied. The flow loop is already filled and the mixture water-Kerdane® is flowing. The circulating baths are turned on. When the desired crystallization temperature 4°C (subcooling of ≈6°C) is attained, the flow loop is pressurized until 80 bar. At first, the automatic pressure compensation control is not turned on, and the pressure is left to decrease for some minutes (maximum of 20 minutes). The pressure decrease data is treated in order to calculate the kinetic coefficient of gas transfer to the shear stabilized emulsion (K_{la}).

The K_{la} is normally determined in closed reactor from the quantity (in moles) of methane solubilized into the shear stabilized emulsion (N_{cf}) during the pressure decrease and the relation of this quantity with time (N_{ct}). These values, calculated from the ideal gas equation (I.58), are used to plot the curve representing "$ln(N_{cf}/N_{cf} - N_{ct})$ *vs. time*". This curve is regressed to linear fitting and the K_{la} is given by the angular coefficient. In experiments performed at the *Archimède* flow loop, the same methodology was applied in order to measure evolution of gas transfer to the shear stabilized

emulsion for the same time interval. This can be observed in the example given in Figure II.23, for the experiment at 80% water cut at 200 $L.h^{-1}$, in this case the K_{la} value is 0.0024 s^{-1}.

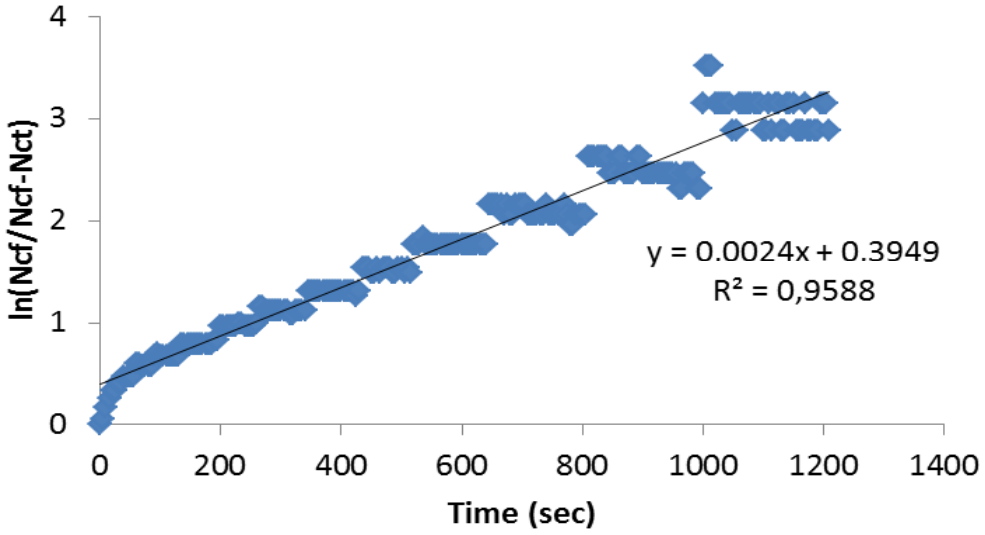

Figure II.23 - K_{la} evolution for the experiment at 80% water cut at 200 $L.h^{-1}$.

II.3.4 Crystallization - Hydrate Formation

After the pressure decrease for calculation of the gas transfer coefficient, the flow loop is pressurized until 80 bar for the second time and the system of automatic pressure control is activated. In this point, the flow loop is in the thermodynamic conditions for hydrate formation. Hereafter, the data is monitored until the end of the crystallization process.

Crystallization beginning is determined by a peak in the temperature due to exothermic characteristic of hydrate crystallization. In general, the increase in the temperature is followed by a pressure drop peak due to the increase in the viscosity of the mixture after hydrate formation. An example can be seen in Figure II.24 (40% water cut and 200 $L.h^{-1}$ flow rate). Other probes of the flow loop can be used to support the observation of crystallization beginning. The study of the crystallization process is performed by analyzing the evolution of the pressure drop, the density, the chord length distribution (and average chord length - FBRM), the images from the PVM, the conversion rate and the percentage in volume of hydrate formed.

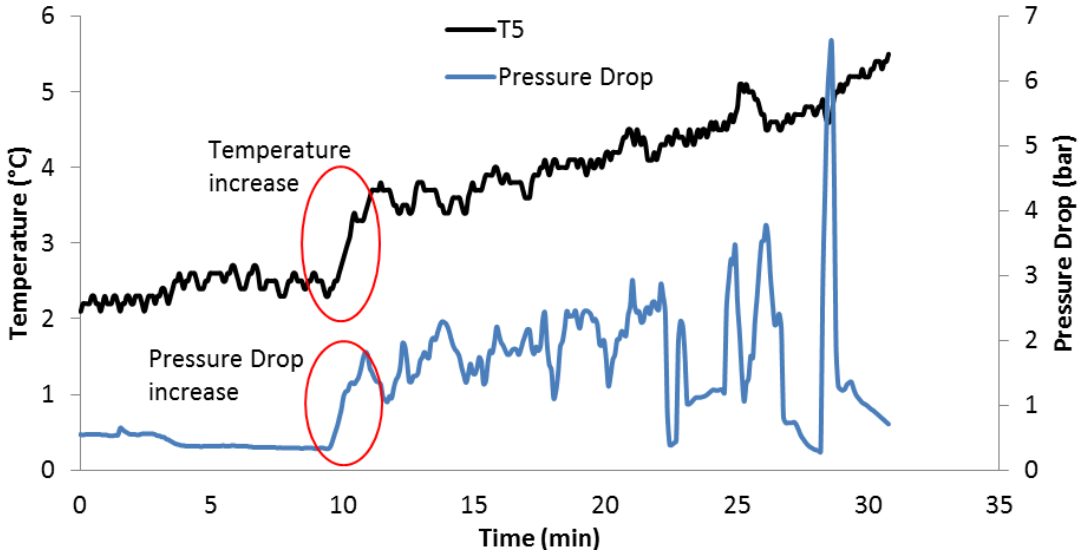

Figure II.24 – Temperature and Pressure Drop evolution with time for the experiment of crystallization at 40% water cut at 200 $L.h^{-1}$

The conversion rate (η) and the percentage in volume of formed hydrates ($\%vol_{Hyd}$) are calculated from the data of gas consumption (obtained by the system of pressure control) from the beginning until the end of the crystallization. In order to proceed with these calculations, it is assumed that after the beginning of hydrate formation all the gas that solubilizes into the system is consumed to form hydrates.

The stoichiometry of the gas hydrate crystallization is given by equation II.1. Fully occupied cages are considered in the calculations. For this case, the amount (in moles) of crystallized water (n_{crw}) is equal to 5.75 times the amount (in moles) of methane (n_{CH_4}) that has been consumed (II.2). The conversion rate (η) of water into hydrates can be determined by equation II.3. The initial quantity of water (n_{iwater}) is easily calculated (II.4) from the mass of water used in each experiment (m) divided by the water molar mass (M_w).

$$CH_{4\,(g)} + 5.75\ H_2O_{(l)} \rightarrow CH_4\ 5.75\ H_2O_{(s)} \quad \text{(II.1)}$$

$$n_{crw} = n_{CH_4} * 5.75 \quad \text{(II.2)}$$

$$\eta = \frac{n_{crw}}{n_{iwater}} \quad \text{(II.3)}$$

$$n_{iwater} = \frac{m_w}{M_w} \quad \text{(II.4)}$$

The volume of hydrates related to the liquid volume (%vol_{hyd}) in the flow loop can also be calculated from the quantity (molecules) of crystallized water (n_{crw}):

$$n_{crw}(molecules) = n_{crw}(moles) * Avogadro \quad \text{(II.5)}$$

The quantity of water molecules crystallized can be related to the number of cells (n_{cells}) of hydrate structure by the equation II.6. Using the number of cells in the system, it is possible to calculate the volume of formed hydrates (V_{Hyd} – Equation II.7), once the volume of the cubic cell (V_{cells}) for the sI hydrate structure can be approximated to 1.728 nm^3. Finally, the volumetric percentage of formed hydrates ($\%vol_{Hyd}$) is obtained by dividing the volume of formed hydrates by the total liquid volume (V_{total}) inside the flow loop.

$$n_{cells} = \frac{n_{crw}(molecules)}{46} \quad \text{(II.6)}$$

$$V_{Hyd} = n_{cells} * V_{cells} \quad \text{(II.7)}$$

$$\%vol_{Hyd} = \frac{V_{Hyd}}{V_{total}} \quad \text{(II.8)}$$

The end of gas hydrate crystallization is determined if no evolution on the pressure drop and no gas compensation are observed for a long period, as the example in Figure II.25 shows. However, the crystallization normally does not achieve the end during one day of experiment and the study needs to be interrupted. This is necessary for a matter of security, because the experimental apparatus cannot stay working overnight without supervision.

The crystallization experiment can be interrupted earlier if pipeline plugging occurs. For the studied system, plugging is stated when it is observed a large increase in the pressure drop followed by flow rate decrease until a point that no flow is detected. Another condition of earlier interruption occurs when no hydrate formation is observed during the first hours of experiment.

Once the experiment of crystallization is finished, the flow loop is depressurized (until atmospheric pressure) and the cooling system is stopped. As consequence, the formed hydrates dissociate since the system is no longer in thermodynamic conditions to have hydrates. The system is kept under flow until the achievement of atmospheric pressure.

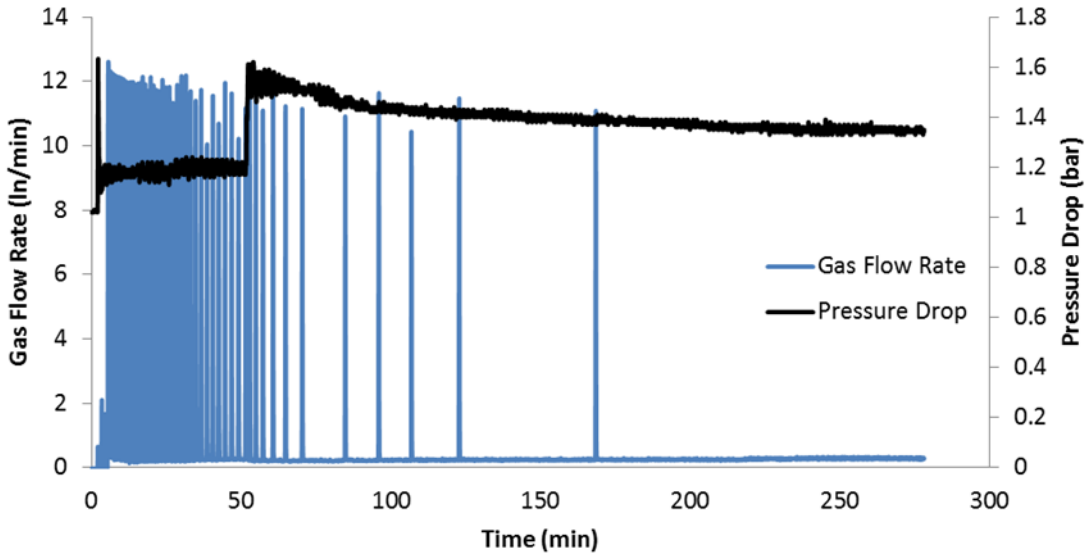

Figure II.25 – Gas flow rate and Pressure Drop evolution with time for the experiment of crystallization at 50% water cut and 400 $L.h^{-1}$.

II.4 Chapter Highlights in French – Aperçu du Chapitre II

L'étude représentative de la formation d'hydrates en lignes d'écoulement à partir de différents types d'émulsion nécessite l'utilisation de systèmes expérimentaux plus complexes que ceux utilisant des réacteurs ou cellules sous pression. L'utilisation d'un pilote expérimental (comme une boucle d'écoulement) est un atout majeur pour reproduire les conditions rencontrées dans les conduites lors de l'extraction du pétrole.

L'étude de la formation des hydrates de méthane développé dans cette thèse a été réalisée dans une boucle d'écoulement (présentée dans la section § II.1 du chapitre II) à partir d'émulsions stabilisées par cisaillement formées d'eau et Kerdane® (C11 - C14), avec et sans anti-agglomérant.

La boucle d'écoulement nommée d'*Archimède* était le dispositif expérimental (Figure II.1) utilisé dans ce travail. Il a été construit au cours de la thèse de doctorat de Fidel-Dufour (2004) pour étudier le transport et l'agrégation des hydrates de méthane. Le pilote est capable de travailler dans des conditions thermodynamiques similaires à celles trouvées lors de l'écoulement pendant l'extraction de pétrole en haute mer (*i.e.*, haute pression et basse température) qui sont les conditions thermodynamiques pour la formation des hydrates.

La boucle d'écoulement est équipée de plusieurs outils pour maintenir le débit (0 à 500 $L.h^{-1}$, vitesse opérationnelle: 0 à 1,7 $m.s^{-1}$), la pression (0 à 100 bars) et la température (0 à 10 °C) constants. La boucle est aussi équipée avec des outils pour surveiller la température, la perte de charge, la masse volumique (et débit), la forme et la taille des gouttelettes et des hydrates et la consommation de gaz pendant les expériences. Ces instruments sont détaillés dans la section § II.1.1 du chapitre II.

Les matériaux utilisés dans les expériences ont été présentés dans la section § II.2, ils sont :

- **Le Kerdane®,** qui est la dénomination commerciale d'un liquide organique fourni par Total *Fluides*, et composé par un mélange variable et complexe d'hydrocarbures paraffiniques et cycliques (C11 - C14). Les propriétés (densité, viscosité) du Kerdane® sont bien connues, il est un liquide de basse volatilité (réduisant ainsi le risque de perte de masse) et transparent, ce qui permet de mieux étudier la taille et la forme des particules présentes dans le système. Ces facteurs, qui facilitent l'analyse expérimentale, ont soutenu le choix du Kerdane® comme la phase huile dans les systèmes étudiés.

- **L'eau ultra pure (type I)**, est obtenue par un système de purification (Milli-Q® Advantage A10) fourni par Merck KGaG. Ce système élimine tous les contaminants ioniques et organiques, en réduisant la conductivité de l'eau et la quantité totale de carbone organique (moins de 5 ppb).
- **Le méthane (CH_4) pur (99,99%)**, qui est utilisé dans les expériences pour former les hydrates, est fourni par Air Liquide.
- **L'additif dispersant**, qui est un anti-agglomérant commercial fourni par Total, est un mélange soluble dans l'eau, principalement composée d'un agent tensio-actif à base d'huile naturelle (30% à 60%, formule du propriétaire) et de méthanol (40% à 50%). La densité du mélange est de 0,8637 $g.mL^{-1}$.

Le protocole expérimental est présenté dans la section § II.3. L'objectif de l'étude est de comprendre la formation d'hydrates à partir d'émulsions stabilisées par cisaillement et composées d'eau et d'huile (Kerdane®). Pour ce faire, une étude paramétrique a été faite pour accéder aux propriétés de la formation d'hydrates. La fraction d'eau et le débit étaient les paramètres systématiquement variés, tandis que la dose d'additif a été modifiée à partir des observations expérimentales (détaillée dans le Chapitre III).

Un total de 110 expériences a été réalisé. Les expériences (Tableau II.3) sans additif anti-agglomérant (AA-LDHI) ont d'abord été réalisées et analysées, visant à mieux comprendre le processus de formation d'hydrates. Ces expériences sont qualifiées de « blancs ». Plus tard, les expériences (Tableau II.4) avec AA-LDHI ont été effectuées, analysées et comparées aux blancs, visant à comprendre l'effet de l'additif sur le système. Les expériences ont été analysées en termes de perte de charge, consommation de gaz, densité, distribution de longueur de corde et forme des particules. Certaines expériences ont été répétées afin de confirmer les résultats obtenus notamment lorsque la formation d'hydrates était très lente.

Pour chaque couple de conditions expérimentales (fraction d'eau et pourcentage d'additif), dans la première journée d'expérience, l'émulsion stabilisée par cisaillement a été préparée dans la boucle d'écoulement et étudiée en termes rhéologiques. Dans la journée suivante, en utilisant le même mélange, la cristallisation d'hydrates a été étudiée à 200 $L.h^{-1}$ et, dans la troisième journée, la cristallisation d'hydrates a été étudiée à un autre débit (400 $L.h^{-1}$), toujours avec la même émulsion stabilisée par cisaillement.

Chapter III – Results and Discussion: Comparing experiments at Different Conditions

"The important thing in science is not so much to obtain new facts as to discover new ways of thinking about them." (William L. Bragg)

The results of hydrate formation processes change varying the experimental conditions (*e.g.*, water cut, flow rate, absence/presence of additive). This chapter will present the experimental results and analysis for different conditions in which experiments were performed. The chapter is divided in three sections: Shear Stabilized Emulsion and Rheological Study (§ III.1), Hydrate Crystallization (§ III.2) and Rheological Comparison between Shear Stabilized Emulsion and Suspension (§ III.3). In order to facilitate the understanding of results hereafter presented, the sections present representative experiments at high (90%), intermediate (60%) and low (30%) water cuts. Each group of water cut (high, intermediate and low) represents the three principal behaviors observed in this work. Each section shows a comparison between blanks and experiments with additive, also including differences observed varying the flow rate.

III.1 Shear Stabilized Emulsion and Rheological Study

As explained in Chapter II, homogeneous and stable emulsion under flow is formed by circulating the mixture in the flow loop at the desired flow rate until the pressure drop and chord length distribution do not present a strong variation with time. For all studied cases, further experiments are only performed if these conditions are achieved.

Concerning the water cut of each experiment, one can suppose that the dispersed phase would be the liquid with the smallest fraction. However, it is not possible to guarantee this assumption and what is the dispersed and the continuous phase. Consequently, water and oil will not be stated as continuous and dispersed phases throughout emulsion and rheological studies.

III.1.1 Experiments without Additive – AA-LDHI

Figure III.1 shows the rheological study for the three water cut groups (high, intermediate and low). During flow rate variation, all experiments present the same plateau of pressure drop for the same flow rate. This can be used to prove the emulsion homogeneity and stability under flow, which is essential to continue the study. Figure III.2 presents the chord length distribution for the same group of experiments. The different scales concerning the number of chords detected when

comparing the experiments in Figure III.2 occur due to the different kinds of dispersion and different fractions of dispersed phase.

During rheological study, experiments at high and intermediate water cuts present stable pressure drop in each studied flow rate (Figure III.1 (a) and (b)). For these water cuts, the number of chord lengths measured by the FBRM probe (displayed from a top view in Figure III.2 (a) and (b)) increases by increasing the flow rate. This means that the increase in the flow rate induces higher homogeneity thus stability by forming more dispersed droplets and consequently increasing the dispersed phase surface area.

The rheological study begins by studying the shear stabilized emulsion under the lowest flow rates (100L.h^{-1} and 200 L.h^{-1}). Regarding experiments in high and intermediate water cuts at this point, the dispersed phase seems not to be completely emulsified (being present as free phase). Later, an enlargement of the interval of measured chord lengths is observed and the free phase disperses partially or completely in the continuous phase when flow rate is increased (300L.h^{-1} and 400 L.h^{-1}). This is the reason for observing an increase in the number of chords lengths measured by the FBRM probe (Figure III.2 (a) and (b)) after increasing the flow rate. In following, the chord length distribution slightly changes when flow rate is decreased, which indicates that the shear stabilized emulsion morphology returns to the initial conditions.

The shear stabilized emulsion at 30% water cut (low water cut, Figure III.1 (c)) presents a particular behavior. Initially, the pressure drop presents a stable behavior for the flow rates of 100L.h^{-1} and 200 L.h^{-1}. After, when the flow rate is increased to 300 L.h^{-1} and 400 L.h^{-1}, the pressure drop values become disturbed. Finally, when the flow rate is decreased to 100 L.h^{-1} and 200 L.h^{-1}, the pressure drop disturbed behavior disappears. Aiming to understand this event, it is necessary to analyze the chord length distribution (displayed from a top view in Figure III.2 (c)).

For the experiment at low water cut (Figure III.2 (c)), the number and the interval of chord lengths measured by the FBRM probe increases until 200 L.h^{-1}. Then, it starts to decrease (at 300 L.h^{-1} and 400 L.h^{-1}) in the same time that the pressure drop measurement becomes noisy. The decrease in the number of chord lengths can be interpreted as the formation of large droplets, not detected by the FBRM probe but that slightly change the chord length distribution by decreasing the measured chord lengths number in smaller classes (Figure III.2 (c)). The shear stabilized emulsion rearrangement destabilizes the system and causes the disturbed behavior in the pressure drop

measurement. Once decreasing the flow rate, the number of chords increases step by step. In the corresponding time, the pressure drop noisy behavior disappears and the shear stabilized emulsion returns to the conditions observed at 200 $L.h^{-1}$, remaining with the same morphology until the end of the experiment, which means that the emulsion is stable and homogeneous under flow.

(a) 90% water cut

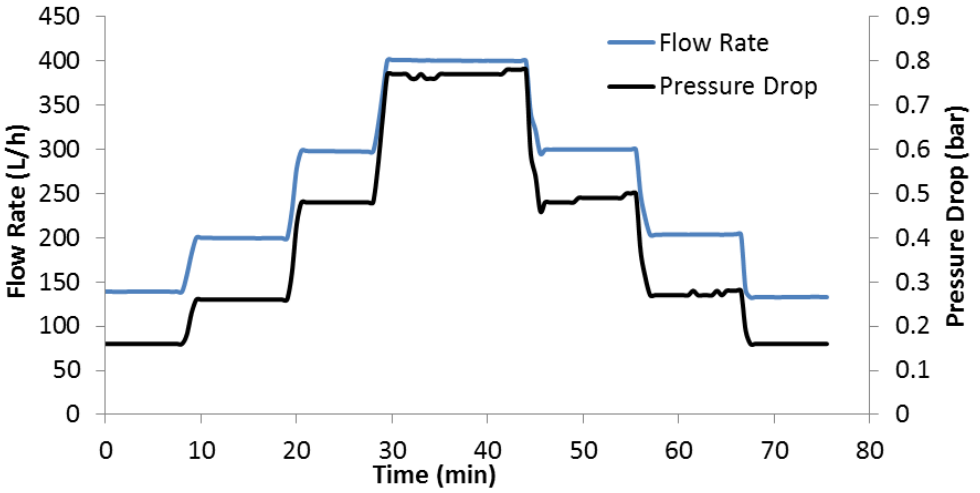

(b) 60% water cut

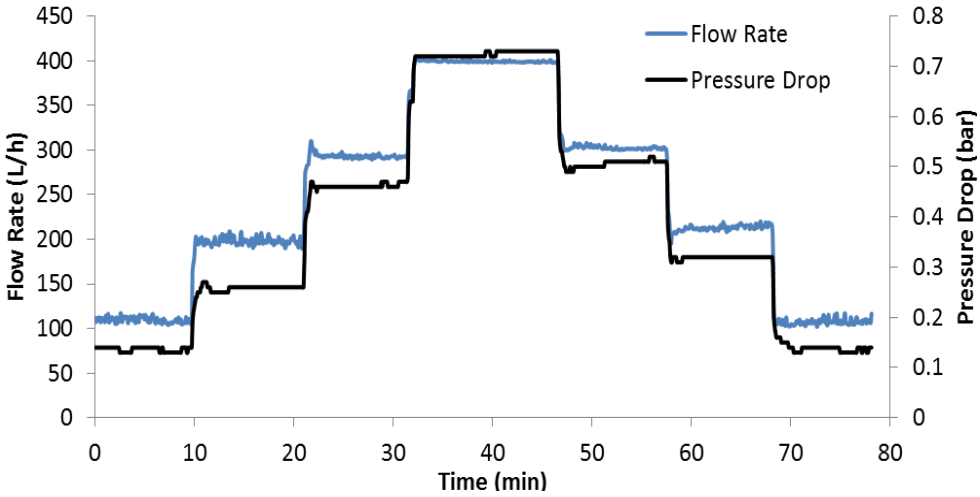

(c) 30% water cut

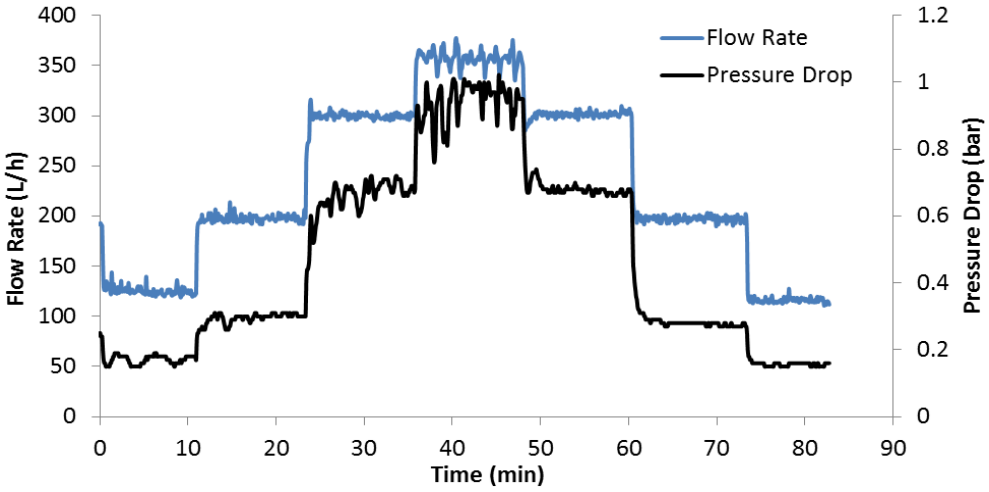

Figure III.1 – Rheological Study for experiments at (a) 90%, (b) 60% and (c) 30% water cut without AA-LDHI.

(a) 90% water cut

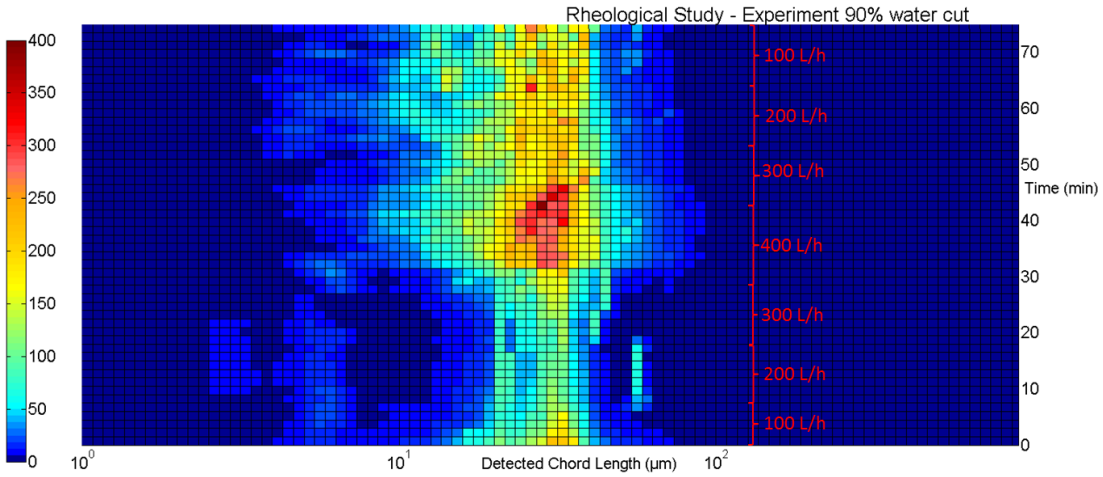

(b) 60% water cut

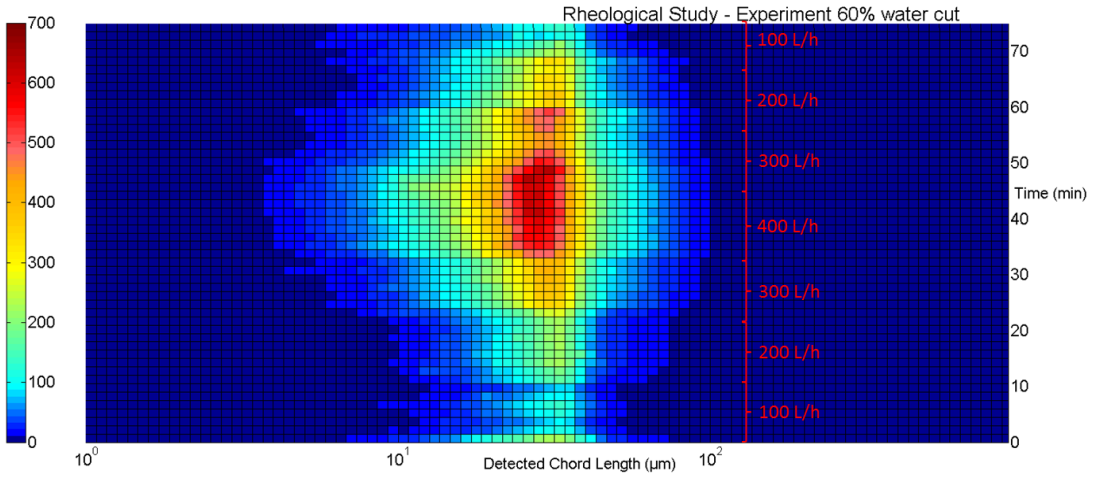

(c) 30% water cut

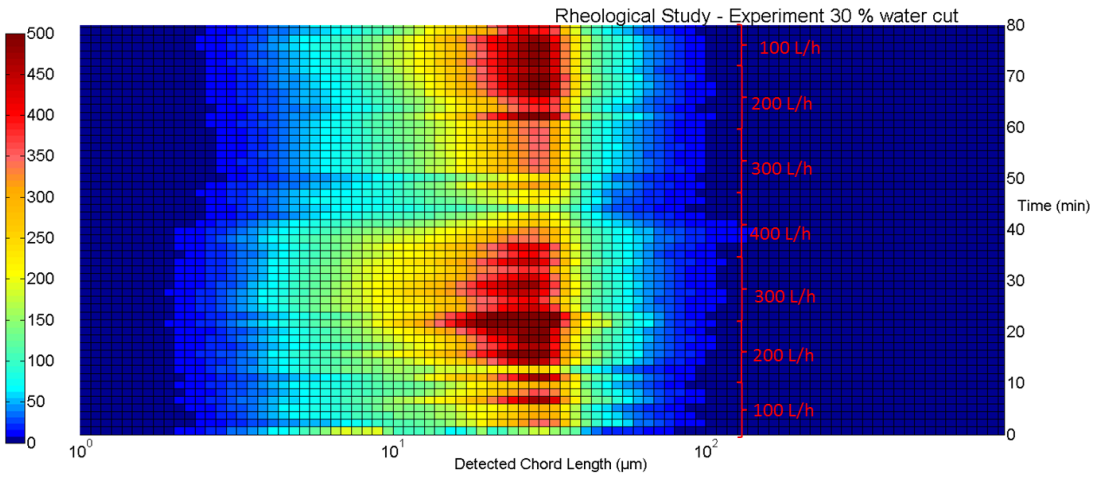

Figure III.2 – Chord Length Distribution in number during Rheological Study for experiments at (a) 90%, (b) 60% and (c) 30% water cut without AA-LDHI.

For experiments with high and intermediate water cuts, the flow rate increase forms some larger droplets, observed by PVM images (Figure III.3). Firstly, comparing the PVM images with the chord length distribution, it is noticed that the FBRM chord length distributions probe does not have detected chords above 100 µm, which were detected by the PVM probe. The appearance of large droplets (not detected by the FBRM probe due to its measure limitation) while increasing the flow rate for experiments at high and intermediate water cuts (Figure III.3 (a) and (b)) was observed together with a large amount of small droplets dispersed in the continuous phase. After decreasing the flow rate, the large droplets are no longer seen by the PVM.

Nevertheless, the chord length distribution shows a higher quantity of chords at the highest flow rate (400 L.h-1, Figure III.2 (a) and (b)). The appearance of large droplets in the PVM images can be interpreted as:

(1) Coalescence of small droplets forming large ones, because increasing the flow rate, the probability of collision between the droplets is increased.

and/or,

(2) Free phase dispersion, which can form small droplets (detected by the FBRM) as well as large droplets (observed with the PVM).

For the experiment at low water cut (Figure III.3 (c)), it is possible to see a large number of small droplets dispersed in the continuous phase at lowest flow rates (until 300 $L.h^{-1}$). The quantity of droplets observed with the PVM probe at low water cut in the lowest flow rates is higher than the one observed for experiments at high and intermediate water cuts (Figure III.3), as confirmed from the chord length distribution (Figure III.2). Nevertheless, when increasing the flow rate, it is observed the formation of large droplets (Figure III.3 (c)). Inside them, there are several small droplets, while in the external continuous phase, very few or no droplets are observed (Figure III.3 (c)). This justifies the decrease of the number of chords detected by the FBRM probe in the highest flow rate (400 $L.h^{-1}$, Figure III.2 (c)). In this case, the increase of flow rate formed complex liquid-liquid dispersion, causing the disturbed behavior detected in the pressure drop measurement. Once decreasing the flow rate, only small droplets dispersed in the continuous phase are observed. This indicates the disappearance of the complex liquid-liquid dispersion and the appearance of a shear stabilized emulsion of the same kind that the one observed in high and intermediate water cuts.

(a) 90 % water cut – 200 $L.h^{-1}$ and 400 $L.h^{-1}$, respectively:

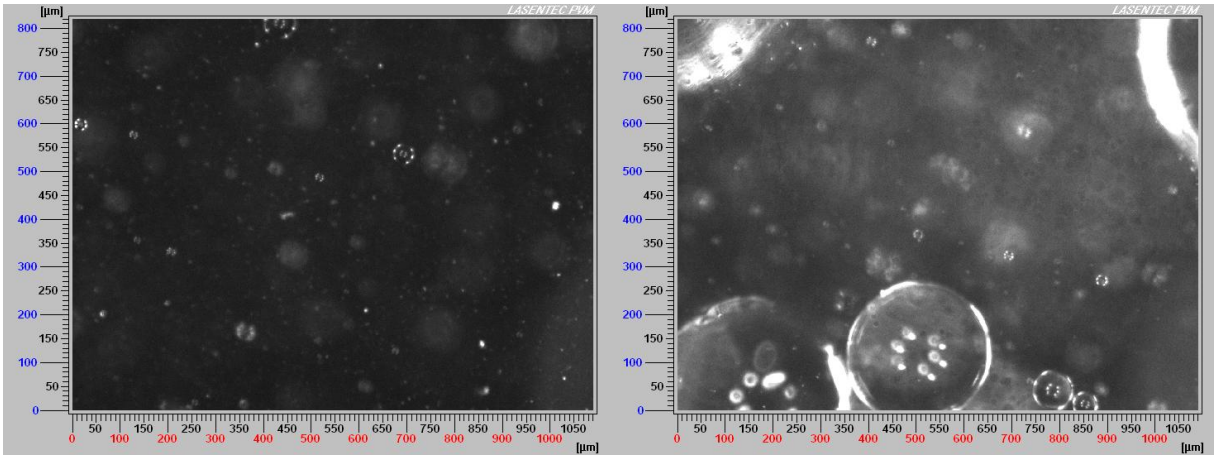

(b) 60 % water cut – 100 $L.h^{-1}$ and 300 $L.h^{-1}$, respectively:

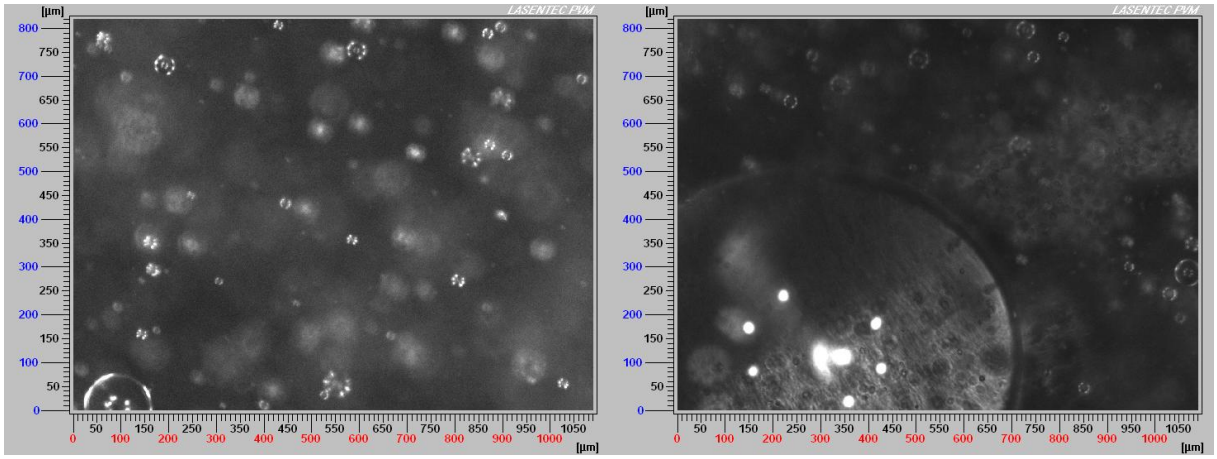

(c) 30 % water cut – 200 $L.h^{-1}$ and 400 $L.h^{-1}$, respectively:

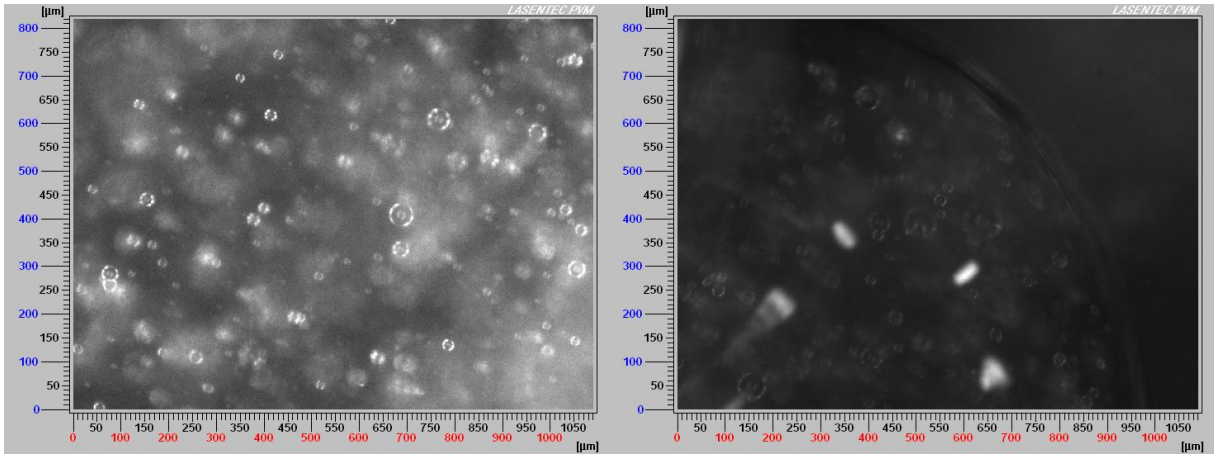

Figure III.3 – PVM images during Rheological Study for experiments at (a) 90%, (b) 60% and (c) 30% water cut without AA-LDHI.

Finally, the density evolution with time during rheological study (Figure III.4) can be analyzed. At high water cut (Figure III.4, red line), it can be noticed that the density is very close to 1000 $kg.m^{-3}$ (water density) for the flow rates of 100 $L.h^{-1}$ and 200 $L.h^{-1}$. This shows that not so much Kerdane® (800 $kg.m^{-3}$) is dispersed in the water phase, an indicative of the presence of a free oil phase. Once the flow rate is increased to 300 $L.h^{-1}$ and 400 $L.h^{-1}$, the dispersion of Kerdane® in water also increases. As consequence, it is detected a decrease on the measured density. Later, when the flow rate is decreased, the density returns to the conditions observed in the beginning of the study.

For low and intermediate water cuts (Figure III.4, green and blue lines, respectively), it can be see that the measured density presents a disturbed behavior for the flow rates of 100 $L.h^{-1}$ and 200 $L.h^{-1}$. Probably, due to the presence of a free phase which is more representative in these cases than in high water cut.

For intermediate water cut (Figure III.4, green line), there are probably large portions of oil still circulating in the lowest flow rates (100 $L.h^{-1}$ and 200 $L.h^{-1}$). Their detection by the probe represents a decrease in the density measurement. For low water cut (Figure III.4 (c), blue line), the same behavior is observed, but in the opposite way because large portions of water are probably circulating.

Once the flow rate (300 $L.h^{-1}$ and 400 $L.h^{-1}$) is increased, the free phase is better dispersed. As consequence, stable density measurement is observed for both intermediate and low water cuts.

However, the density becomes unstable for low water cut in the highest flow rate (400 $L.h^{-1}$), due to the punctual event related to the formation of complex liquid-liquid dispersion. Later, the decrease of the flow rate (100 $L.h^{-1}$ and 200 $L.h^{-1}$) induces the reappearance of the noisy behavior for intermediate and low water cuts.

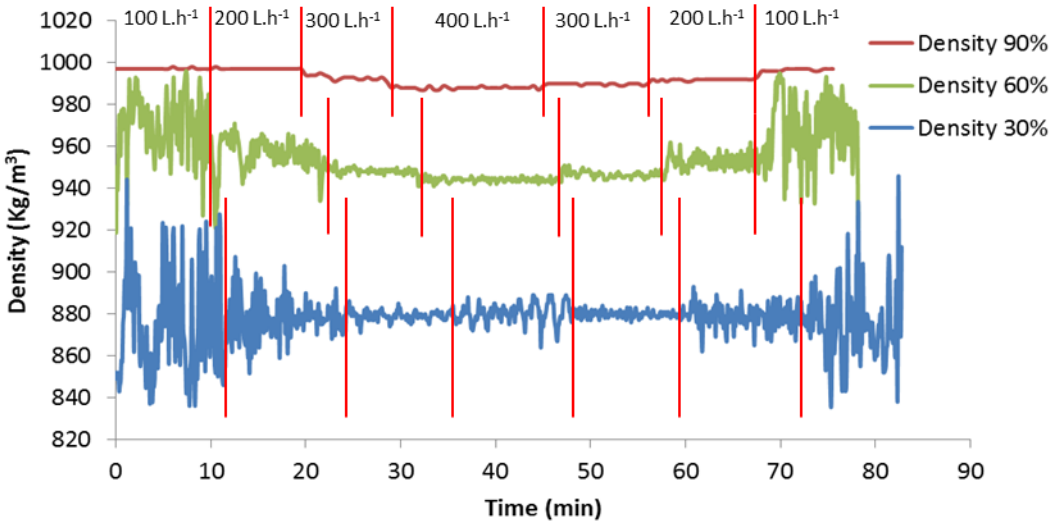

Figure III.4 – Density evolution during Rheological Study for experiments at (a) 90%, (b) 60% and (c) 30% water cut without AA-LDHI.

An overview of the shear stabilized emulsion behavior, for all experiments, throughout the rheological study without anti-agglomerant provides the following conclusions:

(1) At the end of the rheological study, the shear stabilized emulsion presents the same morphology and chord lengths range for the high, intermediate and low water cuts.

(2) After the emulsification and rheological study, all groups present stable and homogeneous emulsion under flow. This behavior is proved by measuring the same pressure drop plateau and the same chord length distribution for the same flow rate. However, concerning the density measurement, some non-homogeneity is detected (mainly at low flow rate).

(3) By varying the flow rate, all water cut groups present a unimodal chord length distribution, with peak between 20 µm and 40 µm at the end of the rheological study.

(4) The chord length distribution changes varying the flow rate. An increase in the flow rate induces a better dispersion by forming more droplets. Sometimes, at low water cut, the new morphology is related to the formation of complex liquid-liquid dispersion, which causes an unexpected behavior of pressure drop, chord length distribution and density evolution.

III.1.2 Experiments with Additive – AA-LDHI

The additive used to avoid hydrate agglomeration is a surface active agent (surfactant). It will act at the droplets interface. As consequence, it also increases homogeneity and stability of the emulsions under flow formed before hydrate formation. Throughout the emulsion formation and

rheological study, this influence should be seen. The additive dosage in each experiment is very low. The different percentages of additive used in this study are a feedback from the hydrate crystallization experiments and will be explained in § III.2.2.

Figure III.5 shows the rheological study for shear stabilized emulsions regarding the three water cut groups (high, intermediate and low) with anti-agglomerant additive. As the blanks (Figure III.1), these experiments (Figure III.5) present the same plateau of pressure drop for the same flow rate during the rheological study. However, it is observed that the pressure drop presents more stable behavior, which means that experiments with additive have higher degree of homogeneity and stability.

With the purpose of understanding what happens in the case where additive is used, it is necessary to evaluate the chord length distribution during the rheological study (Figure III.6). Comparing experiments, it can be observed that the initial chord length distribution shape sharply changes with varying water cut. The sharpest peak of chord length number is of 900 chords at high water cut, 1800 at intermediate water cut and 200 at low water cut, while the corresponding quantity for the blanks does not vary too much when water cut is varied (400, 700 and 500, respectively). The quantity of chords found is related to the dispersed phase. Relating it with the number of chords found in presence and absence of additive, this shows that experiments with additive have more dispersed droplets than experiments without additive. However, the evolution of the number of chords detected in experiments with additive varying the water cut is not similar to blank experiments. Thus, it is necessary to consider that the use of surfactant additive changes the expected shear stabilized emulsion morphology.

The final range (Figure III.6) of measured chord lengths after 400L.h^{-1} is the same for high, intermediate and low water cuts and the attained shear stabilized emulsions remain similar until the end of the rheological study. The small droplets are mainly dependent on the surfactant action: if the dosage of additive is very low, the morphology cannot be completely maintained when the flow rate is decreased and less chord lengths are detected.

In the experiment with low water cut (Figure III.6 (c)), the rheological study already starts with a peak corresponding to small droplets (around 9 µm). This probably happens because the additive dosage used in this water cut is more important than the one used in high and intermediate water cuts. The higher dosage influences the shear stabilized emulsion since the lowest flow rate, inducing

the formation of more and smaller droplets than in experiments at high and intermediate water cuts in same conditions. When the flow rate is increased to 200 $L.h^{-1}$ and 300 $L.h^{-1}$, the distribution is maintained. At the highest flow rate (400 $L.h^{-1}$), it is expected a more important additive effect, in other words, an increase of the peak corresponding to small droplets. However, it is observed the formation of large droplets ranging from 20µm to 40µm. From this, it is possible to interpret that with increasing flow rate droplets coalescence occurs. As the additive is water soluble, its action can be also related to the quantity of water in the system.

(a) 90% water cut and 0.005% AA-LDHI

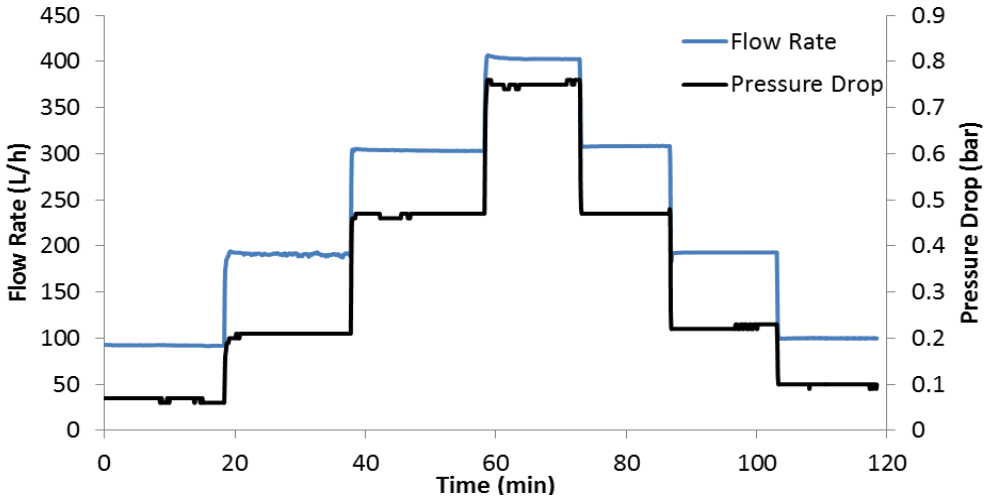

(b) 60% water cut and 0.01% AA-LDHI

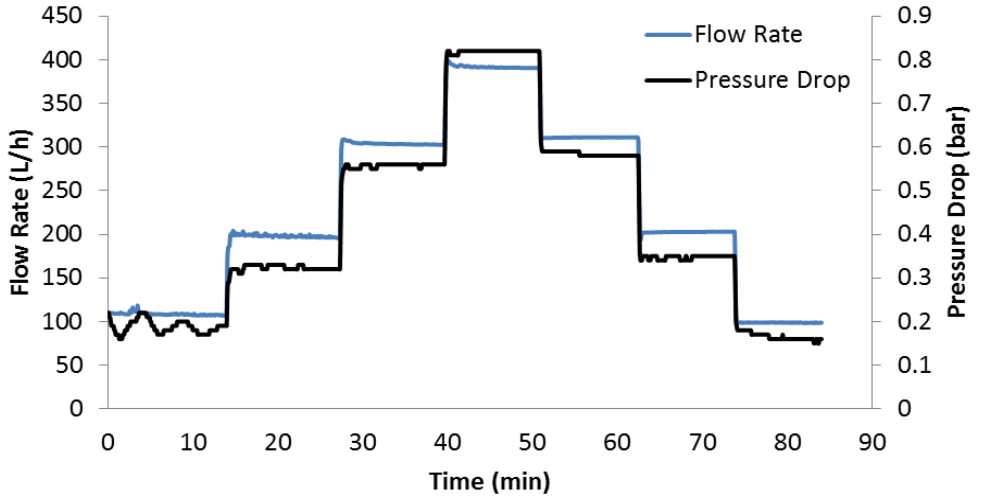

(c) 30% water cut and 0.05% AA-LDHI

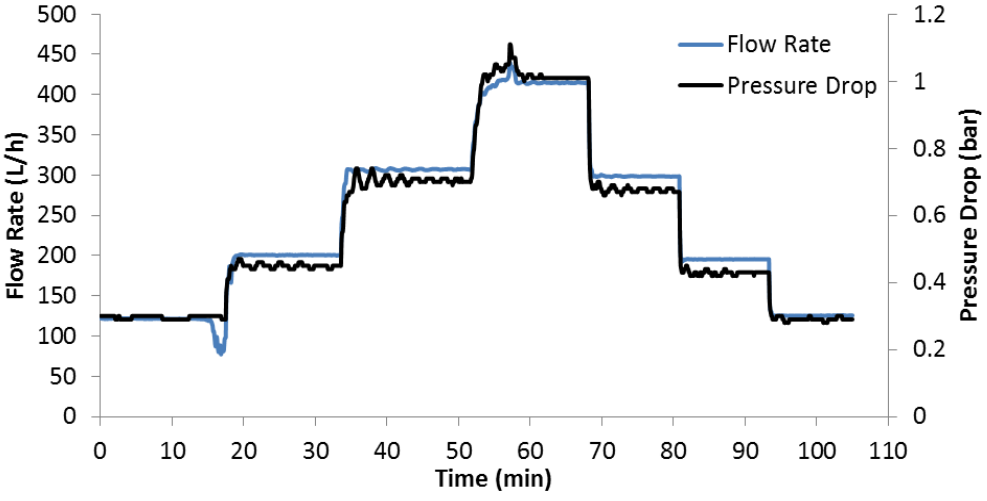

Figure III.5 – Rheological Study for experiments at (a) 90%, (b) 60% and (c) 30% water cut with additive (AA-LDHI).

(a) 90% water cut and 0.005% AA-LDHI

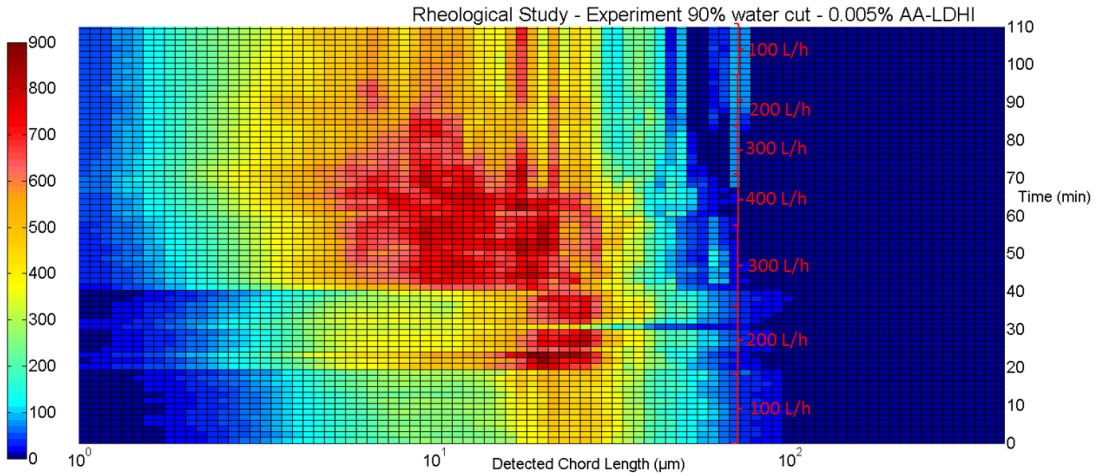

(b) 60% water cut and 0.01% AA-LDHI

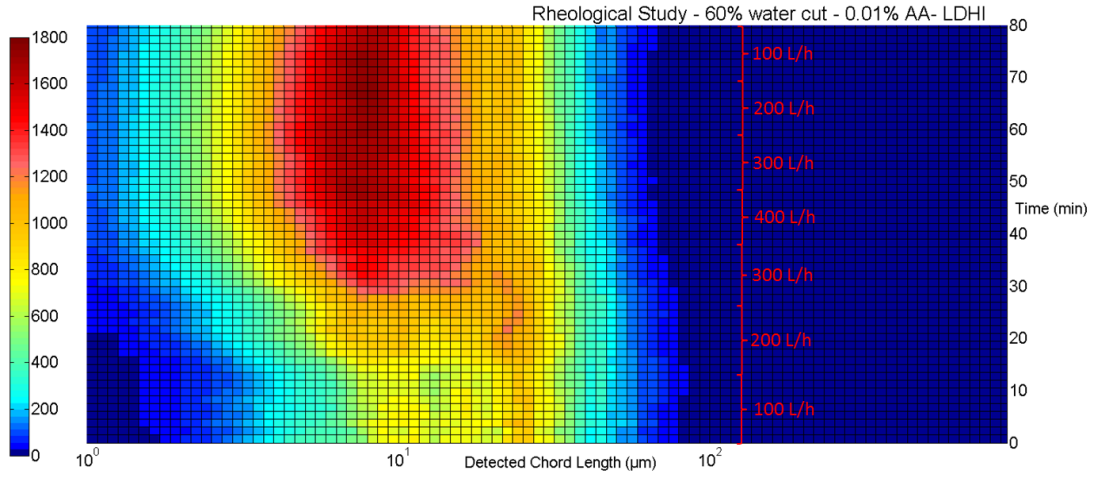

(c) 30% water cut and 0.05% AA-LDHI

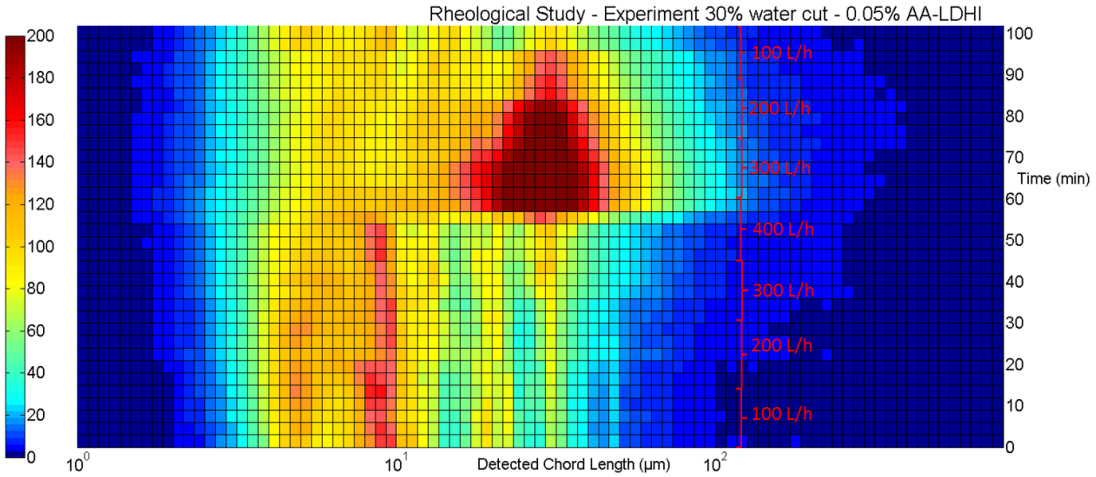

Figure III.6 – Chord Length Distribution in number during Rheological Study for experiments at (a) 90%, (b) 60% and (c) 30% water cut with additive (AA-LDHI).

A final analysis refers to the density evolution throughout the rheological study (Figure III.7). This measurement also evidences the additive effect comparing to the blanks (Figure III.4). The density evolution is more regular and the disturbed behavior presents a narrow range when additive is used.

For all water cuts (Figure III.7), the additive effect is evidenced since the beginning of the experiment by detecting a less noisy density measurement comparing to the blanks (Figure III.4).

For intermediate water cut (Figure III.7, green line) the density is still a little noisy due to the presence of the free phase. Once again, a better dispersion is provided as the flow rate is increased. In agreement with the chord length distribution (Figure III.6 (b)), the density behavior shows that the shear stabilized emulsion partially maintains its new distribution when the flow rate is decreased. Consequently, the noisy behavior does not reappear.

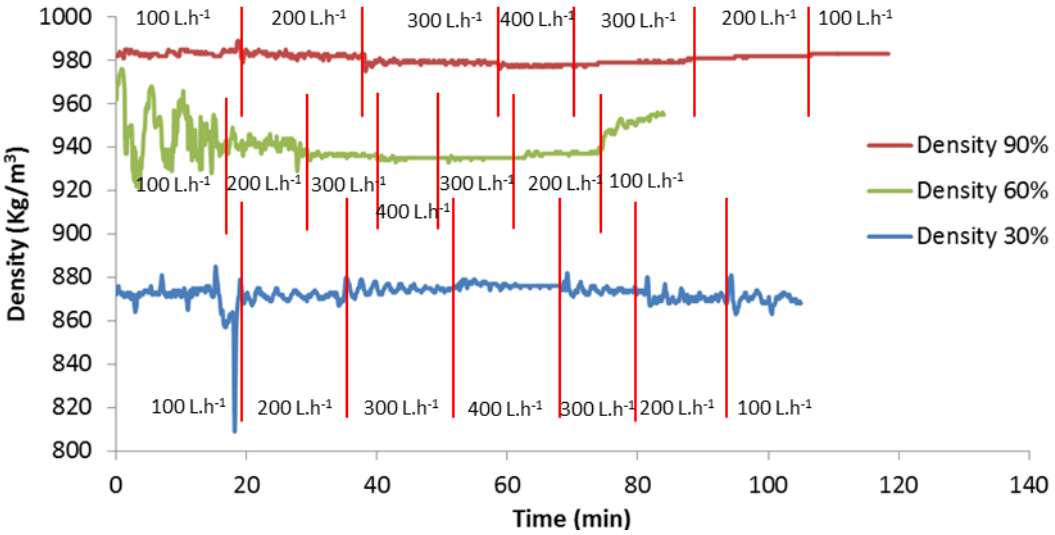

Figure III.7 – Density evolution during Rheological Study for experiments at (a) 90%, (b) 60% and (c) 30% water cut with additive (AA-LDHI).

An overview of the emulsion behavior throughout the rheological study using the surfactant additive gives the following conclusions:

(1) All shear stabilized emulsions, from high to low water cut (independent of the additive dosage), have a better homogeneity and stability under flow when comparing to the blanks. This is confirmed by the pressure drop evolution during the study and also evidenced through the density measurements.

(2) The peaks observed in the chord length distributions change with the flow rate variation, but this change is less important when the flow rate is decreased after 400 $L.h^{-1}$. The presence of additive induces the appearance of smaller droplets with chord length around 10 µm.

(3) A flow rate increase forms a better dispersion with formation of small droplets.

During the rheological study, the flow regime and viscosity is also determined. These topics will be discussed in later section (§ III.3), presenting a comparison between the shear stabilized emulsion and the suspension of hydrates.

Even if these preliminary results were useful to calculate the viscosity of the shear stabilized emulsion and validate its stability and homogeneity under flow, some further work must be done to better understand the behavior of the emulsion and the emulsification process.

III.2 Methane Hydrate Crystallization

III.2.1 Gas Transfer to Shear Stabilized Emulsion

During the methane solubilization into the shear stabilized emulsion (before hydrate formation beginning), the kinetic coefficient (K_{la}) of gas transfer into the shear stabilized emulsion was calculated for some experiments (Table III.1 and III.2). For both groups of experiment, with and without AA-LDHI, experiments at high and intermediate water cuts present a K_{la} (s^{-1}) in the order of magnitude between 10^{-3} and 10^{-4}, while experiments at low water cut range between 10^{-2} and 10^{-3}. The higher K_{la} at low water cut is due to the higher fraction of oil, in which the methane solubilization is larger if compared to water (Figure III.8). The fact that no expressive changes were observed among experiments with and without AA-LDHI evidences that the gas transfer to the shear stabilized emulsion is mostly dependent on the oil fraction of the system and not on the kind of emulsion.

It was observed from the $R^{2(1)}$ analysis that the calculated K_{la} is more reliable for cases in which the pressure decreases more softly (R^2>0.9), probably because the method used for its determination was developed for reactors. However, the present experiments are in a flow loop.

From Tables III.1 and III.2 a connection can be observed between the gas-emulsion transfer rate and the later occurrence of hydrate crystallization: experiments presenting an important pressure decrease (R^2<0.9) during gas solubilization will have a higher probability of later presenting hydrate formation.

[(1)]The R^2 (determination coefficient) indicates the adjustability of the data to the tendency line.

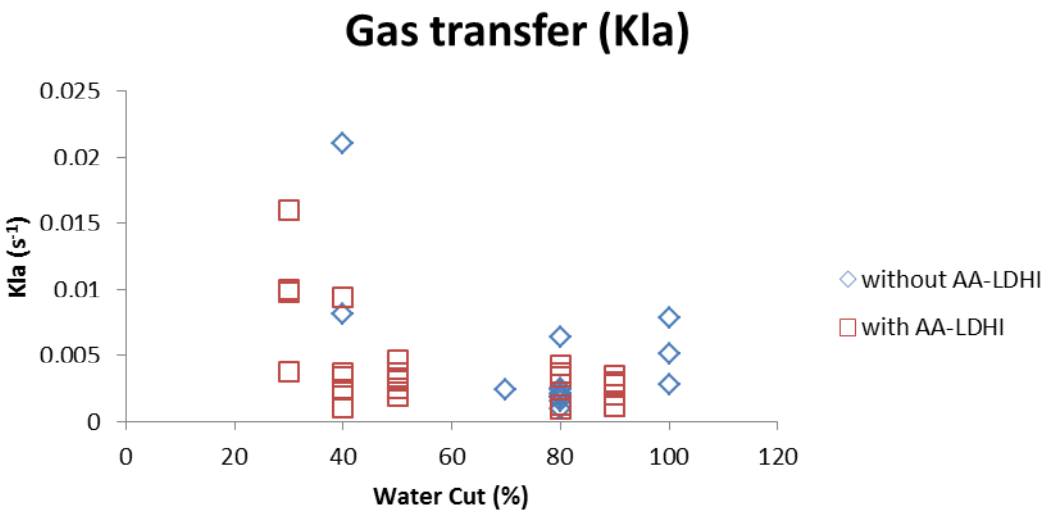

Figure III.8 – Gas transfer (K_{la}) evolution with water cut.

Table III.1 - Kinetic coefficient of gas transfer (K_{la}) for the experiments without additive (AA-LDHI).

Water Cut (vol. %)	Débit (L/h)	K_{la} (s^{-1})	Hydrate Formation after Gas Dissolution	R^2
100	200	5.1E-03	YES	0.88
	200	2.8E-03	YES	0.88
	400	7.8-03	YES	0.89
80	200	2.5E-03	NO	0.91
	200	1.9E-03	NO	0.96
	200	1.8E-03	NO	0.94
	200	2.4E-03	NO	0.96
	200	2.1E-03	NO	0.95
	200	1.5E-03	YES	0.90
	400	9.0E-04	YES	0.86
	400	1.8E-03	NO	0.93
	400	6.4E-03	YES	0.86
70	400	2.4E-03	YES	0.87
40	200	2.1E-02	YES	0.89
	400	8.1E-03	YES	0.78

Table III.2 - Kinetic coefficient of gas transfer (K_{la}) for the experiments without additive (AA-LDHI).

Water Cut (vol. %)	Débit (L/h)	Additif (%)	K_{la} (s^{-1})	Hydrate Formation after Gas Dissolution	R^2
90	200	0.005	2.0E-03	NO	0.92
	200	0.005	3.5E-03	YES	0.86
	400	0.005	2.8E-03	NO	0.95
	400	0.005	1.1E-03	NO	0.97
	400	0.005	3.0E-03	YES	0.90
80	200	0.01	9.0E-04	NO	0.98
	400	0.01	1.2E-03	NO	0.93
	200	0.005	3.4E-03	NO	0.92
	200	0.005	4.2E-03	YES	0.84
	400	0.005	3.6E-03	YES	0.85
50	200	0.01	3.1E-03	NO	0.93
	200	0.01	2.5E-03	NO	0.95
	400	0.01	1.9E-03	NO	0.82
	400	0.01	3.6E-03	NO	0.87
	400	0.01	3.3E-03	NO	0.84
	400	0.01	4.6E-03	YES	0.88
40	200	0.01	3.4E-03	YES	0.89
	200	0.05	1.0E-03	NO	0.93
	200	0.05	3.6E-03	NO	0.93
	200	0.05	2.4E-03	NO	0.94
	400	0.05	9.4E-03	YES	0.88
30	200	0.05	3.7E-03	NO	0.88
	200	0.05	9.8E-03	YES	0.94
	200	0.05	1.0E-02	YES	0.86
	400	0.05	1.6E-02	YES	0.87

III.2.2 Experiments without Additive AA-LDHI

In this section, a qualitative and quantitative description of the crystallization behavior is presented considering each water cut group (high >70%, intermediate 70%-50% and low <50%). Results are supported from probe measurements, but also from the global understanding of the process which will be detailed later in Chapter IV.4.

Methane hydrate formation in flow loop was evaluated for different water cuts (from 30% to 100%) in two different flow rates (200 $L.h^{-1}$ and 400 $L.h^{-1}$) without and with AA-LDHI. The beginning of the hydrate formation is identified by a sudden temperature increase due to the exothermic characteristic of this process. The time elapsed between the moment when the system is in right

conditions of formation (pressure and temperature where hydrate formation is possible) and the moment of the hydrate formation beginning is called induction time. This is a random/stochastic event, *i.e.*, it is not reproducible even applying the same experimental conditions (water cut, flow rate, pressure and temperature). When hydrate formation was observed in a working day of experiment in general the induction time took from 5 to 90 minutes, the lower induction times are observed at intermediate and low water cuts. After the appearance of the first hydrate crystals, each water cut group (at the same flow rate) presents some similarities concerning the experimental data evolution.

The focus of this section is the understanding of the experimental data evolution of pressure drop, density and average chord length for each water cut group without additive (blanks), under different flow rates. These results are supported by the volume of formed hydrates and water conversion in hydrates.

Figure III.9 shows the evolution of pressure drop and density with time during hydrate formation for one example of each water cut group at 200 $L.h^{-1}$ and 400 $L.h^{-1}$. This approach is still valid even if each group does not behave exactly in the same way, because the tendency observed for each group is generally the same.

(a) High water cut without AA-LDHI (Figure III.9 (a)):

The beginning of hydrate formation (nucleation and growth) corresponds to an increase of pressure drop. Nucleation and growth take place at the water/oil interface. The pressure drop increase is consequence of solid particles formation (higher viscosity). The increase is followed by a decrease due to the mixture re-homogenization (hydrates dispersion into the shear stabilized emulsion). The same behavior is observed for both flow rates.

After the initial variation, the pressure drop remains almost constant for a long period. This step also corresponds to hydrate nucleation and growth. This stage is longer in experiments of 200 $L.h^{-1}$ than in experiments of 400 $L.h^{-1}$. As the flow rate increases, the shear stabilized emulsion becomes better dispersed (more droplets), which means a larger water/oil interfacial area. The water/oil interface is the place where hydrate nucleation and growth happen. As consequence, there are more available places for hydrate formation by increasing the interfacial area. A larger interfacial area can also increase the gas solubilization rate into the shear stabilized emulsion, once more interface for gas/liquid transfer is provided. These two factors induce an increase of the hydrate formation kinetic by increasing the flow rate.

The third and last step corresponds to the gradual pressure drop increase thanks also to growth, but mainly to hydrate agglomeration. The formation of solid agglomerates results in the increase of the mixture viscosity and, as secondary effect, the pressure drop increases. The same behavior is observed for both flow rates. However, the gradual increase is faster in high flow rate than in low flow rate. The higher flow rate enhances the probability of collision between the particles, enhancing the agglomeration rate.

In the experiment of 200 $L.h^{-1}$, the beginning of hydrate formation also corresponds to a steep density decrease. This decrease occurs because gas is quickly and strongly consumed by the liquid hydrocarbon phase due to the onset of hydrate formation. The former event is immediately followed by a steep density increase, because the mixture is re-saturated with gas and the system returns to the previous conditions. In this flow rate, the density of the mixture after its re-homogenization is smaller than the one observed in the beginning of the experiment. This happens because the methane hydrate density is lower (900 $kg.m^{-3}$) than the water density (1000 $kg.m^{-3}$). After the detailed variation, the density remains constant until the end of the experiment.

In general, the trend observed in low flow rate (200 $L.h^{-1}$) is also observed in high flow rate (400 $L.h^{-1}$). However, exceptionally in the experiment with 90% water cut and 400 $L.h^{-1}$, the gas compensation was not turned on. For this matter, there is no quick and strong gas consumption in the beginning of hydrate formation, because gas is not being constantly provided to the system. Consequently, the density decrease related to the beginning of hydrate formation is not observed. Only the density increase is observed. In this experiment, a small density decrease is observed when the mixture is re-homogenized. This value remains constant during the second step of crystallization (constant pressure drop). Later, a small density increase is detected in the same time that agglomeration begins (pressure drop increase). After this small increase, the density remains the same until the end of the experiment.

(b) Intermediate water cut without AA-LDHI (Figure III.9 (b)):

For both flow rates, the hydrate formation beginning (nucleation and growth) also corresponds to pressure drop increase as consequence of solid particles formation (higher viscosity). The formation also takes place at the water/oil interface. In the experiment of 400 $L.h^{-1}$, the first pressure drop peak corresponds to gas injection and the second one to beginning of hydrate formation. This last peak is small and hard to observe in Figure III.9 (b) due to the graph scale.

In the experiment of 200 $L.h^{-1}$, the pressure drop signal becomes noisy after the first pressure drop increase. This step also corresponds to hydrate nucleation and growth at the water/oil interface. The

noisy signal of pressure drop measurement means that hydrates are circulating in the flow loop separated by packages, *i.e.*, the re-homogenization is not observed. This indicates that as the water cut decreases, the re-homogenization becomes harder.

After approximately 10 minutes, the pressure drop rises until its maximum due to hydrate formation, and then it starts to decrease. After the decrease, the pressure drop becomes stable with time. The constant pressure drop measurement from this point until the end of the experiment is higher than the one measured before hydrate formation what can be interpreted as hydrate deposition. The pipeline section decreases after hydrates deposition and, consequently, pressure drop increases. This represents a risk of pipeline plugging.

In the experiment of 400 $L.h^{-1}$, pressure drop decreases due to mixture re-homogenization after the first pressure drop increase. For this experiment, hydrate formation started during the gas injection, showing again that higher flow rate implies a faster hydrate formation kinetic.

After re-homogenization, a step where the pressure drop remains constant is observed likewise the experiment at high water cut. This stage is linked to hydrate growth and nucleation at the water/oil interface.

After around 8 minutes (Figure III.9 (b)), it can be observed a large pressure drop increase corresponding to strong hydrate agglomeration. Simultaneously, the flow rate becomes very irregular, reaching values close to zero. When this behavior is observed, the pump is stopped for a matter of security. Following, the pump is re-started, but the pressure drop increases very quickly and the flow rate decreases again to values close to zero. At this point the pipeline is stated as plugged as no flow is observed, this event happened after 19 minutes of experiment. The data showed after this point corresponds to the depressurization step.

Regarding the density evolution for both flow rates, the beginning of hydrate formation corresponds to a steep decrease followed by a steep increase due to strong gas consumption and subsequent gas dissolution in the mixture.

For low flow rate (200 $L.h^{-1}$), the density evolution is noisy at first, as for the pressure drop evolution, due to circulation of hydrates packages in the flow loop. Once the pressure drop starts to decrease due to hydrate deposition, the density measurement becomes more stable. This means better distribution of the remaining solid particles in the liquid phase.

For high flow rate (400 $L.h^{-1}$), the first increase/decrease of the density measurement related to the hydrate formation beginning is followed by another steep decrease with gradual increase. This behavior is related to the fast kinetic of this experiment. Once the density achieves stability, it remains likewise until the beginning of hydrate agglomeration. In this point, the density shows again

a steep decrease followed by increase due to agglomerates formation. The pump is then stopped and the density increases until values observed before agglomeration. Once the pump was re-started, the density decreases again, corroborating with the conclusion that the pipeline is plugged.

(c) Low water cut without AA-LDHI (Figure III.9 (c)):

As for other groups, the beginning of hydrate formation (nucleation and growth at the water/oil interface) corresponds to an increase of pressure drop as consequence of solid particles formation (higher viscosity). However, there is no decrease of pressure drop due to mixture re-homogenization for both flow rates after this first increase. This happens because at low water cut it is harder to re-homogenize the mixture due to faster hydrate formation. The higher oil fraction increases the gas solubilization rate, favoring hydrate formation.

In the experiment of 400 $L.h^{-1}$, hydrate formation and agglomeration started during gas injection due to faster hydrate formation kinetic in higher flow rate. At the same time, the flow rate became very irregular and the pressure compensation system valve remained open because gas was being consumed very fast to form hydrates. For this matter, the flow was stopped for some minutes. After re-starting the pump, the pressure drop remained stable for 1 minute. Afterward, second steep pressure drop increase was observed. This second increase corresponds to new onset of hydrate formation.

After the first increase of pressure drop in experiment of 200 $L.h^{-1}$ and the second one in the experiment of 400 $L.h^{-1}$, the pressure drop continues to increase during approximately 2 minutes. This step corresponds to hydrate nucleation and growth at the water/oil interface. Then, the measure becomes very irregular due to circulation of agglomerates packages. This behavior is observed during 30 minutes in the experiment of 200 $L.h^{-1}$ and during 10 minutes in the experiment of 400 $L.h^{-1}$. Subsequently, the flow rate becomes irregular and decreases to values close to zero. At this point the pump is stopped. After a few minutes, it is re-started. However, no flow is observed and the pipeline is stated plugged. The time between the beginning of crystallization and the pipeline plugging in the experiments of high flow rate (30 minutes) and low flow rate (10 minutes) also evidences how the kinetic of hydrate formation increases by increasing the flow rate.

Regarding the density evolution for both flow rates, it is observed the same behavior detected for the other water cuts, *i.e.*, the beginning of hydrate formation corresponds to a steep decrease followed by a steep increase of the density measurement. When the pressure drop becomes irregular due to the circulation of agglomerates packages, the density measurement also becomes

irregular. After stopping the pump, the density measurement becomes constant. Finally, when the pump is re-started, the density becomes very irregular. This evidences that the pipeline is plugged.

(a) 90% water cut at 200 L.h^{-1} and 400 L.h^{-1}, respectively:

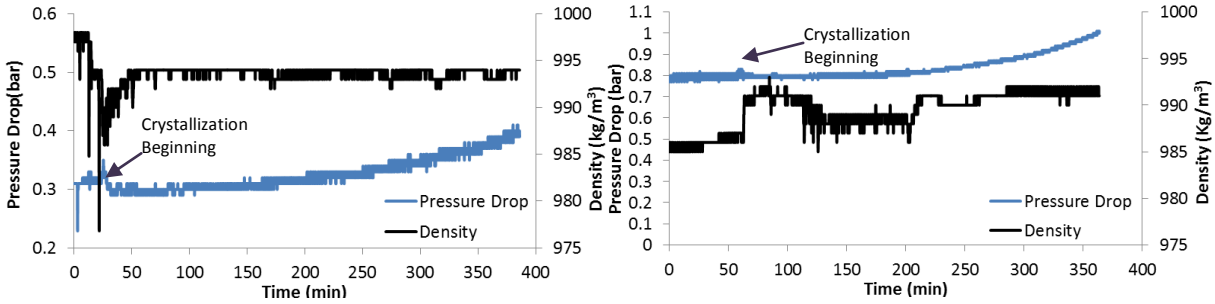

(b) 60% water cut at 200 L.h^{-1} and 400 L.h^{-1}, respectively:

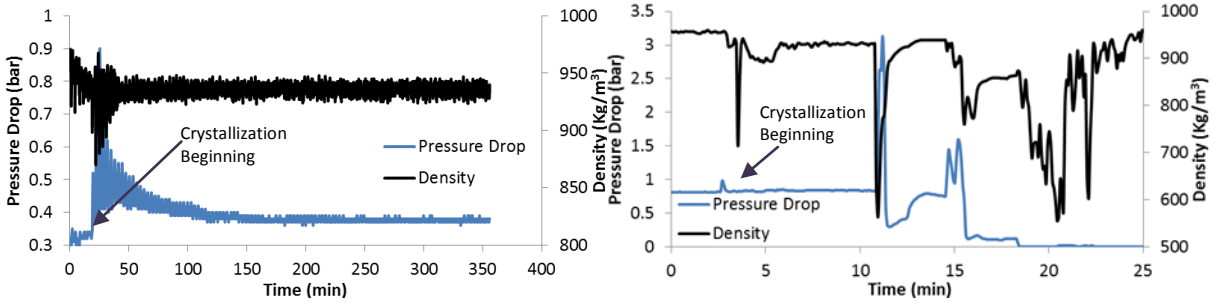

(c) 30% water cut at 200 L.h^{-1} and 400 L.h^{-1}, respectively:

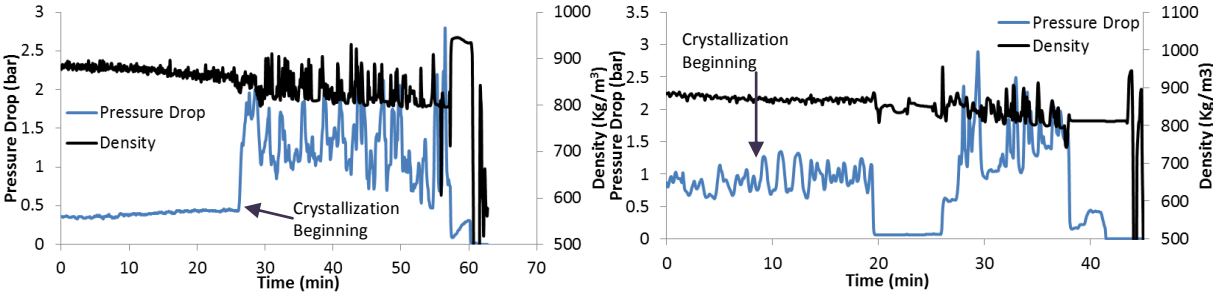

Figure III.9 – Pressure Drop and Density evolution with time during Crystallization at 200 L.h^{-1} and 400 L.h^{-1} for experiments at (a) 90%, (b) 60% and (c) 30% water cut without additive (AA-LDHI).

It can be concluded that hydrate formation kinetic is slower at high water cuts, because there is small amount of oil and smaller water/oil interface. The low solubilization rate of methane in the mixture limits the rate of crystallization.

The slower kinetic at high water cut is reflected in more gradual pressure drop evolution during hydrate formation (Figure III.10 (a)) compared to other water cut groups (Figure III.10 (b) and (c)), both with 200 L.h^{-1} and 400 L.h^{-1}. Decreasing the water cut, the kinetic of hydrate formation becomes

faster, achieving its maximum in experiment at low water cut. These experiments combine large oil amount (increasing the gas solubility) and also larger interfacial area for hydrate formation.

Sometimes volumetric fraction of formed hydrates in experiments at high water cut is higher than in lower water cuts (

Table III.3) due to longer duration of crystallization experiment. However, plug is hardly observed. In high water cut, the aggregates formed by collision between hydrate particles, generally, do not consolidate and do not form agglomerates, because oil is entrapped by hydrate and no more available to dissolve gas. In water dominated systems, the growth rate is also slow due to the small amount of methane dissolved in water phase. As consequence, the aggregates consolidation in agglomerates is less effective. The hydrate plug formation is unlikely at high water cut. In contrast, the possibility of hydrate plugging increases with decreasing water cut, because the consolidation rate is more effective.

The average chord length evolution during hydrate formation (Figure III.10) provides new insights about how hydrates circulate in the flow loop at different flow rates. The observed behavior confirms the conclusions obtained from pressure drop and density measurements. In low flow rate (200 $L.h^{-1}$), hydrates are more prone to circulate in separated groups (packages) even before aggregation (agglomeration) for all water cuts. This is evidenced by the noisy behavior in the average chord length after the beginning of hydrate formation. At high flow rate (400 $L.h^{-1}$), it can be seen that the measurement is not noisy, only becoming disturbed after strong hydrate formation and agglomeration.

As general trend, the kinetic of hydrate formation is faster at higher flow rate, which presents a higher risk of quick hydrate plugging due to the high volume of formed hydrates, even if the suspension is better homogenized compared to lower flow rate where the plugging risk is due to package formation.

In conclusion, there are two main mechanisms for hydrate plugging: from a higher formation rate of a huge hydrate volume (at high flow rate) or from the agglomeration of a small quantity of hydrates into large packages (at low flow rate).

(a) 90% water cut at 200 L.h^{-1} and 400 L.h^{-1}, respectively:

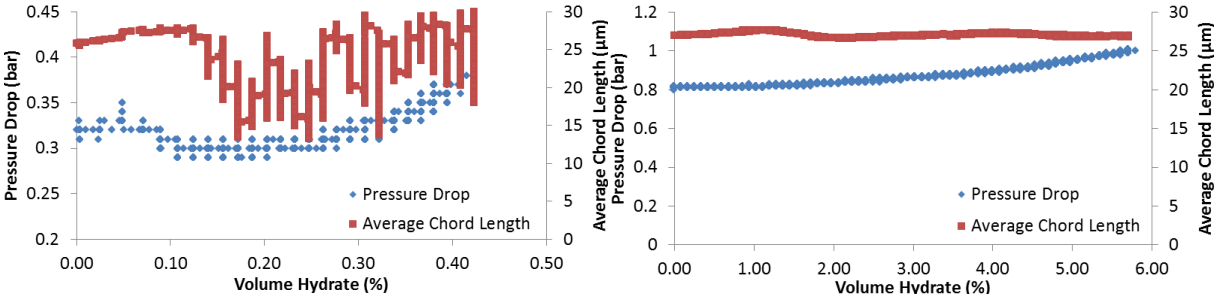

(b) 60% water cut at 200 L.h^{-1} and 400 L.h^{-1}, respectively:

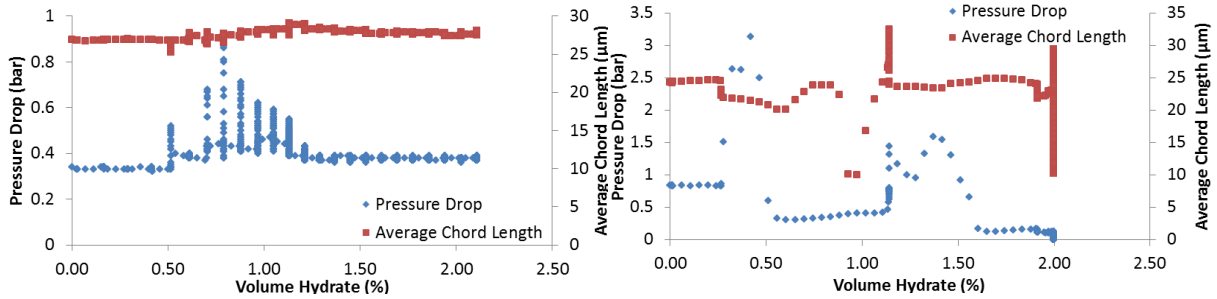

(c) 30% water cut at 200 L.h^{-1} and 400 L.h^{-1}, respectively:

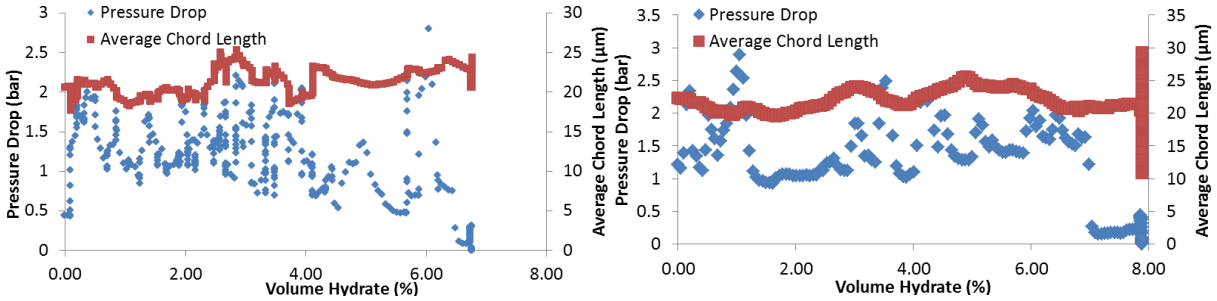

Figure III.10 – Pressure Drop and Average Chord Length evolution during Crystallization at 200 L.h^{-1} and 400 L.h^{-1} for experiments at (a) 90%, (b) 60% and (c) 30% water cut without additive (AA-LDHI).

Table III.3 –Conversion and Volume of Hydrates formed (in percentage) for the Experiments without AA-LDHI.

Water Cut (vol. %)	Flow Rate (L/h)	Conversion (% vs. w)	Volume Hydrate (%)	Plugging
100	200	0.6	0.7	NO
	200	0.6	0.7	NO
	400	2.2	2.6	NO
90	200	2.2	2.5	NO
	400	5.2	5.8	NO
80	200	1.2	1.2	NO
	200	7.8	8.4	NO
	200	0.2	0.2	NO
	400	3.0	3.1	NO
	400	3.0	3.1	NO
70	200	1.3	1.1	YES
	400	7.1	6.6	NO
	400	4.2	3.3	NO
60	200	2.7	2.1	NO
	200	2.3	1.8	NO
	200	3.4	2.6	NO
	400	2.6	2.0	YES
	400	6.3	5.0	NO
50	200	4.4	2.8	NO
	400	6.0	4.1	NO
40	200	19.1	10.5	YES
	400	2.6	1.3	YES
	400	1.9	1.0	NO
30	200	18.2	6.8	YES
	400	22.7	9.4	NO
	400	21.0	7.9	YES

III.2.3 Experiments with Additive AA-LDHI

The focus of experiments presented in this section is the understanding of experimental data evolution considering each water cut group using anti-agglomerant additive (AA-LDHI). Experiments were analyzed in terms of pressure drop, density, volume of hydrate formed (and conversion) and average chord length. Later, these experiments were compared to the blanks. The analysis presented in this section also evidences differences between experiments in different flow rates.

A feedback from the experiments allowed the determination of the best AA-LDHI dosage. At high dosage, it was observed that no experimental data evolution occurred during a day of experiment.

Besides avoiding the agglomeration, the additive was delaying the crystallization beginning, *i.e.*, the AA-LDHI additive also works as kinetic inhibitor. Consequently, no evolution in the measurements was observed. It was perceived that the role of the additive could be studied in two dimensions:

1. The study of the flow when the amount of additive is sufficient to avoid agglomeration and ensure the flow security. In this case, the additive concentration is enough to prevent plugging and, as secondary effect, the crystallization mechanism can be inhibited. These experiments imply long time observations. Consequently, they cannot be done in the *Archimède* flow loop.
2. The study of the additive below its totally effective concentration. In this case, the goal is to analyze different steps of hydrate crystallization in presence of an additive acting to prevent agglomeration. This second dimension of the study concerns aspects of fundamental understanding of crystallization processes.

The second dimension is the one studied in this research. The additive dosage for the set of experiments is under-dosed comparing to real facilities. Although, it is considered *well* dosed concerning the objectives of this study, once:

1. Shear stabilized emulsion and suspension (emulsion after hydrate formation) with AA-LDHI present a smaller average chord length than blanks. This happens due to the fact that the anti-agglomerant, as a surfactant agent, will facilitate the formation of droplets with smaller size. Once hydrates grow at the droplets interface, after hydrate formation the average chord length will remain smaller.
2. The formed hydrates should circulate in the flow loop without causing pipeline plugging (agglomeration in a smaller degree can be observed).

Figure III.11 shows the evolution of pressure drop and density with time during hydrate formation. Following, one example concerning each group of water cut (high, intermediate and low) at 200 $L.h^{-1}$ and 400 $L.h^{-1}$ will be analyzed. In general, these experiments presented an induction time ranging from 20 to 120 minutes, which were always higher than experiments without AA-LDHI. This indicates a secondary kinetic inhibitor after using AA-LDHI.

Although, experiments at same water cut group do not present exactly the same behavior, the data tendency is generally the same, which validates the approach of evaluating experiments by groups of water cut. The presented experiments have the minimum required dosage to

simultaneously observe different crystallization steps and some aspects of the anti-agglomerant effect. Comparing experiments with and without AA-LDHI, it can be observed that plugging can be prevented once additive concentration is enough.

(a) High water cut with AA-LDHI (Figure III.11 (a)):

In general, these experiments followed the same steps than the blanks. The main difference is a smaller conversion ranging from 0.6% to 2.7% (Table III.4) while experiments without AA-LDHI range from 2.2% to 7.8% (Table III.3).

Under effect of anti-agglomerant, the beginning of hydrate formation (nucleation and growth at water/oil interface) corresponds to an increase of the pressure drop slighter than the increase observed for blanks for both flow rates.

A decrease of pressure drop due to re-homogenization is observed in the experiment at flow rate of 200 $L.h^{-1}$. At flow rate of 400 $L.h^{-1}$, the pressure drop increases very slightly after the crystallization beginning. Following it, no decrease is observed. In fact, the pressure drop remains constant until the end of the experiment. This happens because this experiment is kinetically slower than the experiment at 200 $L.h^{-1}$. Thus, there are very few hydrates formed with time (0.6%-0.9%, Table III.4), which does not disturb the mixture organization. In consequence, no re-homogenization occurs. The experiment was repeated and the same tendency was observed. These observations lead to the conclusion that the anti-agglomerant additive leads to some kinetic hydrate inhibitor (KHI) effect.

Regarding the density evolution, the experiment in low flow rate (200 $L.h^{-1}$) presents the same tendency observed for the blanks, where the beginning of hydrate formation corresponds to a steep decrease followed by a steep increase of the density measurement. As hydrate formation continues, the density continues to increase. At the end of the experiment, it slightly overpasses the density values observed before hydrate formation (shear stabilized emulsion without hydrates), which is contrary to what was observed in the blanks due to the morphology of the suspension.

At high flow rate (400 $L.h^{-1}$), only a small density decrease is observed at the beginning of hydrate formation due to the slower kinetic of formation, attaining a value that remains constant until the end of the experiment.

(b) Intermediate water cut with AA-LDHI (Figure III.11 (b)):

As for the other experiments, the beginning of hydrate formation (nucleation and growth at water/oil interface) corresponds to an increase of pressure drop. This behavior is easily observed in the graph of the experiment of 200 $L.h^{-1}$, but hardly detected in the experiment of 400 $L.h^{-1}$ due to

the graph scale. Both experiments follow the same behavior observed for blanks, however, with two important differences:

- At flow rate of 200 $L.h^{-1}$, the time interval from the pressure drop increase until the time that pressure drop achieves its maximum and starts to decrease lasts longer in experiments using anti-agglomerant (80 minutes against 10 minutes without additive). The pressure drop increase corresponds to hydrate nucleation, growth and some agglomeration with hydrates particles circulating in the flow loop in separated package. After the pressure drop decrease, the measured pressure drop is higher than in the one measured in the beginning of the experiment, this corresponds to hydrate deposition after agglomeration. The longer interval observed when anti-agglomerant is used means that the additive postpones the beginning of hydrate deposition, *i.e.*, hydrate agglomeration starts later even if the minimum dosage of anti-agglomerant is used.
- At flow rate of 400 $L.h^{-1}$, the first important remark is the inexistence of pipeline plugging in this experiment, whereas for blanks pipeline plugging was observed. Secondly, it can be noticed that hydrate agglomeration only starts 120 minutes after the beginning of the experiment. For the blank, agglomeration starts a few minutes after beginning of the hydrate formation. One more time, it is possible to detect the anti-agglomerant effect, which makes hydrate agglomeration starts later.

As experiments at high water cut, it can also be observed a slower kinetic of hydrate formation using additive. This can be evidenced by a smaller water conversion into hydrates in a working day of experiment, experiments without AA-LDHI range between 1.3% and 7.1% (Table III.3) of conversion and experiments with AA-LDHI range between 1.6% and 5.6% of conversion (Table III.4).
Concerning the density evolution, it behaves as the blanks for both the flow rates, where the beginning of hydrate formation corresponds to steep decrease followed by steep increase:

- At flow rate of 200 $L.h^{-1}$, there is a disturbed behavior while the formed hydrates circulate as packages in the flow loop. Once hydrate deposition starts to be observed, the remaining solid particles are better dispersed and the density measurement is less noisy.
- At flow rate of 400 $L.h^{-1}$, no disturbed measurement is observed. After the increase due to the gas dissolution, the density keeps almost the same value until the end of the experiment. As hydrates continue to grow and later agglomerate, the density increases as for high water cut.

(c) Low water cut with AA-LDHI (Figure III.11 (c)):

The beginning of hydrate formation (nucleation and growth at the water/oil interface) has the same behavior detected for the corresponding blanks. This first step is characterized by pressure drop increase without subsequent decrease due to mixture re-homogenization due to the high amount of hydrates formed in the first minutes of experiment.

The kinetic of gas consumption and hydrate formation is also faster comparing to other water cut groups thanks to the higher oil content which increases the gas transfer rate. However, no plugging was observed in both flow rates.

- At flow rate of 200 $L.h^{-1}$, the pressure drop evolution immediately after crystallization beginning is similar to the one observed in experiments of the intermediate group, in which the measurement is noisy as consequence of hydrates circulation in packages. Later, the pressure drop starts to increase due to hydrate particles agglomeration instead of decrease and become constant as observed for intermediate water cut. The formed agglomerates continue to flow in low water cut, while hydrate deposition occurs in intermediate water cut. As agglomeration continues, it becomes harder to transport the slurry (around 150 minutes). From this point, a steep pressure drop increase followed by a decrease is detected from time to time; a consequence of the difficulty on keeping the mixture flowing, but no plugging (flow rate close to zero) was detected until the end of the experiment.
- At flow rate of 400 $L.h^{-1}$, the hydrate formation kinetic is slower than at 200$L.h^{-1}$, as observed in the high water cut experiment (Table III.4). In low water cut, gradual pressure drop increase is observed after the onset of hydrate formation. The gradual increase corresponds to hydrates agglomeration. After it, the pressure drop becomes stable with time, which indicates that hydrates started to deposit at the pipeline walls. In this experiment, no significant amount of gas was consumed after 40 minutes of crystallization, which coincides with the onset of the deposition. An interpretation of this event is partial hydrate deposition in the separator, which can work blocking the gas transfer to liquid phase. Consequently, the gas solubilization into the mixture is undermined, which takes the system out of the supersaturated zone and the formation of hydrates will stop. This is reflected in a lower water conversion into hydrates (Table III.4), in a system that normally has higher conversion due to the high amount of oil which normally enhances the gas transfer, as seen in the blanks.

Regarding the density evolution, it is observed the same characteristics than for high and intermediate water cuts.

(a) 90% water cut, 0.005% AA-LDHI at 200 L.h^{-1} and 400 L.h^{-1}, respectively:

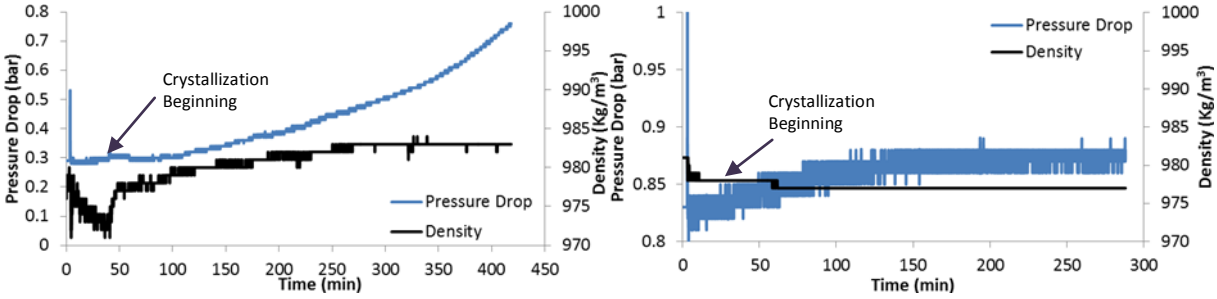

(b) 60% water cut, 0.01% AA-LDHI at 200 L.h^{-1} and 400 L.h^{-1}, respectively:

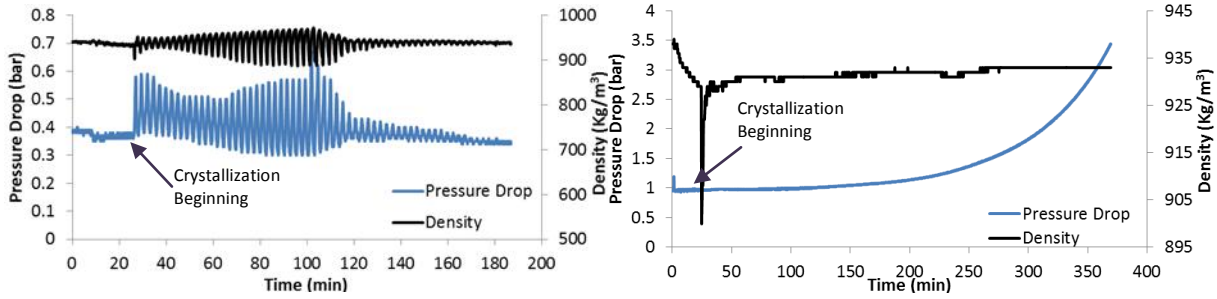

(c) 30% water cut, 0.05% at 200 L.h^{-1} and 400 L.h^{-1}, respectively:[1]

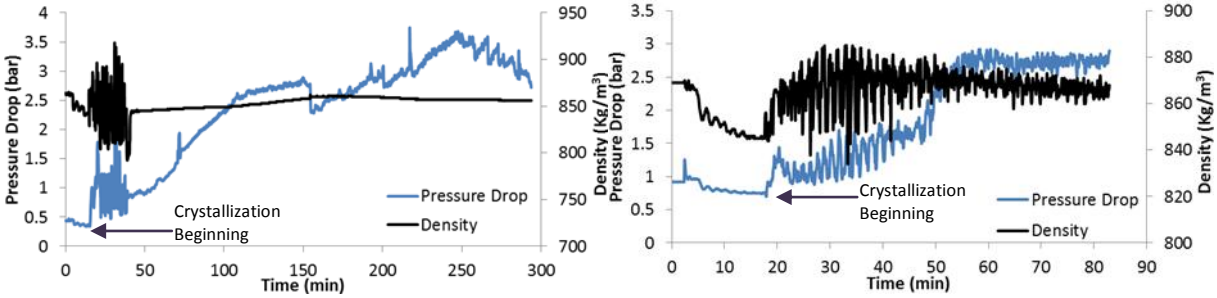

Figure III.11 – Pressure Drop and Density evolution during Crystallization at 200 L.h^{-1} for experiments at (a) 90%, (b) 60% and (c) 30% water cut with additive (AA-LDHI).

From the last analysis, the following main conclusions can be withdrawn:

(1) At a very low dosage, the anti-agglomerant additive (LDHI) is able to avoid hydrate agglomeration until a certain percentage of hydrate volume. This value varies with the water cut and with the dosage of AA-LDHI. For the experiment with water cut of 60% at

400 L.h-1 and AA-LDHI dosage of 0.01%, agglomeration was avoided until the formation of hydrate volume of 2.5% (Figure III.11).

(2) It was observed that the agglomeration beginning was postponed comparing to blanks. Even with agglomeration, this event did not lead to pipeline plugging after a day of experiment.

(3) The additive acts as a kinetic inhibitor, delaying and reducing the quantity of hydrate formed (Table III.4) in comparison with experiments in Table III.3 when no AA-LDHI was used.

(4) In general, the amount of oil provided is directly related to the methane solubilization and to the hydrate formation as for the blanks. Exceptionally, the experiment with 30% water cut and 400L.h^{-1}.

Regarding the average chord length evolution during hydrate formation (Figure III.12), the same behavior observed for the blanks is detected in experiments with AA-LDHI. At flow rate 200 L.h^{-1}, the hydrates are prone to circulate in separated groups (packages). However, this event seems to be less important in experiments with additive, probably because few agglomerates are formed. The measurement is more linear at high flow rate (400 L.h^{-1}), which indicates better dispersion.

After studying experiments without and with AA-LDHI, it can be perceived that generally the average chord length does not give a precise evaluation concerning the methane hydrate formation. Sometimes hydrate formation results in an increase of the average chord length. Nevertheless, for the majority of the experiments little variation is observed during hydrate formation processes. The problem is that the average can hide events related to the crystallization. For this reason, a better analysis shall be done through the study of the chord length distribution with time, which will be the subject of Chapter IV.

(a) 90% water cut, 0.005% AA-LDHI at 200 L.h^{-1} and 400 L.h^{-1}, respectively:

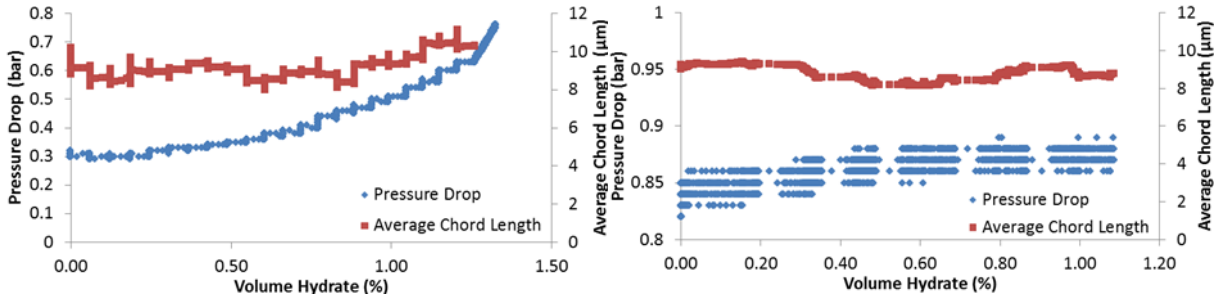

(b) 60% water cut, 0.01% AA-LDHI at 200 L.h^{-1} and 400 L.h^{-1}, respectively:

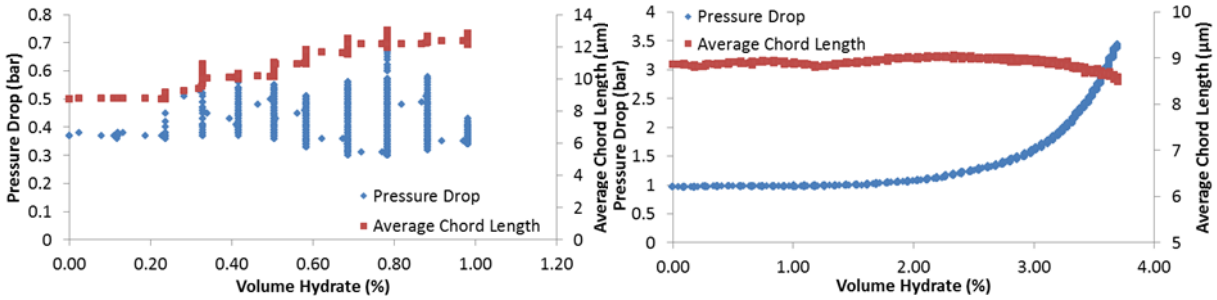

(c) 30% water cut, 0.05% AA-LDHI at 200 L.h^{-1} and 400 L.h^{-1}, respectively:

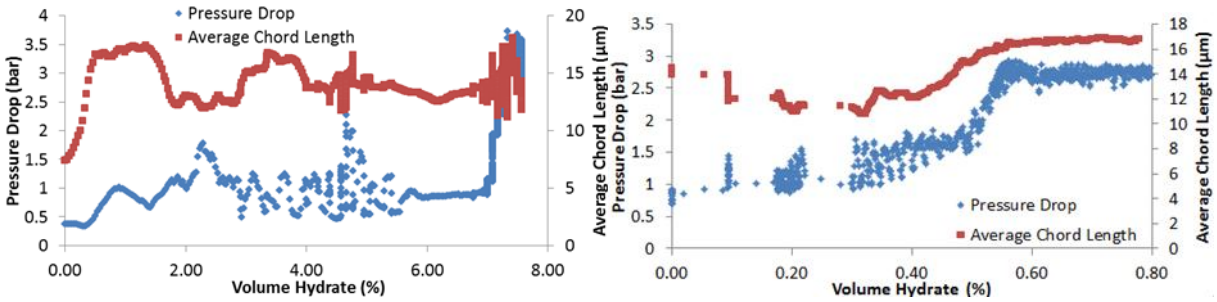

Figure III.12 – Pressure Drop and Average Chord Length evolution during Crystallization at 200 L.h^{-1} and 400 L.h^{-1} for experiments at (a) 90%, (b) 60% and (c) 30% water cut with additive (AA-LDHI).

Table III.4 – Conversion and Volume of Hydrates formed (in percentage) the Experiments with AA-LDHI.

Water Cut (%)	Flow Rate (L/h)	Additive (%)	Conversion (% vs. w)	Volume Hydrate (%)	Plugging
90	200	0.005	1.2	1.3	NO
	400	0.005	0.9	1.1	NO
	400	0.005	0.6	0.7	NO
80	200	0.005	2.7	2.8	NO
	400	0.005	0.7	0.7	NO
70	200	0.01	1.6	1.4	NO
	400	0.01	5.6	5.1	NO
60	200	0.01	1.3	1.0	NO
	400	0.01	4.8	3.7	NO
50	200	0.1	0.9	0.4	NO
	200	0.01	1.4	0.9	NO
	400	0.01	4.1	2.6	NO
40	200	0.01	9.6	5.0	YES
	400	0.01	16.3	8.8	YES
	400	0.05	15.2	8.3	NO
30	200	0.05	2.9	1.1	NO
	200	0.05	18.8	7.6	NO
	400	0.05	2.1	0.8	NO

III.3 Rheological Comparison between Shear Stabilized Emulsion and Suspension

The rheological study was performed for every shear stabilized emulsion tested in the *Archimède* flow loop and for some of the formed suspensions after crystallization. The objective is to enhance the comprehension about the transport of liquid-liquid dispersions and suspensions in the flow loop. The rheological study consists in varying the flow rate and measuring the pressure drop, which allows to calculate the friction factor (f) and determine the flow regime. Also, the viscosity can be calculated from the pressure drop in laminar regime. The rheological study was not performed for all suspensions due to the time limitation of one day per experiment.

Considering each water cut group, experimental results of the rheological study after homogeneous and stable emulsion formation under flow are shown in Figure III.13 (without additive) and Figure III.14 (with additive).

A standard behavior was detected, for all experiments (without additive) at high and intermediate water cuts:

- at the highest flow rate (400 $L.h^{-1}$) the flow is turbulent,
- at the intermediate flow rates (300 $L.h^{-1}$ and 200 $L.h^{-1}$) the flow is in the transition zone,
- at the lowest flow rate (100 $L.h^{-1}$) the flow is laminar.

At low water cut, it is easier to this system to enter in the laminar regime as more oil is present. This is related to the shear stabilized emulsion viscosity, which is higher at low water cut due to higher content of Kerdane® (more viscous than the water). Consequently, the transition from laminar to turbulent regime requires higher flow rates for shear stabilized emulsions with high and intermediate water cuts. For instance, the system is already in the transition zone for the highest flow rate (400 $L.h^{-1}$). The calculated viscosities in the laminar regime are shown in Table III.5.

Concerning experiments with additive (Figure III.14), the first difference noticed is the presence of more points in laminar regime comparing to the blanks. This behavior is highlighted in experiments at intermediate and low water cuts, which have higher additive dosage. This means that the additive forms more viscous shear stabilized emulsions (Table III.5), because droplets are better dispersed in the shear stabilized emulsion continuous phase due to the use of additive. Therefore, it

can be observed that the experiment at low water cut is almost completely in the laminar zone, except in the highest flow rate (400 $L.h^{-1}$). For intermediate water cut, only the two highest flow rates (400 $L.h^{-1}$ and 300 $L.h^{-1}$) are in the transition zone. Finally, for high water cut, it is detected the same tendency observed for blanks, where the system is more viscous due to the higher amount of oil, with a small shift to the laminar regime due to the better dispersion of the droplets.

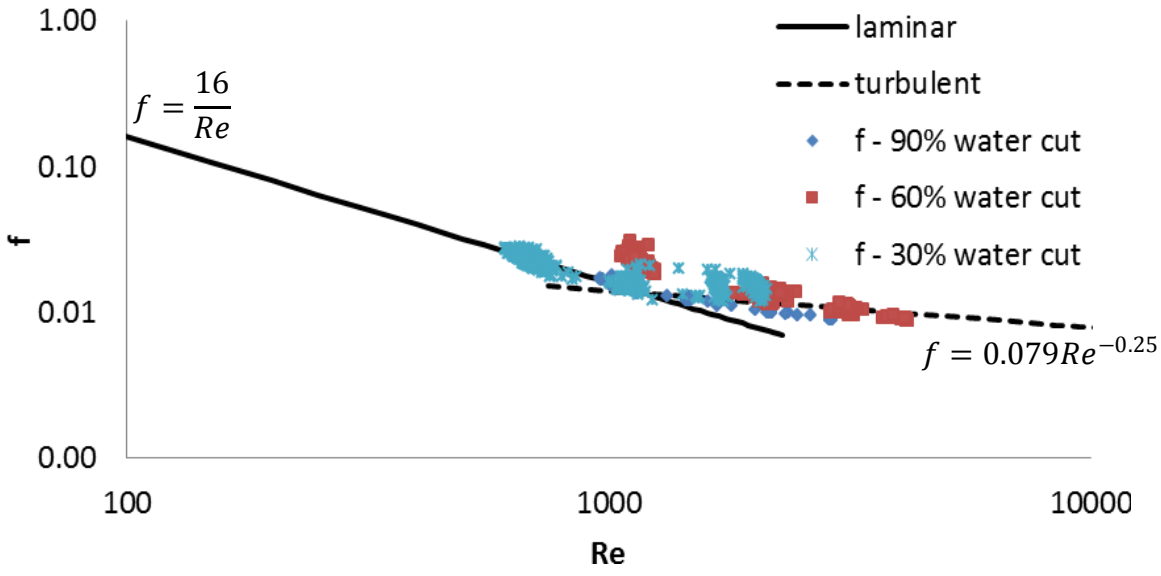

Figure III.13 – Rheological study after emulsification for experiments without AA-LDHI.

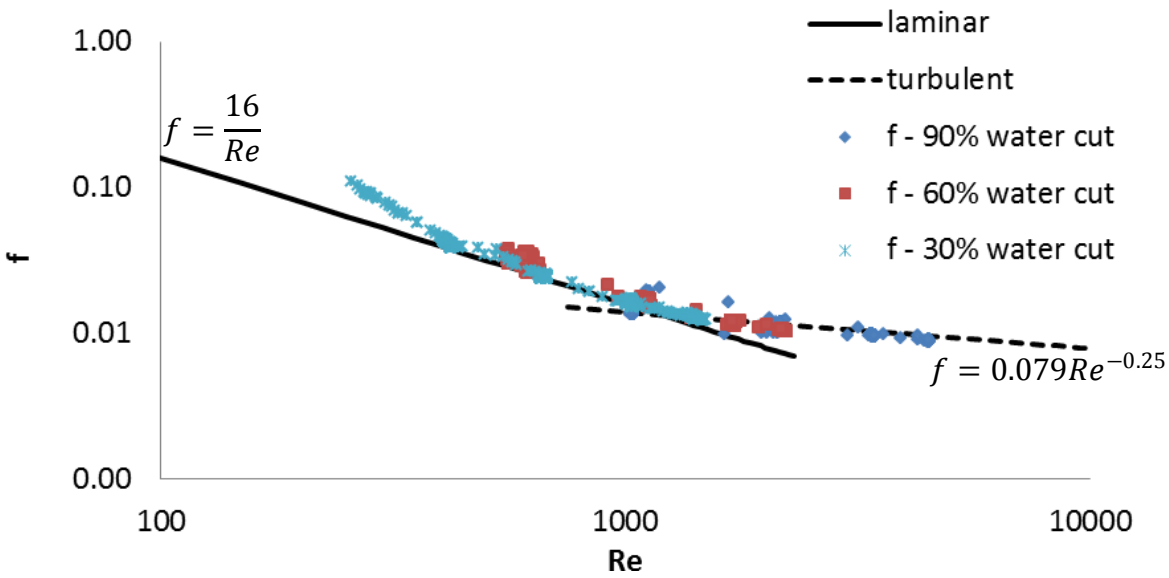

Figure III.14 – Rheological study after emulsification for experiments with AA-LDHI.

The viscosity was calculated from the experimental results by the method described in section II.3.2. In order to validate these results, the viscosity was also calculated (Table III.5) using the equation developed by Pal & Rhodes (Equation I.7, page 30) which is only dependent on the fraction of the dispersed phase, thus presenting the same value for experiments with and without AA-LDHI. The goal was to determine the continuous phase by judging the best fit between experimental and calculated viscosities, because Pal & Rhodes equation distinguishes the behavior for oil or water continuous phase.

The calculated viscosity by Pal & Rhodes equation presents good fit for experiments at high water cut (90% and 80%) when the calculation is done considering water continuous systems. For the experiment at the lowest water cut (30%), the opposite behavior is observed, *i.e.*, the equation fits well the experimental data when is done considering oil continuous systems. The other experiments, mainly at intermediate water cut, do not present a good fit, because Pal & Rhodes equation considers that droplets are well-dispersed and present a spherical shape, which is not the case when a free phase of water or oil exists.

Table III.5 – Experimental and Calculated (considering water dispersed and oil dispersed systems) viscosity without hydrate formation for experiments with and without AA-LDHI.

Water Cut (%)	Experimental Viscosity – without AA-LDHI (mPa.s)	Experimental Viscosity – with AA-LDHI (mPa.s)	Calculated Viscosity (mPa.s) – oil continuous	Calculated Viscosity (mPa.s) – water continuous
90	5.2	4.5	360374.5	**4.1**
80	6.3	5.3	561.2	**5.8**
70	5.7	6.1	109.8	**8.4**
60	5.7	6.7	41.3	**13.2**
50	5.8	7.1	**20.5**	**22.7**
40	6.4	5.7	**11.9**	45.7
30	5.9	8.9	**7.6**	121.6

After crystallization, the presence of hydrates suspended in the shear stabilized emulsion (slurry) changes the rheological behavior of the system by increasing the viscosity. As consequence, the friction factor is shifted in the laminar zone. Regarding water cuts analyzed in Figure III.15 and Figure III.16 (without and with additive, respectively), a laminar behavior is observed even for the highest flow rate (400 $L.h^{-1}$). In Figure III.16, it is interesting to notice, how greatly the points are displaced into the laminar regime in the rheological study concerning the experiment in which the hydrate

formation was performed at 200 L.h^{-1}. This is consequence of the higher fraction of hydrate formed in this experiment (7.6%, Table III.4), that increases the mixture viscosity and enhances the difficulty of transporting the formed slurry.

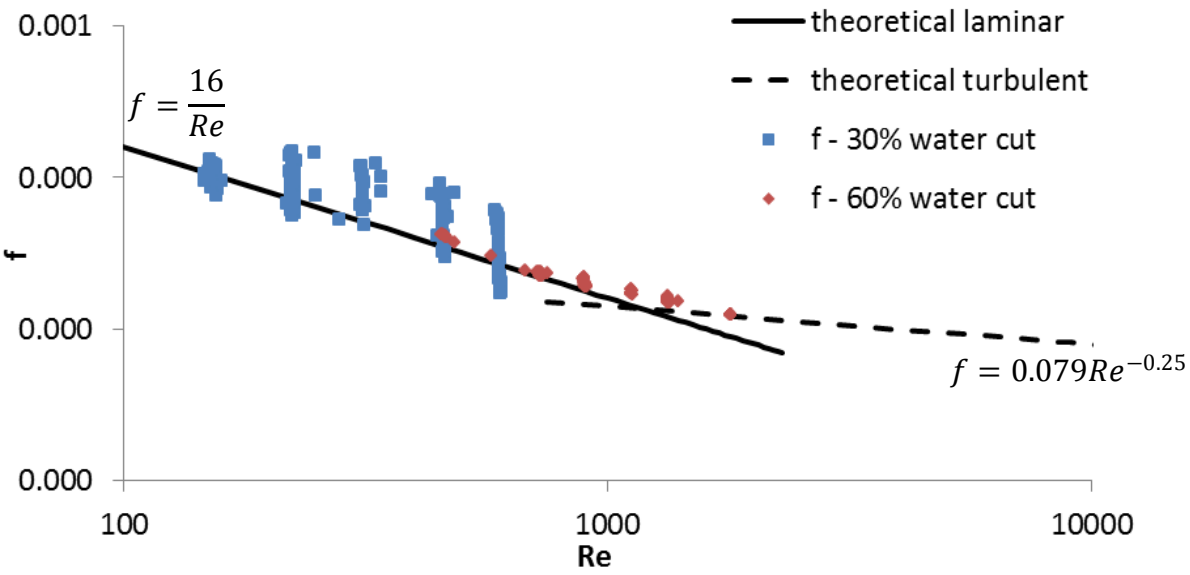

Figure III.15 – Rheological study after crystallization for experiments with 30% and 60% water cut without AA-LDHI at 200 L.h^{-1}.

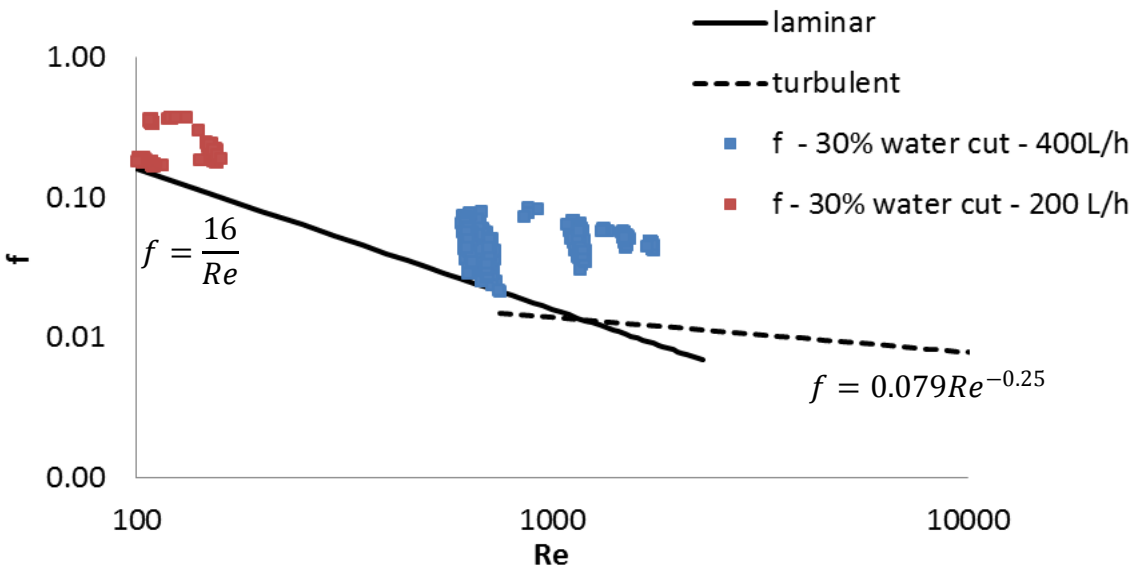

Figure III.16 - Rheological study after crystallization for experiments with 30% water cut with AA-LDHI at 200 L.h^{-1} and 400 L.h^{-1}.

III.4 Conclusions

This chapter presents an overall analysis of experimental results concerning the parametric study of shear stabilized emulsion and hydrate formation (without and with AA-LDHI) performed at the *Archimède* flow loop. Three main groups of behavior were identified (high, intermediate and low water cuts) and analyzed in each section.

Data concerning pressure drop, density, chord length distribution and PVM images for shear stabilized emulsions formation before hydrate crystallization allowed a better understanding about the emulsification process. However, further studies must be performed to better understand the emulsification mechanism. All emulsions were homogeneous and stable under flow before each experiment of crystallization. Even if it has been observed that locally the system can contain free water/oil phase especially at low flow rate.

The dispersed phase is better distributed in the continuous phase by increasing the flow rate through the shear increase. The droplets dispersion can be stabilized by use of an anti-agglomerant additive which increases the emulsion stability under flow by its surfactant effect.

Results concerning the coefficient of gas transfer (K_{la}) showed a link between higher and faster pressure decrease during gas solubilization before hydrate formation and further occurrence of hydrate formation.

In order to summarize all conclusions in one graph, Figure III.17 shows the K_{la} (blue line), the shear stabilized emulsion behavior (represented by the oil/water surface, red line) and the hydrate formation rate (green line) evolution with the water cut.

By increasing the water cut and consequently decreasing the fraction of oil, the K_{la} decreases because methane gas presents higher solubility in hydrocarbon phase than in water. This behavior is detected both in presence and absence of AA-LDHI.

The oil/water surface represents the place where hydrates will nucleate and starts to grow. In experiments without AA-LDHI, it is low at very low water cut and rises softly as the number of dispersed droplets increases. After achieving its maximum, it starts to decrease rapidly as the system enters in the intermediate water cut, because large droplets are formed (representing free phase).

After entering in the high water cut zone, the decline is softer, because the free phase becomes less and less important.

The oil/water surface in experiments in presence of AA-LDHI is more important than in experiments without AA-LDHI due to the formation of smaller droplets. In these experiments, when free phase starts to form at intermediate water cut, the oil/water surface presents a pronounced decrease.

Concerning the rate of hydrate formation without AA-LDHI, it increases gently at very low water cut when the quantity of water available in the system is very low. Once the quantity of water increases, hydrates nucleation and growth are faster, mainly between 30% to 50% water cut. Two main factors contribute to this behavior: (1) droplets are numerous and well distributed in the continuous phase and (2) oil is present in a high amount, which means that the amount of gas transferred to the liquid phase and available to form hydrates is higher.

The rate of hydrate formation decreases when entering in the intermediate zone (water cut higher than 50%). Firstly, because water is present in a higher amount than oil, consequently, the gas transfer to the liquid phase is weaker. Secondly, the appearance of larger droplets decreases the surface to nucleate and to grow hydrates. The rate of formation decreases more softly after entering in the high water cut zone. The decrease continues to occur because fewer droplets are present in a system containing a high amount of water, even if softly because these droplets are better dispersed.

The rate of hydrate formation for experiments with AA-LDHI is less important than the one observed for experiments without AA-LDHI mainly due to the secondary effect of the additive, which works as kinetic inhibitor.

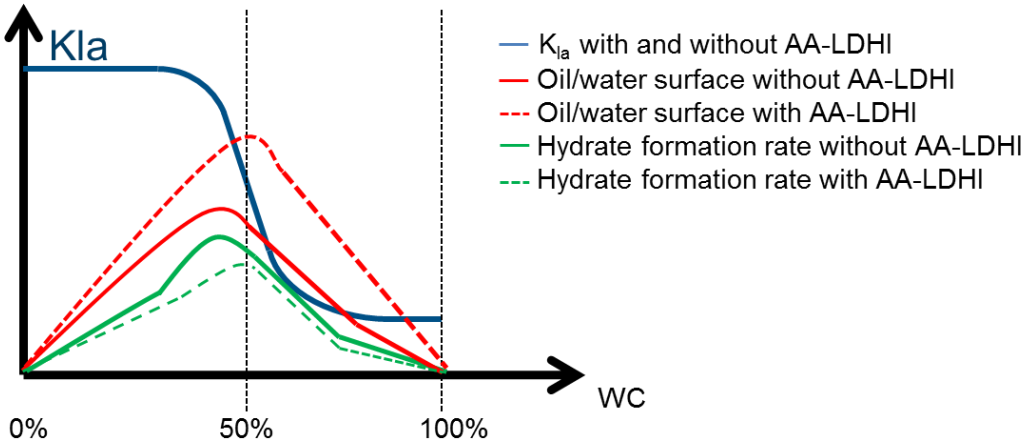

Figure III.17 – Gas transfer coefficient (Kla, blue line), shear stabilized emulsion behavior (oil/water surface, red line) and hydrate formation rate (green line) evolution with the water cut.

III.5 Chapter Highlights in French – Aperçu du Chapitre III

Le processus de formation d'hydrates varie en fonction des conditions expérimentales (par exemple, fraction d'eau, débit, présence / absence d'additif). Le chapitre III a présenté les résultats et analyses expérimentales pour les différentes conditions dans lesquelles les expériences ont été réalisées. Le chapitre était divisé en trois sections : émulsion stabilisée par cisaillement et étude rhéologique (§ III.1), cristallisation d'hydrates (§ III.2) et comparaison entre la rhéologie de l'émulsion stabilisée par cisaillement et de la suspension (§ III.3). Afin de faciliter la compréhension des résultats présentés, les sections présentent des expériences représentatives de trois groupes majeures à forte (90%), intermédiaire (60%) et faible (30%) fraction d'eau. Chaque groupe de fraction d'eau (forte, intermédiaire et faible) est représentatif des trois principaux comportements observés parmi les expériences réalisés dans ce travail. Chaque section a présenté une comparaison entre les blancs et les expériences avec additif AA-LDHI, y compris les différences observées en faisant varier le débit d'écoulement.

Les données concernant la perte de charge, la densité, la distribution de longueur de corde et les images de la sonde microscopique obtenues pendant la formation des émulsions stabilisées par cisaillement (avant la cristallisation d'hydrates) ont permis une meilleure compréhension du processus d'émulsification (§ III.1). Toutes les émulsions étaient homogènes et stables en écoulement avant chaque expérience de cristallisation. Il a été observé que, localement, le système peut contenir une phase huile / eau libre demixée, en particulier à faible débit. Par conséquent, d'autres études doivent être effectuées pour mieux comprendre le mécanisme d'émulsification.

Dans la section § III.1, il a été observé que la phase dispersée est mieux répartie dans la phase continue en augmentant la vitesse d'écoulement, donc par augmentation du cisaillement. La dispersion des gouttelettes peut être stabilisée par l'utilisation d'un additif anti-agglomérant (LDHI) qui augmente la stabilité en écoulement de l'émulsion par son effet secondaire tensio-actif.

Les résultats concernant le coefficient de transfert de gaz (K_{la}) dans la section § III.2.1 montrèrent un lien entre une diminution de pression plus élevée et rapide au cours de la solubilisation du gaz avant la formation d'hydrates de gaz et l'occurrence par la suite de la formation d'hydrates.

Afin d'illustrer toutes les conclusions obtenues avec ce Chapitre dans un graphe, la figure III.16 montre l'évolution du K_{la} (ligne bleue), du comportement de l'émulsion stabilisée par cisaillement

(représenté par la surface huile / eau, ligne rouge) et du taux de formation des hydrates (ligne verte) en fonction de la fraction d'eau.

En augmentant la fraction d'eau et en diminuant par conséquence la fraction de l'huile, le K_{la} diminue parce que le gaz méthane présente une solubilité plus grande dans la phase hydrocarbure que dans l'eau. Ce comportement est détecté à la fois en présence et en l'absence de AA-LDHI.

La surface huile / eau représente l'endroit où les hydrates vont commencer à nucléer et à croître. Dans les expériences sans AA-LDHI, l'évolution est faible à très faible fraction d'eau et monte doucement avec l'augmentation du nombre de gouttelettes dispersées. Après avoir atteint son maximum, elle commence à diminuer rapidement à partir du moment où le système entre dans la zone de fraction d'eau intermédiaire, parce que des grandes gouttelettes sont formées (représentant la phase libre). Après avoir entrée dans la zone de forte fraction d'eau, la diminution est plus douce, parce que la phase libre devient de moins en moins importante.

La surface huile / eau dans les expériences en présence de AA-LDHI est plus importante que dans les expériences sans AA-LDHI en raison de la formation de gouttelettes plus petites. Dans ces expériences, lorsque la phase libre commence à se former à fraction d'eau intermédiaire, la surface de eau / huile présente une diminution prononcée.

Concernant le taux de formation d'hydrate sans AA-LDHI, elle augmente doucement à très faible fraction d'eau parce que la quantité d'eau disponible dans le système est très faible. Une fois que la quantité d'eau augmente, la nucléation et la croissance d'hydrates sont plus rapides, principalement entre 30% à 50% de fraction d'eau. Deux facteurs principaux contribuent à ce problème: (1) les gouttelettes sont nombreuses et bien réparties dans la phase continue et (2) l'huile est présente en grande quantité, ce qui signifie que la quantité de gaz transféré vers la phase liquide et disponible pour former des hydrates est plus élevée.

Le taux de formation d'hydrates diminue quand le système entre dans la zone intermédiaire (fraction d'eau supérieure à 50%). Tout d'abord, parce que l'eau est présente en une quantité supérieure à l'huile, par conséquent, le transfert de gaz vers la phase liquide est plus faible. D'autre part, l'apparition de gouttelettes plus grosses diminue la surface de nucléation et de croissance des hydrates. Le taux de formation diminue plus doucement après être entré dans la zone de forte fraction d'eau. La diminution continue à se produire, car moins de petites gouttelettes sont

présentes dans un système contenant une grande quantité d'eau, même si très doucement parce que ces gouttelettes sont mieux dispersés.

Le taux de formation d'hydrates concernant les expériences avec AA-LDHI est moins important que celui observé pour les expériences sans AA-LDHI principalement en raison de l'effet secondaire de l'additif, qui fonctionne comme inhibiteur cinétique de la formation d'hydrates.

Chapter IV – Model for Under Flow Crystallization of Methane Hydrate Formation from Shear Stabilized Emulsion Systems

"The most exciting phrase to hear in science, the one that heralds the most discoveries, is not Eureka! (I found it!), but 'That's funny...'"(Isaac Asimov)

The previous chapter showed how the understanding of hydrate formation depends on the comprehension of emulsion systems from which hydrates will be formed. Two behavior models were developed comprising shear stabilized emulsion and hydrate formations without free gas phase: the first without anti-agglomerant and the second with anti-agglomerant.

Topological models presented in this chapter are supported by experimental results presented in Chapter III together with PVM and FBRM results here presented. For this reason, a detailed analysis of the chord length distribution results (§IV.1) and PVM images (§IV.2) will be presented aiming to deduce the continuous phase (§IV.1) and the wettability (§IV.3). Finally, the topological models (§IV.4) will be described.

IV.1 Chord Length Distribution – Hydrate Formation

The process of hydrate formation can be evaluated by analysis of the chord length distributions (CLDs) measured using the FBRM probe. The classical way to represent the chord length distribution (Figure IV.1 and also presented in § II.1.1.7) hampers its analysis, thus a different method of analysis will be here described. The CLDs measured in this study have detached three important chord lengths grouping of classes. A more precise way to analyze the results is achieved by separating the chord lengths into these three groups (Figure IV.2). The first one corresponding to chords lower than 10 µm, this class detects hydrates detached from the water/oil interface after nucleation and some growth. The second class presents chords between 10 µm and 100 µm: it corresponds to the detection of not-converted and converted droplets and first agglomerates. The last class presents chords larger than 100 µm, which corresponds to the detection of large agglomerates. The quantity of chords in the larger class was very low for all experiments; hence, this measure will be presented in the secondary axis. In Figure IV.2**,** IV.3 and IV.5, the bar indicates the crystallization beginning.

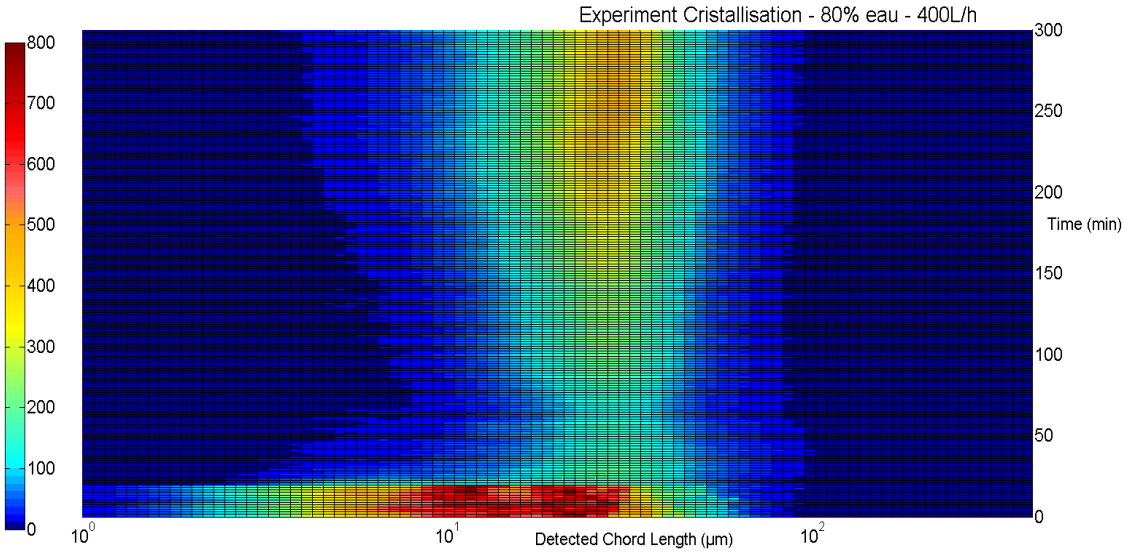

Figure IV.1 - Chord Length Distribution (Experiment at 80 % water cut and 400L/h without AA-LDHI)

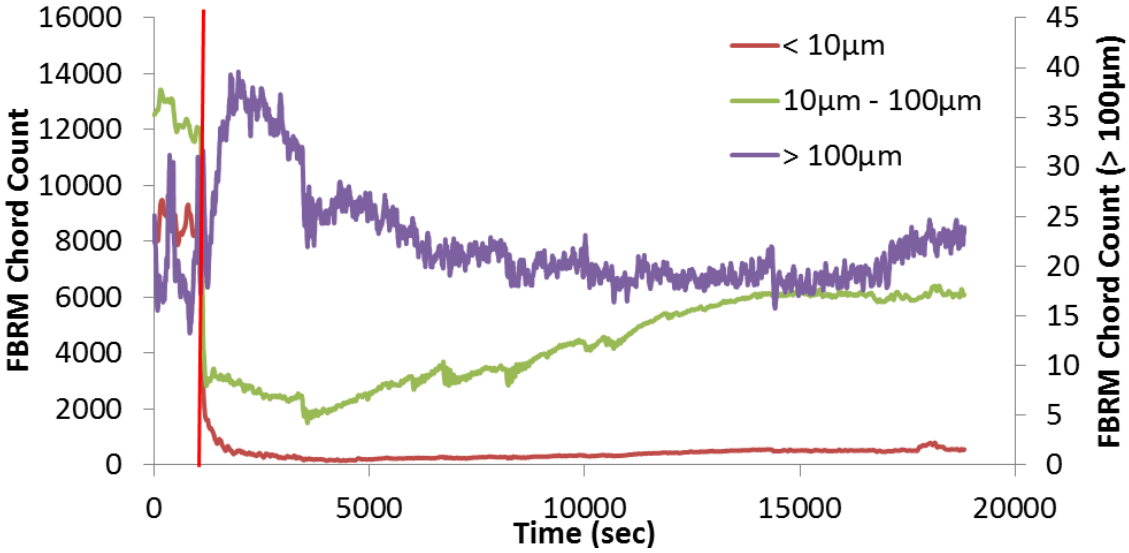

Figure IV.2 – Chord Length Distribution (Experiment at 80 % water cut and 400L/h without AA-LDHI)

Experimental results obtained during the hydrate formation without AA-LDHI will be discussed in section §IV.1.1. Following, experimental results with AA-LDHI will be discussed in section §IV.1.2. A major advance obtained from detailed FBRM data analysis is the determination of the continuous phase, which is of great importance to calculate the wettability (§IV.3) as well as to develop the hydrate crystallization model from shear stabilized emulsion systems (§IV.4).

IV.1.1Experiments without Additive AA-LDHI

In hydrate systems without AA-LDHI, the shear stabilized emulsion changes from oil continuous to water continuous as the water cut increases. From experimental analysis developed in Chapter III, three different groups of behavior were identified (high, intermediate and low). These groups represent three different routes of crystallization. The determination of the continuous phase improved the understanding about hydrate formation processes. Three types of shear stabilized emulsions (water continuous, oil continuous and water continuous with free oil phase) were identified using the FBRM probe (Figure IV.3) and later confirmed by PVM analysis (§IV.2).

During the birth of the first hydrate crystals (nucleation and growth), the number of chord lengths measured by the FBRM in the intermediate class (between 10 and 100 µm) decreases for high and intermediate water cuts (Figure IV.3 (a) and (b)).

The observed decrease in the FBRM measurement for high and intermediate water cuts (Figure IV.3 (a) and (b) and Figure IV.4 (a)) is used as method to identify the continuous phase, once the same behavior is not observed for experiments with oil continuous phase (at low water cut). This is probably consequence of water molecules organization around the *guest* molecule before forming the first methane hydrate crystals (Ribeiro & Lage, 2008; Sloan & Koh, 2007). These arrangements probably change the reflective characteristics of the system, changing the measured number of chord length by the FBRM Probe. Experiments performed by Turner et al. (2005) showed that the number of detected particles using the FBRM depends on the particles reflection. Consequently, it is possible to infer that this measure will also be influenced by the reflective characteristics of the system (external phase).

Experiments with oil continuous phase (Figure IV.3 (c) and Figure IV.4 (b)) do not present the decrease on the number of chord lengths measured around the nucleation step. This happens because there is no change in the external phase before methane hydrates formation. This is a new and major advance on the use of FBRM probe to understand the shear stabilized emulsion. In fact, the change or no-change in the number of measured chord lengths before nucleation gives the nature of the shear stabilized emulsion:

- If the number is decreased, the shear stabilized emulsion is oil-in-water.
- If the number is stable or increased, the shear stabilized emulsion is water-in-oil.

These tendencies are resumed graphically in Figure IV.4, based on the standard evolution of the intermediate chord length class, both to water and oil continuous cases.

Even though high and intermediate water cuts present water as continuous phase, they can be differentiated from each other. At intermediate water cut, the highest class (> 100 µm) presents a steep increase in the beginning of crystallization (Figure IV.3 (b)) due to hydrate formation at the oil/water interface of large oil droplets (stated as free oil phase). These large oil droplets are hardly detected by the FBRM before hydrate formation, since their sizes exceed the upper limit of the probe measurement (3 mm) and also because they are present in low concentration. However, they can be observed by the PVM probe (§IV.2). Once hydrates start to form at these interfaces, these droplets can be more easily detected by the FBRM probe due to the modification of their optical properties. Because hydrates do not completely cover these large droplets, as consequence, they present an underestimated size.

(a) High water cut (90%, 200 L.h^{-1}), beginning of the crystallization at 1400s.

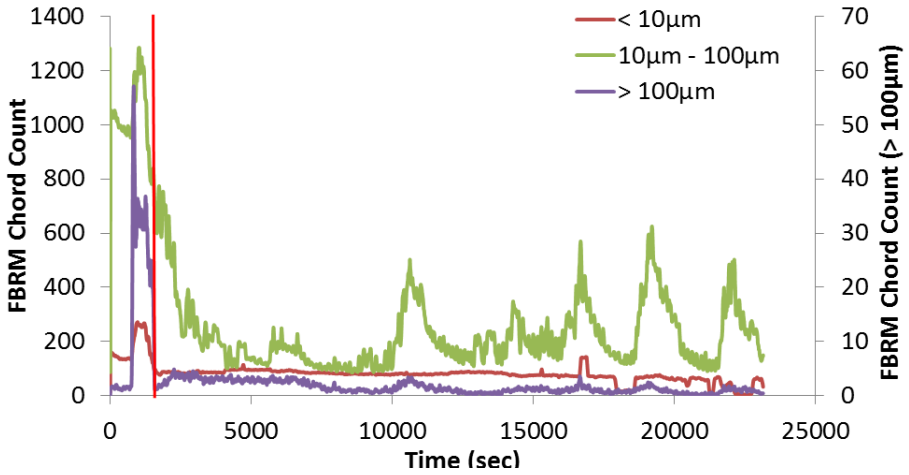

(b) Intermediate water cut (70%, 400 L.h^{-1}), beginning of the crystallization at 5300s.

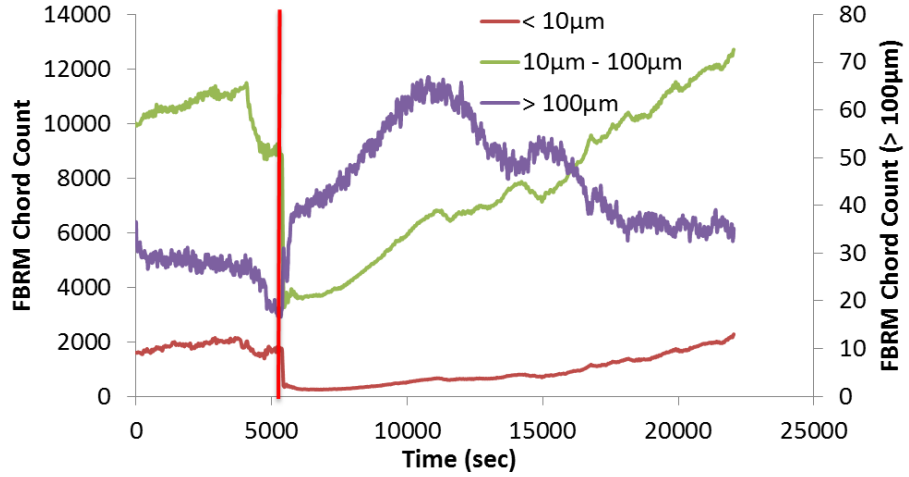

(c) Low water cut (30%, 400 L.h^{-1}), beginning of the crystallization at 1140s

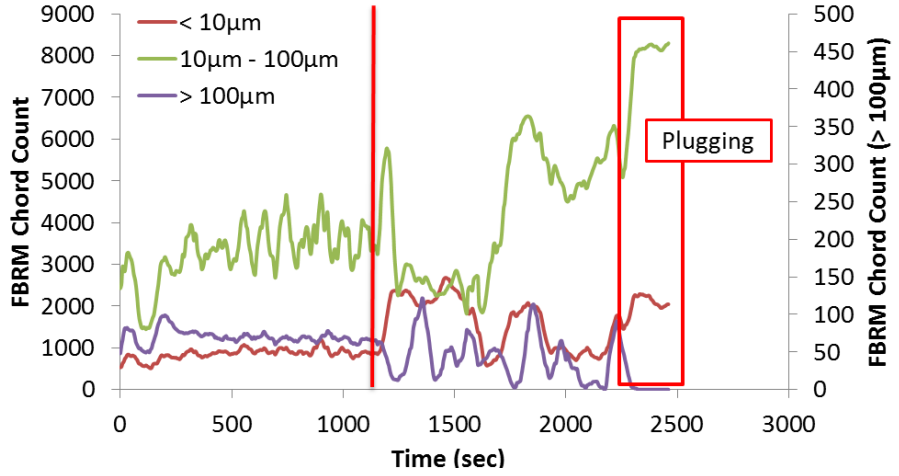

Figure IV.3 – FBRM Chord Length measurements in function of time for some tests with AA-LDHI.

(a) Water continuous

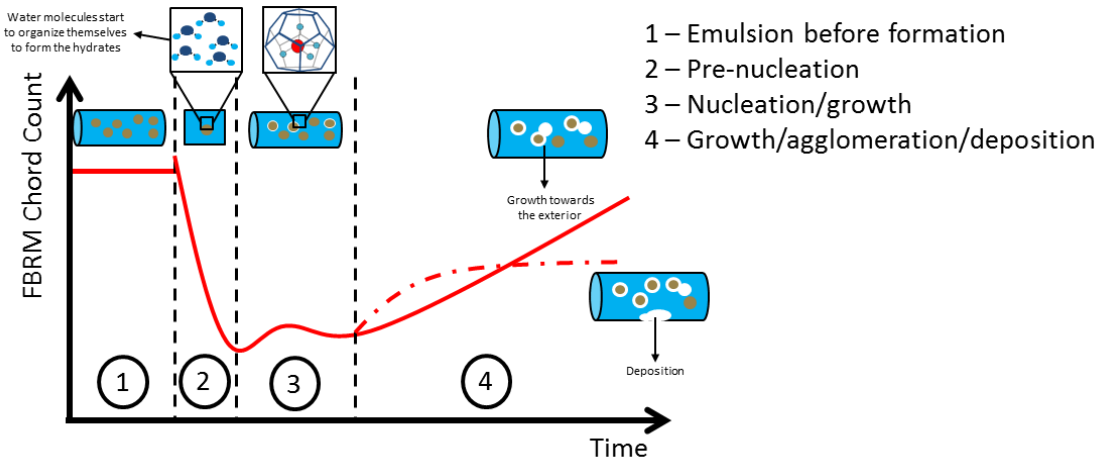

(b) Oil continuous

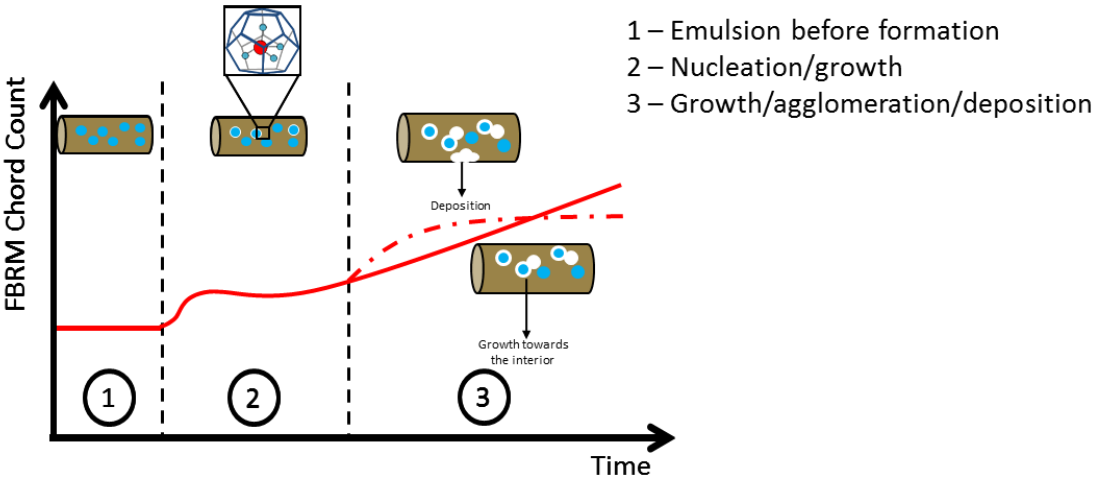

Figure IV.4 – Expected chord length behavior of the intermediate class (10-100 µm) for water and oil continuous without AA-LDHI.

Water Continuous Phase

The beginning of crystallization is accompanied by a decrease number of chords measured in the intermediate grouping of classes (10-100µm, Figure IV.4 (a)) which confirms that the continuous phase is water. Then, the growth occurs around droplets outwardly.

For intermediate water cut, crystallization occurs at the droplets interface, but also at the interface of free oil phase, related to the largest classes (> 100µm). Hydrates can grow at the free oil phase interface justifying why the number of chords related to this group increases after the crystallization beginning. If hydrates grow beyond the limit of detection of the FBRM probe, they

stop to be measured. This explains the decrease later observed for the largest classes (> 100µm). Another possible reason to explain this decrease is to consider the hydrates detachment from the free oil phase interface. Detached hydrates can be under breakage or abrasion and, consequently, will be measured in smallest classes (Figure IV.3 (b)). Hydrates dispersed in the water phase stop to grow due to low gas saturation. A last possible explanation for the decrease observed in the largest group (> 100µm) is considering the deposition of these large hydrates in the pipeline walls, which consequently are not further detected by the FBRM probe. This assumption is supported by the analysis of pressure drop evolution with time (§.III.2.2).

Regarding the agglomeration step, high peaks can be observed in the intermediate class (10-100 µm) for high water cuts (Figure IV.3 (a)). These peaks correspond to large hydrates packages crossing the area of measurement of the FBRM probe.

For intermediate water cut ((Figure IV.3 (b)), the measured chord length number between 10 and 100 µm increases gradually during growth, because converted droplets with sizes between 0 and 10 µm grow and move to the intermediate group of classes (10-100 µm). Later, it continues to increase due to agglomeration between hydrates formed from the free oil phase and from the droplets.

Comparing high and intermediate water cuts, plug is more prone to occur at intermediate water cuts due to the increasing quantity of oil that enhances the gas transfer properties. In high water cut, hydrate formation occurring around oil droplets will block the dissolution of methane in oil. However, in intermediate water cut, free oil phase (large oil droplets) remains in the system and keeps being recharged in methane. Consequently, more hydrates will form at their interface. Hydrates formed at this interface usually detach to flow in the water phase and are measured in lower classes (< 100 µm).

In intermediate water cut experiments, the system keeps being recharged on gas by the free oil phase. Therefore, hydrate growth rate is higher. Comparing the volume of formed hydrates between high and intermediate water cuts, experiments at intermediate water cut generally reach higher values than experiments at high water cut (

Table III.3).

Oil Continuous Phase

Here it is important to remind that when no decrease around the nucleation step is observed for the intermediate group (10-100 µm) in the FBRM measurements, the system is oil continuous. For experiments with oil continuous phase, nucleation and growth start at the water droplets interface, followed by growth inward the water droplets. Consequently, the chord length number does not increase significantly at these steps (Figure IV.4 (b)).

Once the continuous phase is oil, the methane dissolution rate is higher, which keeps constant the driving force for the hydrate crystallization. For this reason, commonly, the appearance of the first hydrates crystals rapidly leads to growth and agglomeration. This is observed in the experiment presented in Figure IV.3 (c), where the step of nucleation and growth is very short, corresponding only to the first minutes of the experiment. After this step, the number of measured chord lengths increases rapidly due to agglomeration until the pipeline plugging (in approximatively 10 minutes).

For oil continuous systems, the quantity of methane dissolved is higher due to the higher gas/liquid transfer. This results in more important hydrate formation which can easily plug the pipeline (

Table III.3).

From the performed experiments with unsalted water and Kerdane®, the transition phase from water to oil continuous of the shear stabilized emulsion was observed at 50% water cut and flow rate of 400L.h^{-1}. Under other experimental conditions and type of oil, the transitions can appear at different water cuts.

IV.1.2 Experiments with Additive AA-LDHI

In order to understand the hydrate formation process with AA-LDHI, the chord length distribution study for this set of experiments was also performed. As explained in Chapter III, the additive is considered *well* dosed, although being under-dosed compared to real facilities. The purpose of this dosage is to observe the anti-agglomerant effect in one way, but also to observe some variations in the behavior of the system due to hydrate formation and some agglomeration. Consequently, although agglomeration is visible in some cases, never a plug situation was observed with *well*-dosage of AA-LDHI.

As consequence of using additive surfactant, which acts reducing the size of the dispersed droplets, the shear stabilized emulsion and the suspension present as the most representative group of classes the smaller one (< 10µm). Hydrates will nucleate and grow at the droplets interface or form in the free phase interface and detach from it. Therefore, this group (< 10µm) shall remain the most representative in absence of agglomeration.

Concerning the FBRM measured chord length number in experiments with AA-LDHI (Figure IV.5 and Figure IV.6); the main difference from experiments without AA-LDHI (Figure IV.3 and Figure IV.4) is that no strong decrease (and sometimes no decrease) is observed around the nucleation step for the most representative class. In other words, this suggests that oil is the continuous phase when AA-LDHI is *well*-dosed.

This conclusion can be linked to the fact that experiments with anti-agglomerant should form hydrates which circulate without agglomeration. One way to achieve this objective is by forming dry hydrates: particles without free water, which do not agglomerate or deposit (Kelland, 2014). The formation of dry particles is possible by forming smaller water droplets dispersed in the oil phase, which can be easily completely converted into hydrates. If formed hydrates do not have accessible water inside or outside it and if these hydrates are not circulating in water phase, no agglomeration is possible, since there is no water available to convert into hydrate and form a solid bridge between hydrates. In other words, the anti-agglomerant induces the formation of dry particles which do not agglomerate once they are circulating in the oil phase.

In the case of hydrates formed at free phase interface, the AA-LDHI will be somehow *consumed* by these hydrates when they leave the water phase into the oil phase. Thus, the system dosage can be not enough to avoid hydrates agglomeration until the end of the experiment. By this way, the fraction of water which was not converted into hydrates is destabilized and can form large droplets by coalescence or Ostwald ripening. In this case, the shear stabilized emulsion can be inverted. In the performed experiments, the chord length number for the smallest group of classes (< 10µm) decreases once agglomeration begins (Figure IV.5) and is overtaken by the intermediate group (10µm – 100µm) in some cases.

(a) High water cut (90%, 400 $L.h^{-1}$) with AA-LDHI, beginning of the crystallization at 1380s.

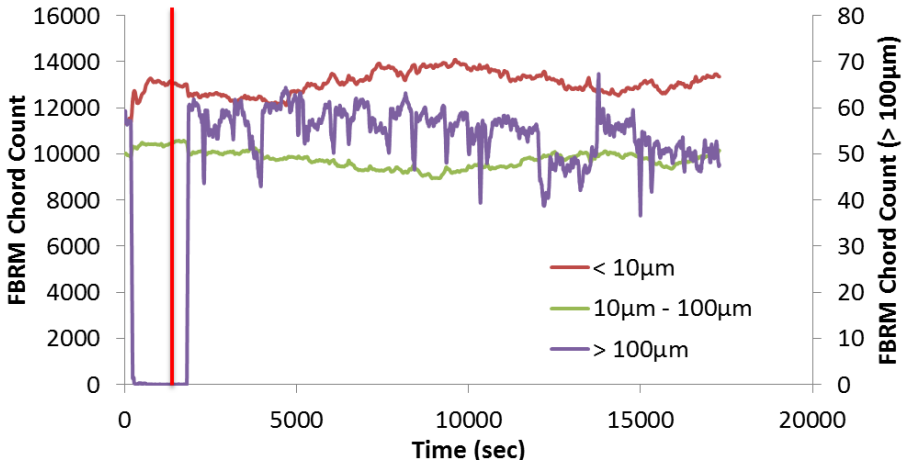

(b) Intermediate water cut (70%, 400 $L.h^{-1}$) with AA-LDHI, beginning of the crystallization at 1740s

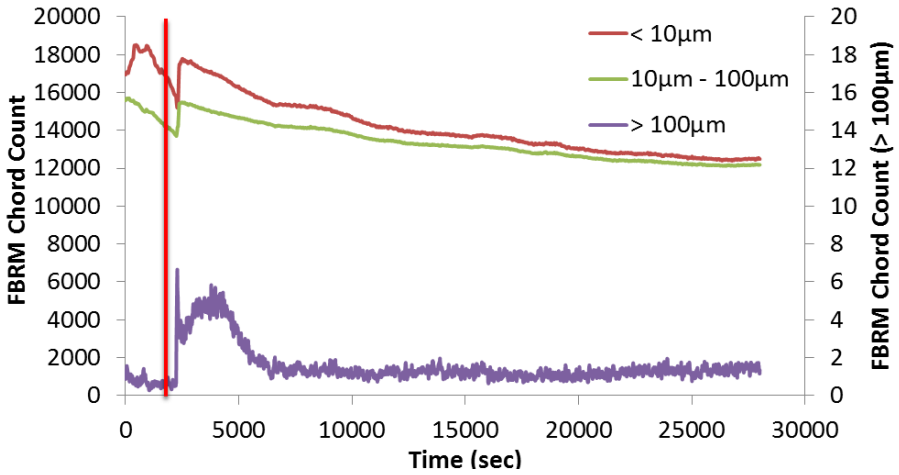

(c) Low water cut (30%, 200 $L.h^{-1}$) with AA-LDHI beginning of the crystallization at 870s

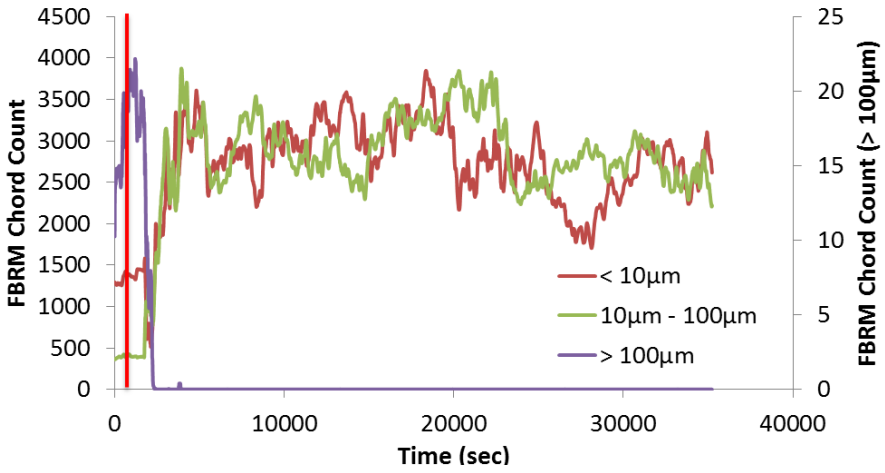

Figure IV.5 – FBRM Chord Length measurements in function of time for some tests with AA-LDHI.

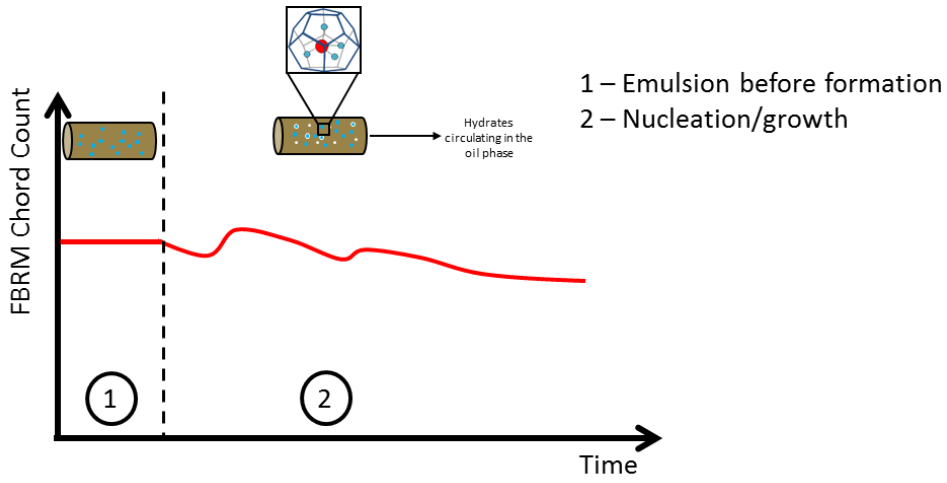

Figure IV.6 – Expected chord length behavior of the intermediate class (10-100 µm) for water and oil continuous with AA-LDHI.

The remaining question is: how a system with high water cut can be oil continuous? The answer is considering a system at high or intermediate water cuts where small droplets of water (average 8 µm) are dispersed in the oil phase together with large water packages, which can be assimilated to a free water phase. In general, the FBRM probe cannot detect these packages, because their sizes exceed the uppermost limit chord measured by the probe (3 mm).

Hydrates nucleation and growth will occur at the water/oil interfaces. Hydrates formed in the interface of water droplets will grow inwardly these droplets. As consequence, the chord length is approximately maintained (< 10µm). If hydrates are formed in the interface of large water packages, they will later detach from this interface and circulate dried in the oil phase. The detached hydrates

will be measured intermediate (10–100µm) or smaller (< 10µm) group of classes. Agglomeration is avoided while the mixture is stabilized by the anti-agglomerant action.

In order to understand the presence of the free water phase, it is interesting to observe the behavior of the highest class (> 100µm), which is hardly detected before hydrate formation and then increases after beginning of crystallization for high and intermediate water cuts (Figure IV.5 (a) and (b)). At high and intermediate water cuts, the free water phase has larger dimension comparing to low water cut and is hardly detected by the FBRM probe. Though, the measurement of larger chord lengths is facilitated when hydrates form in their interface.

For low water cut (Figure IV.5 (c)), the largest group of classes (> 100µm) is more representative before hydrate formation, whether free water phase exists in this case, it is presented in a smaller dimension, so more easily detected by the FBRM. Some minutes after hydrate formation, this measurement decreases as hydrates can be formed in the free water phase interface. Hydrates formation consumes the water of these larger droplets and forms smaller ones. As the amount of oil is larger at low water cut hydrate formation kinetic is faster due to the higher methane transfer rate to the liquid phase. As consequence of faster hydrate formation, the free water phase (> 100µm) quickly decreases.

In resume, by decreasing the water cut, the fraction of free water becomes smaller in size and fewer in quantity. The free water phase flows in the oil phase mixed with small water droplets. At low water cut, there is no significant free water phase and it quickly disappears after the beginning of hydrate formation. Similarly to cases without anti-agglomerant, increasing water cut will generally limit the hydrate formation (Table III.4), due to the low gas solubility in water, combined with the low transfer rate at the gas/liquid phase.

As consequence of low gas solubility in water, the agglomeration at high water cut (Figure IV.5 (a)) is hardly observed through the FBRM measurements, which do not present an important variation during the experiment. Although, hydrates deposition was evidenced by pressure drop analysis (Figure III.9 and Figure III.11).

Agglomeration can be evidenced comparing the behavior of intermediate and smaller group of classes during the experiment. Close to the end of the experiment of intermediate water cut (Figure IV.5 (b)), it can be seen that the intermediate group (10–100µm) almost overtakes the smaller one (<

10µm), as an evidence of agglomeration. Hydrate deposition is also detected through the pressure drop analysis as explained in Chapter III (Figure III.9 and Figure III.11)

Hydrate formation kinetic is faster in the low water cut case. For this reason, fast growth and also agglomeration are observed just some minutes after the beginning of the hydrate formation, evidenced by comparing intermediate (10–100µm) and smaller (< 10µm) group of classes. The intermediate group shows fewer particles than the smaller one before hydrate formation (Figure IV.5 (c)) and after a few minutes of hydrate formation, the intermediate group starts to present the same quantity of particles (and sometimes more) comparing to the smaller one. These conclusions were validated through the pressure drop analysis presented in Chapter III (Figure III.9 and Figure III.11).

The standard behavior for the chord length measurement during hydrate crystallization with *well* dosed AA is summarized in Figure IV.6 from the experimental results analysis (Figure IV.5). After the beginning of hydrate crystallization, there is a global tendency of measured chord length number decrease in the most numerous classes (until 100 µm), but with secondary phenomenon consisting in moderate increasing followed by decreasing. The increase is due to hydrate formation at the interface between free water phase and oil, which can be detected in classes until 100µm. After growth, hydrate can detach and move to the oil phase and the chord length presents a slight decrease. It is assumed that the dispersed hydrate particles are hardly detected compared to the ones attached to a water phase.

If AA-LDHI is not well dosed, the behavior of the hydrate formation is similar to the behavior observed without additive in section §IV.1.1. Experiments show that the quantity of AA-LDHI must be increased with increasing oil cut in order to avoid pipeline plugging, since the higher is the amount of oil, the faster is the kinetic of hydrate formation and the faster is the AA-LDHI *consumption* around hydrates.

IV.2 PVM Images – Experiments without Additive AA-LDHI

Analysis with the Particle Video Microscope (PVM) probe is limited to experiments without anti-agglomerant, as explained in Chapter II. The interpretation of PVM images requires very detailed and careful analysis by comparison between cases of water continuous (Figure IV.7 and Figure IV.8) and oil continuous (Figure IV.9).

For both cases, the beginning of hydrate formation (nucleation and growth) will occur at the droplets interface. This step can be visualized by PVM images, for example in Figure IV.7 (d) and Figure IV.9 (b), where droplets are partially converted into hydrates. It is possible to see that a portion of the droplet is still liquid. This is evidenced by the partial reflection of the laser beams in the non-converted portion of the droplet surface. The other portion of the droplet surface is more irregular without beam reflection due to hydrate formation. The converted portion is also whiter than the liquid portion. Apart from this similarity, some differences can be pointed out between the two cases:

1. **Water continuous without AA-LDHI (Figure IV.7 and Figure IV.8)**:

   Hydrates nucleate and grow at the oil/water droplets interface and grow **outward** the droplets.

   The outward growth is evidenced by PVM images, more clearly seen in Figure IV.8 (d). After the droplets surface conversion into hydrates, the particles start to present a more irregular shape (sometimes even whiter color) when compared to particles with inward growth (Figure IV.9).

   For intermediate water cut ranging from 70% to 50% (Figure IV.8), it was inferred by the FBRM analysis that a free oil phase should be present in this system. This free oil phase can be interpreted as large oil droplets. Observations from PVM analysis can support this conclusion. For example, in Figure IV.8 (c) a large droplet, which exceeds the field of the picture (1050 µm x 800 µm), can be observed. In Figure IV.8 (e), the same is observed, but this time the droplet is, at least, partially converted.

   After hydrate formation and before strong agglomeration, images background in intermediate water cut is normally whiter than in high water cut. This color is influenced by the larger amount of hydrates circulating in the continuous phase. The quantity is larger in the intermediate water cut due to more important hydrate detachment from large oil packages (free oil phase).

Before continuing the PVM analysis, it is essential to notice that for all water cuts the PVM probe detects an important amount of droplets larger than 100 μm which are not detected in the same proportion by the FBRM probe, showing that FBRM measurements are understated comparing to the PVM images. These large droplets are considered to represent free phases when they exceed the field of the photo obtained with the PVM probe.

2. **Oil continuous without AA-LDHI (Figure IV.9)**:

   Hydrates nucleate and grow at the water/oil droplets interface and grow **inward** the droplets while water is available to form hydrates inside them.

   Even if it is possible to see some irregularities of the droplet initial surface due to hydrate formation, the inward growth is evidenced because hydrates formed in oil continuous system present a more regular surface shape (mainly before agglomeration). There is a second evidence concerning the color: hydrates with outward growth are whiter than the continuous phase (Figure IV.7 and Figure IV.8). As hydrate is growing into the continuous phase, this color difference is evidenced by the image. However, for hydrates with inward growth (Figure IV.9), this whiteness is less evident. It seems that hydrate particles have almost the same color of the droplets before hydrate conversion. The color difference comparing the continuous phase surrounding the formed particles and the particles themselves is less pronounced.

   Agglomerates are formed by droplets converted into hydrates that collide with each other and keep together by capillary forces. Generally and mainly in large agglomerates, the initial hydrate particle interface disappears after agglomerate formation. Agglomeration can be observed, for example, in the background of Figure IV.9 (b), (c) and (d) or in Figure IV.9 (b) and (d) which were taken when the pipeline was plugged. In these cases, the agglomerate of hydrate got stuck in the probe window. This event is common for cases of pipeline plug and, consequently, the PVM does not give an accurate image when the system is plugged.

The higher conversion of water into hydrates (Table II.3) as the oil cut increases is also evidenced by the PVM images. For a similar time interval, the images have a higher opacity, meaning a higher formation of hydrates.

(a) 90% 200 $L.h^{-1}$ – 11 min (0.7%)

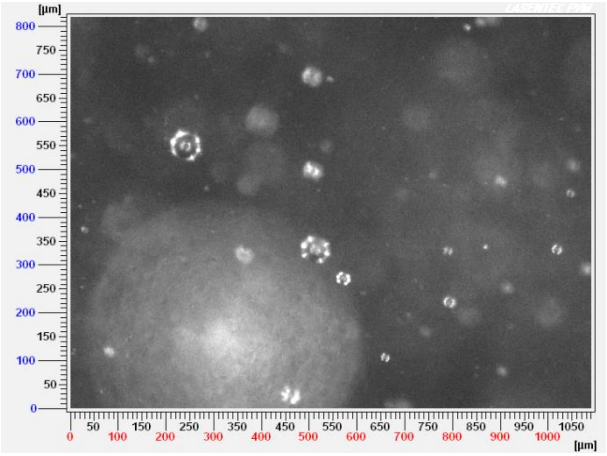

(b) 90% 400 $L.h^{-1}$ – 28 min (1.5%)

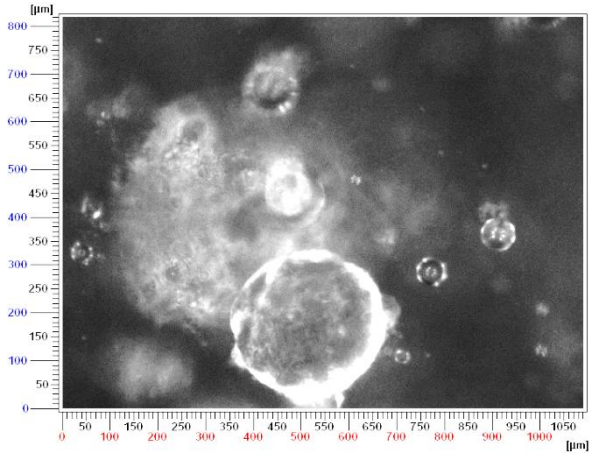

(c) 80% 200 $L.h^{-1}$ – 21 min (0.1%)

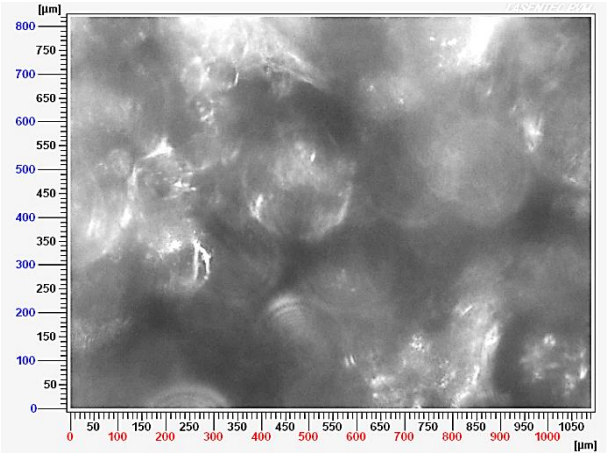

(d) 80% 400 $L.h^{-1}$ – 14 min (1.4%)

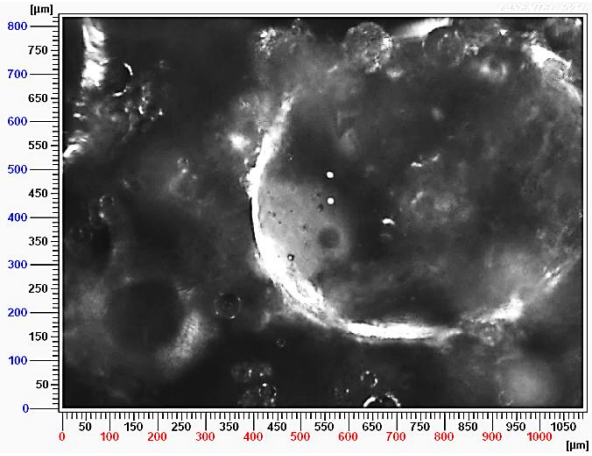

Figure IV.7 – PVM images (1050 µm x 800 µm) from crystallization at high water cut and water continuous phase (200 $L.h^{-1}$ and 400 $L.h^{-1}$) at different times after the beginning of crystallization given in each figure with the volume of hydrates for the respective time.

(a) 70% 200 L.h^{-1} – 3 min (0.4%) Plugging Case

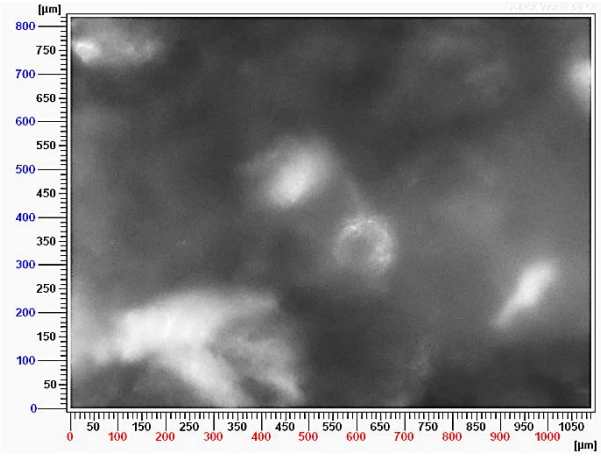

(b) 70% 400 L.h^{-1} – 3 min (0.3%)

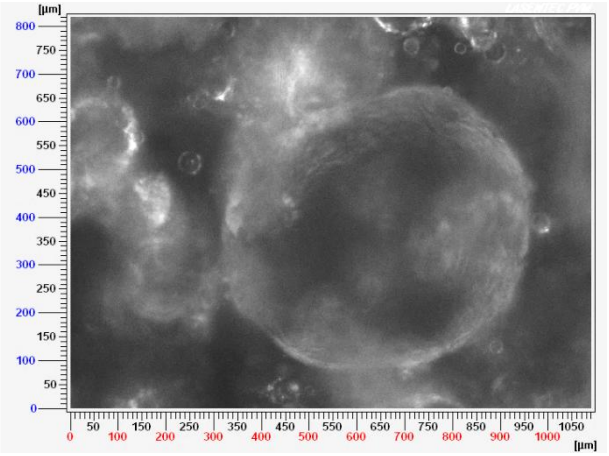

(c) 60% 200 L.h^{-1} – 37 min (1.7%)

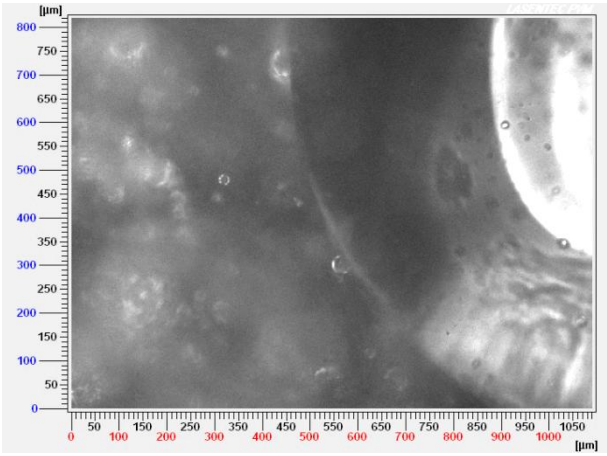

(d) 60% 400 L.h^{-1} – 7 min (1.9%) Plugging Case

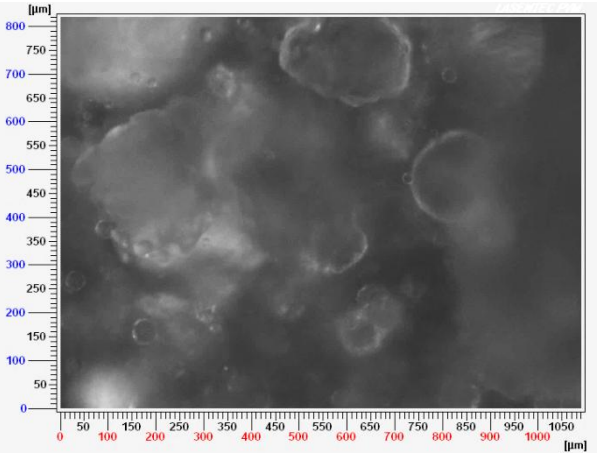

(e) 50% 200 L.h^{-1} – 10 min (0.4%)

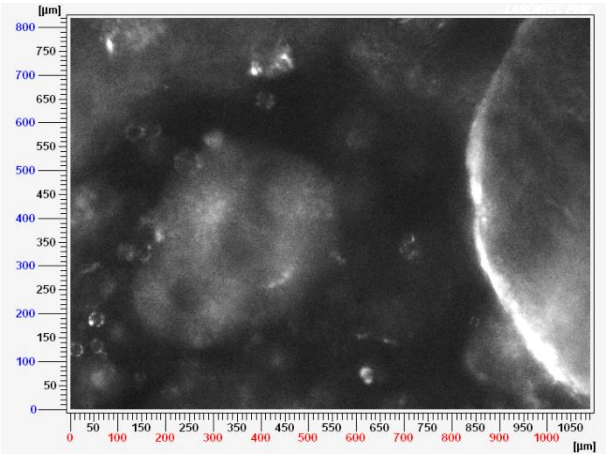

Figure IV.8 – PVM images (1050 µm x 800 µm) from crystallization at intermediate water cut and water continuous phase (200 L.h^{-1} and 400 L.h^{-1}) at different times after the beginning of crystallization given in each figure with the volume of hydrates for the respective time.

(a) 50% 400 L.h^{-1} – 5 min (0.4%)

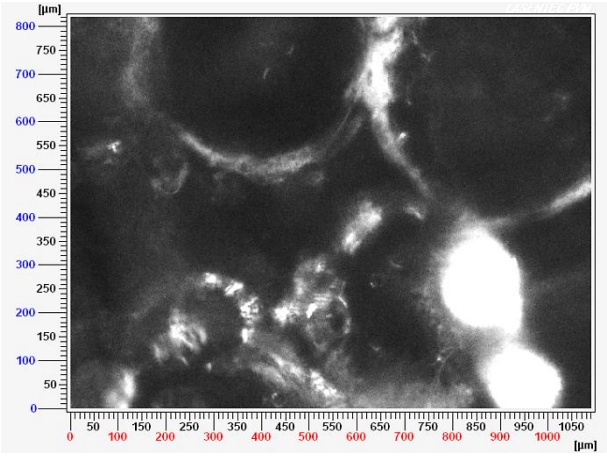

(b) 40% 200 L.h^{-1} – 7 min (4.3%) Plugging Case

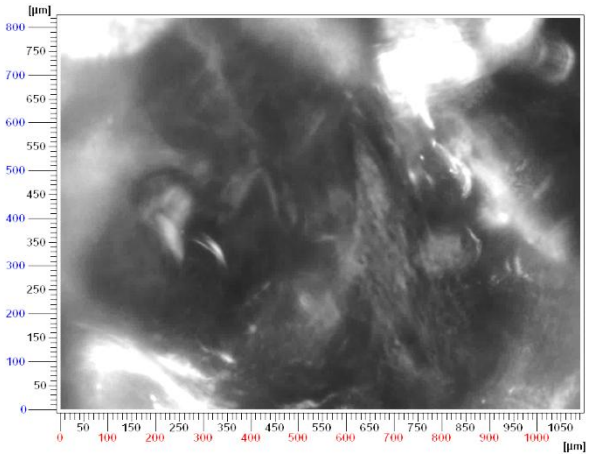

(c) 40% 400 L.h^{-1} – 7min (0.5%)

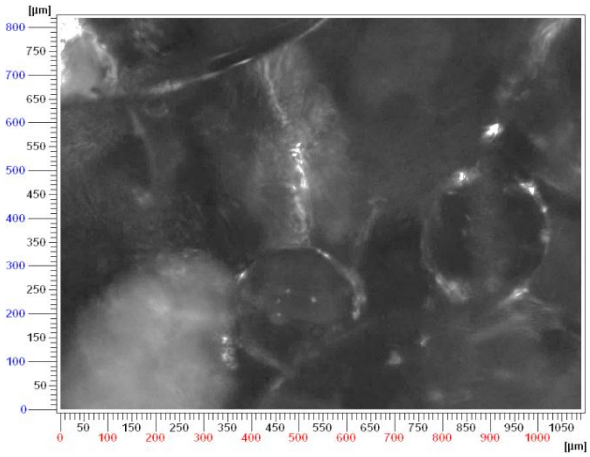

(d) 30% 200 L.h^{-1} – 6 min (1.1%) Plugging Case

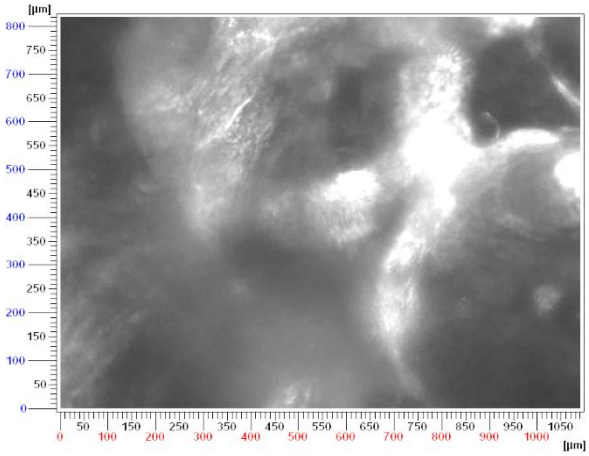

(e) 30% 400 L.h^{-1} – 4 min (2.6%) Plugging Case

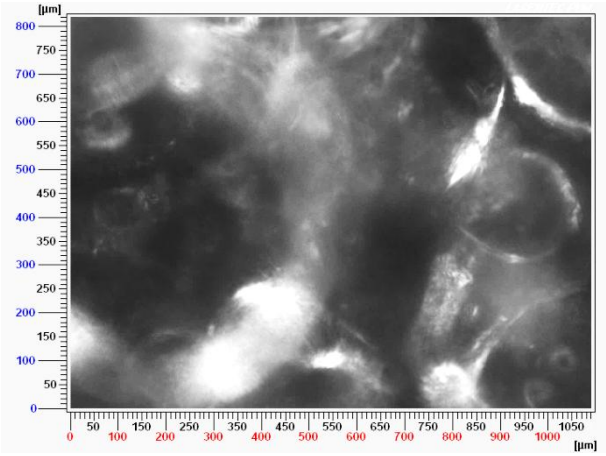

Figure IV.9 –PVM images (1050 µm x 800 µm) from crystallization at low water cut and oil continuous phase (200 L.h^{-1} and 400 L.h^{-1}) at different times after the beginning of crystallization given in each figure with the volume of hydrates for the respective time.

IV.3 Wettability – Experiments without Additive AA-LDHI

Following the studies of Hoiland *et al.* (2005a, b) and Fotland & Askvik (2008) about the hydrate wettability (water or oil wet), they can give a clue about the type of water and oil dispersion and how the process of hydrate formation evolves in the system (Table I.2).

Hoiland *et al.* (2005a, b) developed a qualitative method to determine the hydrate wettability based on the inversion point of mixtures with (φ_w^{inv}) and without hydrates (φ_w^0). The difference between the two inversion points ($\Delta\varphi_w^{inv}$) is related to the wettability (Equation IV.1). Once the inversion point of the system without hydrates influences the inversion point of the system with hydrates, the value of the $\Delta\varphi_w^{inv}$ needs to be normalized (given the wetting index, $\Delta\varphi^*$) to take into account this influence. The calculation to determine the wetting index ($\Delta\varphi^*$), a value between -1 and 1, is given hereafter:

$$\Delta\varphi_w^{inv} = \varphi_w^{inv} - \varphi_w^0 \quad \text{(IV.1)}$$

$$\Delta\varphi_{max} = 1 - \varphi_w^0 \rightarrow when\ \Delta\varphi_w^{inv} > 0 \quad \text{(IV.2)}$$

$$\Delta\varphi_{max} = \varphi_w^0 \rightarrow when\ \Delta\varphi_w^{inv} < 0 \quad \text{(IV.3)}$$

$$\Delta\varphi^* = \frac{\Delta\varphi_w^{inv}}{\Delta\varphi_{max}} \quad \text{(IV.4)}$$

The wetting index ($\Delta\varphi^*$) will be the parameter used to determine if particles are oil or water-wet. Values higher than 0.1 indicate oil-wet particles, values lower than -0.1 indicate water wet particles. Intermediate values indicate intermediate wet, weakly oil and weakly water-wet regimes.

From the presented experimental study, hydrates wettability can only be done accurately for experiments without AA-LDHI, as same conditions were applied and, experimentally, it is possible to detect the phase inversion point. For experiments using AA-LDHI, as the additive dosage was varied, the characteristics of the system were changed, preventing the wettability analysis by the chosen method.

In previous section (§IV.1.1), the continuous phase before the beginning of hydrate formation was identified from the variation of the measured chord length number at the beginning of crystallization, when the chord length number decreases at the beginning of the hydrate formation, it means that the shear stabilized emulsion is water continuous. In order to better evidence this

variation, Figure IV.10 shows the difference between the measured chord lengths number immediately before the beginning of hydrate formation and after the beginning of hydrate formation corresponding to a volume fraction between 0.05% and 0.1% of formed hydrates. For the sake of brevity, only some experiments are shown.

Figure IV.10 shows positive bars when the shear stabilized emulsion is water continuous and negative bars when the shear stabilized emulsion is oil continuous. The experiment with 50% water cut, just before 40% water cut where the bar becomes negative, is considered the inversion point of the mixture without hydrates (φ_w^0), once the volume fraction of hydrate formed is very small.

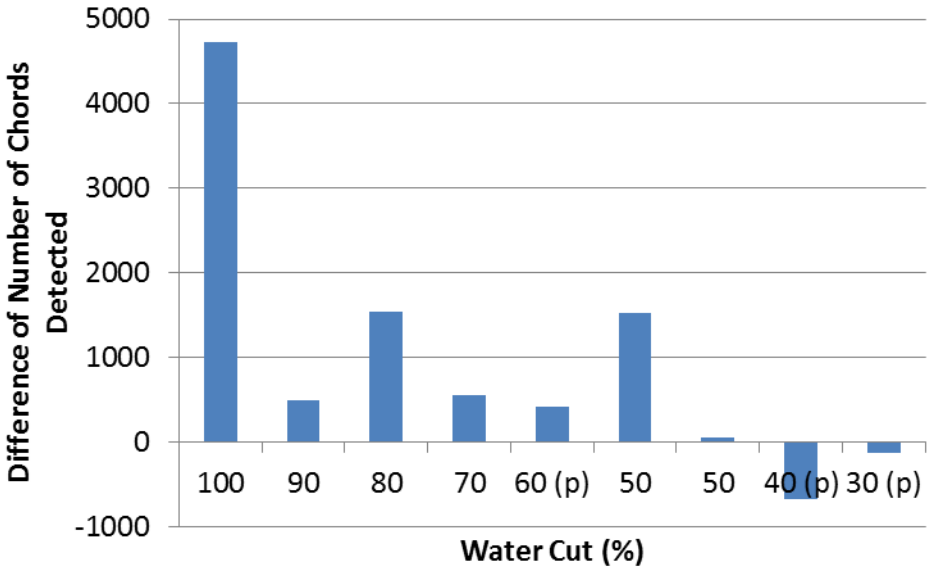

Figure IV.10 – Difference between the number of chords detected by the FBRM probe between the beginning of the hydrate formation and the formation of volume fraction between 0.05% and 0.1% of hydrates for the different water cuts (*p* means plugging).

The probes used to analyze the hydrate crystallization process do not provide an accurate evidence of the inversion point of mixture with hydrates. For this matter, the inversion point for the mixture with hydrates (φ_w^{inv}) is supposed considering the different characteristics of the defined behavior groups (high, intermediate and low water cuts). After this, it is concluded that the inversion point for the mixture with hydrates (φ_w^{inv}) is likely to occur at the intermediate water cut (70% to 50%) due to the existence of a free oil phase which can facilitate the phase inversion as water is being consumed after hydrate formation.

Proceeding with the calculation of the wetting index for the stated range of phase inversion with hydrates, the wetting index for the studied system is placed in the interval from 0 to 0.4. This means formation of intermediate or oil wet particles. Intermediate wet hydrates are associated to a plugging tendency, while oil wet hydrates are associated to a non-plugging (dispersion) tendency.

Although experiments with hydrate formation performed in the *Archimede* flow loop without using AA-LDHI have only presented 25% of plugging (no flow) occurrence, it is not possible to assure that this system has a non-plugging tendency, once experiments are limited to a working day (approximately 7 hours). On the contrary, liquid-liquid mixtures containing light oil as the Kerdane® are well known for their plugging tendency (Hoiland et al., 2005a).

Characteristics of systems with oil and water wet particles were described by Fotland & Askvik (2008) and can be seen in Table I.2. Some behaviors related to water wetted particles characteristics were observed in this work. A very reproducible one is related to water continuous suspensions, in which hydrate formation rate is inhibited some time after the beginning of the hydrate formation. Accordingly to Fotland & Askvik (2008), this event happens before phase inversion. At this point, it is possible to see by comparing the evolution of the hydrate formation through the PVM images that hydrates seems to form in a smaller rate (Figure IV.11 (b)) than the one observed in the beginning of the hydrate crystallization process (Figure IV.11 (a)).

(a) 70% 400 $L.h^{-1}$ – 1 min (0.02%)

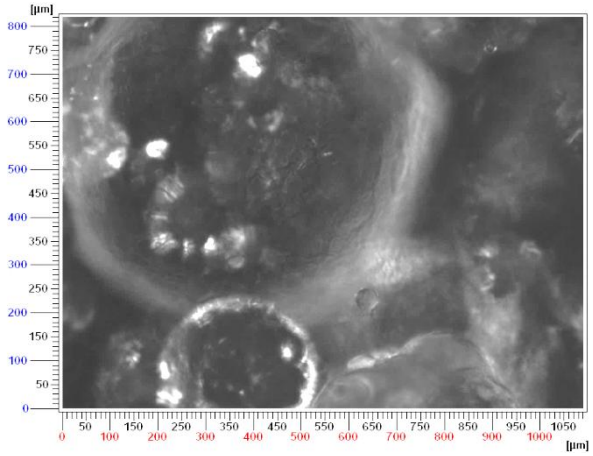

(b) 70% 400 $L.h^{-1}$ –42 min (0.5%)

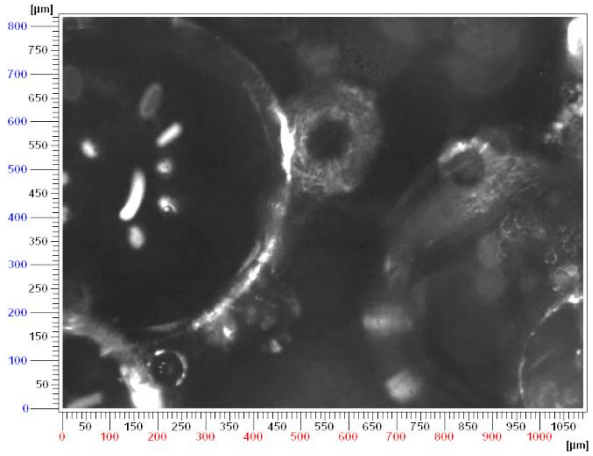

(c) 80% 400 $L.h^{-1}$ – 3 min (1.0%)

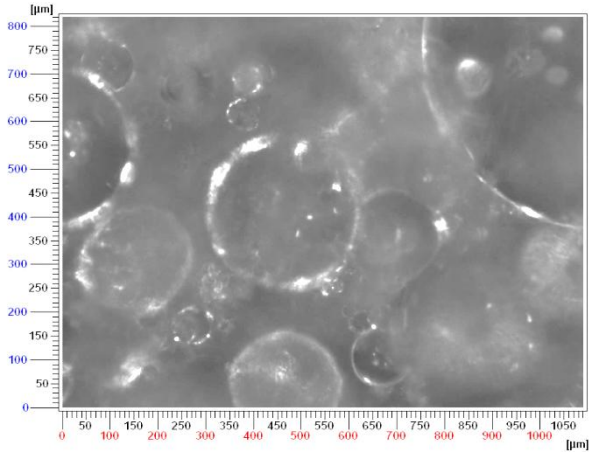

(d) 80% 400 $L.h^{-1}$ – 48 min (1.9%)

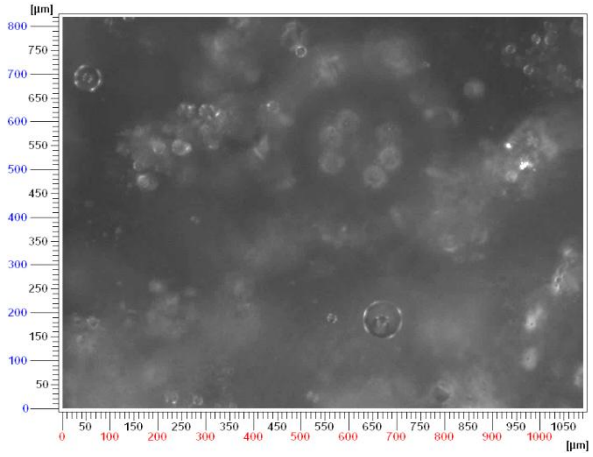

Figure IV.11 - PVM images (1050 µm x 800 µm) showing hydrate formation evolution at different times after the beginning of crystallization given in each figure with the volume of hydrates for the respective time.

IV.4 Shear Stabilized Emulsion and Hydrate Formation Topological Models

Experimental results explored in Chapter III in addition to information acquired by the studies developed in sections §IV.1, §IV.2 and §IV.3 are the basis to develop a topological model for hydrate crystallization from different shear stabilized emulsion systems without free gas phase. The hydrate formation process without anti-agglomerant is different from the process with anti-agglomerant. In consequence, two different models were developed in sections §IV.4.1 and §IV.4.2, respectively.

IV. 4.1 Shear Stabilized Emulsion and Hydrate Formation Models without Additive AA-LDHI

Experimental results without anti-agglomerant presented in Chapter III (§III.1.1 and §III.2.2) and the study developed in Chapter IV (§IV.1.1, §IV.2 and §IV.3) point out the existence of three different behaviors of shear stabilized emulsions, and consequently hydrate formation, depending on the water cut. The topological model shown in Figure IV.12 corresponds to these three different groups of water cuts:

1. **High water cut without AA-LDHI:**

a. Figure IV.12 (a): the shear stabilized emulsion before hydrate formation presents droplets of oil well-distributed in the continuous water phase. For this study, the average droplets size is stable with varying flow rate and equal to approximately 25 µm. However, large oil packages (assimilated to a free oil phase) can exist at low flow rate in a very low amount.

b. Figure IV.12 (b): hydrate nucleation and growth arrive at the oil/water interface, followed by growth **outward** the droplets interface. The hydrate formed at the oil/water interface can detach and flow in the continuous water phase.

   The driving force of nucleation and growth at constant sub cooling is the concentration of methane. When oil droplets are wrapped on hydrate, they block the dissolution of methane in oil and stop hydrates growth.

   Due to the low oil content and to the fact that the formation of a hydrate crust around the oil droplets isolates it from the gas, the quantities of methane dissolved in oil and the rate of dissolution are consequently low. Thus, hydrate formation kinetic is slow. Hence, aggregates formed by collision between hydrates are hardly consolidated to form agglomerates. The hydrate plug formation (stated when no, or very irregular, flow is observed) is unlikely.

2. Intermediate water cut without AA-LDHI:

a. Figure IV.12 (c): regarding the shear stabilized emulsion behavior with increasing oil fraction in the system; an important amount of large oil packages (assimilated to a free oil phase) are dispersed in water together with smaller oil droplets. In this case, the average droplets size significantly decreases with increasing flow rate and the number of chords detected increases, once large oil packages (normally not detected by the FBRM probe) can disrupt into smaller droplets under the effect of the shear stress. In this study, the droplets average size varies from around 30 µm (in lower flow rates) to around 25 µm (in higher flow rates).

b. Figure IV.12 (d): hydrate nucleation and growth start at the oil/water interface. Hydrates will grow **outward** the droplets. Hydrates can detach from the interface where they are growing to flow into the water phase. The quantity of hydrates flowing in the water phase is higher because they also form at the interface between water and free oil phase, detach and circulate in the water phase. It is more difficult to completely cover the free oil phase, thus it will constantly feed the water phase with hydrates. In this case, the hydrate formation kinetic is faster due to the higher amount of oil and consequently of methane.

   The driving force of nucleation and growth at constant sub cooling is dependent on the concentration of methane, when small oil droplets are totally wrapped with hydrate, the dissolution of methane in oil is stopped and inhibits the growth. The remaining free oil phase is finally a semi-continuous hydrate crystallizer that continues dissolving the methane, nucleating and growing hydrates at their interface, and feeding the water continuous phase with hydrate. Because growth kinetics is faster, the aggregates formed by collision between hydrates can consolidate and form agglomerates. Therefore, hydrate plug is likely possible. If high amount of water is transformed into hydrate and/or trapped inside the agglomerates, it can also induce phase inversion of the shear stabilized emulsion.

3. Low water cut without AA-LDHI:

c. Figure IV.12 (e): as the quantity of oil increases, oil becomes the continuous phase with dispersed water droplets. The droplets average size is stable with varying flow rate and equal to approximately 20 µm.

d. Figure IV.12 (f): hydrate nucleation and growth arrive at the oil/water interface. Growth will occur **inward** the water droplets. The growth kinetics is faster because there is a continuous flow of methane dissolving in the shear stabilized emulsion continuous phase (oil). Once the

hydrates growth kinetic is faster, the collision between hydrates will lead to agglomeration and plug (stated I the studied apparatus when no flow is observed).

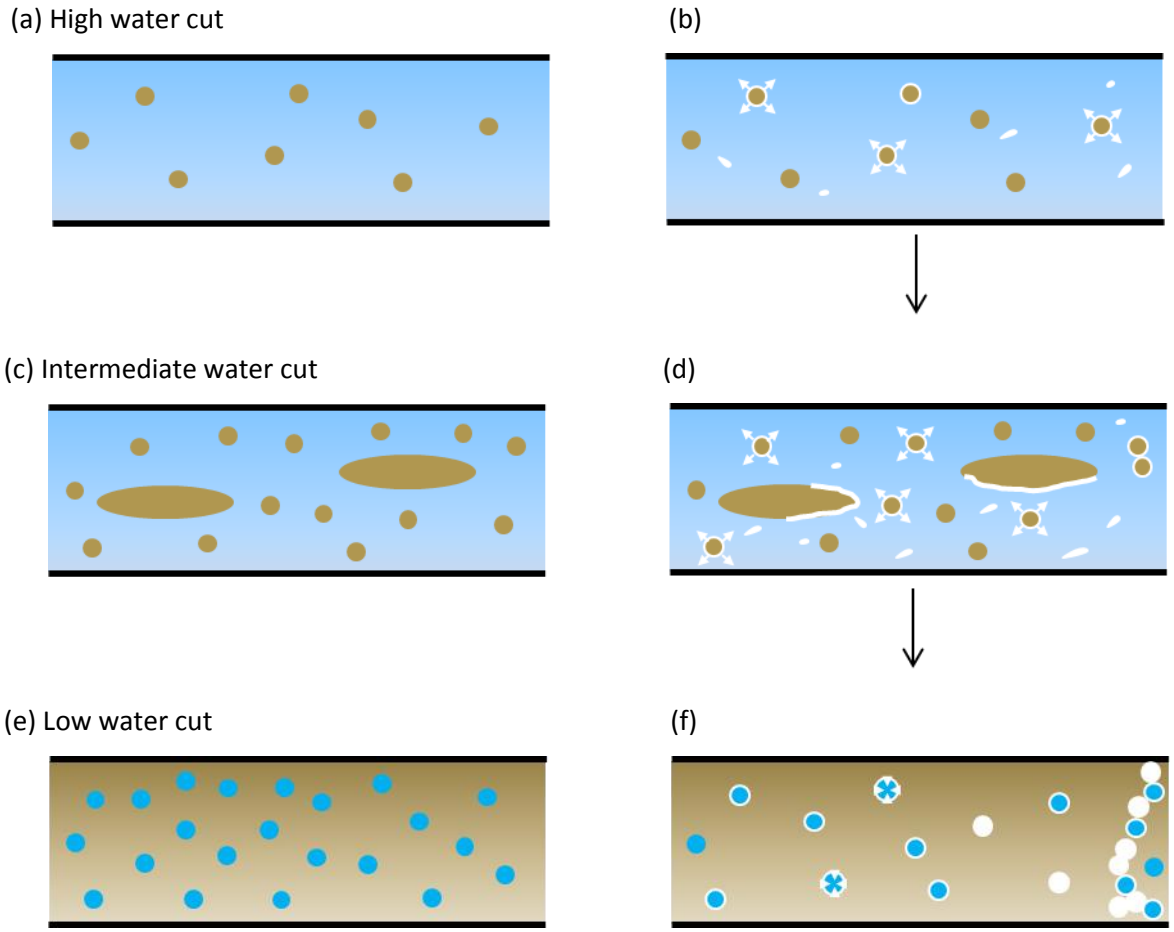

Figure IV.12 – Shear stabilized emulsion (a –high water cut, c – intermediate water cut – and e – low water cut) and hydrate crystallization (b – high water cut, d – intermediate water cut – and f – low water cut) model without AA-LDHI considering Kerdane® and fresh water.

IV.4.2 Shear Stabilized Emulsion and Hydrate Formation Models with Additive AA-LDHI

The crystallization topological model for the case with anti-agglomerant is shown in Figure IV.13. The model is also divided in three cases: high, intermediate and low water cuts. It is important to remind that the additive dosage is low to slightly prevent the agglomeration and plugging, without totally inhibiting hydrate formation and also agglomeration, which can still be observed.

Due to the surfactant properties of the AA-LDHI additive, this kind of system is rather formed by small water droplets dispersed in the oil continuous phase. After hydrate formation, the small

droplets will be more efficiently covered by hydrates and small fraction of water is maintained isolated at the center of droplets. This type of hydrate particles is qualified as dry hydrate, following the definition of Kelland (2014). The aggregates formed in this system after particles collision poorly consolidate into agglomerates due to the weak availability of water inside and around the formed hydrate particles, even if the system is charged with methane.

The different cases observed from the experimental analysis are detailed in sequence (Figure IV.13) considering a system with well-dosed fraction of AA-LDHI. Systems with bad-dosage of AA-LDHI behave likewise systems without AA-LDHI (Figure IV.12).

1. **High water cut with AA-LDHI:**

a. Figure IV.13 (a): due to the high amount of water, large water packages (not detected by the FBRM probe, but observed with the PVM probe) will be formed. The amount of additive is not enough to disperse completely the water phase. The free water phase and small water droplets dispersed will circulate in the continuous oil phase. The droplets average size is stable with varying the flow rate and equal to approximately 9 µm.

b. Figure IV.13 (b): hydrate nucleation and growth start at the oil/water interface. Hydrates will grow **inward** the small droplets. After a while, droplets will fully convert and hydrates will freely circulate in the oil phase as dry particles, thus, avoiding agglomeration. Hydrates formed at the interface of the large water packages will later detach from it. Probably, hydrates are detached due to abrasion and/or breaking. Thus, they form small particles, which freely circulate in the oil phase as dry particles.

2. **Intermediate and Low water cuts with AA-LDHI:**

a. Figure IV.13 (c and e): the amount of large water packages decreases by increasing the oil fraction in the system. For very low water cut, the free water phase completely disappears. These packages circulate in the oil phase with smaller water droplets. The droplets average size is stable with varying flow rate and equal to approximately 9 µm.

b. Figure IV.13 (d and f): hydrate formation has the same behavior as the one presented for high water cuts.

The AA-LDHI efficiency is linked to the volume of hydrate in the system. It means that the more hydrates are formed; the higher is necessary the AA-LDHI dosage to avoid agglomeration. In some cases, if the volume of hydrates is high enough to *consume* all the AA-LDHI, the dispersion can be

destabilized. This event is followed by phase inversion toward water continuous phase at intermediate and high water cut systems and agglomeration may occur.

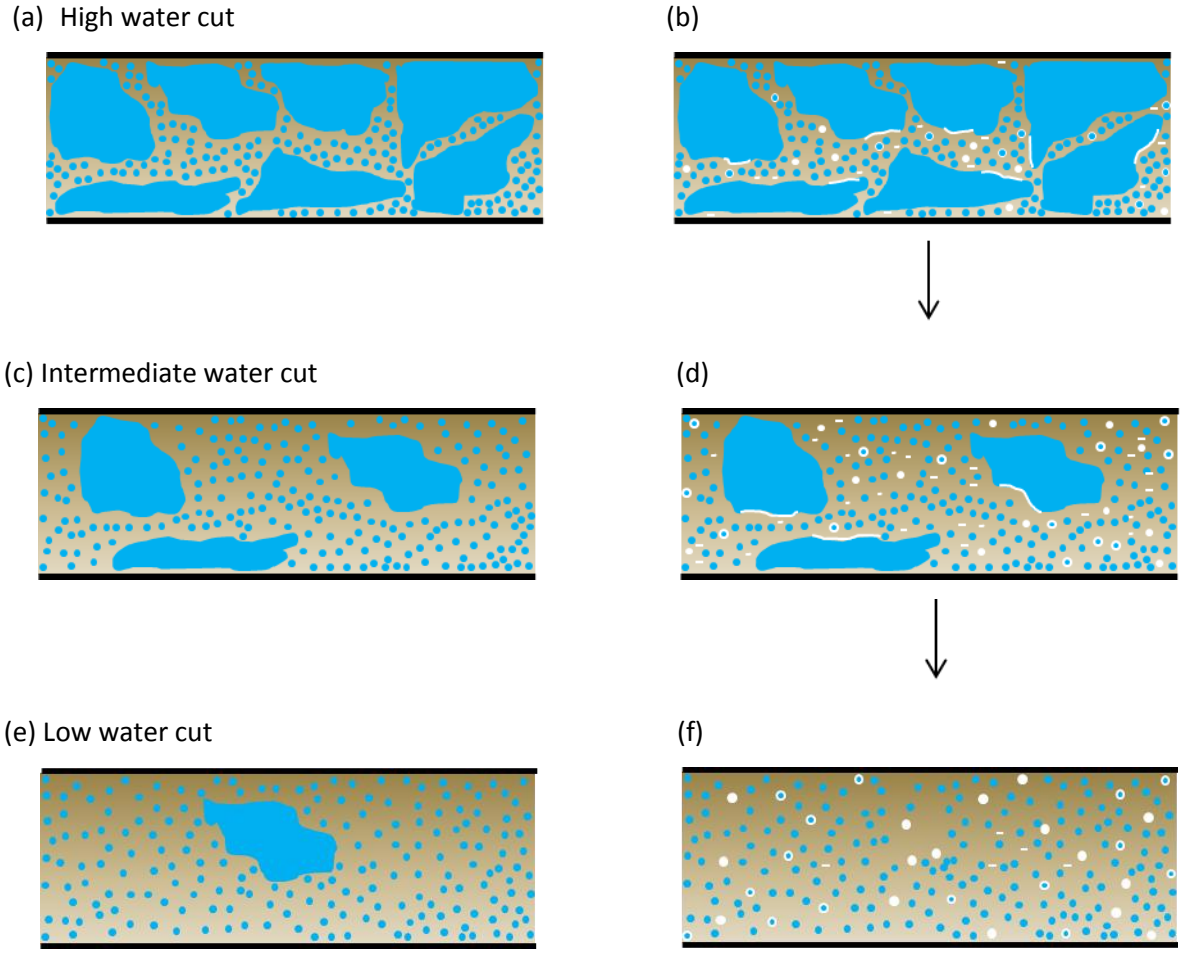

Figure IV.13 – Shear stabilized emulsion (a – high water cut, c – intermediate water cut and e – low water cut) and hydrate crystallization (b – high water cut, d –intermediate water cut and f – low water cut) model with under-dosed AA-LDHI considering Kerdane® and fresh water.

IV.5 Conclusions

In this chapter, experiments of methane hydrate crystallization under constant sub cooling of 6°C were analyzed from the data obtained with FBRM and PVM probes. From a new analysis method of the FBRM results, the shear stabilized emulsion continuous phase was deduced. The measured chord length numbers obtained using the FBRM were grouped in three most representative groups of classes (less than 10µm, between 10µm and 100µm and more than 10µm). The continuous phase was deduced from the results of the most representative group of classes.

From the knowledge of the continuous phase, topological models of crystallization from water or oil continuous shear stabilized emulsions were deduced. They describe crystallization and agglomeration of methane hydrates in systems containing a mixture of water and Kerdane® oil with varying water cut and flow rate, with and without AA-LDHI. The additive mechanism of anti-agglomeration was supported by the continuous phase analysis, which indicates an oil continuous phase when additive dosage was sufficient to avoid pipeline plugging.

Crystallization kinetics in terms of nucleation, growth and agglomeration were described together with the nucleation sites. The nucleation sites are at the interfaces between water and oil. The growth kinetics is outward oil droplets and inward water droplets. The limiting step of crystallization is the gas transfer rates at the gas/liquid interface and at the hydrocarbon/water interface. Gas/liquid transfer is low as water remains the continuous phase, but is enhanced as hydrocarbon content increases and acts as transfer phase. However, the hydrocarbon transfer property is depleted when a continuous and rigid crust of hydrates is formed around droplets, especially in well dispersed emulsions. This behavior is mainly highlighted at high water cut when hydrocarbon is well dispersed in the water continuous phase (experiments without AA-LDHI).

Although the low plugging rate observed in the studied system (25%), the wettability study for the performed experiments without AA-LDHI indicates that the actual system probably forms intermediate-wet particles, which is linked to a system with plugging tendency. The low plugging rate is mostly likely related to the limitation of the experiments to a working day (approximately 7 hours).

In order to prevent agglomeration, the AA-LDHI additive works first by well-dispersing the droplets (and later the formed hydrates) in the emulsion continuous phase. In the performed experiments with AA-LDHI, the shear stabilized emulsion continuous phase was identified as being preferentially the hydrocarbon phase, even at high water cut. Formed hydrates flow as dry particles

in the oil phase without agglomeration, thus preventing the line plugging (which is stated for the studied system when no flow is observed). However, agglomeration was observed in cases where the volume fraction of hydrates formed was large enough to *consume* the additive available in the system. This happened because the additive was intentionally under-dosed to observe the different steps of hydrate formation process including agglomeration.

IV.6 Chapter Highlights in French – Aperçu du Chapitre IV

Dans ce chapitre, deux modèles de comportement ont été développés comprenant la formation de l'émulsion stabilisée par cisaillement et la formation d'hydrates dans un système sans phase gazeuse libre : le premier modèle sans anti-agglomérant et le second avec un anti-agglomérant.

Les modèles topologiques qui ont été présentés dans ce chapitre sont soutenus par les résultats expérimentaux présentés dans le chapitre III, ainsi que les résultats obtenus avec la sonde de granulométrique (FBRM) et avec la sonde microscopique (PVM) qui ont été présentés dans le Chapitre IV. L'analyse détaillée des résultats de distribution de longueur de corde (§IV.1) et des images de la sonde microscopique (§IV.2) ont été présentés en vue d'en déduire la phase continue (§IV.1) et la mouillabilité (§IV. 3). Enfin, les modèles topologiques (§IV.4) ont été décrits.

Dans le chapitre IV, les expériences de cristallisation d'hydrates de méthane sous refroidissement constant de 6 °C ont été analysées à partir des données obtenues avec les sondes FBRM et PVM. A partir d'une nouvelle méthode d'analyse des résultats de la FBRM, la phase continue de l'émulsion stabilisée par cisaillement a été déduite (§IV.1). Les classes mesurées de longueur de cordes obtenues en utilisant la FBRM ont été regroupées en trois groupes concernant les classes les plus représentatives (moins de 10 µm, entre 10 µm et 100 µm et plus de 100 µm). La phase continue a été déduite à partir de l'analyse des résultats concernant le groupe le plus représentatif entre les trois classes.

De la connaissance de la phase continue, les modèles topologiques de cristallisation à partir d'émulsions eau continue ou huile continue stabilisée par cisaillement ont été déduits (§IV.4). Ils décrivent la cristallisation et l'agglomération des hydrates de méthane dans les systèmes d'émulsion d'eau et Kerdane® avec différentes fractions d'eau et débits, avec et sans AA-LDHI. Le mécanisme d'action de l'additif anti-agglomérat a été appuyé par l'analyse de la phase continue, qui indépendamment de la fraction d'eau est la phase huile lorsque la dose d'additif est suffisante, évitant ainsi l'agglomération et le bouchage de la conduite.

Les cinétiques de cristallisation en termes de nucléation, croissance et agglomération ont été décrites ainsi que les sites de nucléation. Les sites de nucléation sont aux interfaces entre l'eau et l'huile. La cinétique de croissance est vers l'extérieur des gouttelettes d'huile et vers l'intérieur des gouttelettes d'eau. Les modèles de nucléation et croissance ont pu être déduites des observations avec la sonde microscopique (§IV.2), et à travers de l'analyse des longueurs de corde (§IV.1).

L'étape qui limite la cristallisation est le taux de transfert de gaz à l'interface gaz / liquide et à l'interface hydrocarbures / eau. Le transfert gaz / liquide est faible tant que l'eau reste la phase continue, mais est accrue lorsque la fraction d'hydrocarbure augmente et agit comme phase de transfert. Toutefois, la propriété de transfert de la phase huile est épuisée quand une croûte d'hydrates continue et rigide se forme autour des gouttelettes d'huile, en particulier dans des émulsions bien dispersée. Ce comportement est mis en évidence principalement lors que la fraction d'eau est élevée et la phase huile est bien dispersée dans l'eau (expériences sans AA-LDHI).

Le taux de bouchage concernant les expériences réalisées dans le système étudié était seulement de 25%. Ce faible taux de bouchage est surtout lié à la limitation des expériences à une journée de travail (environ 7 heures), lorsque les systèmes formés par huiles similaires au Kerdane® ont une tendance plus importante à l'agglomération d'hydrates suivi par bouchage (Hoiland et al., 2005a). En faisant cette considération, l'étude de la mouillabilité pour les expériences effectuées sans AA-LDH indique que le système actuel est constitué probablement par des particules avec mouillabilité intermédiaire, qui est lié à un système avec tendance de bouchage.

Afin d'empêcher l'agglomération, l'additif AA-LDHI fonctionne en premier comme dispersant pour bien disperser les gouttelettes (et plus tard, les hydrates formés) dans la phase continue de l'émulsion. Dans les expériences réalisées avec AA-LDHI, la phase continue de l'émulsion stabilisée par cisaillement a été identifiée comme étant préférentiellement la phase huile, même à haute teneur en eau. Les hydrates formés écoulent comme des particules sèches dans la phase huile, donc sans agglomération, ce qui empêche le bouchage de la ligne d'écoulement. Cependant, l'agglomération a été observée dans les cas où la fraction volumique des hydrates formés a été assez grande pour *« consommer »* l'additif disponible dans le système. Cela est arrivé parce que l'additif était intentionnellement sous-dosé pour observer les différentes étapes du processus de formation d'hydrates y compris l'agglomération.

Conclusions and Perspectives

Gas hydrates, or clathrates, are solid crystalline particles. They can be formed during petroleum extraction inside the flow lines and their formation can change the flow characteristics. Mainly, their formation induces the increase of the pressure drop (viscosity), when they agglomerate they can interrupt the flow due to the formation of a plug or the formation of a mixture highly viscous. The plugging occurrence in on-shore facilities, although being a problem, is easier to localize and to remediate than hydrate plugs in off-shore facilities. Actually, the off-shore oil reserves can reach depths of 7000 meters (pre-salt) away from the coast and longer flow lines are hence necessary. This represents a greater challenge in every angle of risk management, including the hydrate formation

This thesis was part of a collaboration project between the *Ecole Nationale Supérieure des Mines de Saint-Etienne* and *Total S.A.*. The interest was to contribute both to scientific and industrial fields. The main objectives of this work were:

(1) To understand the hydrate formation (crystallization) from different emulsion systems, which were obtained varying the water volume fraction in the system and also the flow rate.

(2) To understand the role of the commercial dispersant additive (anti-agglomerant) in avoiding the hydrate agglomeration.

In order to attain the first objective, a set of experiments of hydrate formation without additive under a sub-cooling of 6°C and pressure of 80 bar were performed in the *Archimède* flow loop. Later, the experimental results were interpreted. After, in order to understand the role of the AA-LDHI additive, experiments in similar conditions to experiments without additive were performed in presence of the AA-LDHI additive. The additive was intentionally under-dosed in order to allow the observation of the different steps of the hydrate formation including some agglomeration.

Concerning the process of hydrate formation, three groups of behavior were identified during the experiments. These groups are: high, intermediate and low water cuts. Data concerning pressure drop, density, chord length and PVM images allowed a better understanding about emulsification and hydrate formation processes. An interesting outcome shows a link between the gas transfer to the shear stabilized emulsion before hydrate formation and the later occurrence of hydrate formation.

From experimental analysis of FBRM measurements, it was possible to deduce the continuous phase of each group of behavior through a new method of analysis by grouping the classes in the most representative ones (less than 10µm, between 10µm and 100µm and more than 100µm). Later, a topological model of the hydrate formation process from different emulsion systems was developed for the different water cut groups with and without anti-agglomerant. The gas transfer rates at the gas/liquid interface and at the hydrocarbon/water interface were identified as limiting parameters of the hydrate crystallization process. The model of hydrate crystallization was supported by the kinetic of nucleation, growth and agglomeration observed throughout the experiments. For future studies, it would be interesting to develop an analytical model to confirm the experimental observations and the topological model.

Concerning the study of the anti-agglomerant additive, it was observed that in order to avoid agglomeration, the system must present an oil continuous phase. Consequently, from the analysis of the continuous phase, it was possible to deduce when the additive dosage was insufficient to avoid the pipeline plugging. The experimental analysis allowed deducing a possible mechanism of action for the anti-agglomerant which acts as a dispersant additive. After hydrate formation at available water/oil interfaces, hydrates will flow in the oil phase without contact to the water phase (dry particles). Thus, no agglomeration will occur and pipeline plugging is prevented.

In future work, the additive effect must be studied in systems where the flow is exposed to unexpected conditions: stopping the flow for a certain time and, later, re-starting it or exposing the flow loop to stronger sub-cooling, etc.. Future work must also be done on the comprehension of the emulsion and emulsification process, once it is decisive to hydrate crystallization and agglomeration processes.

In order to develop a reliable model of growth, the methane concentration in the emulsion must be better known. For instance, by using the Attenuated Total Reflectance (ATR) probe which can be used to determine the gas concentration in the mixture. This method must be tested to confirm if it can also give information on the emulsion continuous phase.

The use of an acoustic emission probe can help to interpret the data obtained with the FBRM probe in order to study the frequency of collision between particles, which can support an agglomeration model.

Conclusions et Perspectives

Les hydrates de gaz, ou clathrates, sont des particules cristallines solides qui peuvent être formés dans les conduites d'écoulement de pétrole en modifiant les caractéristiques de l'écoulement. Ce comportement se reflète principalement dans l'augmentation de la perte de charge (viscosité), quand les hydrates s'agglomèrent et peut interrompre l'écoulement en raison de la formation d'un bouchon ou bien en raison de la trop forte viscosité du système. La survenance d'un bouchage sur les installations terrestres (on-shore), bien que toujours grave, est plus facile à localiser et, en par conséquent à réparer. Cependant, la gestion du risque de bouchage devient plus difficile dans les conditions off-shore, qui sont aujourd'hui plus sévères en raison des profondeurs extrêmes, jusqu'à 7000 mètres (pré-sel), et en raison de l'éloignement de la côte. Cela représente un risque plus élevé pour l'industrie pétrolière, comprenant la formation d'hydrates.

Cette thèse fait partie d'un projet de collaboration entre l'École des Mines de Saint-Etienne et Total S.A., où l'intérêt commun était de contribuer à la fois au domaine scientifique et industriel. Les principaux objectifs de ce travail étaient:

(1) Comprendre la formation des hydrates (cristallisation) à partir de différents types d'émulsion, obtenues en faisant varier la fraction volumique de l'eau dans le système et également la vitesse d'écoulement ;

(2) Comprendre le rôle de l'agent de dispersion commercial, conçu pour prévenir l'agglomération des hydrates.

Pour atteindre le premier objectif, un ensemble d'expériences de formation d'hydrates sans additif avec un sous-refroidissement de 6°C et une pression de 80 bar a été réalisé dans la boucle Archimède et, plus tard, interprété. Dans l'ordre, afin de comprendre le rôle de l'anti-agglomérant, les mêmes expériences ont été réalisées en présence de l'additif. L'additif a été intentionnellement sous-dosé afin d'observer les différentes étapes de la formation d'hydrates, y compris l'agglomération.

En ce qui concerne le processus de formation d'hydrates, trois groupes de comportement ont été identifiés à partir des expériences, qui étaient dépendants du type d'émulsion à partir desquelles les hydrates ont été formés. Ces groupes sont: fort, intermédiaire et faible pourcentage d'eau. Les données concernant la perte de charge, la densité, la longueur de corde et les images de la PVM ont

permis une meilleure compréhension du processus d'émulsification et de formation d'hydrates, avec un résultat intéressant montrant un lien entre la constante de transfert de gaz et l'apparition des hydrates.

De l'analyse expérimentale des résultats obtenus avec la sonde FBRM, il a été possible de déduire la phase continue correspondant à chaque groupe de comportement à partir d'une nouvelle méthode d'analyse en regroupant les classes dans les trois plus représentatives (moins de 10µm, entre 10µm et 100µm et plus de 100µm). Par la suite, un modèle de comportement du processus de cristallisation a été développé pour les différents groupes de pourcentage d'eau, également en décrivant le comportement de l'émulsion stabilisée par cisaillement. Les vitesses de transfert de gaz à l'interface gaz/liquide et à l'interface eau/huile ont été identifiées comme les paramètres limitants de la cristallisation d'hydrate. Le modèle de cristallisation d'hydrate a été soutenu par une approche qualitative des cinétiques de nucléation, croissance et agglomération observées tout au long des expériences. Pour les études futures, il serait intéressant de développer un modèle analytique pour confirmer les observations expérimentales et notre modèle de comportement.

En ce qui concerne l'étude du rôle de l'additif anti-agglomérant, il a été observé que, pour éviter l'agglomération, le système doit présenter une phase huile continue. Par conséquent, à partir de l'analyse de la phase continue, il a été possible de déduire si le dosage de l'additif était insuffisant pour éviter le bouchage de la ligne de flux. L'analyse expérimentale a aussi permis de déduire un possible mécanisme d'action pour l'additif anti-agglomérant qui agit comme un additif dispersant. Après la formation d'hydrate dans les interfaces eau/huile disponibles, les hydrates vont être transportés par la phase d'huile sans contact avec la phase aqueuse, par conséquent l'agglomération ne se produit pas et le bouchage est empêché.

Dans les travaux futurs, l'effet de l'additif doit être étudié dans des systèmes où l'écoulement est exposé à des conditions imprévues : l'arrêt de l'écoulement pendant un certain temps suivi par redémarrage, l'exposition de la boucle à des sous-refroidissements plus forts, etc.. Des futurs travaux doivent également être faits sur la compréhension de l'émulsion et du processus d'émulsification, puisqu'il est décisif sur les processus de cristallisation et d'agglomération d'hydrates.

Afin de développer un modèle fiable de la croissance, la concentration de méthane dans l'émulsion doit être mieux connue. Par exemple, en utilisant la sonde à Réflectance Totale Atténuée (ATR), qui peut être utilisée pour déterminer la concentration de méthane dans le mélange. Cette

méthode doit être testée pour confirmer si elle peut aussi donner des informations par rapport à la phase continue de l'émulsion.

Une autre possibilité est l'utilisation d'une sonde d'émission acoustique, qui peut aider à interpréter les données obtenues avec la sonde FBRM et aussi être un outil pour étudier la fréquence de collision entre les particules, qui peut soutenir par la suite un modèle d'agglomération.

References

Abdallah, W., Buckley, J.S., Carnegie, A., Herold, J.E.B., Fordham, E., Graue, A., Signer, T.H.N.S.C., Hussein, H., Montaron, B., Ziauddin, M., 2007. *Fundamentals of Wettability*. Oilfield Review. 44-61.

Alexiades, V., 2009. *Methane Hydrate Formation and Decomposition*. Seventh Mississippi State - UAB Conference on Differential Equations and Computational Simulations, Electronic Journal of Differential Equations. 1–11.

Anklam, M.R., Firoozabadi, A., 2004. *Driving force and composition for multicomponent gas hydrate nucleation from supersaturated aqueous solutions*. Journal of Chemical Physics, Vol. 121, No. (23), 11867-11874.

Anklam, M.R., York, J.D., Helmerich, L., Firoozabadi, A., 2008. *Effects of Antiagglomerants on the Interactions between Hydrate Particles*. AIChE Journal, Vol. 54, No. 2, 565-574.

Brochette, P., 2013. *Émulsification - Élaboration et étude des émulsions.* Techniques de l'Ingénieur, No. j2150.

Clever, H.L., Young, C.L., Battino, R., Wiesenburg, D.A., Hayduk, W., 1987. Solulibilty Data Series – Methane. Pergamon Press. Vol. 27-28.

Colombel, E., Gateau, P., Barré, L., Gruy, F., Palermo, T., 2009. *Discussion of Agglomeration Mechanisms between Hydrate Particles in Water in Oil Emulsions*. Oil & Gas Science and Technology – Rev. IFP, Vol. 64, No. 5, 629-636.

Cros, C., Pouchard, M., 2009. *Clathrate-type phases of silicon and related elements (C, Ge, Sn): a historic approach*. Comptes Rendus Chimie, Vol. 12, No. 9, 1014-1056.

Darbouret, M., 2005. Etude rhéologique d'une suspension d'hydrates en tant que fluide frigoporteur diphasique. Résultats expérimentaux et modélisation. PhD Thesis. ENSMSE.

Davidson, D. W., 1971. *The Motion pf Guest Molecules in Clathrate Hydrates*. Canadian Journal of Chemistry, Vol. 42, 1224-1242.

Douglas, J.F., Gasiorek, J. M., Swaffield, J.A., Jack L.B., 2005. *Fluid Mechanics, 5th edition*. Pearson Education Limited.

Duan, Z., Moller, N.,Greenberg, J., Weare, J. H., 1992. T*he prediction of methane solubility in natural waters to high ionic strength from 0 to 250°C and from 0 to 1600 bar.* Geochimica et Cosmochimica Acta, Vol. 56, 1451-1460.

Engineering ToolBox << http://www.engineeringtoolbox.com/water-dynamic-kinematic-viscosity-d_596.html >> Accessed October, 2015.

Englezos, P., Kalogerakis, N., Dholabhai, P.D., Bishnoi, P.R., 1987. *Kinetics of gas hydrate formation from mixtures of methane and ethane.* Chemical Engineering Science, Vol. 42, 2659-2666.

Eslamimanesh, A., Mohammadi, A.H., Richon, D., Naidoo P., 2012. Deresh Ramjugernath Application of gas hydrate formation in separation processes: A review of experimental studies. J. Chem. Thermodynamics, Vol. 46, 62-71.

Fidel-Dufour, A., 2004. Influence d'additifs anti-agglomérants sur l'agrégation et les propriétés de transport des hydrates de méthane cristallisant dans des émulsions eau/dodécane (PhD Thesis). ENSMSE.

Fotland P., Askvik K.M., 2008. *Some aspects of hydrate formation and wetting*. J. Colloid Interf. Sci., Vol. 321, No.1, 130-141.

Frostman, L. M., 2000. *Anti-Agglomerant Low Dosage Hydrate Inhibitors (LDHI's)*. Presentation Baker Huges Inc.

Hammerschmidt, E.G., 1934. *Formation of Gas Hydrates in Natural Gas Transmission Lines*. Industrial & Engineering Chemistry, Vol. 26, 851–855.

Herri, J.M., Bouchemoua, A., Kwaterski, M., Fezoua, A., Ouabbas, Y., Cameirao, A., 2010. Gas hydrate equilibria for CO2-N2 and CO2-CH4 gas mixtures - Experimental studies and thermodynamic modelling. Fluid Phase Equilibria, Vol. 301, 171–190.

Herri, J.M., Gruy, F., Pic, J.S., Cournil, M., Cingotti, B., Sinquin, A., 1999b. *Interest of in situ turbidimetry for the characterization of methane hydrate crystallization: Application to the study of kinetic inhibitors.* Chemical Engineering Science, Vol. 54, 1849-1858.

Herri, J.M., Pic, J.S., Gruy, F., Cournil, M., 1999a. *Methane hydrate crystallization mechanism from in-situ particle sizing*. AIChE Journal, Vol. 45, 590-602.

Hill, T., Johnson T., Nicol H.V., 2010. *Steady-state, and interrupted, production through a deep water black oil system*. In: Seventh North American Conference on Multiphase Technology. Canada.

Hoiland, S., Askvik K.M., Fotland, P., Alagic, E., Barth, T., Fadnes, F., 2005a, *Wettability of Freon hydrates in crude oil/brine emulsions*. Journal of Colloid and Interface Science, Vol. 287, No. 1, 217-225.

Hoiland, S., Borgund, A. E., Barth, T., Fotland, P., Askvik K.M., 2005b. *Wettability of Freon hydrates in crude oil/brine emulsions: the effect of chemical additives.* Proceedings of the Fifth International Conference on Gas Hydrates (ICGH-5). Trondheim, Norway.

Huo, Z., Hester, K. C.,Sloan Jr., E.D., Miller, K. T., 2002. *Methane Hydrate Nonstoichiometry and Phase Diagram.* AIChE Journal, Vol. 49, 1300-1305.

Jeffrey, G.A., 1984. *Hydrate inclusion compounds*. Journal of Inclusion Phenomena and Macrocyclic Chemistry, Vol. 1, 211-222.

Jeffrey, G.A., McMullan, R.K., 1967. *The Clathrate Hydrates. in: Progress in Inorganic Chemistry Cotton*. F.A., ed., Interscience, New York, 43-108.

Jones, A. G., 2002. *Crystallization Process Systems*. Butterworth-Heinemann.

Joshi, S.V., Grasso, G.A., Lafond, P.G., Rao I., Webb E., Zerpa L.E., Sloan E.D., Koh C.A., Sum A.K, 2013. *Experimental flow loop investigations of gas hydrate formation in high water cut systems.* Chemical Engineering Science, Vol. 97, 198-209.

Joshi, S.V., Presentation at DeepStar Meeting Houston, TX, December 4, 2008.

Kashchiev, D., Firoozabadi A., 2002a, *Driving force for crystallization of gas hydrates*, Journal of Crystal Growth 241, 220–230

Kashchiev, D., Firoozabadi A., 2002b, *Nucleation of gas hydrates*, Journal of Crystal Growth 243, 476–489

Kelland, M. A., 2014. *Production Chemicals for the Oil and Gas Industry - 2nd Edition*. CRC Press.

Kelland, M. A., Svartaas, T. M., Ovsthus, J., Namba, T., 2006. *A New Class of Kinetic Hydrate Inhibitor*. Annals of the New York Academy of Sciences, Vol. 912, 281-293.

Kvamme, B., 1996. A new theory for the kinetics of hydrate formation. Proceedings of the Second International Conference on Natural Gas Hydrates (ICGH-2), Toulouse, France.

Le Ba, H., 2009. *Formation et agglomération de particules d'hydrate de gaz dans une émulsion eau dans huile : Etude expérimentale et modélisation*. PhD Thesis.ENSMSE.

Liu, Y., Gamwo, I.K., 2012. *Comparison between equilibrium and kinetic models for methane hydrate dissociation*. Chemical Engineering Science, Vol. 69, 193-200.

Livelli,G., 2010. *Innovations in Fluid Flow.* Published in *« http://www.flowcontrolnetwork.com /articles/innovations-in-fluid-flow ». Consulted in March, 2015.*

Long, J.P., 1994*, Gas hydrate formation mechanism and kinetic inhibition*. PhD Thesis. Colorado School of Mines.

Mettler-Toledo Lasentec® Product Group, 2001. *Lasentec® D600 Hardware Manual*. Mettler-Toledo AutoChem, Inc., Redmond, WA.

Mettler-Toledo Lasentec® Product Group, 2011.. *PVM® V819 Hardware Manual*. Mettler-Toledo AutoChem, Inc., Redmond, WA.

Micro Motion® and Rosemount® Flow Product. *Emerson Flow and Density Measurement*. Digital version, accessed « April, 2015 ».

Midoux, N., 1993. *Mécanique et Rhéologie des Fluides en génie chimique*. Edition Lavoisier.

Mullin, J. W., 2001. *Crystallization - 4th edition*. Butterworth-Heinemann.

Natarajan, V., Bishnoi, P.R., Kalogerakis, N., 1994. *Induction phenomena in gas hydrate nucleation*. Chemical engineering science, Vol. 49, 2075-2087.

Nolas, G.S., 2014. *The Physics and Chemistry of Inorganic Clathrates*. Springer.

Palermo, T., Arla, D., Borregales, M., Dalmazzone, C., Rousseau, L., 2005. *Study of the Agglomeration between Hydrate Particles in Oil Using Differential Scanning Calorimetry (DSC)*. Proceedings of the Fifth International Conference on Gas Hydrates (ICGH-5). Trondheim, Norway.

Pauchard, V., Darbouret, M., Palermo, T., Peytavy, J.L., 2007. *Gas Hydrate Slurry Flow in a Black Oil. Prediction of Gas Hydrate Particles Agglomeration and Linear Pressure Drop*. Proceedings of 13th International Conference of Multiphase Production Technology, Edinburgh, UK. 343-355.

PCM Pompes, 2001. *Instruction Manual PCM®-MOINEAU*. PCM Pompes, Inc., Vannes, France.

Potanin A., 1991. *On the mechanism of aggregation in the shear flow of suspensions*. Journal of Colloid Interfaces Science, Vol. 145, No. 1, 140-157.

Preziosi, V., Perazzo, A., Caserta, S., Tomaiuolo, G., Guido, S., 2013. *Phase Inversion Emulsification.* AIDIC Journal, Vol. 32, 1585-1590.

R. Radhakrishnan, B. L. Trout, 2002. *A new approach for studying nucleation phenomena using molecular simulations: Application to CO2 hydrate clathrates*. J. Chem. Phys., Vol. 117, No. 4, 1786.

Ribeiro, J.C.P., Lage, P.L.C., 2008. *Modelling of hydrate formation kinetics: State-of-the-art and future directions*. Chemical Engineering Science, Vol. 63, 2007-2034.

Ripmeester, J. A., 2000. *Hydrate Research – From Correlations to a Knowledge-based Discipline.* Annals of the New York Academy of Sciences, Vol. 912, 1-16.

Ripmeester, J. A., Davidson, D. W., 1981. *^{129}Xe nuclear magnetic resonance in the clathrate hydrate of xenon*. Journal of Molecular Structure, Vol. 75, No. 1,67-72.

Ruppel, *C.*, 2012. *Gas Hydrates Offshore Southeastern United States*. Georgia Institute of Technology, NOAA Ocean Explorer website, accessed March, 2013.

Schramm, L.L., 2005. *Emulsions, Foams, and Suspensions – Fundamentals and Applications.*Wiley-VCH.

Shah, D.O., 1977. *The world of surface science*. Chemical Engineering Education, American Sociey of Engineering Education.

Shia, B.H., Gonga, J., Sunb, C.Y., Zhaoa, J.K., Dinga, Y., Chenb, G.J., 2011. *An inward and outward natural gas hydrates growth shell model considering intrinsic kinetics, mass and heat transfer*. Chemical Engineering Journal, Vol. 171, 1308-1316.

Sjoblom, J., 2006. *Emulsions and Emulsion Stability: Surfactant Science Series.* CRC Press Inc.

Skovborg, P., Rasmussen, P., 1994. *A Mass-Transport Limited Model for the Growth of Methane and Ethane Gas Hydrates*. Chemical Engineering Science, Vol. 49, 1131-1143.

Sloan, E. D., 1990. . *Clathrate Hydrates of Natural Gases.* New York. Marcel Dekker Inc., 641.

Sloan, E. D., Koh, C. A., 2007. *Clathrate Hydrates of Natural Gases - 3rd edition*. CRC Press Inc.

Sloan, E. D., Koh, C. A., Sum, A.K., 2011. *Natural Gas Hydrates in Flow Assurance*. GPP – Elsevier.

Sobrel, T., 2006. *Personal Communication*.

Speight, 2014. *The Chemistry and Technology of Petroleum – 5th Edition*. CRC Press Inc.

Sum, A.K., Koh, C. A., Sloan, E. D., 2009. *Clathrate Hydrates: From Laboratory Science to Engineering Practice.* Ind. Eng. Chem. Res., Vol. 48, 7457-7465.

Talatori, S., Barth, T., 2012. *Rate of hydrate formation in crude oil/gas/water emulsions with different water cuts.* Journal of Petroleum Science and Engineering, Vol. 80, 32-40

Talatori, S., Fotland, P., Barth, T., 2008. *Kinetics of Hydrate Formation in a Water-Oil-Gas System.* Proceedings of the Sixth International Conference on Gas Hydrates (ICGH-6), Vancouver, Canada.

Taylor, P., 1998. *Ostwald ripening in emulsions.* Advances in Colloid and Interface Science, Vol. 75, 107-163.

Turner, D.J., Kleehammer, D.M., Miller, K.T., Sloan, E.D., 2005. *Formation of hydrate obstructions in pipelines: hydrate particle development and slurry flow.* Proceedings of 5th International Conference on Gas Hydrates (ICGH-5), Trondheim, Norvège.

Turner, D.J., Miller, K.T., Sloan, E. D., 2009. *Methane hydrate formation and an inward growing shell model in water-in-oil dispersions*. Chemical Engineering Science, Vol. 64, 3996-4004.

Van der Waals, J., Platteeuw, J., 1959. *Clathrate Solutions*. Adv. Chem. Phys., Vol. 2, 1–57.

Von Stackelberg, M., 1949. *Feste Gashydrate*. Naturwissenschaften, Vol. 36, 327–333.

Von Stackelberg, M., 1956. Rec. Trav. Chim. Pays-Bas, Vol. 75, 902.

Vysniauskas, A., Bishnoi, P.A., 1983. *Kinetic study of methane hydrate formation*. Chemical engineering data, Vol.38, No. 7, 1061-1972.

Zerpa, L.E., 2013. *A Practical Model to Predict Gas Hydrate Formation, Dissociation and Transportability in Oil and Gas Flow lines*. PhD Thesis. Colorado School of Mines.

École Nationale Supérieure des Mines
de Saint-Étienne

NNT : 2016 EMSE 0811

Aline MENDES MELCHUNA

EXPERIMENTAL STUDY AND MODELING OF METHANE HYDRATES CRISTALLIZATION UNDER FLOW FROM EMULSIONS WITH VARIABLE FRACTION OF WATER AND ANTI-AGGLOMERANT

Speciality: Process Engineering

Keywords: crystallization, hydrates, emulsion, flow, flow line, anti-agglomerant.

Abstract:

Crystallization of hydrates during oil production is a major source of hazards, mainly related to flow lines plugging after hydrate agglomeration. During the petroleum extraction, oil and water circulate in the flow line, forming an unstable emulsion. The water phase in combination with light hydrocarbon components can form hydrates. The crystallization of hydrates has been extensively studied, mainly at low water content systems. However, as the oil field matures, the water fraction increases and can become the dominant phase, a system less known in what concerns hydrate formation. Actually, several techniques can be combined to avoid or remediate hydrate formation. Recently, a new class of additives called Low Dosage Hydrate Inhibitor (LDHI) started to be studied, they are classified as Kinetic Hydrate Inhibitors (KHI-LDHI) and Anti-Agglomerants (AA-LDHI).

This work is a parametric study about hydrate formation from emulsion systems ranging from low to high water content, where different flow rates and the anti-agglomerant presence were investigated. The experiments were performed at the Archimède flow loop, which is able to reproduce deep sea conditions. The goal of this study is enhancing the knowledge in hydrate formation and comprehending how the dispersant additive acts to avoid agglomeration. For this matter, it was developed a crystallization topological model for the systems without and with additive. A technique to determine the system continuous phase and a mechanism of the anti-agglomerant action from the chord length measurements were also proposed.

École Nationale Supérieure des Mines
de Saint-Étienne

NNT : 2016 EMSE 0811

Aline MENDES MELCHUNA

ÉTUDE EXPERIMENTALE ET MODELISATION DE LA CRISTALLISATION D'HYDRATES DE METHANE EN ECOULEMENT A PARTIR D'UNE EMULSION A POURCENTAGES VARIABLES D'EAU ET D'ANTI-AGGLOMERANT

Spécialité: Génie des Procédés
Mots clefs : cristallisation, hydrates, émulsion, écoulement, pipeline, anti-agglomérant

Résumé :
La cristallisation des hydrates pendant la production de pétrole est une source de risques, surtout liés au bouchage des lignes de production dû à l'agglomération des hydrates. Pendant l'extraction de pétrole, l'huile et l'eau circulent dans le pipeline et forment une émulsion instable. La phase eau se combine avec les composants d'hydrocarbures légers et peut former des hydrates. La cristallisation des hydrates a été intensivement étudiée, principalement à faible fraction d'eau. Cependant, lorsque le champ de pétrole devient mature, la fraction d'eau augmente et peut devenir la phase dominante, un système peu étudié concernant à la formation d'hydrates. Plusieurs techniques peuvent être combinées pour éviter ou remédier la formation d'hydrates. Récemment, une nouvelle classe d'additifs a commencé à être étudiée : Inhibiteurs d'Hydrates à Bas Dosage (LDHI), divisés en Inhibiteurs Cinétiques (KHI-LDHI) et anti-agglomérants (AA-LDHI).
Ce travail est une étude paramétrique de la formation d'hydrates à partir de l'émulsion, en variant la fraction d'eau, le débit, en absence et en présence d'AA-LDHI. Les expériences ont été réalisées sur la boucle d'écoulement Archimède, qui est en mesure de reproduire les conditions de la mer profonde. L'objectif de cette étude est d'améliorer la compréhension de la formation d'hydrate et de comprendre comment l'additif dispersant évite l'agglomération. Pour ce faire, un modèle comportemental de la cristallisation pour les systèmes sans et avec additif a été développé. Il a également été proposé une technique pour déterminer la phase continue du système et un mécanisme d'action pour l'anti-agglomérant a été suggéré.